The Dissertation Committee for Tania Betancourt Certifies that this is the approved version of the following dissertation:

Targetable Biodegradable Nanoparticles for Delivery of Chemotherapeutic and Imaging Agents to Ovarian Cancer

Committee:

Lisa Brannon-Peppas, Supervisor

R. Malcolm Brown, Co-Supervisor

Nicholas Peppas

Krishnendu Roy

Robert Williams

Targetable Biodegradable Nanoparticles for Delivery of Chemotherapeutic and Imaging Agents to Ovarian Cancer

by

Tania Betancourt, B.S.; M.S.

Dissertation

Presented to the Faculty of the Graduate School of

The University of Texas at Austin

in Partial Fulfillment

of the Requirements

for the Degree of

Doctor of Philosophy

The University of Texas at Austin

December 2007

Dedication

To my loving husband and mother.

For your constant support and encouragement.

Acknowledgements

I would like to sincerely thank my advisor Dr. Lisa Brannon-Peppas for her guidance and support during the course of my Ph.D. I am extremely grateful for the countless opportunities that she provided for my academic and personal growth. Working in her laboratory I learned a great deal not only about science but also about how to approach difficulties positively, how to run a laboratory, and how to balance work and family. I also thank my co-advisor Dr. Malcolm Brown for very helpful research discussions and for providing inspiration through his love for science. I thank Dr. Nicolas Peppas for his guidance and encouragement throughout my doctoral studies, for allowing me to participate with his group in research meetings which were extremely helpful, and providing access to essential laboratory equipment without which I would not have been able to complete this project. I also thank Dr. Krishnendu Roy and Dr. Robert Williams for their helpful research suggestions.

I thank Dr. Maria Jose Alonso and Dr. Patrick Courvreur for having me in their laboratories during my visits to Spain and France. Also thanks to Dayami Carreno and Reddy Harivardhan for their friendship and guidance during these stays abroad.

Special thanks to my colleagues who have been by my side during the course of my studies with helpful discussions, encouraging words, and much patience: Marla Johnson, Amber Doiron, Kimberly Homan, Omar Fisher, Charlie Drinnan, Scott Collins,

Cristal (and Golf) Glangchai, Steve Marek, and Don Owens. Special thanks to Marla for having been such a good friend during the beginning of this stage. Sincere thanks also to Amber for being so patient with me and for having shared so many experiences through this journey. Many thanks to Omar and Charlie for their immense patience while I used their laboratories. I also thank the many other graduate students that have, in some way, helped me during these past years.

Sincere thanks to the wonderful undergraduate researchers that have worked alongside with me to complete this work: Brandon Brown, Jou Lee, Kunal Shah, James Byrne, Shefali Patel, Meena Kadapakkam, Shelly Casciato, Nicole Sunaryo, Spencer Crowder, Jared Chen, and Shelby Pearce. You have all been incredible and I wish you the best in life. I am sure that you will all be very successful in whatever you do.

I would also like to thank John Mendenhall, Angela Bardo and Cassy Horne for all their help with experiment design and use of the equipment in the ICMB facility.

Finally, I would like to thank my family with all my heart for their support. Boran, my loving husband, you have been there for me during the tough times, you have encouraged me to do the best I can in every way, you have been incredibly patient during these four and a half years of living apart. I could not have done this without you. Mami, you have always encouraged me to pursue my dreams, whatever they may be, without pressure. You have also been an incredible role model, and I am especially proud of you for having completed your bachelor's degree concurrently with my Ph.D. Thanks to my dad, my grandparents and the rest of my family for your thoughts and encouragement.

Targetable Biodegradable Nanoparticles for Delivery of Chemotherapeutic and Imaging Agents to Ovarian Cancer

Publication No._____

Tania Betancourt, Ph.D.

The University of Texas at Austin, 2007

Supervisors: Lisa Brannon-Peppas and R. Malcolm Brown

Every year more than 10 million people develop cancers globally. Ovarian cancer, specifically, results in more than 22,000 new cases and 16,000 deaths from this disease yearly, more than any other cancer of the female reproductive system. In addition, because of non-specific symptoms and poor screening techniques, most ovarian cancer cases are discovered after the disease is in an advanced state. Consequently, aggressive and effective treatment options that incur minimal toxic effects to healthy tissue are in great need.

In the present research, stealth biodegradable nanoparticles were developed as vehicles for the controlled and targeted delivery of chemotherapeutic agents for the treatment of ovarian cancer. The design of this delivery system consisted of nanoparticles of biodegradable polymers of the poly(lactic-co-glycolic acid) family loaded with the chemotherapeutic agent doxorubicin or the imaging agents rhodamine 6G, indocyanine green or gadopentetic acid. Nanoparticles were modified by incorporation of functional poly(ethylene glycol) on their surface to improve the stability

of the colloidal suspension, increase their circulation lifetime *in vivo,* and provide a site for conjugation of targeting agents specific to ovarian tissue. Various methods were evaluated for this surface modification, including the use of polymer blends, the chemical conjugation of the polymers, and the polymerization of lactide and glycolide monomers initiated by heterofunctional poly(ethylene glycol). Nanoparticles incorporating poly(ethylene glycol) presented improved characteristics compared to unmodified particles including smaller size, higher stability and slower release of the chemotherapeutic agent doxorubicin The actual drug or agent content was decreased in the case of doxorubicin and rhodamine, but increased for indocyanine green as a result of improved agent-polymer interactions.

Poly(ethylene glycol)-containing nanoparticles were conjugated to monoclonal antibody mAb106-105, which is specific to the extracellular domain of human follicle-stimulating hormone (FSH) receptors. These receptors are only expressed in ovarian cells in women, thus providing a system that is highly specific to ovarian tissue. The interaction and therapeutic potential of nanoparticles with or without targeting antibodies were tested on OVCAR-3, Caov-3, and MDA-MB-231 cancer cells.

Table of Contents

List of Tables

List of Figures

CHAPTER 1

INTRODUCTION

Cancer is a disease that affects millions of people across the globe every year. The World Health Organization estimated that more than 10 million people developed a malignant tumor and more than 6.5 million people died from this disease during the year 2000 (Ferlay, Bray et al. 2004). In the United States, cancer is the second cause of death from disease after heart disease, accounting for more than half a million deaths every year. According to the American Cancer Society Cancer Statistics, the overall cost for cancer for the United States in 2004 was $189.8 billion: $69.4 billion for direct medical costs, $16.9 billion for indirect morbidity costs, and $103.5 billion for indirect mortality costs (American Cancer Society 2005). Most importantly, while mortality rates of other major chronic diseases, such as heart and cerebrovascular disease, decreased significantly in the past half century, cancer mortality rates have remained approximately constant (American Cancer Society 2005). This is a troubling fact because it suggests that recent detection and treatment options have not been able to improve mortality rates substantially.

Ovarian cancer, specifically, currently accounts for 3% of the estimated new cases and 6% of the deaths associated with cancer in women in the United States, which equates to approximately 22,200 cases and 16,200 deaths every year (American Cancer Society 2005). Death rates for ovarian cancer have remained almost constant since the 1950's, and the relative five-year survival rate from 1995 to 2000 was 44%, compared to 88% for breast cancer (American Cancer Society 2005). Unfortunately, symptoms of

ovarian cancer are not specific and current screening methods are not very sensitive. This results delayed detection, usually after the cancer is in an advanced state and has metastasized, and consequently after the chance of survival has been sharply reduced.

The three main treatment options for ovarian cancer patients are surgery, chemotherapy, and radiation therapy. In all cases, the extent of treatment depends on the type of cancer, the stage of the disease, the patient's overall state of health, and personal considerations. In most cases, however, a combination of surgical and chemotherapeutic treatments is utilized. All of these treatment options may lead to permanent menopause and infertility. Chemotherapeutic treatments in general lack specificity because they target all proliferating cells by inhibiting DNA synthesis or interfering with processes of cell division or metabolism (Twardowski and Margolin 2002). As a consequence, chemotherapy leads to the damage of healthy tissue, especially of the normally dividing cells of the bone marrow, skin, and gastro-intestinal mucosa, among other tissues. In addition, neoplastic cells readily mutate, and many cancers develop resistance to chemotherapeutic agents (Twardowski and Margolin 2002). The poor specificity of chemotherapeutic agents commonly prevents aggressive and effective treatment of the cancer.

Targeted delivery of imaging and therapeutic agents with the use of biodegradable nanoparticles promises to improve early detection of the cancer, reduce dose-limiting side effects during treatment, and improve the efficacy of the treatment by controlling the spatial and temporal distribution of the imaging agent or drug *in vivo*. To date, most delivery systems for ovarian cancer have targeted the folate receptors (Li 1998; Sudimack and Lee 2000) and luteinizing hormone-releasing hormone receptors (Wang, Lin et al. 2003; Yang, Chan et al. 2006) that are overexpressed in ovarian cancer cells. However, because these receptors are also expressed in numerous other healthy tissues, only limited

specificity can be achieved. There is, as a result, a great need for the development of a system that can more specifically target ovarian cancer tissue.

1.1 OVERALL RESEARCH OBJECTIVES

The development of an alternative formulation for targeted delivery of imaging and chemotherapeutic agents to ovarian cancer cells based on the concepts of biomaterials, controlled drug delivery and targeted drug delivery could result in a system that overcomes some of the problems associated with current methods. Specifically, the main objectives of the research project described here were to develop, characterize and evaluate an injectable, long-circulating, controlled release system based on biodegradable polymeric nanoparticles that directs imaging and chemotherapeutic agents to ovarian tumors. To achieve the desired specificity of this formulation to ovarian cancer cells these nanoparticles are targeted the follicle stimulating hormone (FSH) transmembrane receptors which are solely expressed in the ovaries and testis (Richards and Midgley 1976; Kangasniemi, Kaipia et al. 1990; Simoni, Gromoll et al. 1997; Meduri, Charnaux et al. 2002). Importantly, expression of FSH receptors has also been observed to occur in samples of numerous types of ovarian epithelial cancers as described in Chapter 2 (Nakano, Kitayama et al. 1989; Zheng, Lu et al. 2000; Parrott, Doraiswamy et al. 2001; Syed, Ulinski et al. 2001; Wang, Lin et al. 2003). It is expected, consequently, that the increased and spatially restricted expression of these receptors in ovarian cancer cells could enhance targeted delivery of imaging and therapeutic agents.

The design of the developed nanoparticles consists of a core of the biodegradable polyesters poly(lactide-co-glycolide) or poly(lactic acid) and free pendant chains of functional poly(ethylene glycol) onto which targeting moieties are conjugated, as depicted in Figure 1.1. The imaging or chemotherapeutic agents to be delivered are

encapsulated within the biodegradable core and are released through a combination of diffusion across the polymeric matrix and degradation of the same.

The system developed is designed to be more efficacious than the current method of systemic bolus administration of chemotherapy and other targeted delivery systems because:

- By releasing the chemotherapeutic agent over time through controlled release, the concentration of this agent is more easily maintained within the therapeutic window for extended periods. This protects the patient from exposure to high concentration bolus doses which are commonly near toxic levels while still delivering therapeutic levels, results in the need for fewer administrations, and increases patient compliance and quality of life during treatment.
- Targeting the nanoparticles loaded with chemotherapeutic agents to cellular receptors of such strict expression profiles as the FSH receptors will provide an extremely specific system that will deliver antineoplastic agents only to the location where they are needed. Consequently, the toxicity that is traditionally induced in other tissues of the body will be significantly reduced. It will then be possible to provide more aggressive chemotherapeutic treatment while minimizing serious side effects to the patient. Additionally, the fact that more of the drug injected is put into intimate contact with the tumor means that therapy will be more efficacious.
- Inclusion of poly(ethylene glycol) chains on the surface of the nanoparticles will result in delayed opsonization, reduced uptake by the reticuloendothelial system, and consequent increased time of residence in the circulation. This alteration increases the likelihood that the therapeutic agent will reach its target without the

need for chemical modification of the drug which may interfere with its *in vivo* activity.

1.2 SPECIFIC RESEARCH AIMS

The specific aims that were addressed in this project were the following:

(i) **To prepare, characterize and optimize formulations of biocompatible, biodegradable nanoparticles of poly(lactic-co-glycolic acid) (PLGA) loaded with chemotherapeutic agents for therapeutic purposes**. Specifically, the chemotherapeutic agent used was doxorubicin, which is currently used in the treatment of recurrent ovarian cancer. Nanoparticles were prepared by oil-in-water nanoprecipitation of a polymer/drug solution upon addition to an aqueous phase. Nanoparticles were characterized with respect to size, loading, encapsulation efficiency, morphology, zeta potential, and in vitro drug release kinetics.

(ii) **To prepare and characterize the formulation of biocompatible, biodegradable nanoparticles of poly(lactic-co-glycolic acid) loaded with fluorescent or electron-dense agents for characterization purposes.** Encapsulation of fluorescent or electron-dense agents within nanoparticles was sought for use in studying the interactions of the nanoparticles with the target cells through fluorescence microscopy and electron microscopy, respectively. The hypothesis here was that if these nanoparticle formulations had similar properties to those loaded with chemotherapeutic agents, then they would be useful for monitoring cellular and tissue uptake and distribution of therapeutic nanoparticles both *in vitro* and *in vivo.* Rhodamine 6G, indocyaninie green and gadopentetic acid were used as fluorescent and electron dense agents.

Nanoparticles were characterized with respect to loading, encapsulation efficiency, particle size and morphology.

(iii) To modify the initial formulations by including poly(ethylene glycol) (PEG) free chains at the surface of the nanoparticles to provide stealth properties. This modified formulation can present enhanced properties such as increased lifetime in the circulation and distinct biodistribution *in vivo*, and provides the possibility for attachment of targeting moieties at the surface of the nanoparticles. Incorporation of functional PEG on the formulation was attempted through polymer blending, polymer conjugation and co-polymerization techniques. Nanoparticle preparation and cryoprotection variables were optimized.

(iv) To incorporate targeting agents specific to ovarian cancer cells on the surface of the nanoparticles. A monoclonal antibody specific to the extracellular portion of the FSHR receptor was introduced on the surface of the nanoparticles through chemical conjugation to the functionalized end of the poly(ethylene glycol) chains. Conjugation of the targeting agents was verified and optimized.

(v) To examine the specificity of cellular uptake, and intracellular distribution of the various formulations of nanoparticles *in vitro*. Cellular studies were carried out in ovarian epithelial cancer cell lines expressing the FSH receptors, in addition to a non-ovarian cancer cell line. Comparative nanoparticle uptake experiments in the different cell lines were performed in order to verify the specificity of the targeted formulation to ovarian cancer cells.

(vi) To determine the therapeutic efficacy of the targeted delivery system *in vitro*. The above mentioned types of cells were exposed to the targeted nanoparticles loaded with chemotherapeutic agents. Cytotoxicity studies revealed the degree of therapeutic effect of the various formulations: free drug, blank nanoparticles,

drug-loaded nanoparticles with or without PEG modification, and drug-loaded nanoparticles with the targeting agent.

1.3 OVERVIEW

Chapter 2 describes background information relevant to the drug delivery system developed. Chapter 3 describes the preparation, characterization and *in vitro* evaluation of poly(lactic-co-glycolic acid) nanoparticles loaded with the chemotherapeutic agent doxorubicin. Chapter 4 describes the preparation and characterization of nanoparticles loaded with the imaging agents rhodamine 6G, indocyanine green and gadopentetic acid for *in vitro* and *in vivo* visualization. Chapter 5 describes the various strategies that were used to incorporate poly(ethylene glycol) on the surface of the nanoparticles to improve the stability of the formulation and provide a site for conjugation of targeting agents . Chapter 6 describes the preparation of targeted nanoparticles containing poly(ethylene glycol) and antibodies for targeting. Chapter 7 describes the results of *in vitro* evaluation of the various formulations on ovarian cancer cells. Finally, Chapter 8 summarizes the conclusions and future prospects for this research project.

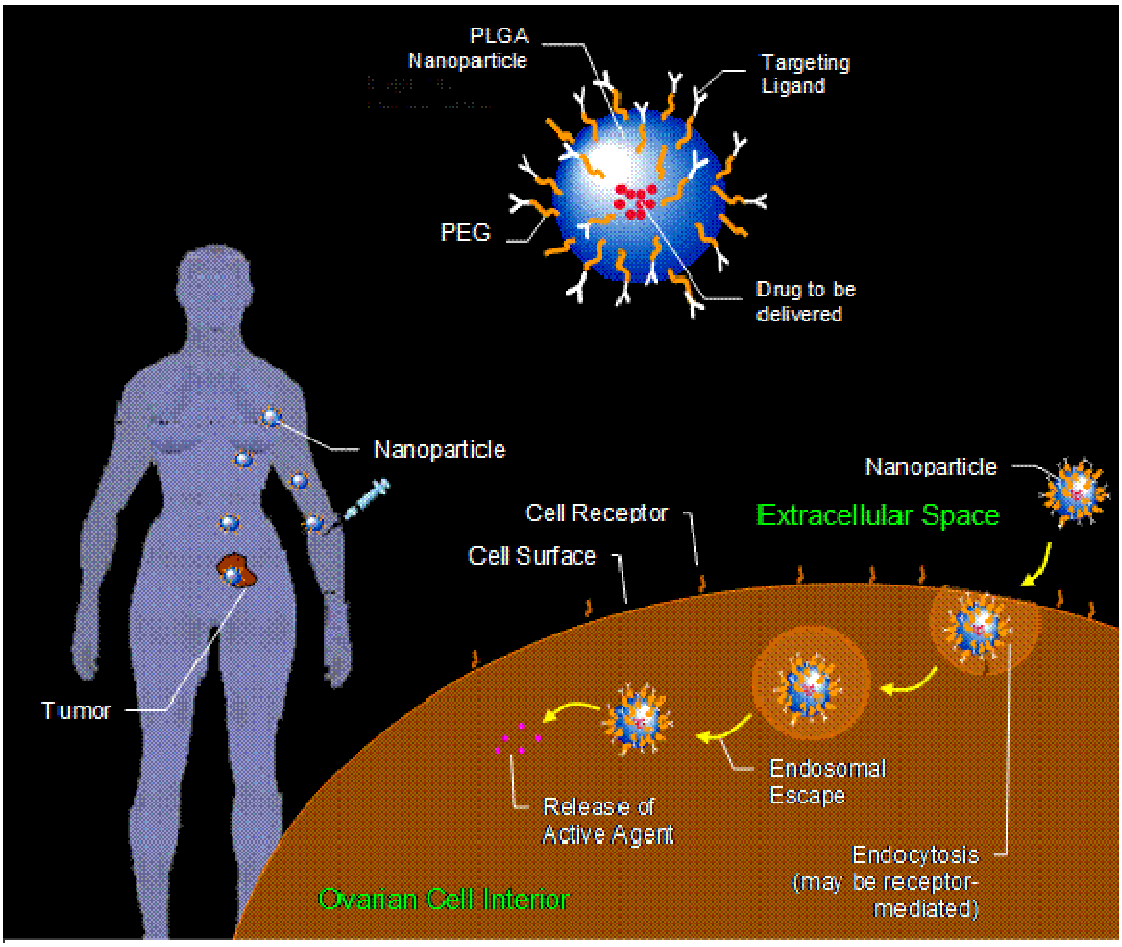

Figure 1.1 Design and Expected Mechanism of Action of Targeted Biodegradable Nanoparticles. Nanoparticles Concentrate at the pathological tissue because of the highly permeable vasculature of cancerous tissue, and specifically interact with the targeted follicle stimulating hormone receptors. The imaging or chemotherapeutic agents loaded within the nanoparticles are released in a controlled manner either intracellularly after receptor-mediated endocytosis, as shown, or extracellularly in close proximity to the cancer cells.

1.4 REFERENCES

American Cancer Society (2005). Cancer Facts & Figures 2005. Atlanta, GA, American Cancer Society.

Ferlay, J., F. Bray, et al. (2004). GLOBOCAN 2002: Cancer Incidence, Mortality and Prevalence Worldwide. IARC CancerBase No. 5. Lyon, IARC Press.

Kangasniemi, M., A. Kaipia, et al. (1990). "Cellular regulation of follicle-stimulating hormone (FSH) binding in rat seminiferous tubules." J Androl 11(4): 336-43.

Li, R. H. (1998). "Materials for Immunoisolated Cell Transplantation." Advanced Drug Delivery Reviews 33: 87-109.

Meduri, G., N. Charnaux, et al. (2002). "Follicle-stimulating hormone receptors in oocytes?" J Clin Endocrinol Metab 87(5): 2266-76.

Nakano, R., S. Kitayama, et al. (1989). "Localization of gonadotropin binding sites in human ovarian neoplasms." Am J Obstet Gynecol 161(4): 905-10.

Parrott, J. A., V. Doraiswamy, et al. (2001). "Expression and actions of both the follicle stimulating hormone receptor and the luteinizing hormone receptor in normal ovarian surface epithelium and ovarian cancer." Mol Cell Endocrinol 172(1-2): 213-22.

Richards, J. S. and A. R. Midgley, Jr. (1976). "Protein hormone action: a key to understanding ovarian follicular and luteal cell development." Biol Reprod 14(1): 82-94.

Simoni, M., J. Gromoll, et al. (1997). "The follicle-stimulating hormone receptor: biochemistry, molecular biology, physiology, and pathophysiology." Endocr Rev 18(6): 739-73.

Sudimack, J. and R. Lee (2000). "Targeted Drug Delivery Via the Folate Receptor." Advanced Drug Delivery Reviews 41: 147-162.

Syed, V., G. Ulinski, et al. (2001). "Expression of gonadotropin receptor and growth responses to key reproductive hormones in normal and malignant human ovarian surface epithelial cells." Cancer Res 61(18): 6768-76.

Twardowski, P. and K. Margolin (2002). Targeting Vascular Endothelium With Antibodies. Cancer Drug Discovery and Development: Tumor Targeting in Cancer Therapy. M. Pagé. Totowa, NJ, Humana Press Inc.: 199-210.

Wang, J., L. Lin, et al. (2003). "Quantitative analysis of follicle-stimulating hormone receptor in ovarian epithelial tumors: a novel approach to explain the field of ovarian cancer development in secondary mullerian systems." International Journal of Cancer 103(3): 328-334.

Yang, C. Q., K. Y. K. Chan, et al. (2006). "Single Nucleotide Polymorphisms of Follicle-Stimulating Hormone Receptor are Associated with Ovarian Cancer Susceptibility." Carcinogenesis 27(7): 1502-1506.

Zheng, W., J. J. Lu, et al. (2000). "Ovarian epithelial tumor growth promotion by follicle-stimulating hormone and inhibition of the effect by luteinizing hormone." Gynecol Oncol 76(1): 80-8.

CHAPTER 2

BACKGROUND AND SIGNIFICANCE

2.1 CONTROLLED DRUG DELIVERY

The properties of the nanoparticle-based system developed in this research are based on the concepts of controlled drug delivery and targeted delivery. Controlled drug delivery utilizes the combination of a bioactive agent with a non-active substance (carrier) in such a way that the drug is released from the carrier in a predetermined manner, whether at a constant rate in what is known as zero-order release, in a cyclic manner, or in response to an external trigger such as a change in pH, ionic strength or temperature of the medium (Brannon-Peppas 1997; Stayton, El-Sayed et al. 2005; Wei, Zeng et al. 2005; Peppas 2006; Sawant, Hurley et al. 2006). The benefits offered by controlled drug delivery over traditional pharmaceutical administration include maintenance of the drug levels within desired limits, maximal use of the pharmaceutical, the need for fewer doses, and better patient compliance (Brannon-Peppas 1997). In addition, association of the drug with a carrier may provide enhanced protection to the active agent from degradation in the physiological environment, and improve the stability of the agent that is required for formulation and administration.

Examples of currently researched methods for drug delivery include prodrugs, dendrimers, liposomes, micelles, hydrogels, implantable systems, micro- and nanofabricated systems, Microparticles, and nanoparticles. Prodrugs are generated through the chemical conjugation of an active agent with a carrier molecule, which could be a polymer or lipid (Lee, Lu et al. 2002; Mhaka, Denmeade et al. 2002). Dendrimers are highly branched macromolecules of very small size, and monodistributed molecular

weight that can be used to deliver high payloads of drugs through conjugation of the active agent with the numerous surface or interior functional groups (Kukowska-Latallo, Candido et al. 2005). Both prodrugs and dendrimers have the disadvantage of chemically modifying the active agent, possibly affecting its *in vivo* activity. Liposomes consist of vesicles formed by phospholipids bilayers, and which deliver the drug into cells by fusing with cellular membranes (Torchilin, Narula et al. 1996; Schiffelers, Koning et al. 2003).

Micelles consist of self-assembled vesicles formed by lipids or other amphiphilic molecules (including polymers), and which can be used for encapsulation and isolation of hydrophobic molecules from the surrounding hydrophilic physiological environment (Yoo and Park 2001; Yoo and Park 2004; Lee, Na et al. 2005; Liu, Tong et al. 2005; Venkatraman, Jie et al. 2005; Nasongkla, Bey et al. 2006). Liposomes and micelles offer advantages such as prolonged circulation time, altered pharmacokinetics, and the ability to encapsulate highly hydrophobic drugs, but do not usually provide controlled release over time. Hydrogels are materials capable of uptaking significant amounts of water and swelling in result to changes in the surrounding environment, resulting in increased pore sizes that allow controlled release of its contents (Torres-Lugo, Garcia et al. 2002; Peppas, Wood et al. 2004; Blanchette and Peppas 2005). Drug delivery systems based on hydrogels have been shown to result in low drug burst effects, but do not usually provide long term drug release. Implantable systems can provide long term drug release, but require invasive interventions for implantation and removal, thus resulting in lower patient acceptability (Desai, Mallery et al. 2007; Huolman and Ashammakhi 2007; Kontakis, Pagkalos et al. 2007).

Micro- and nanofabricated systems have only recently been researched for drug delivery. Although these techniques can produce drug carriers with specific geometrical, structural and functional properties (Betancourt and Brannon-Peppas 2006), the costs

associated with their production may limit their applications. Microparticles (Brannon-Peppas 1995; Kasturi, Sachaphibulkij et al. 2005; Lin, Ng et al. 2005) and nanoparticles (Couvreur, Dubernet et al. 1995; Yoo, Oh et al. 1999; Janes, Fresneau et al. 2001; Brannon-Peppas and Blanchette 2004; Betancourt, Brown et al. 2007)encapsulate drugs in either a reservoir or matrix arrangement, in which the drug is either localized to the center of the particle and surrounded by a polymer layer, or dispersed throughout a polymeric matrix, respectively. Depending on the conformation, and on the material used to fabricate the micro- or nanoparticle, these systems may lead to various drug release kinetic profiles –including constant (zero-order) release– as a result of the combined effects of drug diffusion and carrier degradation (Brannon-Peppas 1997). Nanoparticles, in addition, because of their small size, are able to circulate through capillaries, preferentially escape into tumor tissue because of the enhanced permeability and retention effect (EPR), and may be taken up by cells for intracellular drug delivery, as will be discussed in the "targeted drug delivery" section. It is these properties of nanoparticles that were exploited for the development of the targeted delivery system in this project.

2.1.1 Biomaterials for Drug Delivery

Numerous biopolymers, both synthetic and natural, have been studied for drug delivery applications. As for any other device used for *in vivo* applications, drug delivery systems must result in low or preferably non-detectable adverse physiological reactions such as immunogenicity and toxicity. Natural polymers include cellulose, chitosan, hyaluronic acid, chondroitin sulfate, gelatin, collagen, alginate, carrageenan, dextran, proteins and DNA (Janes, Calvo et al. 2001; Friess 2004). Synthetic polymers include poly(lactic-co-glycolic acid) (PLGA) and other lactide- or glycolide-derived polymers,

polyethylene glycol (PEG), poly(acrylic acids), poly(acrylates), poly(acrylamides), poly(anhydrides), poly(caprolactone), poly(urethanes), among others (Brannon-Peppas 1997; Huh, Cho et al. 2003). Synthetic polymers have a number of benefits including high control of polymer properties, such as molecular weight and functionality, and feasible commercial-scale production. In addition, although both synthetic and natural polymers may activate the complement system, natural polymers can also lead to cellular and humoral immune response as a result of the recognition of foreign organism markers.

The system developed in this research utilizes poly(lactide-co-glycolide) (PLGA), the copolymer of lactide and glycolide, as the main component for the preparation of nanoparticles for delivery of chemotherapeutic or imaging agents. PLGA is a biodegradable polymer that has been approved by the FDA for use as suture material and in various drug delivery systems, including Lupron Depot® formulation of leuprolide acetate for the treatment of prostate cancer and endometriosis (TAP Pharmaceutical Products), Nutropin Depot® PLGA formulation of human growth hormone (Genentech), Sandostatin® Depot PLGA microsphere formulation for inhibition of human growth hormone secretion (Novartis), ProLease® (Alkermes) and Trelstar® Depot (Debiopharm) (Shive and Anderson 1997; Dechy-Cabaret, Martin-Vaca et al. 2004). PLGA degrades by hydrolysis of its ester bonds into lactic acid and glycolic acid, both of which are further metabolized into carbon dioxide and water through the Kreb's cycle (Lewis 1990; Brannon-Peppas 1995). The degradation of this family of polymers can be tailored according to the co-monomer ratio, with a longer degradation time required with increased lactic acid content. Degradation increases under extreme pH conditions. At low pH degradation occurs through random chain cleavage which forms insoluble oligomers and few carboxylic acid groups. In basic conditions, degradation occurs

through preferential cleavage of terminal ester bonds which results in rapid formation of soluble monomers and carboxylic acid groups (Abdelwahed, Degobert et al. 2006).

PLGA microparticles have been formulated in the past as carriers for oral, mucosal and subcutaneous administration (Shive and Anderson 1997; Blanco and Alonso 1998; Fattal, Pecquet et al. 2002; Murillo, Goni et al. 2002; Freitas, Merkle et al. 2005). Polymeric biodegradable nanoparticles, specifically those prepared from PLGA, have only been utilized as drug delivery systems fairly recently (Brannon-Peppas 1995; Panyam and Labhasetwar 2003; Feng, Mu et al. 2004; Astete and Sabliov 2006). These were developed from the modification of well-known microparticle preparation techniques (Jain 2000). PLGA nanoparticles degrade through bulk or uniform degradation throughout the polymeric matrix (Brannon-Peppas 1995; Brannon-Peppas 1997). The research group of Dr. Brannon-Peppas has reported on the optimization (Birnbaum, Kosmala et al. 2000) and scale up production (Brannon-Peppas and Birnbaum 2000) of PLGA nanoparticles to up to 100g per batch, thus demonstrating the feasibility of their production for clinical and commercial applications.

2.1.2 Poly(ethylene glycol) (PEG) in Drug Delivery

Unmodified polymeric nanoparticles administered through intravenous injection are known to be rapidly cleared from the circulation by organs of the reiculoendothelial system, namely the Kuppfer cells in the liver and the macrophages in the spleen (Fawaz, Bonini et al. 1993; Brannon-Peppas and Blanchette 2004). For example, polystyrene particles as small as 60 nm are known to be removed from the circulation within minutes (Gref, Domb et al. 1995). Poly(ethylene glycol) (PEG) has been shown to increase circulation time in the blood, modify the biodistribution, and provide shielding from recognition by the immune system to biologically active agents (Stolnik, Dunn et al.

1994; Gref, Luck et al. 2000; Mehvar 2000; Hu, zhai et al. 2002; Otsuka, Nagasaki et al. 2003). PEG is a hydrophilic, biocompatible, non-biodegradable polymer that has been approved by the FDA for a number of biomedical applications, including suppositories (Graham 1987), contraceptive sponges (Nakaoka, Tabata et al. 1997), and wound healing membranes (Park, Jang et al. 2007). PEG is known to bind 2 to 3 water molecules per ethylene oxide unit, effectively increasing its hydrodynamic size to up to 10 times that of a soluble polymer of comparable molecular weight. Because of this, PEG coating sterically stabilizes the nanoparticles and hinders their interaction with plasma proteins and the immune system. The effect of PEGylation on the serum half life has been shown to correlate with the molecular weight of the PEG chains. Half lives of up to 20 hours have been observed with the use of 190 kDa PEG chains (Yokoyama and Okano 1996). Although PEG is not biodegradable, PEG molecules of less than about 30 kDa can be excreted from the body through renal clearance.

2.1.3 Targeted Drug Delivery

Targeted delivery utilizes unique phenotypic features of diseased tissues and cells in order to concentrate the drug at the location where it is needed. Targeted delivery can be divided into passive and active targeting. Passive targeting tries to minimize non-specific interactions between the drug carrier and non-target sites in the body by detailing its physiochemical properties such as size, morphology, hydrophilicity, and surface charge (McDonald and Baluk 2002; Torchilin 2002). When targeting tumor tissue, the enhanced permeability and retention effect (EPR) acts as a passive targeting approach because it allows passage of drug carriers ranging in size from 10 to 500 nm through the highly-permeable blood vessels that supply growing tumors, and leads to entrapment of large molecules as a result of deficient lymphatic drainage (Yokoyama and Okano 1996;

McDonald and Baluk 2002). In fact, it has been reported that the intra-cellular openings in vascular endothelium of tumor blood vessels can be of up to 2 μm in diameter, and that the vessel porosity in tumor vasculature can be up to an order of magnitude higher than that of normal blood vessels (McDonald and Baluk 2002). The abnormal architecture of tumor vasculature is a result of the process of neovascularization directed by tumor factors, a process that is crucial for tumor growth and metastasis (Folkman, Merler et al. 1971; Folkman 2003). The ability of therapeutic NPs to utilize the EPR can translate into improved anti-tumor efficacy, better use of the encapsulated pharmaceutical agent, and increased patient compliance and quality of life.

Active targeting utilizes biologically specific interactions including antigen-antibody and ligand-receptor binding, and may seek drug uptake by receptor-mediated endocytosis through association of the drug or drug carrier with such antigen or ligand (Torchilin 2002; Fahmy, Samstein et al. 2005). Receptor-mediated endocytosis commonly occurs through clathrin-coated vesicles, and is carried out in mammalian cells continuously for the uptake of nutrients, and for modulation of signal transduction through the up- or down-regulation of signaling receptors (Conner and Schmid 2003). Signaling receptors, such as the ones that are targeted with the present nanoparticles, are commonly endocytosed in response to elevated hormone levels as a feedback regulation mechanism. Targeted delivery avoids the need for high systemic drug levels for the drug to be effective, and consequently offers a more economic alternative for treatment. Targeted delivery is not only useful for therapeutic purposes, but has also been researched for its ability to concentrate imaging or contrast agents for the detection of malignancies and for monitoring the effects of therapeutic agents (Brannon-Peppas and Blanchette 2004; Gao, Cui et al. 2004).

Most systems for targeted delivery to cancer have utilized drug conjugates, liposomes or micelles. Recently, however, various nanoparticle-based targeted systems have been developed. Table 2.1 and Table 2.2 summarize some of the targeted drug delivery systems or polymeric nanoparticle systems, respectively, for cancer treatment that have been recently reported. To date, the vast majority of systems developed for targeted drug delivery for the treatment of ovarian cancer target the folate receptor with monoclonal antibodies or folic acid itself (Sudimack and Lee 2000; Turk, Waters et al. 2004; Yoo and Park 2004). Folate receptors are overexpressed in many tumor types, including more than 90% of ovarian carcinomas (Sudimack and Lee 2000; Yoo and Park 2004). However, folate receptors are also expressed on epithelial cell in the placenta, breast, lung, kidney, proximal tubles, choroid plexus, fallopian tubes, uterus, endocervix, and salivary glands (Veggian, Fasolato et al. 1989; Weitman, Lark et al. 1992), as well as in myelomonocytes and lymphoid cells (Shen, Ross et al. 1994; Ross, Wang et al. 1999). Consequently, such systems will result in significant effects to these non-cancerous tissues when administered systemically *in vivo*. Other systems have been designed to target the Luteinizing Hormone-Releasing Hormone (LHRH) receptors (Arencibia, Schally et al. 2001; Dharap, Qiu et al. 2003; Dharap, Wang et al. 2005) but run into the same type of limitations as folate targeting.

As mentioned in Chapter 1, the system developed in the present project was designed to actively target the follicle stimulating hormone (FSH) receptors for the treatment of ovarian cancer by taking advantage of their exquisite ovarian-specific expression profile.

2.1.4 Multi-Drug Resistance and Drug Delivery Systems

Many types of tumor cells have developed resistance to treatment with commonly-used chemotherapeutic agents with unrelated structures, including doxorubicin. This multi-drug resistance is associated with the overexpression of transmembrane ATP-binding transporters such as the P-glycoprotein (Pgp) and multidrug resistance-related proteins (Yoo and Park 2004). These transport proteins are able to excrete drugs that have diffused into the plasma membrane.

Drug delivery systems promise to increase therapeutic efficacy of chemotherapeutic agents by delivering the drugs intracellularly to the cytoplasm or endosomal compartments, thus avoiding recognition and excretion by these transporters in the plasma membrane (Torchilin 2002). For example, folate-decorated doxorubicin loaded nano-aggregates were found to be more effective than the free drug *in vitro* and *in vivo* with human squamous carcinoma KB cells which are known to present severe multi-drug resistance (Wong, Rauth et al. 2006). Solid lipid nanoparticles with doxorubicin were seen to be eight times more effective than the free drug in multidrug resistant breast cancer cells MDA435/LCC6/WT (Lee, Na et al. 2005). Doxorubicin-loaded pH sensitive nanoparticles made from blends of poly(L-histidine)-poly(ethylene glycol)-folate and poly(lactic acid)-PEG-folate resulted in 90% cytotoxicity of doxorubicin-resistant MCF-7 cells and significantly improved *in vivo* therapeutic effect in a MCF-7 mice xenograft model (Lu, Zheng et al. 2000). In all three examples, increased therapeutic effect was attributed to bypass of Pgp efflux pump and consequent high drug concentrations intracellularly.

As part of the present research project, we investigated the therapeutic efficacy of targeted nanoparticles targeted to the follicle stimulating hormone receptor in multi-drug resistant ovarian cancer cells, as discussed in Chapter 7.

2.2 CONTRAST AGENTS IN MOLECULAR AND CLINICAL IMAGING

Clinical imaging is an important aspect of cancer detection and therapeutic monitoring. Depending on the imaging modality, imaging tests can show the location and some of the properties of a mass in the body. Ultrasound, for example, can be used to determine whether a mass is solid or fluid. Computer Tomography (CT) scans can give information about mass location and size. Magnetic Resonance Imaging (MRI) produces images from variables that are determined by the chemical characteristics of tissue, and consequently provides detailed anatomical information. Nuclear imaging, which includes Positron Emission Tomography (PET) and Single Photon Emission Computed Tomography (SPECT), can provide molecular information because it utilizes radioactively-labeled materials that specifically accumulate at sites of disease. However, this imaging modality provides images of considerable low resolution (5 to 7 mm) when compared to CT and MRI images (~ 1mm). Despite the valuable information that all of these imaging modalities provide in the clinical setting, to date only invasive biopsies are able to reliably reveal whether a growth is cancerous.

Contrast agents have been extensively used in clinical settings to provide enhanced specificity and contrast for imaging with the above-mentioned imaging systems. In MRI specifically, various negative and positive contrast agents, which result in dark and bright images respectively, are clinically used and many more are being researched. Example of novel negative MRI contrast agents are superparamagnetic iron oxide nanoparticles (Chertok, Moffat et al. 2007; Kumar, Leuschner et al. 2007; Liu, Dahnke et al. 2007; Morello, Burrill et al. 2007). Positive contrast agents are commonly small molecular weight compounds with unpaired electron spins in their outer shells, such as compounds of the paramagnetic metal ion gadolinium, manganese or iron

(D'Arceuil, de Crespigny et al. 2004; Lee and Koretsky 2004; Lee, Silva et al. 2005; Silva, Lee et al. 2007). Commercially available gadolinium-based positive contrast agents include Magnevist® (Schering, Germany), Gadovist® (Schering, Germany), and Optimark® (Mallinkrodt, USA). The active agent in Magnevist®, which was the first MRI contrast agent approved for clinical use, is gadopentetic acid (Gd-DTPA), a chelate complex of the gadolinium ion. Magnevist® distributes in the intravascular and extracellular fluid spaces, does not cross the blood brain barrier, and is excreted rapidly by glomerular filtration via the kidneys. Contrast agents are also being developed for use in molecular imaging, including its application in targeted drug delivery (Lanza, Winter et al. 2004).

Encapsulation of contrast agents within drug delivery systems, such as the targeted nanoparticles here developed, will change their biodistribution and pharmacokinetics according to those of the carrier. Nanoparticles loaded with imaging agents could be used for *in vivo* detection and monitoring of tumors, as well as for monitoring the retention, biodistribution, and tumor uptake of the nanocarriers. In addition, because of the increased circulation time and the narrow spatial localization offered by the targeted nanoparticles, it is expected that they could provide a significant increase in tumor-specific image contrast *in vivo*.

2.3 OVARIAN CANCER

Ovarian tissue contains three main types of cells: germ cells, stromal cells, and epithelial cells. Germ cells are responsible for the production of oocytes (eggs). Stromal cells surround the germ cells and produce most of the female hormones (estrogen and progesterone). Epithelial cells line the ovary. Ovarian tumors are classified according to the type of cell in which they originate. Germ cell tumors account for less than 5% of

ovarian tumor cases, and usually occur in young women (American Cancer Society 2005). Since up to 70% of patients with germ cell tumors are diagnosed during the first stage of the disease, the outcomes are generally positive. There are two types of germ cell tumors: dysgerminomonas, the most common, and nondysgerminomatous.

Stromal tumors normally develop in post-menopausal women and also account for about 5% of all ovarian cancers (American Cancer Society 2005). These tumors are formed from the cells of the sex cord or early connective tissue, and commonly include granulosa cells, Sertoli cells, thecal cells, and fibroblasts. Granulosa cell tumors are the most prevalent of the stromal tumors, and are commonly accompanied by elevated levels of the tumor marker *inhibin* in the circulation. Inhibin is responsible for the inhibition of follicle stimulating hormone (FSH) secretion.

Cancers originating in the epithelial lining of the ovaries account for 90% of ovarian cancers (Nitta, Katabuchi et al. 2001). Epithelial tumors can be further classified into serous, endometroid, mucinous, and clear cells tumors. Ovarian epithelial cells are involved in secretion of lysosomal enzymes to digest the follicular stroma during ovulation and are degraded during this process. The rapid rate of epithelial cell proliferation during healing after ovulation has been suggested to be a possible source of mutagenic potential (Lu, Zheng et al. 2000).

Numerous factors have been associated with the risk for ovarian cancer. Elevated levels of the pituitary gonadotropins luteinizing hormone and follicle stimulating hormone, such as in postmenopausal women or women treated for infertility, have been connected with a higher risk for ovarian cancer (Dias, Lindau-Shepard et al. 1998; Choi, Choi et al. 2004). In contrast, reduced gonadotropin levels, such as in women who have had multiple pregnancies, are breast feeding, use oral contraceptives, or are receiving

estrogen replacement therapy, are associated with a reduced risk (Dias, Lindau-Shepard et al. 1998; Lu, Zheng et al. 2000; Nitta, Katabuchi et al. 2001).

Early detection of tumors in general is usually regarded as the best method for increased patient survival because it improves the chances of successful treatment. In fact, the 5-year survival rate for patients diagnosed during stage I of ovarian cancer is more than 90%, compared to 30-60% and 20% for stages III and IV, respectively (American Cancer Society 2005). However, less than 20% of cases are discovered at an early stage because of the non-specific symptoms and poor detection methods. The symptoms associated with ovarian tumors usually include abdominal fluid buildup, unusual vaginal bleeding, pelvic pressure, back or leg pain, and digestive symptoms such as gas, bloating and indigestion. These symptoms, unfortunately, are often caused by conditions other than cancer and commonly delay identification of the tumor until it has spread beyond the ovaries.

Regular gynecological exams commonly fail to identify ovarian tumors because the ovaries are internal organs that are difficult to palpate. Although a number of screening tests are available, these were found not to lower the number of deaths caused by ovarian cancer in studies, and, consequently, are only performed on women with known high risk of developing ovarian tumors. Screening tests for epithelial ovarian cancer include transvaginal sonography for ultrasound-based detection of masses – whether cancerous or not–, and blood tests for quantifying levels of cancer antigen CA-125 which have been correlated with ovarian cancer (Jacobs and Bast 1989). The CA-125 test is very non-specific because a number of other gynecological conditions in addition to hepatitis, pancreatitis, cirrhosis, and other cancers may result in elevated levels of this marker. There are no tests available for screening for germ cell or stromal tumors.

Treatment options for ovarian cancer patients include surgery, chemotherapy, and radiation therapy. In all cases, the extent of treatment depends on the type of cancer, the stage of the disease, the patient's overall state of health, and personal considerations. In most cases, however, a combination of surgical and chemotherapeutic treatments is utilized. Surgical options include uni- or bilateral oophorectomy, salpingectomy, and/or hysterectomy, corresponding to the removal of the ovaries, fallopian tubes and uterus, respectively. Cytoreduction or debulking of the tumor is also performed in order to improve the patient's prognosis. For stages III and IV the recommended surgical treatment includes removal of the uterus, both fallopian tubes, both ovaries, and omentum (fatty tissue from upper abdomen), in addition to tumor cytoreduction. Such treatment completely eliminates the possibility of the patient ever becoming pregnant. After surgery, combination chemotherapy is most commonly used, as will be described in the following section.

Progress in the development of better treatments for ovarian cancer has been slow because of numerous factors. There are no acceptable animal models that develop ovarian epithelial cancers (Choi, Choi et al. 2004). Existing models are frequently deemed not relevant as this disease almost never occurs in non-primate animals (Nitta, Katabuchi et al. 2001). Little information has been gathered regarding the formation and progression of human epithelial ovarian cancer as a result of late diagnosis and consequent lack of human tissue at the early stages of the disease (Nitta, Katabuchi et al. 2001). Also, even though ovarian surface epithelial cells have been cultured and characterized, their growth is not adequate for in vitro investigations (Nitta, Katabuchi et al. 2001). A recent achievement has been the immortalization of normal ovarian epithelial cells for research purposes (Nitta, Katabuchi et al. 2001). In addition, xenograft models of human ovarian cancer have been reported to result in the formation

of intraperitoneal carcinomatosis and metastasis in similarity to human tumors which suggest that these models may provide valuable information for future studies (Nitta, Katabuchi et al. 2001).

2.3.1 Chemotherapeutic Treatment of Ovarian Cancer

Combination chemotherapy is the standard therapeutic approach for the treatment of epithelial cancerous tumors. As first-line therapy, a taxane such as paclitaxel in combination with a platinum compound such as cisplatin is indicated. Recurrent epithelial tumors are treated with either additional cycles of the above chemotherapeutic combination, or with agents such as topotecan, doxorubicin, liposomal doxorubicin (Doxil®), cyclophosphamide, vinorelbine (Navelbine®), hexamethylmelamine, ifosfamide, etoposide, or topotecan with fluorouracil (American Cancer Society 2005). There are no standard chemotherapy treatments for recurrent stromal cancer, but some of the antineoplastic agents used are vincristine, cisplatin, doxorubicin, and cyclophosphamide (American Cancer Society 2005). Doxorubicin was utilized in for the preparation of therapeutic targeted nanoparticles in this research project.

2.4 FOLLICLE STIMULATING HORMONE AND RECEPTOR

The follicle stimulating hormone (FSH) is one of the two glycoprotein hormones secreted by the pituitary gland, commonly referred to as gonadotropin hormones, that regulate the function of the gonads (testes and ovaries) (Dias, Lindau-Shepard et al. 1998). The other gonadotropin hormone is the luteinizing hormone (LH). FHS is essential for female fertility as it is key for the formation and development of follicles, but not for male fertility (Vannier, Loosfelt et al. 1996; Lindau-Shepard, Brumberg et al.

2001; Choi, Choi et al. 2004). FSH acts through receptors on granulosa cells in females and on Sertoli cells in males (Vannier, Loosfelt et al. 1996). Structurally, it is composed of two subunits (α and β) and two glycosilation sites on each unit (Dias, Lindau-Shepard et al. 1998).

The follicle stimulating hormone receptor (FSHR) is a transmembrane protein from the family of G protein-coupled signaling surface receptors (Lu, Zheng et al. 2000). Its transmembrane domain its composed of seven α-helices (Vannier, Loosfelt et al. 1996; Lindau-Shepard, Brumberg et al. 2001). The size of FSHR is of 74 kDa as determined by Western Blot using a monoclonal antibody against the receptor (Vannier, Loosfelt et al. 1996). The protein consists of 695 amino acids (Lindau-Shepard, Brumberg et al. 2001). Specifically, it has been determined that the extracellular domain comprises approximately 346 amino acids (residues 18–364) and contains the N-terminus of the protein, the transmembrane domain contains 264 amino acids (residues 365-629), the intracellular region consists of 65 amino acids (residues 630-695) and contains the C-terminal end of the protein, and the signal peptide consists of amino acids 1-17 (Vannier, Loosfelt et al. 1996; Lindau-Shepard, Brumberg et al. 2001).

The extracellular region has a leucine-rich repeat segment located within amino acid residues 200-500 (Jiang, Dreano et al. 1995). Such leucine-rich repeats are believed to be involved in protein-protein interaction and, consequently, to home the binding site for FSH. Further studies have shown that the binding site is in close proximity to amino acid residues 300-315 (Lindau-Shepard, Brumberg et al. 2001). Binding of FSH to FSHR results in a conformational change that activates a signaling pathway through the intracellular G-protein. This pathway consists of activation of adenylyl cyclase (cAMP) followed by indirect activation of mitogen activated protein (MAP) kinases (Vannier, Loosfelt et al. 1996).

2.4.1 Expression and Function of FSHR in Ovarian Cancer

In this project, the possibility of using the FSH receptor for ovarian-specific delivery of anti-tumor agents loaded in biodegradable nanoparticles was investigated. FSH receptors have one of the most restricted cell distribution patterns, being expressed only in the ovaries and testis (Richards and Midgley 1976; Kangasniemi, Kaipia et al. 1990; Simoni, Gromoll et al. 1997; Meduri, Charnaux et al. 2002). Expression levels of FSHR on ovarian cells *in vitro* and *in vivo* both in healthy and diseased conditions have been studied in numerous reports. Studies have identified high affinity binding sites for FSH on samples of human serous and mucinous cystoadenomas of epithelial origin and on samples of theca/theca-granulosa cell tumors (Nakano, Kitayama et al. 1989). Additionally, FSH receptors have been identified on many ovarian cancer cell lines (Parrott, Doraiswamy et al. 2001; Syed, Ulinski et al. 2001). In one study, expression of FSHR was detected in 100% of ovarian epithelial inclusions, 100% of cystoadenomas, 94% of borderline tumors and 60% of carcinomas (Zheng, Lu et al. 2000). Increasing levels of FSHR expression were observed with increased malignancy level from precursor lesions to ovarian inclusions, benign ovarian epithelial tumors and borderline ovarian epithelial tumors, in that order (Wang, Lin et al. 2003). However, the same group also observed that FSHR expression decreased as the level of malignancy increased from borderline ovarian epithelial tumors to ovarian carcinomas (Wang, Lin et al. 2003).

Because of varying expression of FSHR in tumors with malignancy stage, a role of FSH and FSHR on the development of the tumor has been suggested. The effect of FSH exposure and FSHR expression on the presentation of oncogenes has been investigated previously *in vitro*. After transfection of immortalized ovarian surface epithelial cells IOSE-80 with an FSHR overexpression vector, overexpression of

epidermal growth factor receptor (EGFR), c-myc and HER-2/neu oncogenes but not of K-Ras oncogene were observed (Choi, Choi et al. 2004). This study also found that overexpression of FSHR resulted in increased phosphorilzation of ERK1/2 but not of p38 or pJNK (Choi, Choi et al. 2004). A separate study reported that exposure of normal ovarian cells, immortalized ovarian surface epithelial cells and some ovarian cancer cells to FSH results in increased growth in a dose and time-dependent manner (Parrott, Doraiswamy et al. 2001; Syed, Ulinski et al. 2001). These results suggest that FSHR expression may be associated with an increased oncogene activation and proliferation in preneoplastic and ovarian cancer cells.

Despite the fact that the role of FSHR in tumor development is not completely clear to date, the fact that the expression of this receptor is limited to ovarian tissue offers a possibility for enhancing the specificity of delivery of therapeutic nanoparticles to ovarian cancer.

Table 2.1 Targeted drug delivery systems reported in the literature. Abbreviations: 5-fluorodeoxyiridine (5-FU), epidermal growth factor (EGF), epidermal growth factor receptor (EGFR), poly(ethylene glycol) (PEG).

Targeted Epitope	Targeting Agent	Drug Delivery System	Reference
EGFR	Fragment of humanized anti- EGFR monoclonal antibody Matuzumab	Liposomes with Doxorubicin	(Mamot, Ritschard et al. 2006)
	EGF	Micelles of methoxy PEG-b-poly(delta valerolactone) with ellipticine or EGF as an apoptotic factor	(Zeng, Lee et al. 2006; Lee, Hu et al. 2007)
	Antibody C225	Prodrug of poly(L-glutamic acid)-co-PEG-doxorubicin	(Vega J 2003)
	EGF and EGF receptor-binding fragment	Doxorubicin-antibody conjugate	(Lutsenko SV 2002)
Folate Receptors	Folic acid	Poly(amidoamine) dendrimers loaded with paclitaxel	(Majoros, Myc et al. 2006)
		Temperature sensitive micelles with doxorubicin	(Liu SQ 2007)
		Poly(lactide-co-glycolide)-PEG micelles with doxorubicin	(Yoo and Park 2004)
		Nano-aggregates of doxorubicin-PEG-folic acid conjugate	(Yoo and Park 2004)
		Micelles of PEG-poly(ε-caprolactone) loaded with paclitaxel	(Park, Kim et al. 2005; Park, Lee et al. 2005)
		Micelles of PEG-poly(ε-caprolactone) loaded with multi-drug resistance modulator FG02326	(Yang, Deng et al. 2007)
		Paclitaxel-folic acid prodrug	(Lee, Lu et al. 2002)

Targeted Epitope	Targeting Agent	Drug Delivery System	References
Transferrin receptors	Transferrin	Liposomes with doxorubicin or verapamil	(Wu J 2007)
		Cyclodextrin polyplexes stabilized with adamante-PEG loaded with DNAzyme (RNA-cleaving enzyme)	(Pun SH 2004)
Hyaluronan receptors	Hyaluronan	N-(2-hydroxypropyl) methacrylamide-doxorubicin prodrug	(Luo Y 2002)
CD166 (Prostate Cancer)	Single chain variable fragment Anti-CD166 antibody	Liposomes with topotecan, vinorelbine or doxorubicin	(Roth, Drummond et al. 2007)
Prostate Specific Antigen	Anti-prostate specific antigen peptide	5-FU-targeting peptide prodrug	(Mhaka, Denmeade et al. 2002)
Hsp47/CBP2 receptor (Squamous carcinoma of head & neck)	Hsp47/CBP2 binding peptide	N-(2-hydroxypropyl)-methacrylamide-doxorubicin prodrug	(Nan, Ghandehari et al. 2005)

Table 2.2 Targeted drug delivery systems based on polymeric nanoparticles for cancer treatment

Cancer Type	Targeted Epitope	Targeting Agent	Nanoparticle Description	References
Breast Cancer	HER2	Trastuzumab (anti-HER2 human epidermal growth factor receptor)	Poly(d,l-lactide-co-glycolide)-montmorillonite NPs with Paclitaxel	(Sun B 2007)
Prostate Cancer	Prostate Specific Antigen	A10 RNA aptamer to the prostate specific membrane antigen	Poly(lactic acid)-poly(ethylene glycol) NPs with Paclitaxel	(Farokhzad, Jon et al. 2004; Farokhzad, Cheng et al. 2006; Farokhzad, Karp et al. 2006; Cheng, Teply et al. 2007)
General Cancers	Transferrin Receptors	Tranferrin	Poly(lactic-co-glycolic acid) NPs with Paclitaxel	(Sahoo, Wenxue et al. 2004; Sahoo and Labhasetwar 2005)
Liver Cancer	Galactosamine	Asialoglycoprotein receptors	poly(gamma-glutamic acid)-poly(lactide) NPs with Paclitaxel	(Liang, Chen et al. 2006)
Melanoma, hepatocellular carcinoma and breast cancer	SM5-1 binding protein	Polylysine modified SM5-1 single chain antibody	Poly(lactic-co-glycolic acid) NPs with Paclitaxel	(Kou G 2007)

2.5 REFERENCES

Abdelwahed, W., G. Degobert, et al. (2006). "Freeze-drying of nanoparticles: Formulation, process and storage considerations." Advanced Drug Delivery Reviews 58(15): 1688-1713.

American Cancer Society (2005). Cancer Facts & Figures 2005. Atlanta, GA, American Cancer Society.

Arencibia, J. M., A. V. Schally, et al. (2001). "In vitro targeting of a cytotoxic analog of luteinizing hormone-releasing hormone AN-207 to ES-2 human ovarian cancer cells as demonstrated by microsatellite analyses." Anticancer Drugs 12(1): 71-8.

Astete, C. E. and C. M. Sabliov (2006). "Synthesis and characterization of PLGA nanoparticles." Journal of Biomaterials Science Polymer Edition 17(3): 247-289.

Betancourt, T. and L. Brannon-Peppas (2006). "Micro- and nanofabrication methods in nanotechnological medical and pharmaceutical devices." International Journal of Nanomedicine 1(4): 483-495.

Betancourt, T., B. Brown, et al. (2007). "Doxorubicin-loaded PLGA nanoparticles by nanoprecipitation: preparation, characterization and in vitro evaluation." Nanomedicine 2(2): 219-232.

Birnbaum, D. T., J. D. Kosmala, et al. (2000). "Optimization of preparation techniques for poly(lactic acid-co-glycolic acid) nanoparticles." Journal of Nanoparticle Research 2(2): 173-181.

Blanchette, J. and N. A. Peppas (2005). "Oral chemotherapeutic delivery: design and cellular response." Ann Biomed Eng 33(2): 142-9.

Blanco, D. and M. J. Alonso (1998). "Protein encapsulation and release from poly(lactide-co-glycolide) microspheres: effect of the protein and polymer properties and of the co-encapsulation of surfactants." Eur J Pharm Biopharm 45(3): 285-294.

Brannon-Peppas, L. (1995). "Recent advances on the use of biodegradable microparticles and nanoparticles in controlled drug delivery." Int J Pharm. 116(1): 1-9.

Brannon-Peppas, L. (1997). "Polymers in Controlled Drug Delivery." Medical Plastics and Biomaterials Magazine 4: 34-44.

Brannon-Peppas, L. and D. T. Birnbaum (2000). Process to Scale-Up the Production of Biodegradable Nanoparticles. American Institute of Chemical Engineers Annual Meeting, Los Angeles, CA.

Brannon-Peppas, L. and J. O. Blanchette (2004). "Nanoparticle and targeted systems for cancer therapy." Advanced Drug Delivery Reviews 56(11): 1649-1659.

Cheng, J., B. A. Teply, et al. (2007). "Formulation of functionalized PLGA-PEG nanoparticles for in vivo targeted drug delivery." Biomaterials 28(5): 869-76.

Chertok, B., B. A. Moffat, et al. (2007). "Iron oxide nanoparticles as a drug delivery vehicle for MRI monitored magnetic targeting of brain tumors." Biomaterials.

Choi, J.-H., K.-C. Choi, et al. (2004). "Overexpression of Follicle-Stimulating Hormone Receptor Activates Oncogenic Pathways in Preneoplastic Ovarian Surface Epithelial Cells." The Journal of Clinical Endocrinology & Metabolism 89(11): 5508-5516.

Conner, S. D. and S. L. Schmid (2003). "Regulated portals of entry into the cell." Nature 422(6927): 37-44.

Couvreur, P., C. Dubernet, et al. (1995). "Controlled Drug Delivery with Nanoparticles: Current Possibilities and Future Trends." European Journal of Pharmaceutics and Biopharmaceutics 41(1): 2-13.

D'Arceuil, H. E., A. J. de Crespigny, et al. (2004). "An MRA study of vascular stenosis in a pig model using CH3-DTPA-Gd (NMS60) and Gd-DTPA." Magn Reson Imaging 22(9): 1243-8.

Dechy-Cabaret, O., B. Martin-Vaca, et al. (2004). "Controlled Ring-Opening Polymerization of Lactide and Glycolide." Chemical Reviews 104(12): 6147-6176.

Desai, K. G., S. R. Mallery, et al. (2007). "Formulation and Characterization of Injectable Poly(DL: -lactide-co-glycolide) Implants Loaded with N-Acetylcysteine, a MMP Inhibitor." Pharm Res.

Dharap, S. S., B. Qiu, et al. (2003). "Molecular targeting of drug delivery systems to ovarian cancer by BH3 and LHRH peptides." Journal of Controlled Release 91(1-2): 61-73.

Dharap, S. S., Y. Wang, et al. (2005). "Tumor-specific targeting of an anticancer drug delivery system by LHRH peptide." Proc Natl Acad Sci U S A 102(36): 12962-7.

Dias, J. A., B. Lindau-Shepard, et al. (1998). "Human Follicle-Stimulating Hormone Structure-Activity Relationships." Biology of Reproduction 58: 1331-1336.

Fahmy, T. M., R. M. Samstein, et al. (2005). "Surface modification of biodegradable polyesters with fatty acid conjugates for improved drug targeting." Biomaterials 26.

Farokhzad, O. C., J. Cheng, et al. (2006). "Targeted nanoparticle-aptamer bioconjugates for cancer chemotherapy in vivo." Proc Natl Acad Sci U S A 103(16): 6315-20.

Farokhzad, O. C., S. Jon, et al. (2004). "Nanoparticle-aptamer bioconjugates: a new approach for targeting prostate cancer cells." Cancer Res 64(21): 7668-72.

Farokhzad, O. C., J. M. Karp, et al. (2006). "Nanoparticle-aptamer bioconjugates for cancer targeting." Expert Opin Drug Deliv 3(3): 311-24.

Fattal, E., S. Pecquet, et al. (2002). "Biodegradable microparticles for the mucosal delivery of antibacterial and dietary antigens." Int J Pharm. 242(1-2): 15-24.

Fawaz, F., F. Bonini, et al. (1993). "Influence of poly(DL-lactide) on the biliary clearance and enterohepatic circulation of indomethacin in the rabbit." Pharmaceutical Research 10(5): 750-756.

Feng, S. S., L. Mu, et al. (2004). "Nanoparticles of biodegradable polymer for clinical administration of paclitaxel." Current Medicinal Chemistry 11(4): 413-424.

Folkman, J. (2003). "Fundamental Concepts of the Angiogenic Process." Current Molecular Medicine 3(7): 6423-651.

Folkman, J., E. Merler, et al. (1971). "Isolation of a Tumor Factor Responsible for Angiogenesis." The Journal of Experimental Medicine 133(2): 275-288.

Freitas, S., H. P. Merkle, et al. (2005). "Microencapsulation by solvent extraction/evaporation: reviewing the state of art of microsphere preparation process technology." Journal of Controlled Release 102(2): 313-332.

Friess, W. (2004). Biopolymers for Parenteral Drug Delivery in Cancer Therapy. Drug Delivery Systems in Cancer Therapy. D. M. Brown. Totowa, New Jersey, Humana Press: 62-95.

Gao, X., Y. Cui, et al. (2004). "In vivo cancer targeting and imaging with semiconductor quantum dots." Nature Biotechnology 22(8): 969-971.

Graham, N. B. (1987). Poly(ethylene oxide) and related hydrogels. Hydrogels in Medicine and Pharmacy; Volume II Polymers. N. A. Peppas. Boca Raton, FL, CRC Press: 95-114.

Gref, R., A. Domb, et al. (1995). "The Controlled Intravenous Delivery of Drugs Using PEG-Coated Sterically Stabilized Nanospheres." Advanced Drug Delivery Reviews 16: 215-233.

Gref, R., M. Luck, et al. (2000). "'Stealth' corona-core nanoparticles surface modified by polyethylene glycol (PEG): influences of the corona (PEG chain length and surface density) and of the core composition on phagocytic uptake and plasma protein adsorption." Colloids Surf B Biointerfaces 18(3-4): 301-313.

Hu, R. G., Q. W. zhai, et al. (2002). "Bioactivities of ricin retained and its immunoreactivity to anti-ricin polyclonal antibodies alleviated through pegylation." International Journal of Biochemistry and Cell Biology 34(4): 396-402.

Huh, K. M., Y. W. Cho, et al. (2003). "PLGA-PEG Copolymers." Drug Delivery Technology 3(5)?

Huolman, R. and N. Ashammakhi (2007). "New multifunctional anti-osteolytic releasing bioabsorbable implant." J Craniofac Surg 18(2): 295-301.

Jacobs, I. and R. C. Bast (1989). "The CA 125 tumor-associated antigen: a review of the literature." Human Reproduction 4(1): 1-12.

Jain, R. A. (2000). "The manufacturing techniques of various drug loaded biodegradable poly(lactide-co-glycolide) (PLGA) devices." Biomaterials 21(23): 2475-2490.

Janes, K. A., P. Calvo, et al. (2001). "Polysaccharide colloidal particles as delivery systems for macromolecules." Adv Drug Deliv Rev 47(1): 83-97.

Janes, K. A., M. P. Fresneau, et al. (2001). "Chitosan nanoparticles as delivery systems for doxorubicin." Journal of Controlled Release 73(2-3): 255-267.

Jiang, X., M. Dreano, et al. (1995). "Structural predictions for the ligand-binding region of glycoprotein hormone receptors and the nature of hormone-receptor interactions." Structure 3(12): 1341-53.

Kangasniemi, M., A. Kaipia, et al. (1990). "Cellular regulation of follicle-stimulating hormone (FSH) binding in rat seminiferous tubules." J Androl 11(4): 336-43.

Kasturi, S. P., K. Sachaphibulkij, et al. (2005). "Covalent conjugation of polyethyleneimine on biodegradable microparticles for delivery of plasmid DNA vaccines." Biomaterials 26(32): 6375-6385.

Kontakis, G. M., J. E. Pagkalos, et al. (2007). "Bioabsorbable materials in orthopaedics." Acta Orthop Belg 73(2): 159-69.

Kou G, G. J., Wang H, Chen H, Li B, Zhang D, Wang S, Hou S, Qian W, Dai J, Zhong Y, Guo Y (2007). "Preparation and Characterization of Paclitaxel-loaded PLGA nanoparticles coated with cationic SM5-1 single-chain antibody." Journal of Biochemistry and Molecular Biology 40(5): 731-739.

Kukowska-Latallo, J. F., K. A. Candido, et al. (2005). "Nanoparticle Targeting of Anticancer Drug Improves Therapeutic Response in Animal Model of Human Epithelial Cancer." Cancer Research 65(12): 5317-5324.

Kumar, C. S., C. Leuschner, et al. (2007). "Glutaric acid as a spacer facilitates improved intracellular uptake of LHRH-SPION into human breast cancer cells." Int J Nanomedicine 2(2): 175-9.

Lanza, G. M., P. Winter, et al. (2004). "Novel paramagnetic contrast agents for molecular imaging and targeted drug delivery." Curr Pharm Biotechnol 5(6): 495-507.

Lee, E. S., K. Na, et al. (2005). "Doxorubicin loaded pH-sensitive polymeric micelles for reversal of resistant MCF-7 tumpr." Journal of Controlled Release 103: 405-418.

Lee, H. S., M. Hu, et al. (2007). "Apoptotic epidermal growth factor (EGF)-conjugated block copolymer micelles as a nanotechnology platform for targeted combination therapy." Molecular Pharmaceutics 4(5): 769-781.

Lee, J. H. and A. P. Koretsky (2004). "Manganese enhanced magnetic resonance imaging." Curr Pharm Biotechnol 5(6): 529-37.

Lee, J. H., A. C. Silva, et al. (2005). "Manganese-enhanced magnetic resonance imaging of mouse brain after systemic administration of MnCl2: dose-dependent and temporal evolution of T1 contrast." Magn Reson Med 53(3): 640-8.

Lee, J. W., J. Y. Lu, et al. (2002). "Synthesis and evaluation of taxol-folic acid conjugates as targeted antineoplastics." Bioorg Med Chem 10(7): 2397-414.

Lewis, D. H. (1990). Controlled Release of Bioactive Agents from Lactide/Glycolide Polymers. Biodegradable Polymers as Drug Delivery Systems. M. Chasin and R. Langer. New York, Marcerl Dekker: 1-41.

Liang, H.-F., C.-T. Chen, et al. (2006). "Paclitaxel-loaded poly(γ-glutamic acid)-poly(lactide) nanoparticles as a targeted drug delivery system for the treatment of liver cancer." Biomaterials 27(9): 2051-2059.

Lin, R., L. S. Ng, et al. (2005). "In vitro study of anticancer drug doxorubicin in PLGA-based microparticles." Biomaterials 26: 4476-4485.

Lindau-Shepard, B., H. A. Brumberg, et al. (2001). "Reversible immunoneutralization of human follitropin receptor." Journal of Reproductive Immunology 49: 1-19.

Liu, S. Q., Y. W. Tong, et al. (2005). "Incorporation and in vitro release of doxorubicin in thermally sensitive micelles made from poly(N-isopropylacrylamine-co-N,N-dimethylacrylamide)-b-poly(D,L-lactide-co-glycolide) with varying compositions." Biomaterials 26: 5064-5074.

Liu SQ, W. N., Gao SJ, Tong YW, Yang YY (2007). "Bio-functional micelles self-assembled from a folate-conjugated block copolymer for targeted intracellular delivery of anticancer drugs." Biomaterials 28(7): 1423-1433.

Liu, W., H. Dahnke, et al. (2007). "In vivo MRI using positive-contrast techniques in detection of cells labeled with superparamagnetic iron oxide nanoparticles." NMR Biomed.

Lu, J. J., Y. Zheng, et al. (2000). "Decreased Luteinizing Hormone Receptor mRNA Expression in Human Ovarian Epithelial Cancer." Gynecologic Oncology 79: 158-168.

Luo Y, B. N., Lu ZR, Kopecek J, Prestwich GD (2002). "Targeted delivery of doxorubicin by HPMA copolymer-hyaluronan bioconjugates." Pharmaceutical Research 19(4): 396-402.

Lutsenko SV, F. N., Severin SE (2002). "Cytotoxic and antitumor activities of doxorubicin conjugates with the epidermal growth factor and its receptor-binding fragment." Journal of Drug Targeting 10(7): 567-571.

Majoros, I. J., A. Myc, et al. (2006). "PANAM dendrimer-based multifunctional conjugate for cancer therapy: synthesis, characterization, and functionality." Biomacromolecules 7(2): 572-579.

Mamot, C., R. Ritschard, et al. (2006). "EGFR-targeted immunoliposomes derived from the monoclonal antibody EMD72000 mediate specific and efficient drug delivery to a variety of colorectal cancer cells." Journal of Drug Targeting 14(4): 215-223.

McDonald, D. M. and P. Baluk (2002). "Significance of Blood Vessel Leakiness in Cancer." Cancer Research 62(18): 5381-5385.

Meduri, G., N. Charnaux, et al. (2002). "Follicle-stimulating hormone receptors in oocytes?" J Clin Endocrinol Metab 87(5): 2266-76.

Mehvar, R. (2000). "Modulation of the pharmacokinetics and pharmacodynamics of proteins by polyethylene glycol conjugation." Journal of Pharmacy and Pharmacetuical Sciences 3(1): 125-136.

Mhaka, A., S. R. Denmeade, et al. (2002). "A 5-fluorodeoxyuridine prodrug as targeted therapy for prostate cancer." Bioorganic & Medicinal Chemistry Letters 12(17): 2459-2461.

Morello, A. P., 3rd, R. Burrill, et al. (2007). "Preparation and characterization of poly(methyl methacrylate) - iron (III) oxide microparticles using a modified solvent evaporation method." J Microencapsul 24(5): 476-91.

Murillo, M., M. M. Goni, et al. (2002). "Modulation of the cellular immune response after oral or subcutaneous immunization with microparticles containing brucella ovis antigens." J Control Release. 85(1-3): 237-246.

Nakano, R., S. Kitayama, et al. (1989). "Localization of gonadotropin binding sites in human ovarian neoplasms." Am J Obstet Gynecol 161(4): 905-10.

Nakaoka, R., Y. Tabata, et al. (1997). "Prolongation of the serum half-life period of superoxide dismutase by poly(ethylene glycol) modification." Journal of Controlled Release 46(3): 253-261.

Nan, A., H. Ghandehari, et al. (2005). "Water-soluble polymers for targeted drug delivery to human squamous carcinoma of head and neck." Journal of Drug Targeting 13(3): 189-197.

Nasongkla, N., E. Bey, et al. (2006). "Multifunctional Polymeric Micelles as Cancer-Targed, MRI-Ultrasensitive Drug Delivery Systems." Nano Letters 6(11): 2427-2430.

Nitta, M., H. Katabuchi, et al. (2001). "Characterization and Tumorigenecity of Human Ovarian Surface Epithelial Cells Immortalized by SV40 Large T Antigen." Gynecologic Oncology 81: 10-17.

Otsuka, H., Y. Nagasaki, et al. (2003). "PEGylated nanoaprticles for biological and pharmaceutical applications." Advanced Drug Delivery Reviews 55(3): 403-419.

Panyam, J. and V. Labhasetwar (2003). "Biodegradable nanoparticles for drug and gene delivery to cells and tissue." Advanced Drug Delivery Reviews 55(3): 329-347.

Park, E. K., S. Y. Kim, et al. (2005). "Folate-conjugated methoxy poly(ethylene glycol)/poly(epsilon-caprolactone) amphiphilic block copolymeric micelles for tumor-targeted drug delivery." J Control Release 109(1-3): 158-68.

Park, E. K., S. B. Lee, et al. (2005). "Preparation and characterization of methoxy poly(ethylene glycol)/poly(epsilon-caprolactone) amphiphilic block copolymeric nanospheres for tumor-specific folate-mediated targeting of anticancer drugs." Biomaterials 26(9): 1053-61.

Park, S. N., H. J. Jang, et al. (2007). "Preparation and characterization of biodegradable anti-adhesive membrane for peritoneal wound healing." J Mater Sci Mater Med 18(3): 475-82.

Parrott, J. A., V. Doraiswamy, et al. (2001). "Expression and actions of both the follicle stimulating hormone receptor and the luteinizing hormone receptor in normal ovarian surface epithelium and ovarian cancer." Mol Cell Endocrinol 172(1-2): 213-22.

Peppas, N. A. (2006). "Intelligent Biomaterials as Pharmaceutical Carriers in Microfabricated and Nanoscale Devices." MRS Bulletin 31: 888-893.

Peppas, N. A., K. M. Wood, et al. (2004). "Hydrogels for oral delivery of therapeutic proteins." Expert Opin Biol Ther 4(6): 881-7.

Pun SH, T. F., Bellocq NC, Cheng J, Grubbs BH, Jensen GS, Davis ME, Brewster M, Janicot M, Janssens B, Floren W, Bakker A (2004). "Targeted delivery of RNA-cleaving DNA enzyme (DNAzyme) to tumor tissue by transferrin-modified, cyclodextrin-based particles." Cancer Biology & Therapy 3(7): 641-650.

Richards, J. S. and A. R. Midgley, Jr. (1976). "Protein hormone action: a key to understanding ovarian follicular and luteal cell development." Biol Reprod 14(1): 82-94.

Ross, J. F., H. Wang, et al. (1999). "Folate receptor type beta is a neutrophilic lineage marker and is differentially expressed in myeloid leukemia." Cancer 85(2): 348-57.

Roth, A., D. C. Drummond, et al. (2007). "Anti-CD166 single chain antibody-mediated intracellular delivery of liposomal drugs to prostate cancer cells." Molecular Cancer Therapeutics 6(10): 2737.

Sahoo, S. K. and V. Labhasetwar (2005). "Enhanced antiproliferative activity of transferrin-conjugated paclitaxel-loaded nanoparticles is mediated via sustained intracellular drug retention." Molecular Pharmaceutics 2(5): 373-383.

Sahoo, S. K., M. Wenxue, et al. (2004). "Efficacy of transferrin-conjugated paclitaxel-loaded nanoparticles in a murine model of prostate cancer." International Journal of Cancer 112(2): 335-340.

Sawant, R. M., J. P. Hurley, et al. (2006). ""SMART" drug delivery systems: double-targeted pH-responsive pharmaceutical nanocarriers." Bioconjug Chem 17(4): 943-9.

Schiffelers, R. M., G. A. Koning, et al. (2003). "Anti-tumor efficacy of tumor vasculature-targeted liposomal doxorubicin." Journal of Controlled Release 91: 115-122.

Shen, F., J. F. Ross, et al. (1994). "Identification of a novel folate receptor, a truncated receptor, and receptor type beta in hematopoietic cells: cDNA cloning,

expression, immunoreactivity, and tissue specificity." Biochemistry 33(5): 1209-15.

Shive, M. S. and J. M. Anderson (1997). "Biodegradation and biocompatibility of PLA and PLGA microspheres." Advanced Drug Delivery Reviews 28(1): 5-24.

Silva, A. C., J. H. Lee, et al. (2007). "Detection of cortical laminar architecture using manganese-enhanced MRI." J Neurosci Methods.

Simoni, M., J. Gromoll, et al. (1997). "The follicle-stimulating hormone receptor: biochemistry, molecular biology, physiology, and pathophysiology." Endocr Rev 18(6): 739-73.

Stayton, P. S., M. E. El-Sayed, et al. (2005). "'Smart' delivery systems for biomolecular therapeutics." Orthod Craniofac Res 8(3): 219-25.

Stolnik, S., S. E. Dunn, et al. (1994). "Surface modification of poly(lactide-co-glycolide) nanospheres by biodegradable poly(lactide)-poly(ethylene glycol) copolymers." Pharm Res 11(12): 1800-8.

Sudimack, J. and R. J. Lee (2000). "Targeted drug delivery via the folate receptor." Adv Drug Deliv Rev 41(2): 147-62.

Sun B, R. B., Feng SS (2007). "Multifunctional poly(d,l-lactide-co-glycolide)/montmorillonite (PLGA/MMT) nanoparticles decorated by Trastuzumab for targeted chemotherapy of breast cancer." Biomaterials In Press.

Syed, V., G. Ulinski, et al. (2001). "Expression of gonadotropin receptor and growth responses to key reproductive hormones in normal and malignant human ovarian surface epithelial cells." Cancer Res 61(18): 6768-76.

Torchilin, V. P. (2002). Strategies and Means for Drug Targeting: An Overview. Biomedical Aspects of Drug Targeting. V. R. Muzykantov and V. P. Torchilin, Kluwer Academic Publishers: 3-26.

Torchilin, V. P., J. Narula, et al. (1996). "Poly(ethylene glycol)-coated anti-cardiac myosin immunoliposomes: factors influencing targeted accumulation in the infarcted myocardium." Biochimica Biophysica Acta 1279: 75-83.

Torres-Lugo, M., M. Garcia, et al. (2002). "pH-Sensitive hydrogels as gastrointestinal tract absorption enhancers: transport mechanisms of salmon calcitonin and other model molecules using the Caco-2 cell model." Biotechnol Prog 18(3): 612-6.

Turk, M. J., D. J. Waters, et al. (2004). "Folate-conjugated liposomes preferentially target macrophages associated with ovarian carcinoma." Cancer Lett 213(2): 165-72.

Vannier, B., H. Loosfelt, et al. (1996). "Anti-Human FSH Receptor Monoclonal Antibodies: Immunochemical and Immunocytochemical Characterization of the Receptor." Biochemistry 35: 1358-1366.

Vega J, K. S., Fan Z, Wallace S, Charsangavej C, Li C (2003). "Targeting doxorubicin to epidermal growth factor receptors by site-specific conjugation of C225 to poly(L-glutamic acid) through a polyethylene glycol spacer." Pharmaceutical Research 20(5): 826-832.

Veggian, R., S. Fasolato, et al. (1989). "Immunohistochemical reactivity of a monoclonal antibody prepared against human ovarian carcinoma on normal and pathological female genital tissues." Tumori 75(5): 510-3.

Venkatraman, S. S., P. Jie, et al. (2005). "Micelle-like nanoparticles of PLA-PEG-PLA triblock copolymer as chemotherapeutic carrier." Int J Pharm 298(1): 219-32.

Wang, J., L. Lin, et al. (2003). "Quantitative analysis of follicle-stimulating hormone receptor in ovarian epithelial tumors: a novel approach to explain the field of ovarian cancer development in secondary mullerian systems." International Journal of Cancer 103(3): 328-334.

Wei, J. S., H. B. Zeng, et al. (2005). "Temperature- and pH-sensitive core-shell nanoparticles self-assembled from poly(n-isopropylacrylamide-co-acrylic acid-co-cholesteryl acrylate) for intracellular delivery of anticancer drugs." Front Biosci 10: 3058-67.

Weitman, S. D., R. H. Lark, et al. (1992). "Distribution of the folate receptor GP38 in normal and malignant cell lines and tissues." Cancer Res 52(12): 3396-401.

Wong, H. L., A. M. Rauth, et al. (2006). "A New Polymer-Lipid Hybrid Nanoparticle System Increases Cytotoxicity of Doxorubicin Against Multidrug-Resistant Human Breast Cancer Cells." Pharmaceutical Research 23(7): 1574-1585.

Wu J, L. Y., Lee A, Pan X, Yang X, Zhao X, Lee RJ (2007). "Reversal of multidrug resistance by tranferrin-conjugated liposomes co-encapsulating doxorubicin and verapamil." Journal of Pharmacy and Pharmacetuical Sciences 10(3): 350-357.

Yang, X., W. Deng, et al. (2007). "Folate-functionalized polymeric micelles for tumor targeted delivery of a potent multidrug-resistance modulator FG020326." J Biomed Mater Res A.

Yokoyama, M. and T. Okano (1996). "Targetable Drug Carriers: Present Status and Future Perspectives." Advanced Drug Delivery Reviews 21(2): 77-80.

Yoo, H. S., J. E. Oh, et al. (1999). "Biodegradable Nanoparticles Containing Doxorubicin-PLGA Conjugate for Sustained Release." Pharmaceutical Research 16(7): 1114-1118.

Yoo, H. S. and T. G. Park (2001). "Biodegradable Polymeric Micelles Composed of Doxorubicin Conjugated PLGA-PEG Block Copolymer." Journal of Controlled Release 70(1-2): 63-70.

Yoo, H. S. and T. G. Park (2004). "Folate-receptor-targeted delivery of doxorubicin nano-aggregates stabilized by doxorubicin-PEG-folate conjugate." Journal of Controlled Release 100(2): 247--256.

Yoo, H. S. and T. G. Park (2004). "Folate receptor targeted biodegradable polymeric doxorubicin micelles." Journal of Controlled Release 96(2): 273-283.

Zeng, F., H. Lee, et al. (2006). "Epidermal growth factor-conjugated poly(ethylene glycol)-block- poly(delta-valerolactone) copolymer micelles for targeted delivery of chemotherapeutics." Bioconjugate Chemistry 17(2): 399-409.

Zheng, W., J. J. Lu, et al. (2000). "Ovarian epithelial tumor growth promotion by follicle-stimulating hormone and inhibition of the effect by luteinizing hormone." Gynecol Oncol 76(1): 80-8.

CHAPTER 3

FORMULATION, CHARACTERIZATION AND IN VITRO EVALUATION OF DOXORUBICIN LOADED NANOPARTICLES

3.1 INTRODUCTION

Chemotherapeutic agents commonly lead to the damage of healthy cells, especially those of the bone marrow, skin, and gastro-intestinal mucosa because they act on rapidly-proliferating cells by inhibiting DNA synthesis and interfering with the processes of cell division and metabolism (Twardowski and Margolin 2002). Engineered drug delivery systems for cancer treatment aim to increase the therapeutic efficacy of chemotherapeutic agents while minimizing their interaction with non-pathological sites in the body by modifying their biodistribution and controlling the rate at which the agent is released from the carrier to the systemic circulation or tissues. The design and consequent physiochemical properties of the drug carrier determine the results observed *in vivo*.

DOX (M.W. 580 g/mol), known under the trade name of Adriamycin® (Pharmacia & Upjohn, Kalamazoo, MI), is an anthracycline antibiotic that blocks DNA synthesis and transcription by intercalating between DNA nucleotides interacting specifically with guanine and cytosine, inhibits the action of Topoisomerase II, and generates damaging radicals from its metabolism (Blasiak, Gloc et al. 2002). DOX has been clinically used for the treatment of lymphoma, acute leukemia, soft tissue sarcoma, and breast, ovarian, testicular, lung, bladder, and gastric cancers (IARC 1976). DOX is usually administered intravenously at a maximum bolus dose of 60-90 mg/m^2 at 21-day intervals (IARC 1976). A maximum lifetime dose of 550 mg/m^2 is allowed because of known cumulative

cardiotoxicity associated with anthracycline treatment (Lum, Svec et al. 1985). In addition to cardiotoxicity, DOX is also known to cause severe myelosupression, which limits the aggressiveness and extent of treatment possible.

Development of drug delivery systems for the controlled delivery of DOX has been the focus of much research to date. In fact Doxil® (ALZA Corporation), a controlled release injectable formulation based on pegylated DOX-loaded liposomes, is approved by the FDA for the treatment of AIDS-related Kaposi's sarcoma and refractory ovarian cancer. This formulation efficiently targets tumors by taking advantage of the enhanced permeability and retention effect, and has shown to result in drastically different toxicity profiles than free DOX. Specifically, Doxil is known to cause dose-limiting toxicity to the skin and musosa, while significantly reduced myelosuppression, alopecia and cardiotoxicity (Gabizon 2001). DaunoXome® (Gilead Sciences Ltd.) is a similar liposomal formulation of the antineoplastic anthracycline antibiotic daunorobicin. DaunoXome is indicated for the treatment of advanced AIDS-related Kaposi's sarcoma. Another formulation of DOX that has proven efficacious in *in vitro* and *in vivo* animal studies for the treatment of chemoresistant hepatocellular carcinoma consists of DOX-loaded polyisohexylcyanoacrylate nanoparticles (Barraud, Merle et al. 2005) and is currently undergoing phase I/II clinical trials in Europe under the name of Transdrug® (Bioalliance Pharma, France).

DOX formulations based on the biodegradable polymers poly(lactic acid) or PLGA have also been reported in the literature. These formulations include DOX-loaded microparticles (Ike, Shimizu et al. 1991; Lin, Ng et al. 2005; Tan, Lin et al. 2005), PLGA NPs, PLGA-PEG micelles, and PLGA-vitamin E tocopheryl polyethylene glycol succinate NPs with DOX covalently conjugated to the PLGA polymer (Yoo, Oh et al. 1999; Yoo and Park 2001; Yoo and Park 2004; Zhang, Lee et al. 2007), pH sensitive

DOX-loaded micelles of poly(L-histidine)-PEG-folate and PLA-PEG-folate blends (Lee, Na et al. 2005), self-assembled NPs of PLGA-g-pullulan loaded with DOX (Jeong, Na et al. 2006), and multifunctional micelles of PLA-PEG loaded with superparamagnetic iron oxide NPs and DOX (Nasongkla, Bey et al. 2006), among others. Microparticle formulations have limited clinical potential because they must be locally administered or implanted. Formulations in which DOX is chemically conjugated to the drug carrier are often problematic because modification of the drug may lead to changes in its *in vivo* activity and creates the risk for creation of non-biocompatible products of drug-polymer metabolism.

In this chapter, the preparation, characterization, and *in vitro* evaluation of DOX-loaded PLGA NPs is described. DOX NPs were prepared through a nanoprecipitation technique followed by solvent evaporation. DOX NPs were characterized with respect to size, morphology, zeta potential, loading, encapsulation efficiency, and release profile. The therapeutic efficacy and cellular interaction of DOX NPs was studied *in vitro* in MDA-MB-231 breast cancer cells. Encapsulation of DOX within PLGA NPs will protect the patient from toxic effects associated with high-concentration bolus doses because the NPs will release the drug in a controlled manner so that its available concentration is maintained within therapeutic levels –above the minimum effective concentration but below the toxic concentration— for longer periods of time.

3.2 METHODS

3.2.1 Materials

PLGA (molecular weight 11 kD) with 50/50 lactide/glycolide molar percent and carboxylic acid end group was purchased from Medisorb (Cincinnati, OH, USA).

Doxorubicin hydrochloride was purchased from Fisher Scientific (Fair Lawn, NJ, USA). Bovine serum albumin, phosphate buffer saline (PBS) packs (0.01M buffer, 0.138M NaCl, 0.0027M KCl, pH 7.4) and 3,3-dimethyl glutaric acid were purchased from Sigma/Aldrich (St. Louis, MO, USA). All solvents were of at least ACS grade.

3.2.2 Preparation of Blank and DOX-Loaded NPs

PLGA NPs with no drug (blank NPs) or with DOX were prepared through a modified oil-in-water (o/w) nanoprecipitation technique (Fessi, Devissaguet et al. 1986). This technique has been used in the past for the preparation of NPs and nanocapsules with various polymers and drugs (Stolnik, Dunn et al. 1994; Barichello, Morishita et al. 1999; Furtado Mosquera, Legrand et al. 2000; Peltonen, Koistinen et al. 2003; Arica and Lamprecht 2005; Leo, Contado et al. 2006). DOX was dissolved in methanol at concentration of 2.2mg/l, 4.2 mg/ml and ~5.8mg/ml for 2.1, 3.9 and 5.3 wt.% targeted loadings (i.e. the desired weight percent of DOX in the NPs assuming a 100% encapsulation efficiency). Separately, 100 mg of PLGA were dissolved in 3ml of acetone. The organic phase was formed by combining 1.0 ml of the DOX solution and the 3ml of PLGA solution. This phase was added to 10 ml of an aqueous phase containing 10 mg/ml bovine serum albumin (BSA) as a suspension stabilizer, followed by sonication for 30 seconds. NPs form spontaneously as a result of the migration of the water-miscible acetone and methanol into the water phase, and the consequent precipitation of PLGA in the form of NPs. The solvents were removed by stirring under vacuum for 45 minutes at room temperature. NPs were recovered by centrifugation for 10 minutes at 48k g in a Beckman J2-21 refrigerated centrifuge (Beckman Instruments Inc., Palo Alto, CA, USA), and washed three times by resuspending the pellet in 10 ml of 10 mg/ml BSA solution followed by centrifugation to remove any unencapsulated DOX.

Supernatants were collected for analysis. NPs were frozen in a -20°C freezer overnight, lyophilized without any cryoprotectant using a Freeze Dryer 4.5 (Labconco, Kansas City, MO, USA), and stored at -20°C for further use. All characterization and evaluation studies described below were done utilizing lyophilized NPs. Blank NPs were similarly prepared, except that no DOX was utilized in the formulation.

3.2.3 Physiochemical Characterization of NPs

The yield of the formulation was determined by weighting the total mass of NPs recovered after lyophilization, and comparing it to the mass of polymer and drug used during preparation. A Coulter® NanoSizerTM (Coulter Electronics LTD., Harpenden Herts, UK) was utilized to determine the size and relative polydispersity of freeze-dried NPs resuspended in de-ionized water with sonication. Each batch was sized three times independently. The polydispersity index provides an indication of the variation in the NP size for each batch of NPs. This index, as given by the NanoSizer, ranges from 0 to 9, where 0 indicates a monodispersed distribution and 9 a distribution in which the ratio of the largest to the smallest particle is 5 or more.

The morphology of the NPs was studied with a Hitachi 4500 scanning electron microscope (SEM). NPs were resuspended in water with sonication, mounted onto a carbon conductive tab (Ted Pella, Inc., Redding, CA, USA), dried at room temperature overnight, and sputter coated with metal plasma prior to SEM imaging. A Phillips EM 208 transmission electron microscope (TEM) was used to confirm NP size and to study their internal structural features. NPs were resuspended in water, applied to a 300 mesh copper TEM grid with a carbon film (Electron Microscopy Sciences, Hatfield, PA, USA), and stained with uranyl acetate (J. T. Baker Chemical Co., Phillipsburg, NJ, USA).

The surface charge of NPs was studied through zeta potential measurements with a ZetaPlus (Brookhaven Instruments Corporation, Holtsville, NY, USA). NPs were resuspended at a concentration of 1mg/ml by sonication in a 1mM KCl solution (pH 7.5). A minimum of 9 zeta potential readings were obtained per batch.

3.2.4 DOX Encapsulation Efficiency and Loading

Drug loading (the weight percent of DOX in the final NP formulation) and encapsulation efficiency (*EE* ; percent of the DOX that was actually encapsulated out of that used for the preparation of DOX NPs) were assessed by two methods: (i) quantifying the amount of DOX recovered from wash supernatants ($M_{DOX_{SUPERNATANTS}}$) and assuming that the rest of the drug used during preparation ($M_{DOX_{PREP}}$) had been encapsulated, and (ii) by dissolving a known mass of NPs (M_{NPs}) with a mixture of dichloromethane and methanol (60:40 v/v%), filtering through a 0.45 μm nylon syringe filter to remove insoluble fractions and determining the mass of DOX found in the solution ($M_{DOX_{inNPs}}$). Absorbance at 480 nm was used to determine these concentrations based on standard curves ($r^2 > 0.99$).

Equations 3.1 and 3.2 were utilized to calculate encapsulation efficiency and loading:

$$EE = \frac{\left(M_{DOX_{PREP}} - M_{DOX_{SUPERNATANTS}}\right)}{M_{DOX_{PREP}}} \times 100\% \quad (3.1)$$

$$Loading = \frac{M_{DOX_{inNPs}}}{M_{NPs}} \times 100\% \quad (3.2)$$

Dissolved blank NPs did not show absorbance at 480nm.

3.2.5 *In Vitro* DOX Release

Drug release studies were performed *in vitro* in 10mM phosphate buffered saline (PBS, pH 7.4) or isotonic 10mM dimethylglutaric acid buffer (DMGA buffer, pH 4.0, 0.006M DMGA, 0.0039M NaOH, 150mM NaCl). DMGA buffer was utilized to mimic the conditions to which the NPs would be exposed during the process of vesicular endocytosis, specifically the pH in endo-lysosomal compartments (Chapman 2002; Panyam, Sahoo et al. 2003). For these studies, a known mass of DOX-loaded NPs was suspended in the appropriate buffer with sonication in centrifuge tubes and maintained in a water bath at 37^{o}C. At specific times the samples were centrifuged for 10 minutes at 48k g and an aliquot of the supernatant was removed, collected for analysis, and replaced with a known volume of fresh buffer. Absorbance at 480 nm of the supernatants was used to determine the amount of DOX released based on a standard curves ($r^2 > 0.99$) in each buffer.

3.2.6 *In Vitro* Therapeutic Efficacy

The therapeutic properties of the DOX NPs were evaluated in MDA-MB-231 human mammary gland epithelial adenocarcinoma cells (Generous gift from Dr. Dharmawardhane, previously from the Section of Molecular, Cell and Developmental Biology at The University of Texas at Austin). Cells were maintained in Dulbecco's Modified Eagle Medium supplemented with 10% fetal bovine serum (Tissue Culture Biologicals, Tulare, CA), 1% HEPES buffer, 1% L-glutamine (Mediatech Cellgro, Herndon, VA), and 1% sodium pyruvate at 37^{o}C in a humidified CO_2 incubator. All cell culture products were purchased from Invitrogen (Carlsbad, CA) unless otherwise specified.

For the studies, cells were seeded on 48-well plates at a cell density of 15,000 cells per well and incubated under normal growth conditions. After 24 hours of incubation, the cell media was replaced with suspensions of DOX-loaded or blank NPs, or solutions of free DOX in Dulbecco's phosphate buffered saline with $CaCl_2$ and $MgCl_2$ (DPBS, BioWhittaker^{TM}, Cambrex Bio Science Walkersville Inc., Walkersville, MD) in 4 different concentrations equivalent to 1.0, 10.0, 50.0 or 100.0 μg/ml of DOX for a 5.0% drug loading in the NPs. Fresh DPBS was used as a control. Each condition was repeated in three separate wells. Cells were then incubated for 2 hours, after which the DOX/NP-containing media was removed and the cells were washed three times with DPBS. An exposure time of 2 hours was chosen in order to try to isolate the therapeutic effect of the DOX NPs from that caused by DOX released from the NPs after longer exposure times in aqueous media. As will be described in the results section, after 2 hours of exposure significant amounts of DOX NPs had interacted with the cells. The cells were subsequently incubated for 2 days in complete growth medium before cell viability was assessed with the MTT Assay (Toxicolology Assay Kit TOX-1, Sigma). Lower cell viability represents a higher therapeutic efficacy.

3.2.7 Microscopy Studies of Cell-NP Interaction

The fluorescence of DOX was utilized to study the interaction of DOX NPs with MDA-MB-231 breast cancer cells through fluorescence confocal microscopy (Leica SP2 AOBS). Cells were seeded in 6-well plates containing a pre-sterilized coverslip in complete cell media at a density of 100,000 cells per well. After 48 hours of incubation, the media was replaced DPBS, with $CaCl_2$ and $MgCl_2$, including suspended DOX NPs, free DOX, or blank NPs at concentrations equivalent to 1.0 or 10.0 μg/ml of free DOX for a theoretical loading of 6.0 wt.%. DPBS was used as a control. The Cells were

incubated under normal conditions and at specific time points (1 or 2 hours) the media was removed and the cells were washed 3 times in ice cold DPBS to remove NPs that had not entered or adhered to the cells. Cells were then fixed with -20^{o}C methanol for 5 minutes and mounted onto microscopy slides utilizing Fluoromount-G mounting medium (Southern Biotech, Birmingham, AL).

Confocal microscopy images of representative cell groups were obtained at the plane of maximal fluorescence intensity or at consecutive z-planes with a 63x water objective. Image acquisition variables such as gain, offset, and zoom were adjusted in to obtain readable fluorescent signal from all concentration levels –which required some of the highest concentration samples to be saturated— and maintained constant during the study for all samples.

Separate studies were performed to determine if the fixation protocol had affected the results obtained. In one study, cells were fixed with 3.7% formalin for 15 minutes, washed three times with DPBS and mounted onto microscope slides as described above. In a separate study, cells were seeded onto Lab-Tek^{TM} chambered coverslips and imaged while live after exposure to 0.1 mg/ml of doxorubicin-loaded nanoparticles. Samples were imaged as described above.

3.2.8 Statistical Analysis

Statistical significance of differences between data sets was determined by Students' t-test at a 95% or 97.5% confidence level ($p < 0.05$ or 0.025) as indicated in the results.

3.3 RESULTS

3.3.1 NP Characterization

Blank and DOX-loaded PLGA NPs were prepared through a nanoprecipitation technique. Table 3.1 summarizes size and zeta potential results. The percent recovery, or yield, for each batch of NPs ranged from 60 to 90 percent. This percent recovery was calculated from comparison of the mass of NP powder recovered and the initial mass of polymer and drug used for preparation of the NPs. The mass of BSA that remained adsorbed to the surface of the NPs was not taken into account for determination of the percent recovery. Although this oversight could lead to slightly elevated calculated yields, we belive that the amount and variability of the yield was mainly affected by the process of purification and recovery which involved repeated centrifugation and resuspension, as well as the retrieval of NP powder from freeze drying tubes which was hindered by static.

NPs are roughly spherical, as seen in the SEM image in Figure 3.1A. The average diameter of the NPs resuspended in de-ionized water after lyophilization was determined to be about 230 nm and was found to be independent of DOX loading. The average polydispersity of the NP size as determined by a Coulter NanoSizer was 3 in a range from 0 to 9. The size and internal structural features of the NPs were also studied by TEM, as shown in Figure 3.1B. The perturbations on the surface of the NPs can be attributed to drying effects. Because of the uniformity of the uranyl acetate stain across the NPs, this image suggests a matrix type drug delivery system in which the drug is uniformly dispersed within the polymer matrix that forms the NP, as expected from a particulate formulation in which the drug is co-dissolved with the polymer prior to the formation of

the NP. The average size of the NPs measured from TEM images was determined to be 174 nm with a standard deviation of 76 nm, consistent with the SEM findings.

The average zeta potential of the NPs was determined to be -45 mV and to be independent of the amount of DOX loaded. The zeta potential of PLGA NPs depends on the end groups of the PLGA, the type of drug encapsulated and the type of stabilizing agent utilized during their preparation. The zeta potential of uncoated PLGA NPs has been reported to be -40.3 mV and to increase toward neutrality after coating with poloxamines (Stolnik, Dunn et al. 1994). PLGA NPs prepared with poly(vinyl alcohol) as a stabilizer have been reported to have a zeta potential in the range of -10.0 to -20.0 mV. The zeta potential of the NPs is key for their stability. Highly charged NPs are better able to remain stable as colloidal suspensions since the Coloumbic repulsion forces arising from their surface charge can overcome the Van der Waals attractive forces between them (Heurtault, Saulnier et al. 2003).

3.3.2 DOX Encapsulation

Several batches of DOX-loaded NPs with three different drug loadings were prepared for this study. Table 3.2 summarizes the results of DOX encapsulation efficiency and loading within PLGA NPs obtained from quantification of (1) non-encapsulated drug found in supernatants from NP washes, and (2) drug found from dissolved freeze-dried NPs. As can be seen from this table, the maximum DOX loading achieved was close to 5 mg of DOX per 100 mg of NPs (5 wt. %) with an average of 4.7 wt%, and the average encapsulation efficiency was 80%. The difference in drug loading calculated from both analyses is not significantly different ($p > 0.25$).

Previous accounts of encapsulation of DOX in particle-based drug delivery systems have reported DOX loadings in the order of less than 0.1 wt.% in cholesterol-

bearing pullulan hydrogel NPs (Akiyoshi, Taniguchi et al. 1996), 3.45 wt. % in PLGA NPs in which DOX was chemically conjugated to PLGA (Yoo, Oh et al. 1999), 2.2 wt. % in micelles composed of DOX conjugated to PLGA-PEG block copolymers (Yoo and Park 2001), 4.23 wt. % in micelles formulated with a copolymer of cholesterol and poly(2-methacryloyloxyethyl phosphorylcholine) (Xu, Ji et al. 2005), and 4.0 wt. % in chitosan NPs prepared by a ionotropic gelation with sodium tripolyphosphate (Janes, Fresneau et al. 2001).

3.3.3 *In Vitro* Drug Release

Drug release studies were performed in buffered saline pH 7.4 and 4.0 to observe the effect of pH on the release rates in the conditions that would most closely mimic those that the NPs would encounter *in vivo*. Figure 3.2 displays the observed release profiles. The release rate of DOX from PLGA NPs at pH 4.0 is significantly higher than at pH 7.4 ($p < 0.05$). In fact, at the acidic pH more than 50% of the drug had been released during the first hour, and more than 90% after 12 hours. On the other hand, the release at pH 7.4 indicates that the formulation is able to deliver the drug in a controlled manner over an extended period of time. Only 20 to 30% of the drug was released within the first hour depending on the loading of the formulation, while only about 65 to 75% was released within the first day. Drug continued to be released from this formulation at a slower rate for over 3 days, after which the rate of release was minimal. Drug loading did not appear to result in significantly different release profiles for a threshold of statistical difference of $p < 0.025$. However, if a threshold for statistically significant difference of $p < 0.05$ was used, NPs with lower loading appeared to result in significantly higher cumulative release at various time points at pH 7.4.

It is hypothesized that the difference in release rates at the different pH conditions is influenced by two phenomena. First, the degradation of PLGA is accelerated in acidic conditions and is further auto-catalyzed as the local concentration of lactic and glycolic acids increases. Since the degradation of PLGA NPs is known to occur through bulk erosion (Brannon-Peppas 1995; Brannon-Peppas 1997), the accelerated degradation results in faster decrease in polymer molecular weight and NP mass loss, easier access of physiological fluids into the NPs, quicker dissolution of the drug in physiological fluids and consequent enhanced release of the drug.

The second phenomenon that could be involved in the enhanced release of DOX at endo-lysosomal pH is related to the ionic interaction of the weakly basic DOX with the carboxylic acid groups of acid-capped PLGA, lactic acid and glycolic acid. As can be appreciated from Figure 3.3, DOX exists mostly as a single cation at the pH range of interest up to 7.0 (Sturgeon and Schulman 1977). Above pH 7.0, DOX can become a zwitterion or neutral compound by losing a proton from a phenolic hydroxyl group or from the sugar amino group, respectively (Sturgeon and Schulman 1977). Utilizing its pKA of 8.15 which accounts for dissociation from the single cationic state (C) to the zwitterion and the neutral species (here combined into the term N) (Sturgeon and Schulman 1977), one can determine the ratio of cationic DOX to the neutral or switterion configurations at specific pH values, as described by Equation 3.3.

$$K = \frac{[N]\cdot[H^+]}{[C]} = 10^{-8.15} \quad \longrightarrow \quad \frac{[C]}{[N]} = \frac{10^{-pH}}{10^{-8.15}} = 5.62 \qquad (3.3)$$

Thus, at pH 7.4 nearly 85% of the DOX molecules will be in the cationic state, as compared to 100% of the molecules at pH 4.0.

At a pH of 7.4 almost 100% of the acid groups in PLGA and the degradation products will be in the deprotonated (anionic) configuration, while at a pH of 4.0 almost 50% of the acid groups are in the protonated neutral form. As a result, at a pH of 7.4, DOX present mostly in its cationic state interacts favorably with the anionic PLGA. As the pH is reduced closer to the pKa of the acid groups in PLGA and the degradation products, it is thus possible that the ionic interaction with the cationic DOX is lost and results in faster release of the drug.

Scanning electron microscopy images of the NPs after the end of the release of the drug show that although degradation of the polymer has occurred, much of the morphology of the NPs remains, thus suggesting that most of the release of the drug occurs through diffusion across the polymeric matrix. Figure 3.4 shows SEM images of DOX-loaded PLGA NPs after release. Larger particle sizes and significant inter-particle fusing can be observed in the SEM of particles exposed to the more acidic conditions, thus confirming the contribution of the degradation of the NPs to the overall faster release rate observed at pH 4.0.

The polymer degradation characteristics at pH 7.4 for NPs prepared with the same PLGA type as that used in the present study have been previously reported by our group (Birnbaum and Brannon-Peppas 2003). The molecular weight of these NPs is known to decrease rapidly during the first week of degradation, followed by a slower rate of molecular weight loss. After 18 days under release conditions, the weight-average molecular weight was found to decrease from over 30K Da to about 2700 Da in previous studies (Birnbaum and Brannon-Peppas 2003). Such reduction in molecular weight would allow high water and drug diffusion rates, while still maintaining enough of the polymer in cohesive semi-spherical form.

3.3.4 *In Vitro* Therapeutic Efficacy

The *in vitro* anti-tumor efficacy of DOX-loaded NPs was evaluated with the cytotoxicity MTT assay in MDA-M-231 breast cancer cells. Cell viability data, as a fraction of control, are summarized in Figure 3.5. Lower cell viability represents a higher anti-tumor therapeutic effect.

Free DOX and DOX-loaded NPs significantly reduced viability compared to control and to blank NPs at concentrations equivalent to or higher than 10 μg/ml of DOX ($p < 0.05$). Blank NPs did not show reduced cell viability compared to control at the concentrations tested. Cytotoxicity induced by DOX encapsulated within NPs was not significantly different than that caused by the free drug in solution within the concentration range tested. However, it is important to note that since the drug and NP-containing media was removed after 2 hours of exposure, the cytotoxicity caused by the NPs had to be mainly associated with endocytosed particles or drug that was released from the particles and that entered the cells during these two hours. According to the data obtained from *in vitro* release studies in buffered media, the amount of drug that would have been released during this time is between 25 and 35%. These data indicate that despite the lack of significant increase in cytotoxicity by the NPs, this formulation (1) maintains the activity of DOX, (2) readily interacts with the cells despite the macromolecular size, and (3) is at least as effective as the free drug.

3.3.5 Microscopy Studies of NP/Cell Interaction

Figure 3.6 displays the fluorescence signal at the plane of maximum intensity for representative groups of fixed cells. High fluorescence intensity was observed even after 1 hour of cell incubation with NPs or free drug. An increase in fluorescence intensity was observed with increased concentration of DOX NPs or free DOX, and with increased

time of exposure, as expected. For all times of incubation, the fluorescence intensity of cells exposed to DOX NPs was significantly higher than that of cells exposed to free DOX. The low but detectable level of fluorescence observed in cells exposed to blank NPs did not appear to differ from that of the control samples, and is a result of cellular auto-fluorescence.

Figure 3.7A and B show differential interference contrast and the corresponding confocal fluorescence plane for cells exposed to DOX NPs or free DOX, respectively, in solution for 2 hours. High fluorescence intensity corresponding to high concentration of the nuclear drug DOX is observed at the nuclei of the cells. Since NPs are not able to enter the nuclei because of their large size, it is probable that upon particle endocytosis, the release rate from DOX NPs was accelerated in the acidic conditions of late endosomes and endo-lysosomal compartments. Once in solution at high concentrations within the cells, DOX was free to enter the nuclei. Figure 3.7C shows the fluorescence signal of a cell exposed to the same concentration of DOX NPs for 2 hours along the x-y plane and the z cross-section. Similar results were obtained when cells were fixed with formalin instead of methanol (data not shown) and with live cells, as can be observed in Figure 3.8.

3.4 DISCUSSION

Encapsulation of chemotherapeutic agents, and specifically of DOX, into injectable drug delivery systems has been reported in several instances. Encapsulation of hydrophilic molecules such as DOX in PLGA NPs is most commonly carried out through water-in-oil-in-water procedures in which the drug is first dissolved in the inner aqueous medium. However, the loading and encapsulation efficiency permissible are less than

acceptable because (1) the volume of the inner aqueous phase and consequently the mass of the active agent that can be used in the preparation must be small in order to prepare a stable initial water-in-oil emulsion and (2) the drug will have the tendency to diffuse into the outer aqueous phase during the preparation process because of concentration gradient.

Here an oil-in-water nanoprecipitation process was utilized for the preparation of DOX-loaded NPs. The use of an oil-in-water process, nanoprecipitation, and an acid-capped polymer resulted in higher drug loadings than those reported for other systems in the past (Akiyoshi, Taniguchi et al. 1996; Yoo, Oh et al. 1999; Janes, Fresneau et al. 2001; Yoo and Park 2001; Xu, Ji et al. 2005). Incorporation of DOX hydrochloride in the organic phase of the oil-in-water system together with the polymer was achieved by first dissolving it in the polar protic solvent methanol which is fully miscible with acetone. Co-dissolving the drug with the polymer permits the incorporation of higher mass than would otherwise be possible with a water-in-oil-in-water process.

Nanoprecipitation offers various benefits compared to more commonly-used emulsion processes. First and most importantly, NPs are formed spontaneously as the solvents of the polymer and drug diffuse into the water phase causing the precipitation of the water-insoluble polymer. The speed for NP solidification enables the drug to be rapidly entrapped, thus preventing its diffusion into the outer aqueous phase. Second, the nanoprecipitation process is simple and highly reproducible, and results in the formation of NPs or nanocapsules –depending on the protocol-- of about 200 nm in size with little influence from stirring or sonication (Couvreur, Dubernet et al. 1995; Legrand, Barratt et al. 1999). Such NP size is optimal for the ability of the NPs to be used for intravenous administration and passive targeting to tumors taking advantage of the EPR effect. NPs larger than about 250-300 nm would be at higher risk of being seized by the filtration in the spleen (Brannon-Peppas 1995). Finally, the use of acid-capped PLGA in the present

formulation is also believed to improve the encapsulation of the mildly basic DOX because, as described earlier, DOX is present as a single cation within the pH range at which is exposed during the preparation of the NPs while the carboxylic acid at the end of the PLGA chains is deprotonated, thus resulting in a moderate favorable ionic interaction between these two compounds. As observed from the *in vitro* release data, this interaction is lost when the loaded particles are exposed to acidic conditions and results in rapid release of the drug.

For the preparation of stable NPs with the nanoprecipitation method, a surfactant is normally required in the aqueous phase. Albumin has been previously utilized as a surface agent for the preparation of NPs (Bazile, Ropert et al. 1992; Verrecchia, Huve et al. 1993; Verrecchia, Spenlehauer et al. 1995). Albumin acts as a tensioactive agent by exposing its hydrophilic and hydrophobic regions toward the aqueous and organic phases during the process of NP formation, respectively. Once the organic solvent is removed, albumin remains associated with the hydrophobic NP surface, and in fact, part of the albumin is permanently bound (Bazile, Ropert et al. 1992; Verrecchia, Huve et al. 1993; Verrecchia, Spenlehauer et al. 1995). Utilization of BSA as a stabilizing agent in the present formulation was found to prevent aggregation of the NPs during the repeated centrifugation-resuspension cycles utilized to wash un-encapsulated drug, and to eliminate the need for a separate cryoprotectant. In addition to BSA, our group has worked on the preparation of NPs with other stabilizers such as poly(vinyl alcohol) and sodium cholate.

BSA adsorbed on the surface of the NPs was not taken into account in the determination of the yield percent for the present formulation. Previous studies by Verrecchia and colleages have shown that poly(lactic acid) (PLA) NPs prepared by an emulsion and solvent evaporation method in the presence of radiolabeled human serum

albumin have shown that the amount of albumin bound to the NP surface was inversely proportional to the NP diameter and that, for their formulation, approximately 5.7 μg of albumin remain bound per square meter of NP surface area (Verrecchia, Huve et al. 1993). According to this surface concentration, our NPs could contain around 125 μg of albumin per mg of polymer, or about 10mg of albumin for an 80mg batch. However, this comparison could be misleading because the cited study used different polymer, solvent, and albumin type, did not encapsulate a drug, and used different preparation and recovery procedures. In fact, the sizes of the particles in that study were markedly different when prepared with the same albumin concentration in the aqueous phase compared to those here reported. In addition, it is not clear whether the NPs in the cited study were freeze dried or whether freeze drying would have changed their results. Further studies will be necessary to determine the albumin fraction that remains adsorbed to the surface of the present NPs.

The *in vitro* interaction of DOX-loaded PLGA NPs with MDA-MB-231 breast cancer cells presented promising results. Cell exposure to DOX-loaded NPs or free DOX in solution resulted in comparable cancer cell viability. Studies demonstrated higher uptake and nuclear localization of DOX in the cells when presented in the form of NPs. Although it was expected that the negatively-charged surface of the NPs would hamper their interaction with negatively-charged cell membranes, the results suggest that the NP-cell interaction is modulated by phenomena more complex than just charge effects and must be further investigated. In addition, it is possible that the high cellular uptake could be a result of the high DOX payload in the NPs (each NP could contain more than 400 DOX molecules as calculated from the drug loading, particle size and polymer density) which would result in substantial intracellular delivery even if only small number of NPs were able to enter the cells. Further studies will need to be performed to investigate why

the increased DOX nuclear localization did not result in higher therapeutic efficacy *in vitro*. Nonetheless, the data suggests that the encapsulated drug is active and that the formulation could possibly lead to significantly higher therapeutic effect *in vivo* as result of the improved biodistribution of the NPs and the pH-dependent release of the drug from these particles.

The biodistribution of polymeric NPs *in vivo* is known to be distinctly different from that of low-molecular weight drugs. NPs are known to undergo rapid opsonization and be quickly sequestered by the macrophage phagocytic system. Bazile, et al. studied the distribution and pharmacokinetics of albumin-coated PLA NPs and found that despite longer circulation times compared to uncoated particles, the NPs were still captured by liver, bone marrow, lymph nodes, spleen and peritoeal macrophages (Bazile, Ropert et al. 1992). Although this disctinct localization can be exploited for targeting of drugs to these organs, its use for the delivery of chemotherapeutic agents to tumors could lead to undesired toxicity. For this reason, further studies are underway in our laboratory to modify the surface of the NPs in order to delay opsonization and provide specific targeting capabilities.

3. 5 CONCLUSION

The use of an oil-in-water nanoprecipitiation technique for the encapsulation of the chemotherapeutic drug DOX into acid-capped PLGA NPs was proven in this work to be a satisfactory method. By co-dissolving the drug with the polymer, high entrapment efficiency was achieved as the polymer precipitated into solid particles. In vitro studies revealed a pH-dependent release profile that would result in slow drug release at physiological pH and fast release within the more acidic endolysosomal compartments after endocytosis. Increased degradation of the polymer at acidic pH as well an ionic

interaction between the polymer and the mildly basic DOX are hypothesized to influence its release from the NPs. DOX NPs were found to result in a therapeutic efficacy comparable to the free drug, while blank NPs did not reduce cell viability. Confocal microscopy studies revealed that exposure of MDA-MB-231 breast cancer cells to DOX NPs resulted in higher intracellular drug concentrations than exposure to free DOX, and that the level of intracellular accumulation increased in a time- and dose-dependent manner as expected for both DOX NPs and free DOX.

Having satisfactorily prepared nanoparticles loaded with a chemotherapeutic agent that could be used for therapeutic purposes, the following chapter describes the preparation of nanoparticles loaded with imaging agents for *in vitro* and *in vivo* monitoring of the biological distribution and activity of the nanoparticles.

Table 3.1 Size and zeta potential of blank and doxorubicin-loaded nanoparticles. Values represent the average ± standard deviation for n batches of equivalent targeted drug loading. DOX: Doxorubicin; NP: Nanoparticle; SD: Standard deviation; SE: Standard error.

Group	Targeted Loading (wt. %)	Number of Batches (n)	Size ± Std. Dev (nm)	Polydispersity ± Std. Dev	Zeta Potential ± SE (mV)
Blank NPs	0	4	225 ± 49	3 ± 1.3	-44.7 ± 1.7
DOX NPs 1	2.1	1	249	3	-46.5 ± 1.5
DOX NPs 2	3.9	1	173	3	-46.4 ± 1.5
DOX NPs 3	5.3 ± 0.1	6	239 ± 27	3 ± 0.7	-44.9 ± 1.4

Table 3.2 Doxorubicin encapsulation efficiency and loading within PLGA nanoparticles. Results represent the average ± standard deviation for n batches of equivalent targeted drug loading. DOX: Doxorubicin; NP: Nanoparticle.

Targeted Loading (wt. %)	Number of Batches (n)	Encapsulation Efficiency (wt. %)		Drug Loading (wt. %)		Mass of DOX Accounted (%)
		Supernatant Analysis	Dissolved NPs	Supernatant Analysis	Dissolved NPs	
2.1	1	80.9	95.4	1.7	2.0	114.5
3.9	1	75.6	72.7	2.9	2.9	97.1
5.3 ± 0.1	3	79.5 ±6.9	65.4 ±4.6	4.3 ±0.4	4.7 ±1.1	85.8 ±10.7

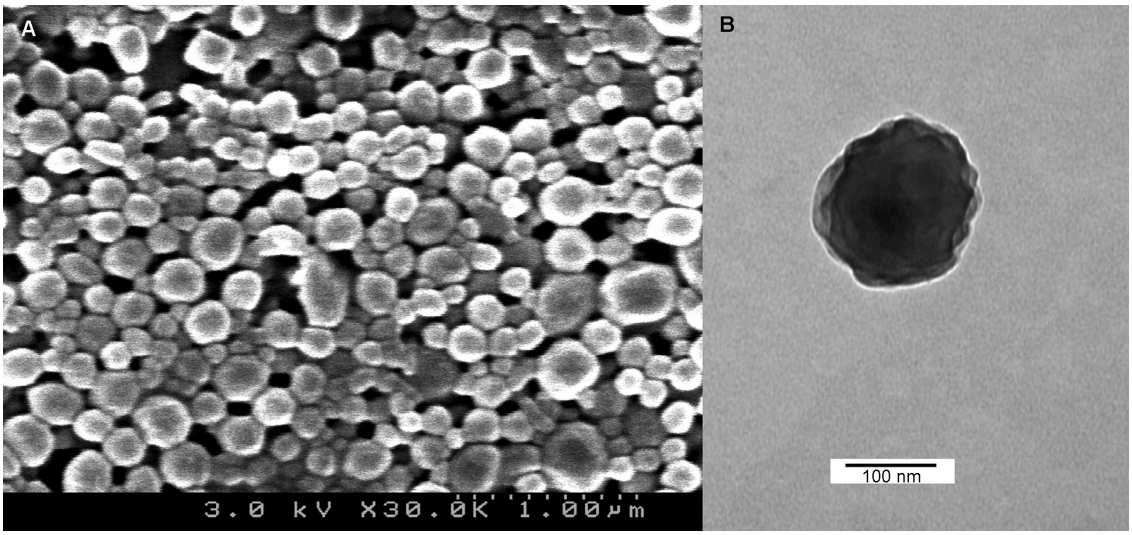

Figure 3.1 (A) Scanning electron microscopy image of doxorubicin-loaded poly(lactic-co-glycolic acid) nanoparticles prepared by a nanoprecipitation method. (B) Transmission electron microscopy image of doxorubicin-loaded nanoparticle stained with uranyl acetate.

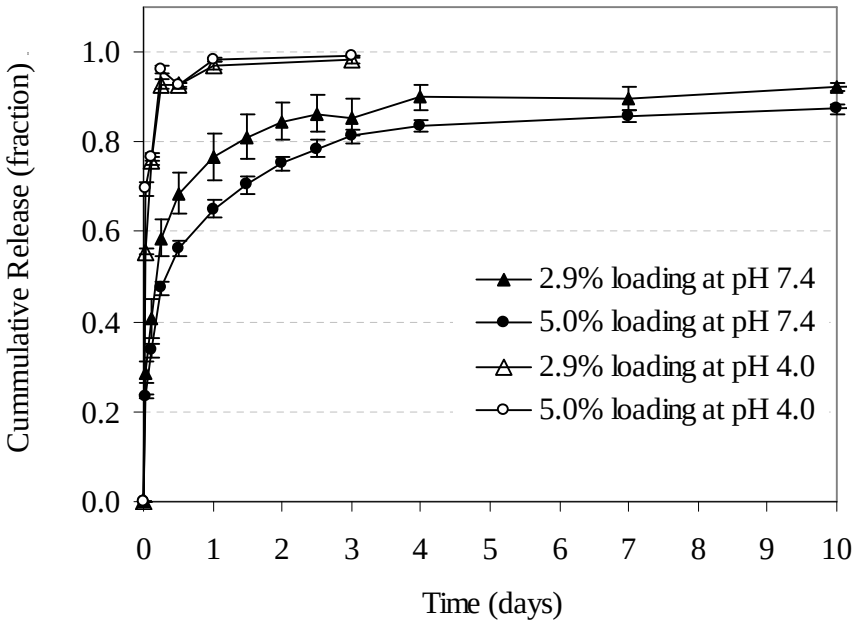

Figure 3.2 *In vitro* release of doxorubicin from poly(lactide-co-glycolide) nanoparticles in buffered saline, pH 7.4 and 4.0. Values represent release data for 2 batches of nanoparticles with different loadings, each batch in triplicate. Error bars represent the standard deviation in the release for each batch.

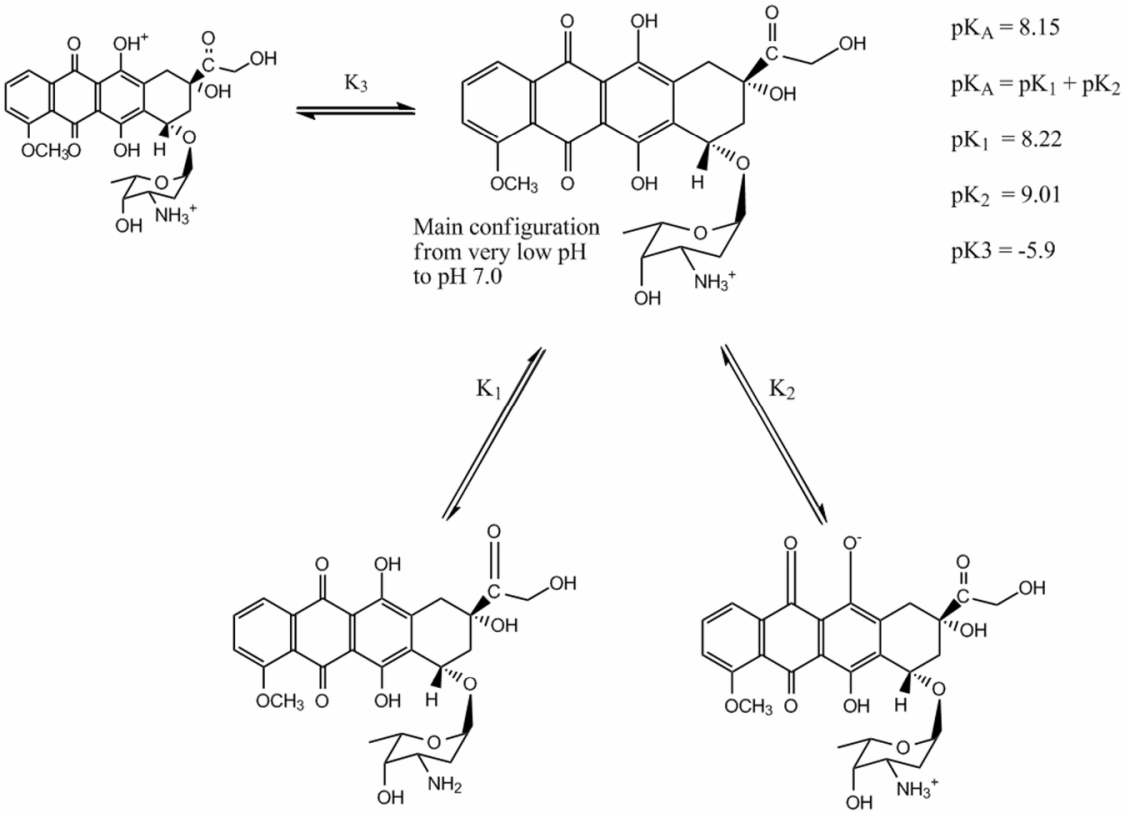

Figure 3.3 Possible ionic configurations of doxorubicin within the pH range of 4.0 to 9.0. Data obtained from Sturgeon et al. (1977).

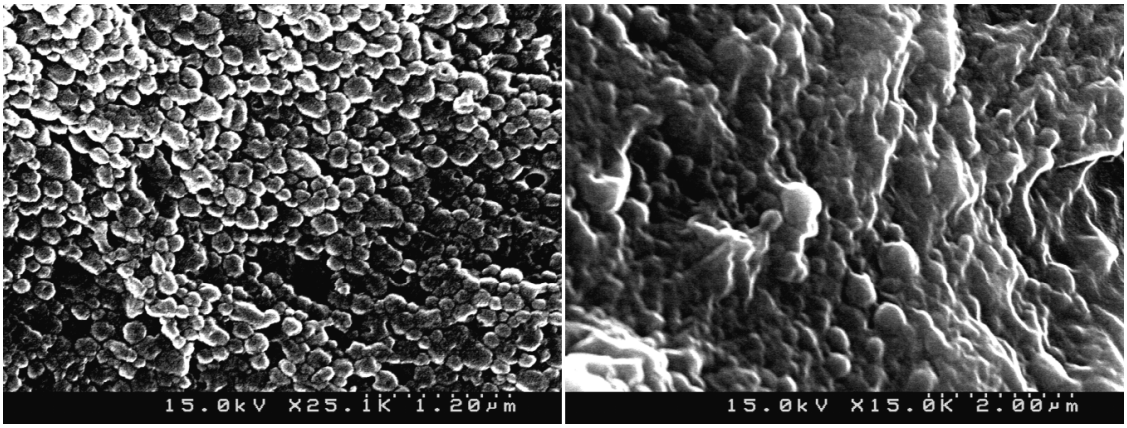

Figure 3.4 Scanning electron microscopy (SEM) image of PLGA nanoparticles after a 16-day in vitro release study in 10mM phosphate buffered saline pH 7.4 (left) and after 4 days of release in 10mM dimethyl glutaric acid/NaOH buffer pH 4.0 (right) at 37C. Nanoparticles were recovered from release vials, washed with water to remove excess salt, and freeze dried prior to SEM sample preparation.

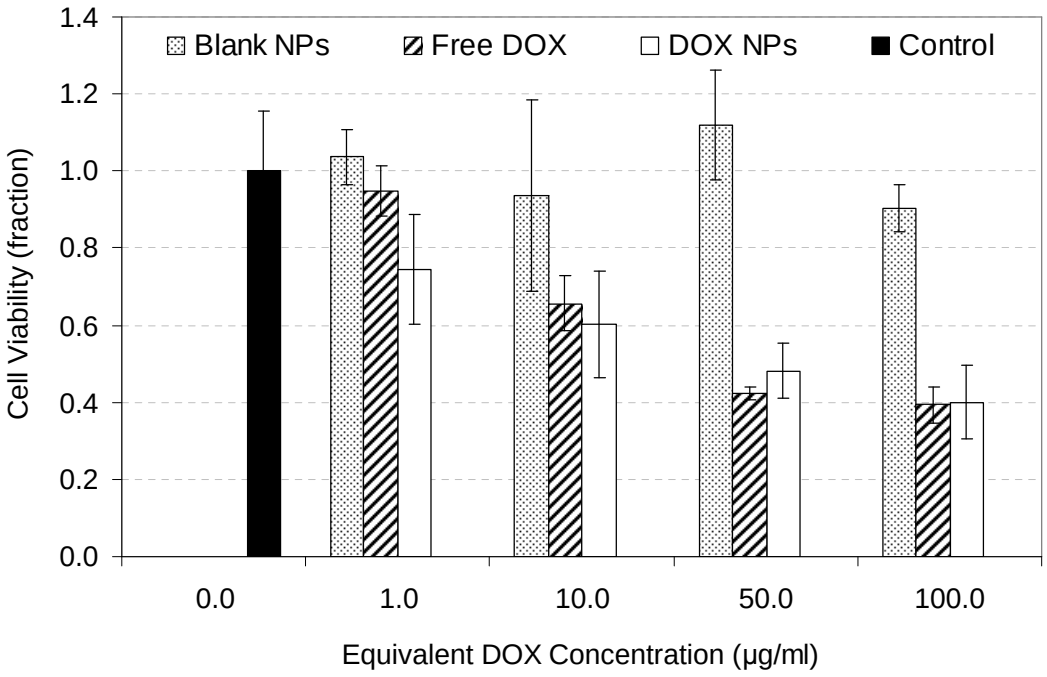

Figure 3.5 Viability of MDA-MB-231 mammary gland epithelial adenocarcinoma cells after exposure to doxorubicin-loaded nanoparticles (white bars), free doxorubicin in solution (dark gray bars), or blank nanoparticles (light gray bars) at concentrations equivalent to 1.0, 10.0 and 100.0 µg/ml of doxorubicin. Control data (black bar) is for cells maintained in DPBS. Data presented as a percentage of control average. Error bars represent the standard deviation of the data. Abbreviations: NPs = nanoparticles, DOX = doxorubicin.

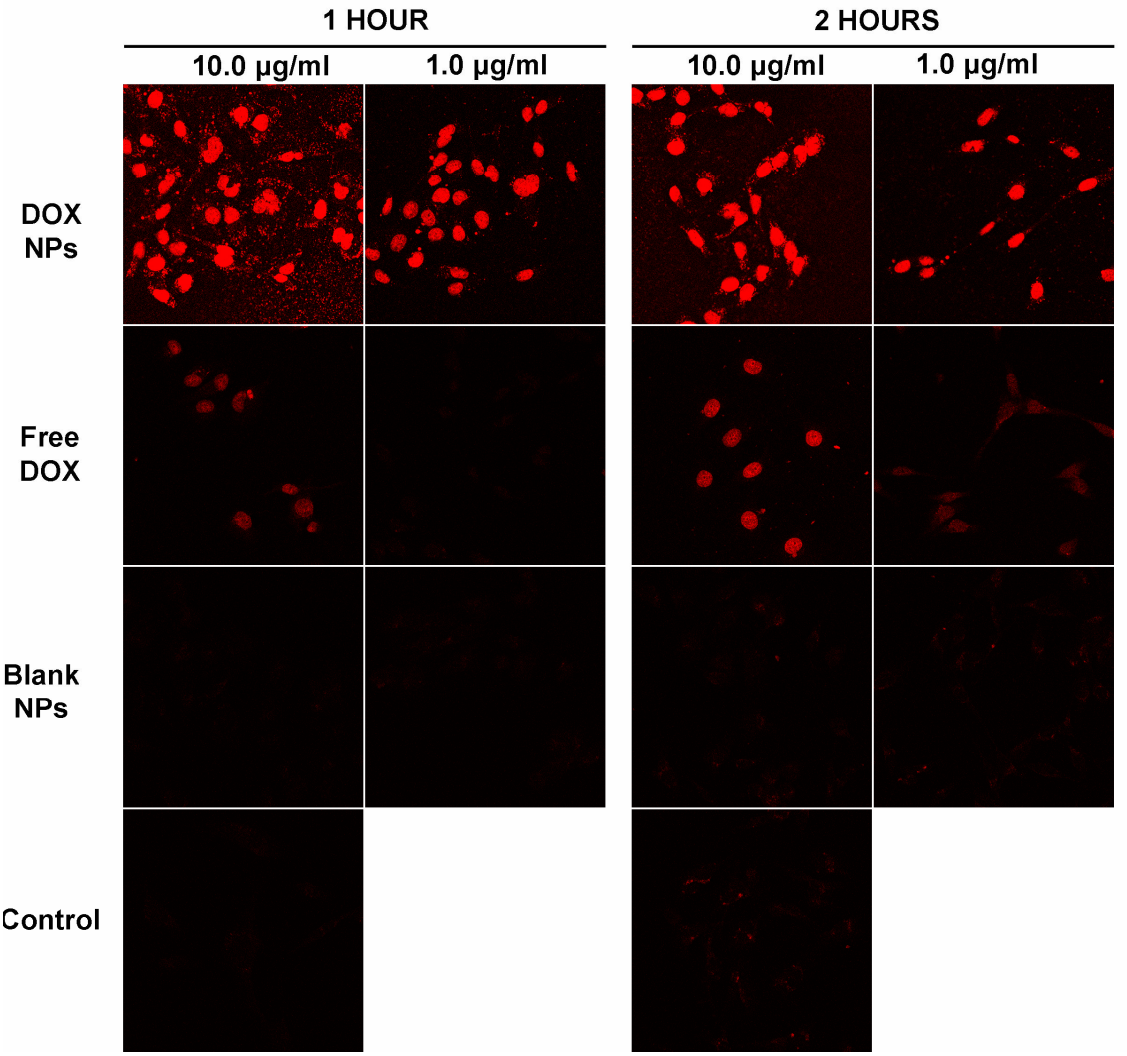

Figure 3.6 Confocal microscopy images of MDA-MB-231 breast cancer cells exposed to doxorubicin-loaded PLGA nanoparticles (DOX NPs), free doxorubicin (free DOX), or blank PLGA nanoparticles (Blank NPs) at concentrations equivalent to 10.0 and 1.0 µg/ml of DOX for 1 or 2 hours. Cells in control samples were incubated in DPBS for the same time periods. Cells were fixed with -20^{o}C methanol.

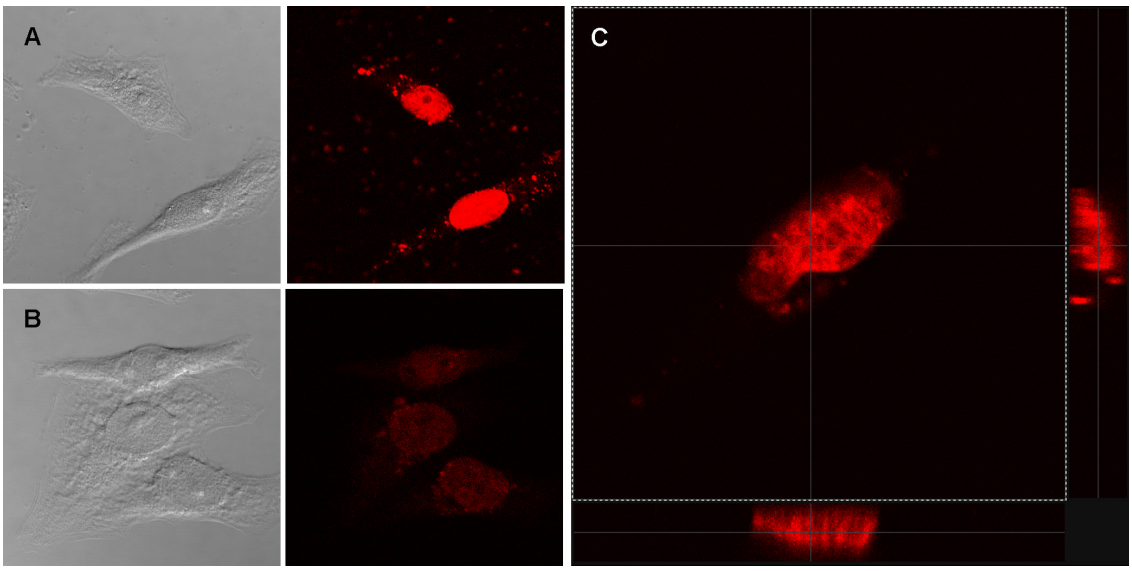

Figure 3.7 Differential interference contrast (DIC) images (left) and corresponding confocal fluorescence images (right) of MDA-MB-231 cells after exposure to doxorubicin-loaded nanoparticles (A) or free doxorubicin in solution (B) at a concentration equivalent to 1.0 μg/ml of doxorubicin for 2 hours. (C) Cross-sectional view of cell exposed to doxorubicin-loaded nanoparticles for 2 hours at the same concentration along its depth. Cells were fixed with ice-cold methanol. Doxorubicin preferentially localizes at the nucleus of the cells when administered in nanoparticles or in solution.

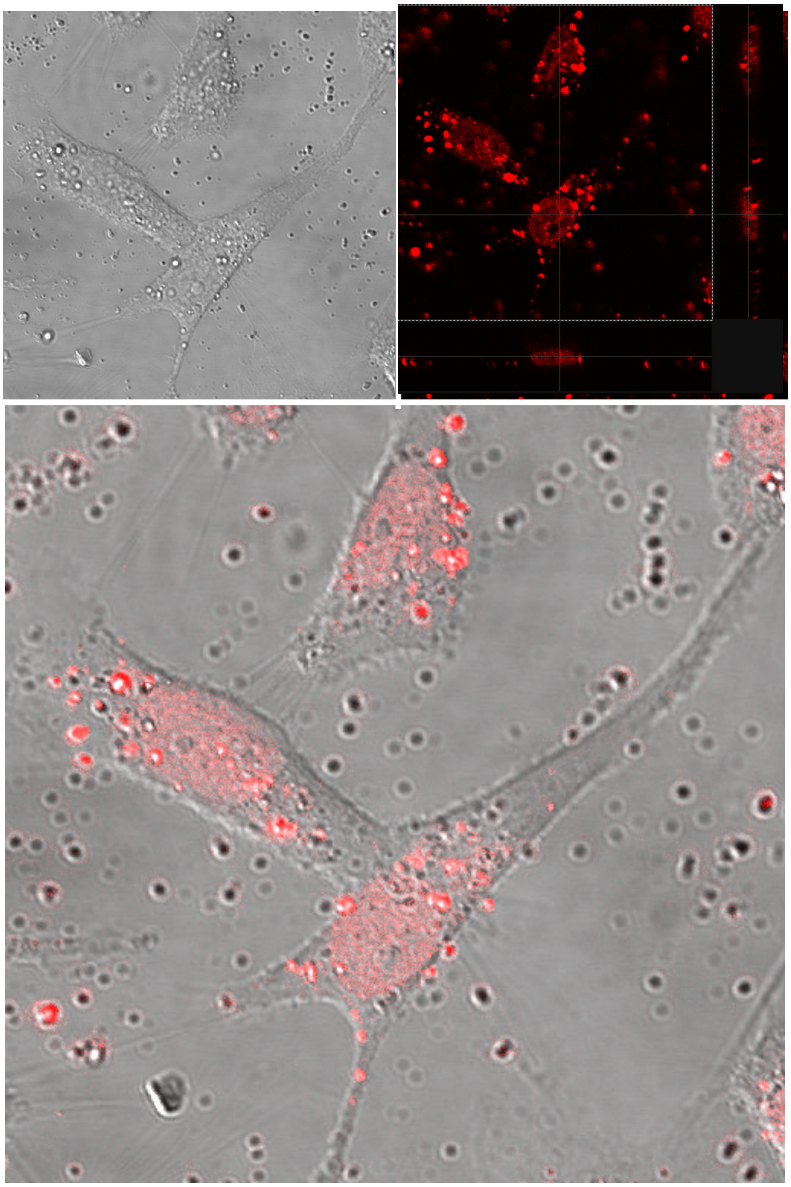

Figure 3.8 Differential interference contrast images (left), corresponding confocal fluorescence images along the x-y-z axes (right) and overlay of these images (bottom) of live MDA-MB-231 cells after exposure to doxorubicin-loaded nanoparticles at a concentration of 0.1 mg/ml of nanoparticles (5 μg/ml doxorubicin) for 4 hours. As observed in fixed cells, doxorubicin preferentially localizes at the nucleus of the cells after entering the cells.

3.6 REFERENCES

Akiyoshi, K., I. Taniguchi, et al. (1996). "Hydrogel nanoparticle formed by self-assembly of hydrophobized polysaccharide. Stabilization of Adriamycin by complexation." European Journal of Pharmaceutics and Biopharmaceutics 42(4): 286-290.

Arica, B. and A. Lamprecht (2005). "In Vitro Evaluation of Betamethasone-Loaded Nanoparticles." Drug Development and Industrial Pharmacy 31(1): 19-24.

Barichello, J. M., M. Morishita, et al. (1999). "Encapsulation of Hydrophilic and Lipophilic Drugs in PLGA Nanoparticles by the Nanoprecipitation Method." Drug Development and Industrial Pharmacy 25(4): 471-476.

Barraud, L., P. Merle, et al. (2005). "Increase of doxorubicin sensitivity by doxorubicin-loading into nanoparticles for hepatocellular carcinoma cells in vitro and in vivo." Journal of Hepatology 42: 736-343.

Bazile, D. V., C. Ropert, et al. (1992). "Body distribution of fully biodegradable [14C]-poly(lactic acid) nanoparticles coated with albumin after parenteral administration to rats." Biomaterials 13(15): 1093-1102.

Birnbaum, D. T. and L. Brannon-Peppas (2003). "Molecular weight distribution changes during degradation and release of PLGA nanoparticles containing epirubicin HCl." Journal of Biomaterials Science Polymer Edition 14(1): 87-102.

Blasiak, J., E. Gloc, et al. (2002). "A comparison of the in vitro genotoxicity of anticancer drugs idarubicin and mitoxantrone." Acta Biochimica Polonica 49(1): 145-155.

Brannon-Peppas, L. (1995). "Recent advances on the use of biodegradable microparticles and nanoparticles in controlled drug delivery." Int J Pharm. 116(1): 1-9.

Brannon-Peppas, L. (1997). "Polymers in Controlled Drug Delivery." Medical Plastics and Biomaterials Magazine 4: 34-44.

Chapman, A. P. (2002). "PEGylated Antibodies and Antibody Fragments for Improved Therapy: a Review." Advanced Drug Delivery Reviews 54(4): 531-545.

Couvreur, P., C. Dubernet, et al. (1995). "Controlled Drug Delivery with Nanoparticles: Current Possibilities and Future Trends." European Journal of Pharmaceutics and Biopharmaceutics 41(1): 2-13.

Fessi, H., J. P. Devissaguet, et al. (1986). Procédé de préparation des systèmes colloïdaux dispersibles dune substance sous forme de nanoparticules. F. P. Application. French.

Furtado Mosquera, V. C., P. Legrand, et al. (2000). "Poly(D,L-Lactide) Nanocapsules Prepared by a Solvent Displacement Process: Influence of the Composition on Physiochemical and Structural Properties." Journal of Pharmaceutical Sciences 89(5): 614-626.

Gabizon, A. A. (2001). "Pegylated Liposomal Doxorubicin: Metamorphosis of an Old Drug into a New Form of Chemotherapy." Cancer Investigation 19(4): 424-436.

Heurtault, B., P. Saulnier, et al. (2003). "Physico-chemical stability of colloidal lipid particles." Biomaterials 24: 4283-4300.

IARC (1976). IARC Monographs on the Evaluation of the Carcinogenic Risk of Chemicals to Man. Some Naturally Occurring Substances. I. A. f. R. o. Cancer. Lyon, France, IARC. 10: 353 pp.

Ike, O., Y. Shimizu, et al. (1991). "Biodegradation and antitumor effect of adriamycin-containing poly(L-lactid acid) microspheres." Biomaterials 12(8): 757-762.

Janes, K. A., M. P. Fresneau, et al. (2001). "Chitosan nanoparticles as delivery systems for doxorubicin." Journal of Controlled Release 73(2-3): 255-267.

Jeong, Y.-I., H.-S. Na, et al. (2006). "Adriamycin release from self-assembling nanospheres of poly(D,L-lactide-co-glycolide)-grafted pullulan." International Journal of Pharmaceutics 322(1-2): 154-160.

Lee, E. S., K. Na, et al. (2005). "Doxorubicin loaded pH-sensitive polymeric micelles for reversal of resistant MCF-7 tumor." Journal of Controlled Release 103(2): 405-418.

Legrand, P., G. Barratt, et al. (1999). "Polymeric Nanocapsules as Drug Delivery Systems." S.T.P. Pharma Sciences 9(5): 411-418.

Leo, E., C. Contado, et al. (2006). "Nanoparticle formulation may affect the stabilization of an antiischemic prodrug." International Journal of Pharmaceutics 307(1): 103-113.

Lin, R., L. S. Ng, et al. (2005). "In vitro study of anticancer drug doxorubicin in PLGA-based microparticles." Biomaterials 26: 4476-4485.

Lum, B. L., J. M. Svec, et al. (1985). "Doxorubicin: alteration of dose scheduling as a means of reducing cardiotoxicity." Drug Intelligence & Clinical Pharmacy 19(4): 259-264.

Nasongkla, N., E. Bey, et al. (2006). "Multifunctional Polymeric Micelles as Cancer-Targed, MRI-Ultrasensitive Drug Delivery Systems." Nano Letters 6(11): 2427-2430.

Panyam, J., S. K. Sahoo, et al. (2003). "Fluorescence and electron microscopy probes for cellular and tissue uptake of poly(D,L-lactide-co-glycolide) nanoparticles." International Journal of Pharmaceutics 262(1-2): 1-11.

Peltonen, L., P. Koistinen, et al. (2003). "Preparation of Nanoparticles by the Nanoprecipitation of low molecular weight poly(l)lactide." S.T.P. Pharma Sciences 13(5): 299-304.

Stolnik, S., S. E. Dunn, et al. (1994). "Surface Modification of Poly(lactide-co-glycolide Nanospheres by Biodegradable Poly(lactide)-Poly(ethylene glycol) Copolymers." Pharmaceutical Research 11(12): 1800-1808.

Sturgeon, R. J. and S. G. Schulman (1977). "Electronic Absorption Spectra and Protolytic Equilibria of Doxorubicin: Direct Spectrophotometric Determination of Microconstants." Journal of Pharmaceutical Sciences 66(7): 958-961.

Tan, E. C., R. Lin, et al. (2005). "Fabrication of double-walled microspheres for sustained release of doxorubicin." Journal of Colloild and Interface Science 291: 134-143.

Twardowski, P. and K. Margolin (2002). Targeting Vascular Endothelium With Antibodies. Cancer Drug Discovery and Development: Tumor Targeting in Cancer Therapy. M. Pagé. Totowa, NJ, Humana Press Inc.: 199-210.

Verrecchia, T., P. Huve, et al. (1993). "Adsorption/desorption of human serum albumin at the surface of poly(lactic acid) nanoparticles prepared by a solvent evaporation technique." Journal of Biomedical Materials Research 27(8): 1019-1028.

Verrecchia, T., G. Spenlehauer, et al. (1995). "Non-stealth (poly(lactic acid/albumin)) and stealth (poly(lactic acid-polyethylene glycol)) nanoparticles as injectable drug carriers." Journal of Controlled Release 36(1-2): 49-61.

Xu, J.-P., J. Ji, et al. (2005). "Novel biomimetic polymersomes as polymer therapeutics for drug delivery." Journal of Controlled Release 107(3): 502-512.

Yoo, H. S., J. E. Oh, et al. (1999). "Biodegradable Nanoparticles Containing Doxorubicin-PLGA Conjugate for Sustained Release." Pharmaceutical Research 16(7): 1114-1118.

Yoo, H. S. and T. G. Park (2001). "Biodegradable Polymeric Micelles Composed of Doxorubicin Conjugated PLGA-PEG Block Copolymer." Journal of Controlled Release 70(1-2): 63-70.

Yoo, H. S. and T. G. Park (2004). "Folate receptor targeted biodegradable polymeric doxorubicin micelles." Journal of Controlled Release 96(2): 273-283.

Zhang, Z., S. H. Lee, et al. (2007). "Folate-decorated poly(lactic-co-glycolide)-vitamin E TPGS nanoparticles for targeted drug delivery." Biomaterials 28(10): 1889-1899.

CHAPTER 4

FORMULATION, CHARACTERIZATION AND EVALUATION OF IMAGING NANOPARTICLES

4.1 BACKGROUND

As mentioned in Chapter 2, imaging methods are currently utilized for clinical detection of tumors, although to date biopsies are the gold standard for final diagnosis and staging. Contrast agents are invaluable for the detection of tumors as they provide the means for distinguishing them from surrounding normal tissue by taking advantage of various physiologic, metabolic or molecular differences. Contrast agents can also be used for studying and monitoring the distribution and interaction of drug delivery systems with cancer cells *in vitro* and with tumor tissue *in vivo*.

In this chapter, the formulation of biodegradable nanoparticles loaded with imaging agents is described. Fluorescent or electron-dense agents were investigated with the purpose creating formulations that could be used for study the interactions of the nanoparticles with target cells through fluorescence microscopy or electron microscopy, respectively. The hypothesis here was that these nanoparticles could be used to elucidate the behavior of the formulations containing chemotherapeutic agents both *in vitro* and *in vivo* through imaging methods. For this to be true, these nanoparticles must have properties equivalent to the nanoparticles loaded with chemotherapeutic agents, i.e. similar size, morphology, and surface chemistry.

Rhodamine 6G and Indocyanine Green were used as fluorescent agents while gadopentetic acid (Gd-DTPA) was used as an electron dense agent. While the use of

rhodamine-loaded nanoparticles would be limited to *in vitro* studies, use of indocyanine green and Gd-DTPA as fluorescent and electron dense agents was motivated by the desire to create formulations that, in addition, could be potentially used for clinical detection and monitoring of tumors *in vivo* through photoacoustic computer tomography and magnetic resonance imaging (MRI), respectively. Table 4.1 and the following sections describe some of the characteristics of these agents. Figure 4.1 displays the chemical structure of each of these imaging agents.

4.1.1 Rhodamine 6G

Rhodamine 6G (RHO) is a fluorescent dye that is commonly used as a label for detection and monitoring of molecules in fluorescence microscopy, flow cytometry, immunohistochemistry and spectroscopy. RHO has a molecular weight of 479 g/mol. Its structure is depicted in Figure 4.1A. RHO is highly soluble in water, ethanol, methanol, acetone and dimethyl sulfoxide, among other agents. It presents absorption and fluorescence peaks at about 530nm and 550nm, respectively. RHO has been previously used as a dye for mitochondrial staining and as an inhibitor of mitochondrial function in cells (Gear 1974; Hu, Zhao et al. 2007), for general cellular staining (Tang, Yang et al. 2007) and also as a dye for imaging of nanoparticles for gene delivery *in vivo* (Vila, Gill et al. 2004; Vila, Sanchez et al. 2004; Bejiani, BenEzra et al. 2005). In the present work, RHO was used a means for monitoring the interactions of poly(lactic-co-glycolic acid) nanoparticles with breast cancer cells *in vitro* by confocal fluorescence microscopy and flow cytometry.

4.1.2 Indocyanine Green

Indocyanine green (ICG) is a fluorophore that exhibits high absorbance and fluorescence in the near-infrared region. It has a molecular weight of 775 g/mol and is highly soluble in aqueous solutions and polar solvents. Its chemical structure is shown in Figure 4.1B. ICG presents absorbance and emission maxima at about 790 and 820 nm, respectively. ICG and other near-infrared fluorophores have been widely accepted for diagnostic applications because these molecules offer low background interference since almost no biological molecules absorb or emit in the near-infrared region and because infrared light offers the highest penetration depth in biological tissue. The absorption and emission peaks of ICG are in the range of the isobestic point of 800nm, where oxygenated and de-oxygenated hemoglobin have the same extinction coefficient, and consequently permit imaging of tissues independently of oxygenation status (Kalliokoski, Scheede-Bergdahl et al. 2006).

ICG has been widely used for imaging-based characterization of blood volume, cardiac output, hepatic function, retinal blood flow, and pharmacokinetic behavior. The main problems associated with the use of indocyanine green as an imaging agent have to do with its small circulation half life, instability in aqueous solutions and its photosensitivity. The circulation half life of ICG is only between 2 and 4 minutes (Desmettre, Devoisselle et al. 2000). ICG has been reported to form aggregates and undergo irreversible degradation in aqueous media (Saxena, Sadoqi et al. 2003). These transformations result in decreased absorption and fluorescence, discoloration, and shifts in the wavelength of maximum absorption. Some of the factors that influence the optical behavior of ICG are: concentration, light exposure, temperature, and pH. The fluorescence of ICG in aqueous solutions has been observed to decrease with

concentration above 2μg/ml, phenomenon that has been attributed to the formation of aggregates, self quenching, and overlap of the absorption/emission spectra at higher concentrations (Saxena, Sadoqi et al. 2003).

The effect of light exposure on the photostability of ICG has been reported to be dependent on the type and intensity of the light. The half life of ICG was reported to be 2.3 hours when continuously exposed to light from a 786 nm laser, compared to a half life of 14 hours when exposed to normal room lighting (Saxena, Sadoqi et al. 2003). The mechanism of ICG degradation with light has been proposed to be associated with the creation of a photoexcited molecule that is easily transformed into reactive radicals, which can then react with ions and other radicals present in the solvent to form leucoforms (Holzer, Mauerer et al. 1998).

When protected from light, the temperature of storage also has an effect on the half life of ICG, with higher temperatures reducing its half life (Saxena, Sadoqi et al. 2003). The mechanism of degradation as a function of temperature has also been proposed to be associated with the formation of radicals through vibrational, librational, and translational agitation processes (Holzer, Mauerer et al. 1998). Finally, degradation of ICG was reported to occur faster when stored at lower initial concentrations (Holzer, Mauerer et al. 1998; Saxena, Sadoqi et al. 2003).

Depending on the solvent, ICG may be found in the monomeric form or as a dimer or oligomer with absorption maxima at 780, 680 and 890 nm respectively (Holzer, Mauerer et al. 1998). Dimerization occurs at very low concentrations in water. In water and deuterated water at concentrations above 1.15 mg/ml ICG self-organizes into aggregates that lead to a red-shifted narrow absorption band that is the result of delocalized excitation by light (Holzer, Mauerer et al. 1998). This state is normally referred to as J-aggregation, and is characteristic of relatively high stability compared to

monomeric ICG. In organic solvents such as methanol or dimethyl sulfoxide, on the other hand, the critical concentration for dimerization is very high (Holzer, Mauerer et al. 1998). In human plasma dimerization occurs at about 387 μg/ml, although ICG normally exists as a conjugate with plasma proteins (Holzer, Mauerer et al. 1998).

Encapsulation of ICG within nanoparticles can protect ICG from rapid clearance and degradation, while at the same time modifying its biodistribution according to that of the nanoparticles. As will be discussed in this chapter, the instability of ICG greatly complicates characterization of nanoparticles loaded with this agent as it makes its quantification difficult. However, by choosing appropriate solvents and being meticulously careful with readings, it is possible to quantify ICG encapsulation efficiency and weight percentage within nanoparticles.

4.1.3 Gd-DTPA

Diethylenetriaminepentaacetic acid Gd (III) dihydrogen salt hydrate or gadopentetic acid (Gd-DTPA) is a gadolinium chelate approved for clinical use as a positive MRI contrast agent. It is currently marketed under the brand name of Magnevist® (Schering, Germany). Magnevist® distributes in the intravascular and extracellular fluid spaces, does not cross the blood brain barrier, and is excreted rapidly by glomerular filtration via the kidneys.

Gd-DTPA has a molecular weight of 548 g/mol. Its structure can be seen in Figure 4.1C. Gd-DTPA is a hydrophilic agent that is not soluble in alcohols. As such, encapsulation of this agent within the hydrophobic core of polymeric nanoparticles is a challenge. A water-in-oil-in-water method was investigated for its incorporation of this agent within nanoparticles, as described in the materials and methods section. This method is based on the modification of a microparticle formulation that was previously

reported (Faranesh, Nastley et al. 2004). Gd-DTPA provides the ability to visualize the interaction of nanoparticles with cells and tissue with electron microscopy and MRI.

4.2 MATERIALS AND METHODS

4.2.1 Materials

Rhodamine-6G was obtained from ACROS Organics. Indocyanine green, bovine serum albumin, sodium cholate hydrate and gadopentetic acid (Gd-DTPA) were obtained from Sigma-Aldrich (Saint Louis, MO, USA). Acetone, methanol and ethyl acetate were obtained from Fisher Scientific (Waltham, MA, USA) and were of HPLC grade. Poly(lactic-co-glycolic acid) (formerly PLGA 50:50 DL 2A, now 5050 DLGA 2A, 50/50 D,L-lactide to glycolide ratio, molecular weight 11,000, carboxylic acid and hydroxyl end groups) was obtained from LakeShore Biomaterials (Birmingham, AL, USA).

4.2.2 Preparation of Nanoparticles Loaded With Imaging Agents

The preparation methods described in Table 4.1 were utilized for encapsulation of imaging agents. The specific method of nanoparticle preparation depended mainly on the solubility properties of each of the imaging agents. Nanoparticles with rhodamine 6G or indocyanine green were prepared with oil-in-water nanoprecipitation or emulsification methods, while encapsulation of Gd-DTPA was carried out with the water-in-oil-in-water method. Figure 4.2 displays the general steps that were taken for the preparation of imaging agent-loaded particles.

4.2.2.1 Rhodamine Loaded Nanoparticles

RHO was first dissolved in acetone at concentrations ranging from 0.017 to 0.1 mg/ml. A volume of 3 to 4.35ml of this solution was then used to dissolve 100 mg of PLGA. This organic solution was then added to 10 ml of an aqueous solution containing 10 mg/ml of bovine serum albumin, vortexed and sonicated for 30 seconds to form a nanoparticle suspension. Organic solvents were evaporated by stirring under vacuum for 45 minutes. Nanoparticles were recovered by centrifugation for 10 minutes at 48,000xg with a refrigerated Beckman J2-21 centrifuge. The particles were washed three times by resuspending in surfactant solution through sonication and/or vortexing, followed by centrifugation. Supernatants from each centrifugation were collected for determination of the amount of the imaging agent that had not been encapsulated within nanoparticles. Small samples of the nanoparticle suspension were taken throughout the preparation procedure in order to identify and troubleshoot any step at which the particles aggregated. After 3 washes, the nanoparticle pellet was frozen at -20°C, freeze dried in a Labconco Freeze Dryer 4.5 for 2 days and stored at -20^{o}C.

4.2.2.2 Indocyanine Green Nanoparticles

ICG loaded nanoparticles were prepared similarly to RHO nanoparticles, except for the fact that ICG was first dissolved in methanol at a concentration of 2.5 to 10 mg/ml depending on the desired loading and then mixed with a solution of 100 mg of PLGA in 3 ml of acetone to form the organic phase. In addition, sodium cholate (SC) was used as the surfactant instead of bovine serum albumin. Sodium cholate has been widely used as a surfactant for nanoparticle preparation and has been observed to result in the

preparation of particles with smaller and more homogeneous size distributions (Lamprecht, Ubrich et al. 2001; Arica and Lamprecht 2005; Leo, Contado et al. 2006).

4.2.2.3 Gd-DTPA Nanoparticles

Nanoparticles loaded with Gd-DTPA were prepared by a water-in-oil-in-water process. Gd-DTPA was first dissolved in DI water at a concentration of 14 mg/ml. A volume of 100 to 500 µl of this solution was then added to a solution of 100 mg of PLGA in 3 ml of acetone or ethyl acetate, vortexed and sonicated for 1 minute to form a stable water-in-oil emulsion. This emulsion was then added to 10 ml of an aqueous solution of 10 mg/ml bovine serum albumin or sodium cholate, vortexed and sonicated until a homogeneous water-in-oil-in-water suspension was formed. The solvent was then removed by evaporation and the nanoparticles washed as described for RHO nanoparticles.

4.2.3 Nanoparticle Size

Particle size was determined using a Coulter Nanosizer or a dynamic light scattering (DLLS) based instrument (Brookhaven Instruments Corporation) from suspensions of nanoparticles in water. Particle sizes were determined during the preparation process by diluting samples of nanoparticle suspensions in DI water and after freeze drying by resuspending a small amount of dry nanoparticles in DI water with sonication.

4.2.4 Nanoparticle Morphology

Nanoparticle morphology was studied through scanning electron microscopy (SEM). A small amount of freeze dried nanoparticles was suspended in DI water with sonication and vortexing and dried at room temperature on top of a carbon conductive tab held on top of a aluminum sample disk. SEM samples were sputter coated with metal plasma and imaged with a Hitachi 4500 electron microscopy.

4.2.5 Agent Encapsulation Efficiency

Encapsulation efficiency (EE), or the percentage of the total amount of imaging agent used in the preparation that was actually encapsulated, was determined by quantifying the amount of agent found in supernatants collected during the cycles of nanoparticle washes ($M_{AGENT\text{-}Supernatants}$) and comparing it to the mass of agent used for nanoparticle preparation ($M_{AGENT\text{-}Preparation}$), as described in Equation 4.1.

$$EE = \frac{\left(M_{AGENT-Preparation} - M_{AGENT-Supernatants}\right)}{M_{AGENT-Preparation}} \cdot 100\% \qquad (4.1)$$

The mass of the RHO or ICG lost in the supernatants was determined by absorption spectroscopy using standard curves ($r^2 > 0.99$) of known concentrations of the agent in the respective surfactant solution (bovine serum albumin or sodium cholate solutions) used for nanoparticle suspension and washing. A Shimadzu UV-1201 UV/Vis spectrophotometer is with an optical range from 200 to 1100nm was used for this purpose. RHO absorbance was measured at the peak wavelength of 530 nm in bovine serum albumin solution, while ICG absorbance was read at 795 nm in sodium cholate and 800 nm in bovine serum albumin.

The mass of Gd-DTPA in supernatants was determined by elemental analysis using inductively-coupled mass spectroscopy (ICP-MS). A GBC Optimass 8000 ICP-MS instrument from the group of Dr. James Holcombe in the Department of Chemistry of The University of Texas at Austin was used for this purpose. ICP-MS is a highly-sensitive technique, being able to detect concentrations of Gd-DPTA in the range of 10^2 to 10^6 ppt, or 0.1 to 1000 ng/ml. Supernatants from nanoparticle purification steps were diluted from 100 to 10,000 times with deionized water and analyzed by introducing directly into the ICP-MS. Concentrations were determined by comparing the average intensity of the most commonly-occurring gadolinium isotopes –molecular weight of 152, 154, 155, 156, 157, 158, and 160 (Leland 1950) -- to a calibration curve based on known Gd-DTPA concentrations. The mass of Gd-DTPA in the supernatants was determined by multiplying the concentration by the total volume of each supernatant and the dilution factor. The encapsulation efficiency was determined by comparing the mass of Gd-DTPA found in the supernatants to that used for preparation of the nanoparticles.

4.2.6 Agent Loading

Loading, or the weight percent of the agent in the final formulation, was determined by dissolving a known mass of nanoparticles in an organic solvent and comparing the absorbance of these solutions to a standard curve ($r^2 > 0.99$) of known concentrations of the agent in the same organic solvent. Loading was calculated as described in Equation 4.2.

$$\text{Loading} = \frac{M_{\text{AGENT-IN-NPs}}}{M_{\text{NPs}}} \cdot 100\% \qquad (4.2)$$

RHO nanoparticles were dissolved in dichloromethane while ICG nanoparticles were dissolved in dimethylsulfoxide.

Determination of the loading of Gd-DTPA nanoparticles by ICP-MS by direct injection, as was done with supernatants, was not assessed as the presence of the polymer and surfactant was expected to cause problems with quantification. However, at the end of this part of the project, this was determined to not be a problem. Data for direct injection of nanoparticle suspensions is not presented here.

A Jeol 2010F transmission electron microscope with energy dispersive spectroscopy (EDS) capability was used as an alternative for elemental detection of gadolinium within solid Gd-DTPA nanoparticles. A single nanoparticle was focused , scanned and analyzed for its elemental composition.

4.2.7 *In Vitro* Agent Release Experiments

The release of rhodamine and ICG under simulated physiological conditions from nanoparticles was studied. A known mass of nanoparticles was suspended in a specific volume of 0.01M phosphate buffered saline, pH 7.4, and incubated in poly(carbonate) centrifuge tubes in a 37°C water bath. At specific time points, the samples were centrifuged for 15 minutes at 48,000xg and a portion of the supernatant was removed for analysis and replaced with fresh buffer. Absorption spectroscopy was used to determine the mass of agent released with time. Each set of data was run in independent triplicates. The average and standard deviation between repetitions was determined.

At the end of the release study, the nanoparticle suspension was centrifuged and all the supernatant was removed. The nanoparticle pellet was resuspended in water and centrifuged to remove excess buffer salts. The supernatant was again removed and the

pellet was freeze dried for determination of remaining dry weight and agent content by spectrophotometry.

4.2.8 Studies of Nanoparticle Interaction with Model Cancer Cells *In Vitro*

Human mammary gland adenocarcinoma cell line MDA-MB-231 was generously provided by Dr. Dharamawhardane, formerly from the Section of Molecular, Cell and Developmental Biology of The University of Texas at Austin. Cells were incubated at 37°C under a 5% CO_2 atmosphere and maintained with Dulbecco's Modified Eagle Medium (DMEM) supplemented with 10% fetal bovine serum, 1% HEPES buffer, 1% L-glutamine and 1% sodium pyruvate.

For microscopy studies, cells were seeded in four 6-well plates that contained a pre-sterilized coverslip at a concentration of 300,000 cells per well. A day after seeding, the cells were pre-treated with endocytosis inhibitors including 10mM ammonium chloride or 450mM sucrose for 1 hour, or 30μM cytochalasin D, 33μM nocodazole, or 1μg/ml filipin for 30 minutes. A separate plate of cells was placed incubated at 4C for 1 hour to study the effect of cell metabolism on the uptake or rhodamine or rhodamine-loaded nanoparticles. After the specific pre-treatment time, the cell media was replaced with media containing the appropriate inhibitor at the pre-treatment concentration and 100 μg/ml of rhodamine-loaded nanoparticles or the equivalent rhodamine concentration in solution (0.28 μg/ml – based on the loading for the batch used). After a 2 hour exposure to the rhodamine-containing formulations, the media was removed and cells were washed three times with Dulbecco's phosphate buffered saline (DPBS), fixed for 15 minutes in 3.7% formalin and again washed. Coverslips were then mounted onto microscopy slides using Fluoromount-G (Southern Biotech, Birmingham, AL, USA) to protect the samples. Microscopy slides were observed with a Leica SP2 AOBS confocal

microscope using laser sources at 476, 488 and 496 nm to excite rhodamine and detecting the fluorescence signal in the 550-650 nm range. All microscopy gain and offset settings were maintained constants throughout the study.

For flow cytometry studies, cells were seeded at a concentration of 500,000 cells per well in 6-well plates. Growth media was replaced with rhodamine-containing formulations 24 hours after seeding. The tested formulations included rhodamine-loaded nanoparticles, rhodamine in solution, blank nanoparticles and DPBS as a control. The concentrations used were 5, 50 and 500 μg/ml in DPBS for nanoparticles. Equivalent rhodamine solution concentrations of 0.014, 0.14 and 1.4 μg/ml were used based on a nanoparticle loading of 0.28 wt%. After exposure to these formulations for 2, 4 or 8 hours, cells were washed three times with DPBS and a cell suspension was created using trypsin/EDTA. Cells suspensions were diluted in growth media, centrifuged and washed three times with DPBS. Cells were finally resuspended in 1 ml of DPBS without Ca/Mg and immediately analyzed with a FACS Calibur flow cytometer (Beckton & Dickinson, Franklin Lakes, NJ, USA) using a 488nm laser for excitation of rhodamine and a band centered at 585 nm for detection of fluorescence. Flow cytometer channel voltage and gain were maintained constant throughout the analysis.

Flow cytometry data were processed to remove the events associated to free nanoparticles according to their light scattering properties. From the filtered data, the arithmetic mean of the fluorescence intensity of cells exposed to the various formulations was determined.

4.2.9 *In Vivo* Imaging Study with Indocyanine Green Nanoparticles

A preliminary study of *in vivo* fluorescence imaging was performed with ICG-loaded nanoparticles to determine if their ICG content was sufficiently high for *in vivo*

detection and to observe their biodistribution. These studies were done in collaboration with Dr. Keith Stantz from Purdue University, School of Health Sciences. ICG nanoparticles with a loading of 967 ng/mg were suspended in water at 2.5 mg/ml by sonication. Approximately 0.7 ml of this suspension was injected intravenously into mice. The mouse model had two xenographs of MCF-7 human breast adenocarcinoma cells, one originated with wild type (WT) cells and another of cells transfected with vascular endothelial growth factor (VEGF). Fluorescence images were obtained by photoacoustic computer tomography spectroscopy. Initial readings were done after injection of known concentrations of free ICG in solution to establish the concentration required for detection.

4.2.10 Statistical Analysis

Significant difference between the means of sample groups was determined using Sudent's t-test based on a confidence level of 95% ($p < 0.05$). Statistical analysis was performed for sizing, zeta potential, yield, encapsulation efficiency and loading data.

4.3 RESULTS AND DISCUSSION

4.3.1 Rhodamine Loaded Nanoparticles

Rhodamine nanoparticles were successfully prepared using nanoprecipitation by co-dissolving rhodamine and PLGA in acetone and precipitating the polymer into nanoparticles in an aqueous phase having bovine serum albumin as a stabilizer. Table 4.2 summarizes the results of RHO nanoparticle characterization. Batch mass recovery, or yield, ranged from the 70 to 90% and was not dependent on the loading of rhodamine.

The average nanoparticle size was of 290 nm before freeze drying and of 317 nm after freeze drying. No significant difference was observed in the size of the particles loaded with 0.15 or 0.30 wt% RHO compared to blank nanoparticles, or between samples of a given targeted loading before or after freeze drying ($p >> 0.05$). Approximately 86% encapsulation efficiencies were achieved. No statistically significant difference was observed between the encapsulation efficiency for the desired loading levels of 0.075, 0.15 or 0.30 wt% RHO. The actual weight percent of RHO that was found to be loaded within dissolved PLGA nanoparticles was very close to the targeted loading. Figure 4.3 is a scanning electron microscopy image of RHO loaded PLGA nanoparticles. As displayed, the nanoparticles have a spherical morphology and range in size between 150 and 300 nm, thus agreeing with the results described above.

In vitro release studies demonstrated that RHO-loaded nanoparticles were an optimal formulation for imaging studies because the hydrophobic RHO was released very slowly, as shown on Figure 4.4. Specifically, within 12 hours less than 15% of the agent had been released when incubated at 37°C at pH 7.4. On the other hand, and as described for doxorubicin-loaded nanoparticles in Chapter 3, at pH 4.0 the nanoparticles rapidly released the agent, with 75% being released within the same 12 hours. Importantly, controlled release of this fluorescent agent over a time period of 12 hours is sufficient for studying the interaction and uptake of nanoparticles by cells *in vitro*.

4.3.1.1 Cellular Studies with Rhodamine-Loaded Nanoparticles

Microscopy and flow cytometry studies of the interaction of rhodamine-loaded nanoparticles and breast cancer cells were conducted. Microscopy studies, as seen in Figure 4.5 and 4.6, show that the cells are able to uptake rhodamine both when presented in the form of nanoparticles or as a solution. Studies performed at 4°C showed that

rhodamine uptake was not an active process as the reduced metabolism of the cells under this condition did not seem to significantly decrease the level of rhodamine observed in the cells (Figure 4.6). This observation had also been reported for retinal pigment epithelial cells upon exposure to rhodamine-loaded poly(lactic acid) nanoparticles prepared by precipitation from dimethylsulfoxide (Bejjani, BenEzra et al. 2005). It is possible, then, that nanoparticle binding and uptake was mediated by interaction of residual albumin on the surface of the particles and albumin receptors on the cells. These receptors are normally involved in albumin transcytosis across endothelial tissue as have been recently suggested to be participants in the delivery of paclitaxel-albumin bound nanoparticles marketed under the name of Abraxane® (Green, Manikhas et al. 2006).

As can be seen in Figures 4.5 and 4.6, high level of nanoparticle adhesion to cells and culture substrate was observed. This made objective comparison of fluorescence intensities between the formulations more challenging, although there appeared to be higher fluorescence from the cells exposed to rhodamine-loaded nanoparticles. It is also important to note that rhodamine distributed throughout the cytoplasm of the cells, contrary to the nuclear localization observed with the chemotherapeutic agent doxorubicin as described in Chapter 3.

Flow cytometry was used in separate experiments to try to filter out the fluorescence associated with nanoparticles that were adhered to the cell culture substrate as opposed to being associated with the cells. For flow cytometry, suspensions of blank or rhodamine-loaded nanoparticles and cells were analyzed after exposure of adhered cells to nanoparticle suspensions or free rhodamine for specific periods of time. In these studies, laser light of a wavelength of 488 nm was focused on a narrow stream of the flowing suspension. Upon interaction of the light with a particle, which could be a polymeric nanoparticle or a cell, the light scattered in line with the laser source (forward

scattering) or perpendicular to it (side scattering), and the fluorescence produced by the sample were detected. As expected, nanoparticles resulted in significantly greater side scattering as a result of their high opacity while cells are able to scatter light in the forward direction in a much greater amount as a result of their low index of refractivity. This difference was used to separate the data of independent nanoparticles that had remained in the samples of cells exposed to nanoparticles as the purpose of the experiment was to obtain a quantitative measure of rhodamine (whether entrapped in attached or endocytosed nanoparticles or free) directly associated with the cells. Figure 4.7 shows the side and forward scattering of rhodamine-loaded and blank nanoparticles, and of control and nanoparticle-exposed cells.

After removal of the data of independent nanoparticles, the fluorescence associated which each cell after exposure to rhodamine in solution or in nanoparticles was determined. Figure 4.8A is a histogram that summarizes the number of events or cells recorded (counts) and the fluorescence intensity of each event after exposure of the cells for 4 hours with all the formulations. Figure 4.8B shows the arithmetic mean of the fluorescence intensity recorded in the cells exposed to each dosage. As can be seen in both of these figures, the fluorescence associated with cells exposed to rhodamine-loaded nanoparticles was significantly higher than that of cells exposed to rhodamine in solution for all concentrations and exposure times tested. No fluorescence was detected on cells exposed to blank nanoparticles or to DPBS (control). As can be seen in figure 4.8B, the fluorescence of cells exposed to rhodamine in solution appeared to decrease with exposure time. The fluorescence intensity of cells exposed to rhodamine-loaded nanoparticles increased from 2 to 4 hours but appeared to decrease after 8 hours of cell exposure. This observation could be a result of cellular efflux mechanisms since rhodamine molecules have been reported to be substrates for the P-glycoprotein (P-gP)

transmembrane receptor associated with multidrug resistance (Yoshimura, Shudo et al. 1990; Sarver, Klis et al. 2002). P-gP is overexpressed in cell lines that are resistant to chemotherapeutic agents, but could be expressed in normal levels by the MDA-MB-231 breast cancer cell line. This cell line is known to be sensitive to chemotherapeutic agents unless specifically adapted to grow under constant chemotherapeutic agent exposure (Schneider, Fuqua et al. 1990; de la Torre, Hao et al. 1993; Betancourt, Brown et al. 2007).

4.3.2 Indocyanine-Green Loaded Nanoparticles

Quantification of ICG for determination of encapsulation efficiency and loading was a difficult task as a result of the severe instability of ICG when dissolved in various media. An initial attempt to quantify the weight percent of ICG within nanoparticles was made by dissolving the particles in a mixture of 60:40 v/v% dichloromethane/methanol and utilizing absorbance spectroscopy for quantification. Interestingly, when running samples of ICG in this medium to create a standard curve, a rapid and linear decrease in absorbance was observed when an ICG solution sample was maintained under continuous illumination within the spectrophotometer, as shown in Figure 4.9A. The absorbance of a 0.977 μg/ml ICG solution in 60:40 v/v% dichloromethane/methanol decreased to about 1.5% of the original absorbance within 50 minutes. After 50 minutes of continuous illumination no further changes in absorbance were observed, although by then the absorbance was so low that any changes may not have been detectable by the instrument. Although continuous illumination of the sample was not necessary for quantification of ICG, the changes in absorbance occurred fast enough to be significant for the time of a single absorbance scan (about 2 minutes).

A second experiment was performed to determine if the rapid decrease in absorbance of ICG could be minimized by protecting the samples from both environmental and spectrophotometer light. The absorbance at 795 nm of a number of ICG solutions in 60:40 v/v% dichloromethane/methanol was obtained. No spectrum scans were done so that the time of light exposure was reduced to a few seconds. Figure 4.9A shows the effect of storage time on the absorbance of ICG solutions in this solvent mixture. It was found that a decrease in absorbance was also observed even when light exposure had been minimized. Interestingly, the rate of absorbance decrease was only slightly lower than that of the samples continuously illuminated in the spectrophotometer. For the 0.977 μg/ml sample stored in the dark, the absorbance decreased to about 4% the initial reading after 1 hour. These experiments pointed out the need to be extremely consistent and careful when utilizing absorbance spectroscopy for quantification of ICG.

As described earlier in this chapter, time and intensity of illumination, pH, solvent, concentration, temperature and other factors significantly affect the optical stability of ICG (Gathje, Steuer et al. 1970; Holzer, Mauerer et al. 1998; Saxena, Sadoqi et al. 2003; Saxena, Sadoqi et al. 2004). Since the type of solvent is one of the main factors determining the stability of ICG, the absorbance of this agent was probed in other solvents to determine if its stability could be improved compared to that in dichloromethane/methanol mixtures. Standard curves of ICG were procured in dimethyl sulfoxide (DMSO) as an alternative solvent for quantification of ICG within solid nanoparticles. The absorbance of ICG was observed to be stable and behave linearly DMSO for up to 17 hours when stored at 4°C and protected from light. Figure 4.10 shows the data for ICG solutions in DMSO at three concentrations and 2 different time points.

Table 4.3 displays the properties of the various formulations of ICG-loaded nanoparticles that were prepared. Yields ranged from 50 to 65% for all batches and did not depend on the amount of ICG used in the preparation. The average size of ICG-loaded particles ranged from 140 to 170 nm before freeze drying and increased to about 200 nm after freeze drying. Size was not found to be significantly different between the particles of different targeted loadings neither before nor after freeze drying ($p > 0.1$), as expected for the low loading of a small molecular weight agent. The size of these nanoparticles, which were prepared with sodium cholate as the surfactant, was smaller than that of blank or rhodamine-loaded nanoparticles prepared with bovine serum albumin as the surfactant (see Table 4.2). Nanoparticle size reduction and a more homogenous size distribution has been observed in the past with the use of sodium cholate as a surfactant compared to particles prepared with poly(vinyl alcohol) (Lamprecht, Ubrich et al. 2001; Arica and Lamprecht 2005; Leo, Contado et al. 2006).

Accurate determination of ICG encapsulation efficiency was not achieved as a result of ICG instability in aqueous solutions and the presence of small nanoparticles in the supernatants which could not be successfully centrifuged or filtered as a result of their small size. The presence of nanoparticles in the samples resulted in light scattering and higher absorbance values during spectrophotometric analysis. For these particles only determination of ICG loading from dissolved nanoparticles was deemed accurate.

The loading of ICG achieved was about two orders of magnitude lower than the targeted loading, but it was clearly dependent on the amount of ICG used for preparation of the particles ($p < 0.05$). Specifically, the loadings of ICG achieved ranged from 85 to 1028 ng of ICG per milligram of nanoparticles. It is possible that the maximum encapsulation of ICG within PLGA nanoparticles is controlled by the partitioning of ICG between the hydrophobic core of the particles and the outer aqueous phase. It is

expected, consequently, that if a lower amount of ICG were used to make the nanoparticles, even lower loadings would have been achieved. Alternative preparation methods that utilize specific affinities between ICG and nanoparticle contents or that prevent ICG diffusion into the outer emulsifying phase will need to be studied to achieve better loadings.

Results of *in vitro* release studies can be seen in Figure 4.11. An initial burst release of 15% of the ICG was observed within the first hour. By one day, 25% of the ICG had been released. After this, ICG release was controlled at constant rate over a period of 12 days. The initial burst release is most likely a result of rapid solubilization of ICG that had been adsorbed to the surface of the nanoparticles instead of encapsulated within their core. Once all adsorbed ICG has been dissociated, ICG within the particles is released through a combination of diffusion and degradation of the polymeric matrix.

4.3.2.1 In Vivo Imaging Study with ICG Nanoparticles

A preliminary study in mice was performed to determine if the ICG content that was achieved in the PLGA nanoparticles was adequate for its use as an image contrast agent. From initial readings with free ICG solution, it was determined that a concentration of 0.3μg/ml of ICG was required to detect a decent fluorescent signal within VEGF-transfected tumors. This concentration also resulted in enhanced signal in the liver and heart, while only a small enhancement was observed in the wild type tumor and muscle. Imaging after nanoparticle injection revealed that ICG-loaded nanoparticles were able to clearly highlight with the wild type tumor vasculature a high level of contrast. In the VEGF-transfected tumor, slight and non-uniform enhancement was observed shortly after injection but disappeared after 20 minutes. Figure 4.12 display the fluorescent image of a mouse after exposure to ICG nanoparticles and the relative levels

of fluorescence intensity in tissues compared to background, respectively. Similar images were obtained at 50, 200 and 500 ms. These results demonstrate that the ICG nanoparticles could be successfully imaged *in vivo* despite the low encapsulation efficiency and loading achieved.

Preferential distribution of ICG-loaded nanoparticles on wild-type tumor as opposed to VEGF-transfected tumor is possibly a result of tumor characteristics. The VEGF-transfected tumors were observed to have high blood flow and vascular blood volume in comparison to the wild type with dynamic contrast enhanced computer tomography. It is possible that high blood flow rates, and consequent low residence time, prevented nanoparticles from extravasating from the tumor vasculature of VEGF-transfected tumors.

4.3.3 Gd-DTPA Loaded Nanoparticles

Preparation of Gd-DTPA loaded nanoparticles was performed by a water-in-oil-in-water technique. A volume of 100 to 500 μl of Gd-DTPA solution was added to an organic solution of the polymer. This first mixture was then added to an outer aqueous phase containing a surfactant. Table 4.4 displays the various combinations of solvent, inner aqueous phase volume, outer aqueous phase surfactant and Gd-DTPA loading that were attempted. This table also displays the resulting nanoparticle sizes before and after freeze drying, and the percent recovery. For a given solvent/surfactant combination, the volume of the inner aqueous phase was increased with the purpose of achieving higher Gd-DTPA loading until the size of the particles became too large as a result of aggregation or un-controlled polymer precipitation.

As can be seen in Table 4.4, the best results were obtained using a combination of acetone and bovine serum albumin as this was the only method in which 500 μl of the

inner aqueous phase and a enough Gd-DTPA for a maximum loading of 6.4wt.% were incorporated without increasing the size of the particles above 1 μm. The size of these particles ranged from 218 to 340 nm before freeze drying and from 230 to 570nm after freeze drying. A scanning electron microscopy image of these particles is shown in Figure 4.13. Acceptable results were also obtained using a combination of ethyl acetate and sodium cholate, although the size of the particles increased significantly and even above 1 um after freeze drying, depending on the volume of the inner aqueous phase that was used. The remaining combinations, which included ethyl acetate with bovine serum albumin and acetone with sodium cholate, only allowed addition of 100-200 μl of Gd-DTPA solution before their size escalated. Figure 4.14 shows a scanning electron microscopy image of particles made with 500 μl of Gd-DTPA solution, ethyl acetate and bovine serum albumin. As can be seen, particles are visible but are surrounded by large polymer precipitates.

The yield of the formulations ranged from 50 to 80% for nanoparticles made with bovine serum albumin as a surfactant and from 30-60% for nanoparticles made with sodium cholate. As described for ICG nanoparticles previously, sodium cholate commonly results in smaller particle sizes and lower polydispersity. Lower nanoparticle sizes prior to freeze drying result in lower recovery as a result of the centrifugation process.

Quantification of Gd-DTPA in aqueous supernatants collected during nanoparticle preparation by ICP-MS led to inconclusive results. Numerous variables resulted in highly inconsistent encapsulation efficiency values, including the need for dilution of samples to up to 10,000 times their initial concentration, the need for creating standard curves of concentrations in the parts-per-trillion concentration range, possible contamination of samples with low levels of gadolinium in the laboratory, and instrument

instability during readings. For a single control sample containing 10,000 ppt Gd-DTPA, the concentration between runs varied by up to 30% as a result of instrument stability issues. When the supernatants of a single batch were run on two different occasions, the encapsulation efficiency was determined to be 40.1% the first time and 12.5% the second time. In any case, the need for substantial dilution of supernatants demonstrated the low encapsulation efficiency of Gd-DTPA within PLGA nanoparticles.

Energy dispersive spectroscopy analysis of Gd-DTPA loaded nanoparticles via transmission electron microscopy was able to identify the presence of gadolinium within a single nanoparticle, as shown on Figure 4.15, although the signal is very close to the noise level. Elemental analysis of that sample revealed that Gd was approximately 0.07% of the weight of the nanoparticle.

4.4 CONCLUSIONS

Emulsification and nanoprecipitation methods were utilized for preparation of poly(lactic-co-glycolic acid) nanoparticles loaded with the imaging agents RHO, ICG and Gd-DTPA. Various modifications to the preparation protocols were investigated to try to achieve nanoparticles of properties similar to those of drug-loaded particles that were described in Chapter 3, but with sufficient imaging agent loading to be used for imaging studies.

RHO particles were prepared through nanoprecipitation of a solution of PLGA, rhodamine and acetone after addition to an aqueous phase containing bovine serum albumin as a stabilizer. *In vitro* studies with RHO nanoparticles revealed that MDA-MB-231 breast cancer cells were better able to intake this agent when presented in the form of a nanoparticle suspension rather than as a rhodamine solution, result that agrees with what was observed with doxorubicin-loaded nanoparticles in Chapter 3.

Indocyanine green particles were best prepared by first dissolving it in methanol, mixing the solution with a polymer-acetone solution and then precipitating the polymer upon addition to an aqueous phase containing sodium cholate. Although the loading achieved was much lower than desired, an *in vivo* study revealed that ICG content was sufficient for detection through photoacoustic computer tomography spectroscopy.

Gd-DTPA-loaded nanoparticles were obtained by oil-in-water-in-oil methods using acetone or ethyl acetate as the solvent and bovine serum albumin or sodium cholate as the surfactant in the outer aqueous phase. Determination of actual Gd-DTPA loading within nanoparticles was unsuccessful although EDS analysis was able to identify its presence on a single nanoparticle even if at low levels.

Although use of alternative methods of nanoparticle preparation could have resulted in higher loading of ICG and Gd-DTPA, this would also have resulted in nanoparticles with properties different from those of the chemotherapeutic agent-loaded particles described in Chapter 3. Dissimilar physiochemical characteristics between the therapeutic and imaging nanoparticles would surely result in different interactions with biological systems, and consequently would not be representative of one another.

Up to this point, research efforts resulted in the preparation of biodegradable nanoparticles which could deliver a high payload of the chemotherapeutic agent doxorubicin in a pH-dependent manner, and at least two similar formulations containing imaging agents for *in vitro* cellular studies. The following chapter describes the modification of these preparations for incorporation of poly(ethylene glycol) on the surface of the nanoparticles in order to improve the fate of the particles *in vivo* and to provide external sites for conjugation of targeting agents.

Table 4.1 Properties of imaging agents and methods used for their encapsulation and quantification

Imaging Agent	Type	Imaging Method	Solubility	Particle Preparation Method	Agent Quantification
Rhodamine 6G	Fluorophore	Fluorescence microscopy	Soluble in water, alcohols and organic solvents	o/w	Absorbance spectroscopy
Indocyanine Green	Fluorophore	---	Soluble in water and alcohols	o/w	Absorbance spectroscopy
Gd-DTPA	Electron Dense Paramagnetic	Electron microscopy	Water soluble	w/o/w	Inductively-coupled mass spectroscopy (ICP-MS)

Abbreviations:
o/w oil-in-water
w/o/w water-in-oil-in-water

Table 4.2 Properties of rhodamine-loaded poly(lactic-co-glycolic acid) nanoparticles. Values shown are the average ± standard deviation for samples of a given targeted loading.

Targeted Rhodamine Loading (wt. %)	Number of Samples	Batch Yield (%)	Size Before Freeze Drying (nm)	Size After Freeze Drying (nm)	Encapsulation Efficiency (%)	Loading (wt. %)
0	4	74.1 ± 3.9	293 ± 32	332 ± 104	---	---
0.075	2	81.5 ± 2.8	376 ± 109	310 ± 153	90 ± 0.4	0.08 ± 0.002
0.15	4	82.8 ± 3.6	258 ± 54	333 ± 219	83 ± 8	0.15 ± 0.03
0.3	4	79.1 ± 7.6	282 ± 63	291 ± 51	90 ± 8	0.29 ± 0.01

Table 4.3 Properties of Indocyanine Green (ICG)-loaded poly(lactic-co-glycolic acid) nanoparticles. Values displayed are averages ± standard deviation for samples of a given targeted loading.

Targeted ICG Loading (wt. %)	Number of Samples	Yield (%)	Size Before Freeze Drying (nm)	Size After Freeze Drying (nm)	Actual ICG Loading (wt. %)	Actual ICG Loading (ngICG / mgNP)
1.22	4	55.6 ± 2.1	142 ± 10	205 ± 46	0.009 ± 0.004	85.0 ± 36
2.41	8	53.3 ± 5.3	166 ± 26	194 ± 28	0.014 ± 0.005	139.5 ± 49
4.71	8	51.2 ± 8.6	172 ± 32	207 ± 19	0.028 ± 0.151	284.1 ± 151
9.07	2	64.6 ± 2.0	152 ± 10	157 ± 1.2	0.103 ± 0.009	1028.5 ± 86

Table 4.4 Properties of Gd-DTPA loaded poly(lactic-co-glycolic acid) nanoparticles

Surfactant Type	Solvent Type	Volume of Inner Aqueous Phase (ul)	Targeted Loading (wt. %)	Number of Samples	Size Before Freeze Drying (nm)	Size After Freeze Drying (nm)	Yield (mg)
Bovine Serum Albumin	Acetone	100	1.4	5	234 ± 60	228 ± 43	66 ± 11
		500	3.6	4	218 ± 13	226 ± 12	79 ± 2
		500	6.4	8	343 ± 69	570 ± 513	72 ± 4
Bovine Serum Albumin	Ethyl Acetate	100	1.4	1	168	354	53
		200	2.7	1	189	236	47
		300	4	1	> 3,000	---	---
		400	5.2	2	> 3,000	---	---
		500	3.6	4	> 3,000	---	---
		500	6.5	2	> 3,000	---	---
Sodium Cholate	Acetone	100	1.4	1	188	144	56
		200	2.7	1	> 3,000	---	---
		300	4.0	1	> 3,000	---	---
Sodium Cholate	Ethyl Acetate	200	2.7	1	247	749	27
		300	4	1	251	214	28
		400	5.3	1	896	896	34
		500	6.5	1	453	1400	33

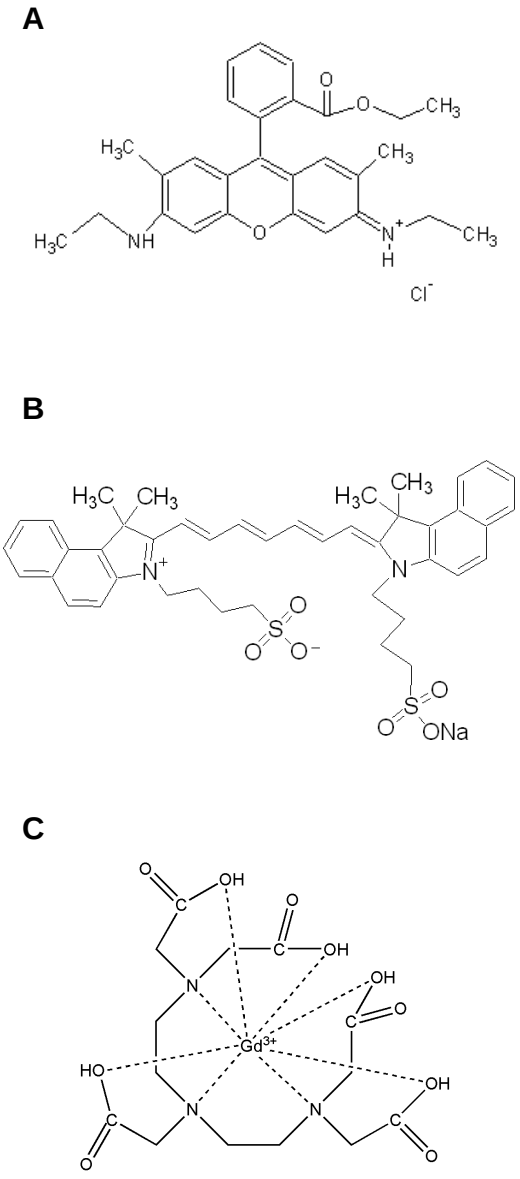

Figure 4.1 Chemical structure of (A) Rhodamine 6G, (B) indocyanine green and (C) gadopentetic acid

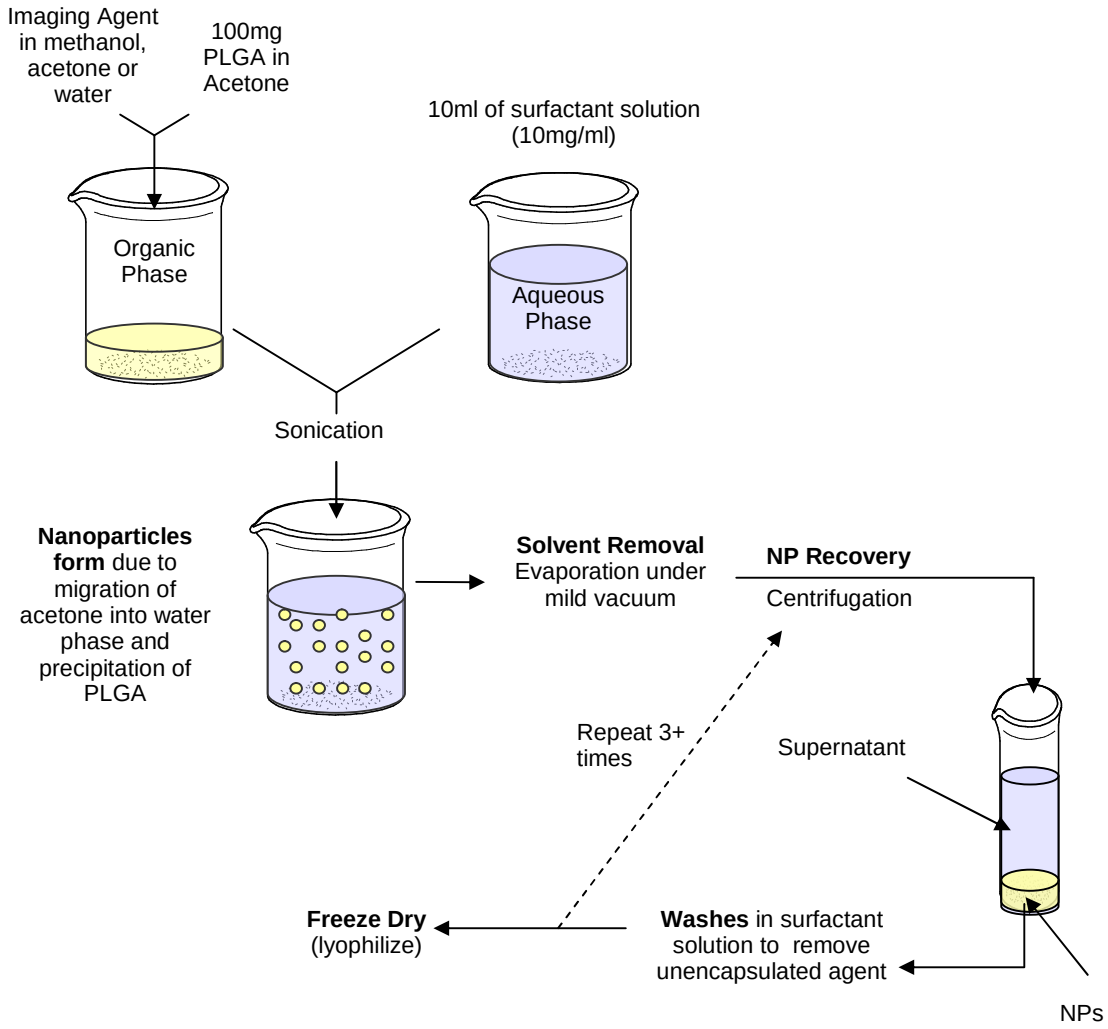

Figure 4.2 Schematic of preparation of PLGA nanoparticles loaded with imaging agents.

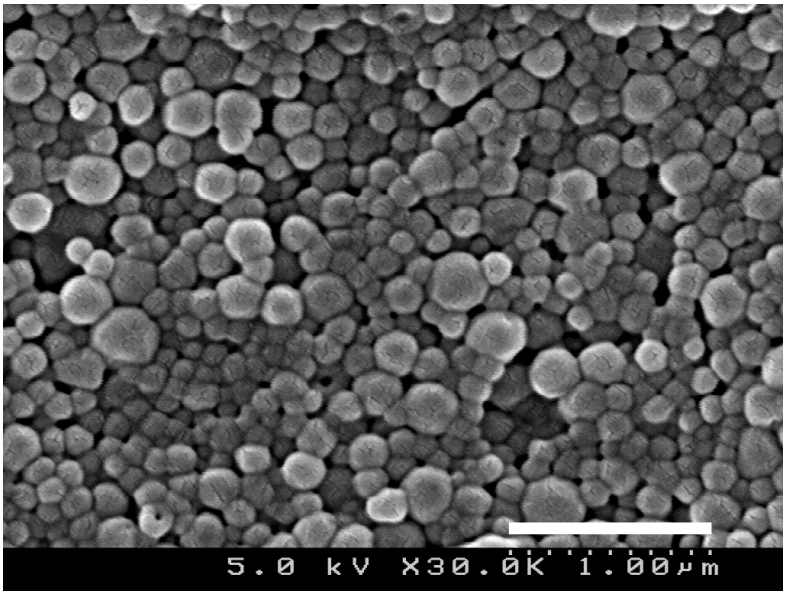

Figure 4.3 Scanning electron microscopy image of rhodamine-loaded poly(lactic-co-glycolic acid) nanoparticles. White bar represents a length of 1µm.

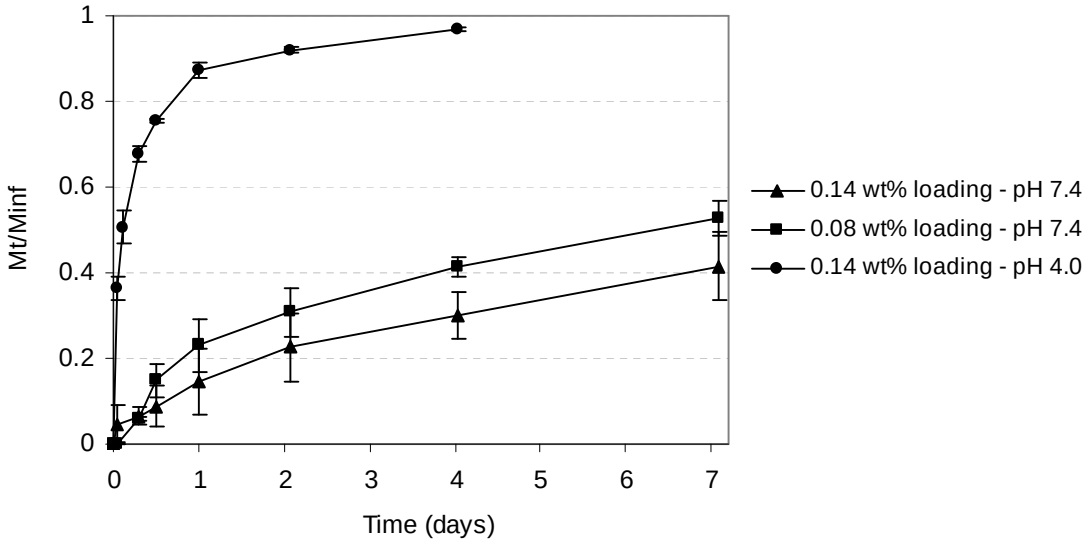

Figure 4.4 *In vitro* release of rhodamine from poly(lactic-co-glycolic acid) nanoparticles as a function of rhodamine loading and pH. The y axis, M_t/M_{inf}, corresponds to the cumulative fraction of rhodamine mass released (Mt) over time compared to the total mass of rhodamine that was released or found in the remaining nanoparticles (M_{inf}). Y bars represent the standard deviation between 3 independent samples for each condition.

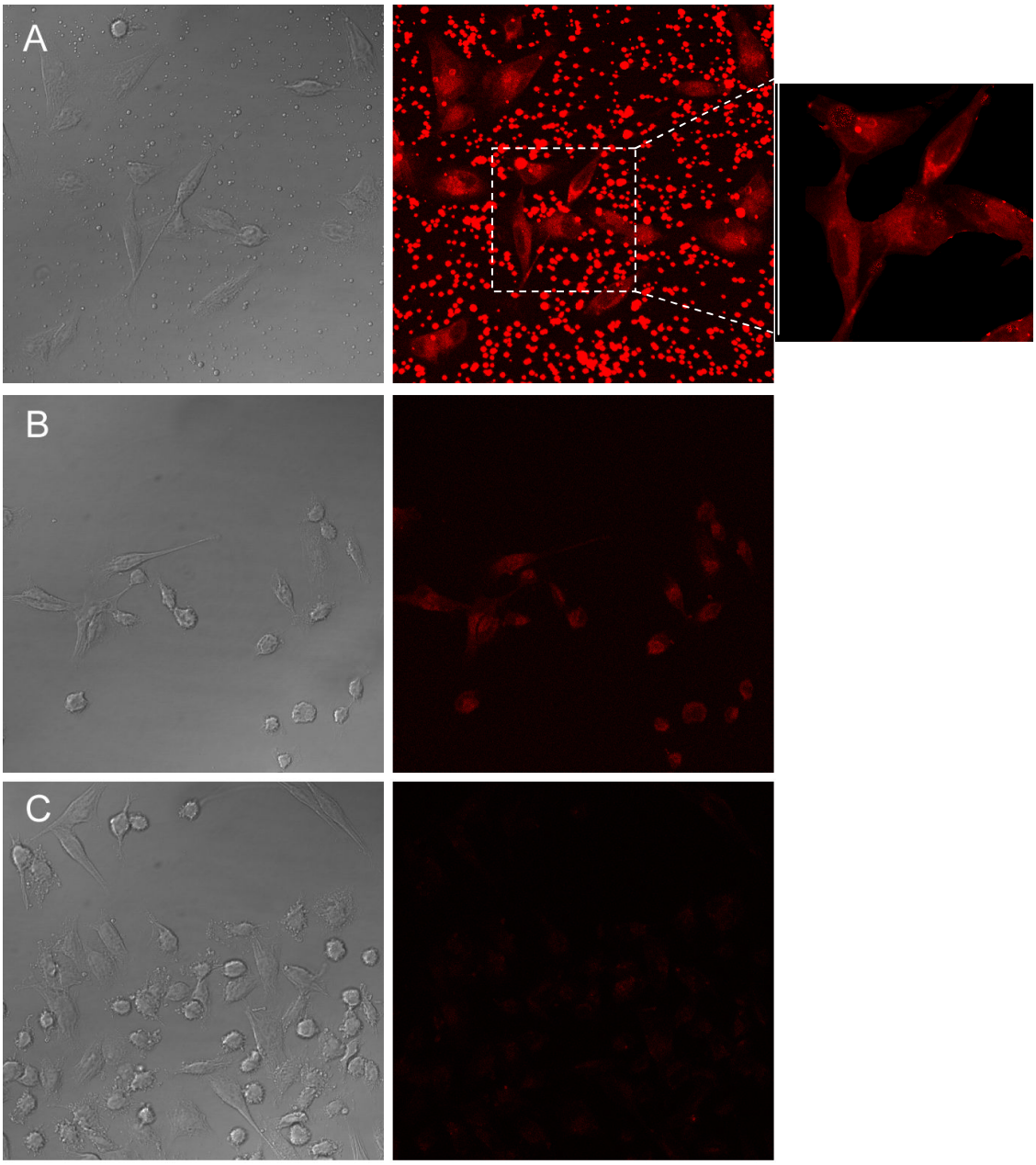

Figure 4.5 Confocal microscopy images at the plain of maximum cellular fluorescence of MDA-MB-231 breast cancer cells after exposure to (A) rhodamine loaded nanoparticles, (B) rhodamine in solution or (C) growth media as a control for 2 hours at 37°C. Cells were exposed to 280 ng/ml of rhodamine or to equivalent nanoparticle concentrations based on rhodamine loading.

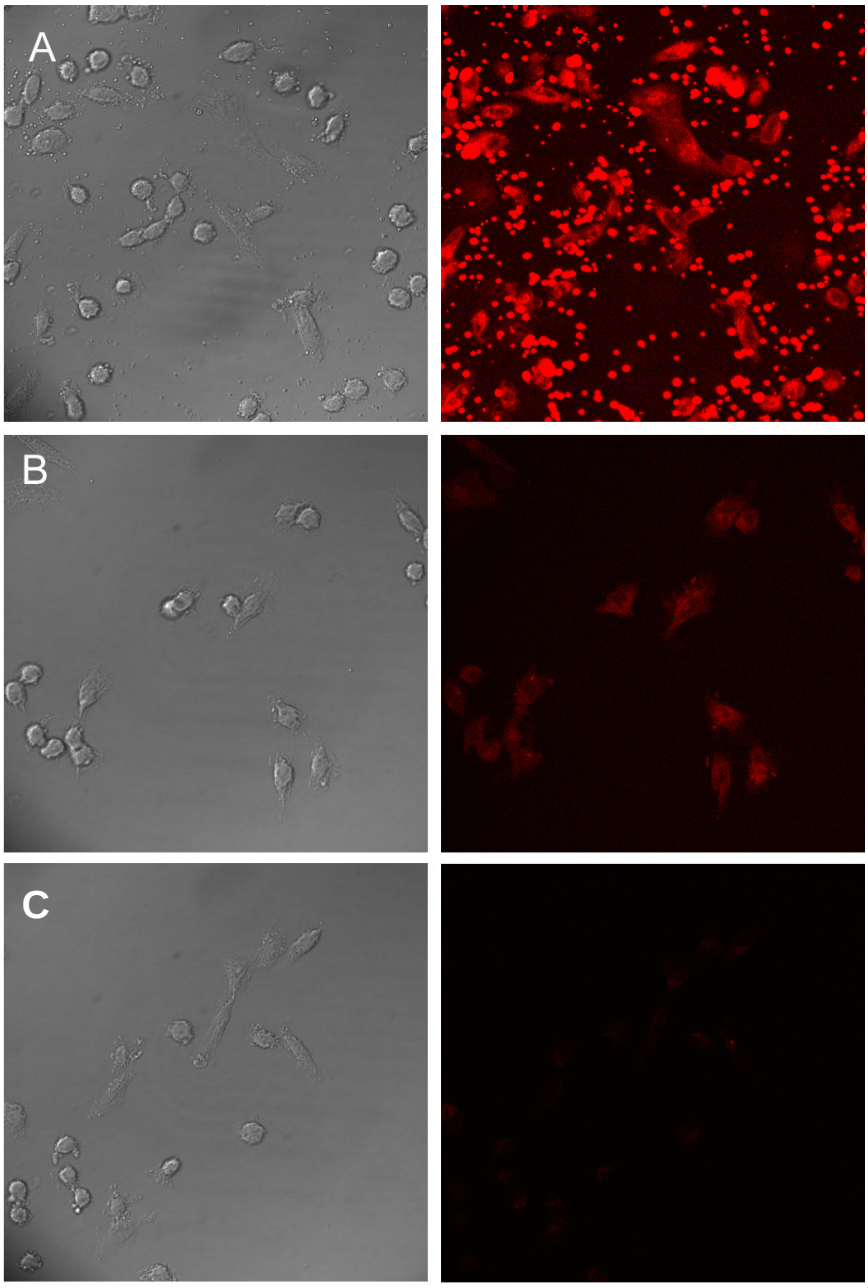

Figure 4.6 Confocal microscopy images at the plain of maximum cellular fluorescence of MDA-MB-231 breast cancer cells after exposure to (A) rhodamine loaded nanoparticles, (B) rhodamine in solution or (C) growth media as a control for 2 hours at 4°C. Cells were exposed to 280 ng/ml of rhodamine or to equivalent nanoparticle concentrations based on rhodamine loading.

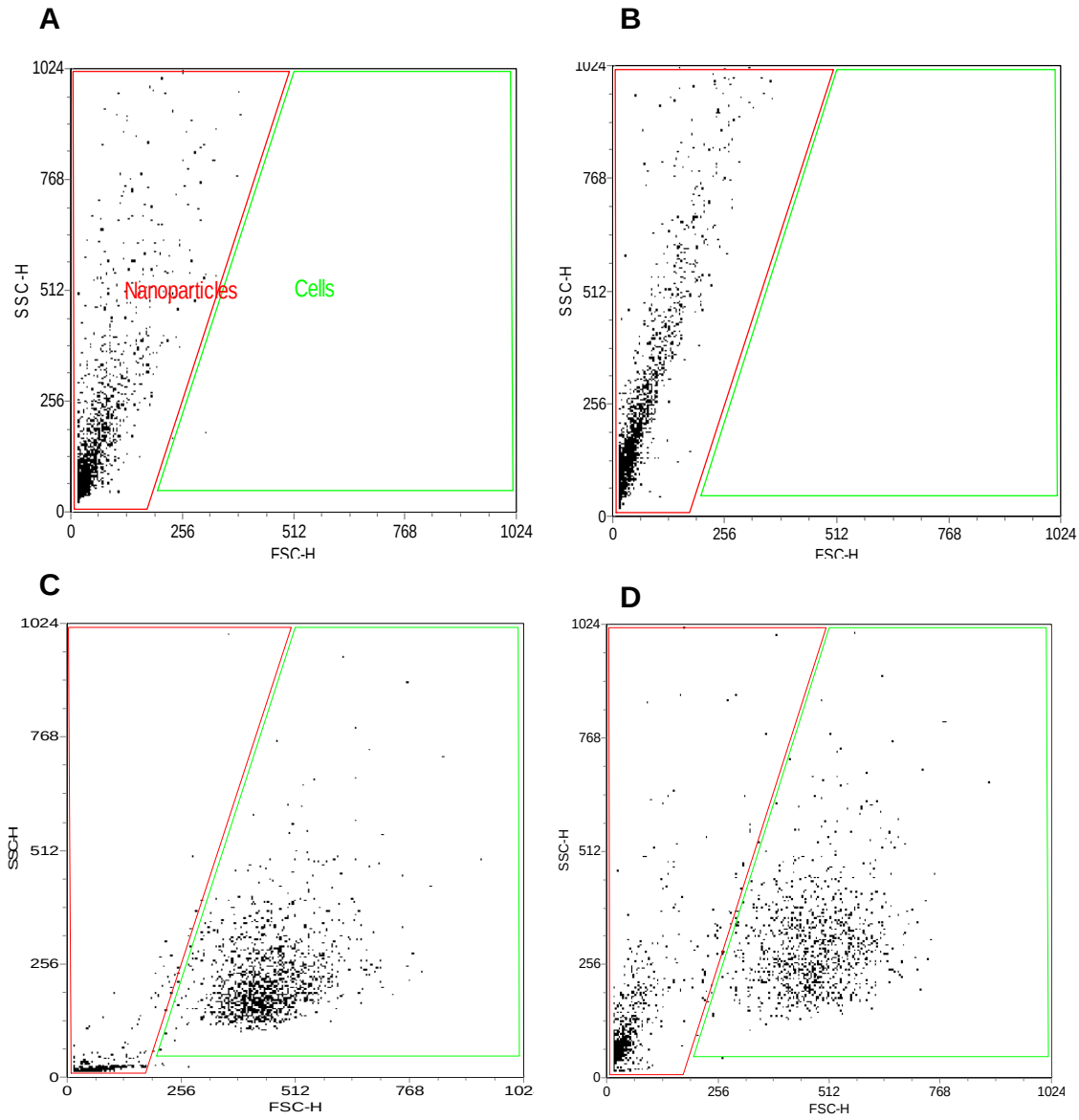

Figure 4.7 Plot of forward versus side scattering (x and y axis, respectively) of nanoparticle or cell suspensions obtained after flow cytometry analysis. Scattering profile of (A) rhodamine-loaded nanoparticles, (B) blank nanoparticles, (C) MDA-MB-231 breast cancer cells and (D) cells exposed to rhodamine-loaded nanoparticles. Red- and green-lined regions on each plot represent the gates used for separating the data associated with nanoparticles or cells, respectively.

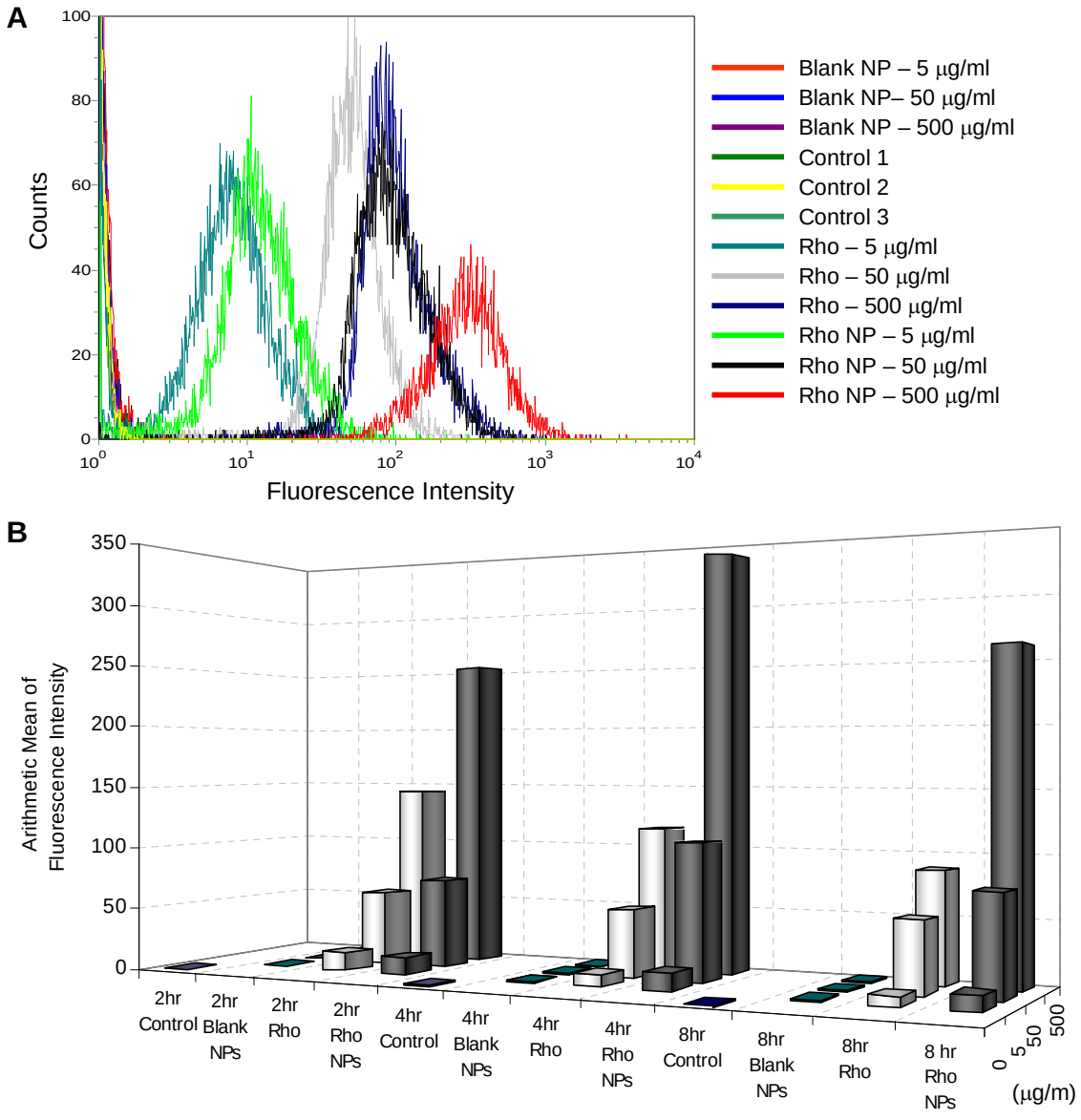

Figure 4.8 Fluorescence intensity of cells exposed to rhodamine (RHO)-loaded nanoparticles or free RHO in solution obtained by flow cytometry. Fluorescence associated with independent nanoparticles has been removed. (A) Histogram of fluorescence intensity of cells exposed to blank nanoparticles, RHO in solution or RHO-loaded nanoparticles for 4 hours at nanoparticle concentrations of 5, 50 and 500 μg/ml. (B) Arithmetic average of the fluorescence intensity of cells exposed to the same formulations for 2 or 4 hours. RHO solution concentrations for cell exposure were determined according to the loading of the RHO-loaded nanoparticles.

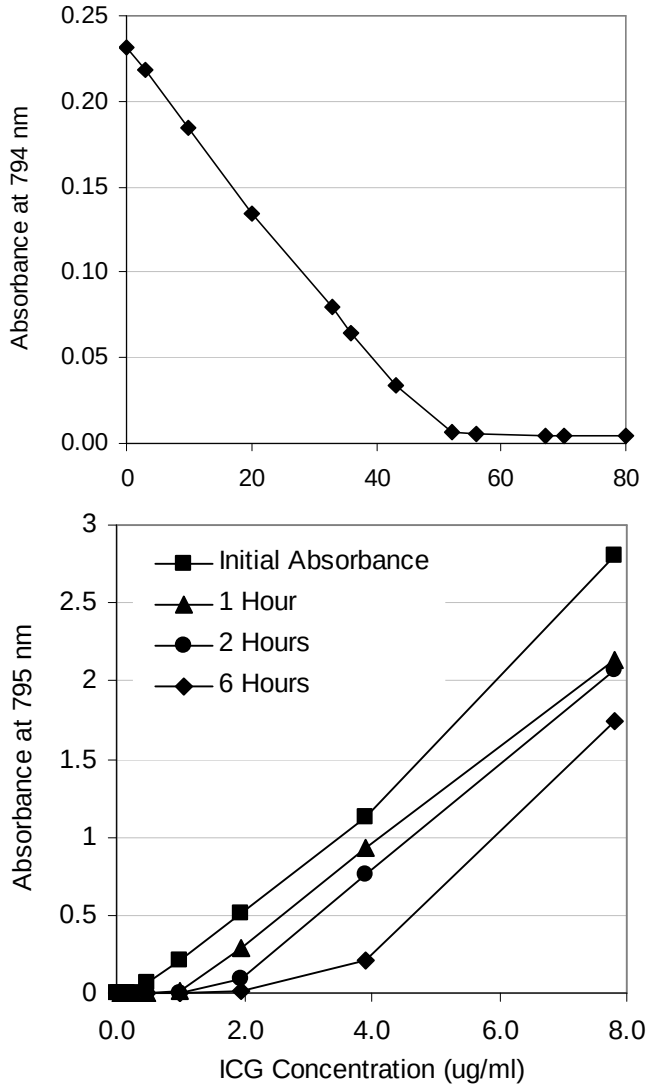

Figure 4.9 (A) Effect of illumination and storage time on indocyanine green (ICG) absorbance. A 0.977 μg/ml sample of ICG in a 60/40 v/v% dichloromethane/methanol was continuously illuminated in a Shimadzu UV-1201 spectrophotometer. Absorbance readings at the peak wavelength of 794 nm were taken at specific time points. (B) Time-dependence of absorbance of ICG at 795 nm in 60/40 v/v% dichloromethane/methanol after storage at room temperature for specific time periods in the dark. Samples were exposed to the spectrophotometer light for only a few seconds.

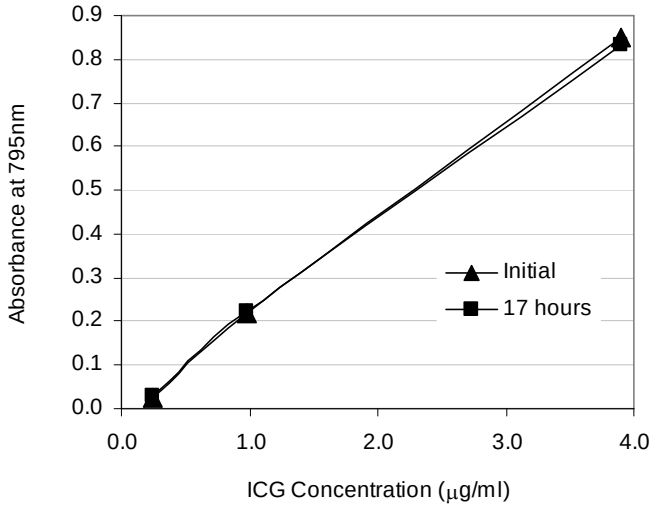

Figure 4.10 Concentration and time dependence of absorbance of indocyanine green (ICG) dissolved in dimethyl sulfoxide initially and after 17 hours of storage at 4°C in the dark.

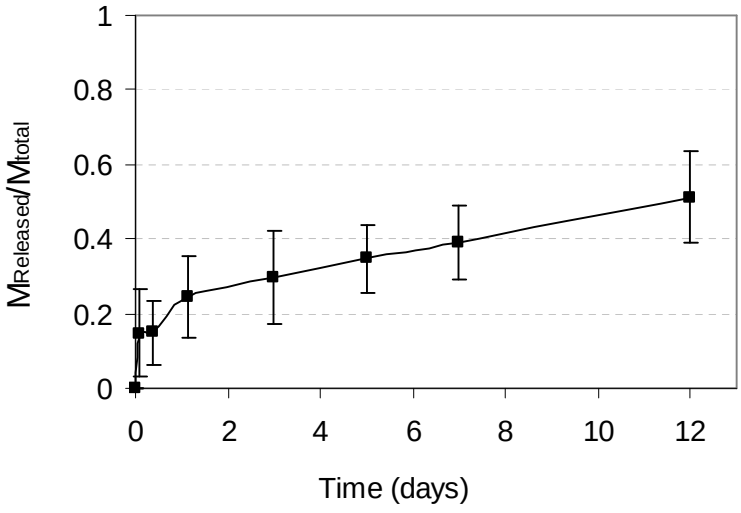

Figure 4.11 *In vitro* release of ICG from poly(lactic-co-glycolic acid) nanoparticles. Nanoparticles with a loading of 967 ngICG/mg were suspended in 0.01M phosphate buffered saline, pH 7.4, and at 37°C.

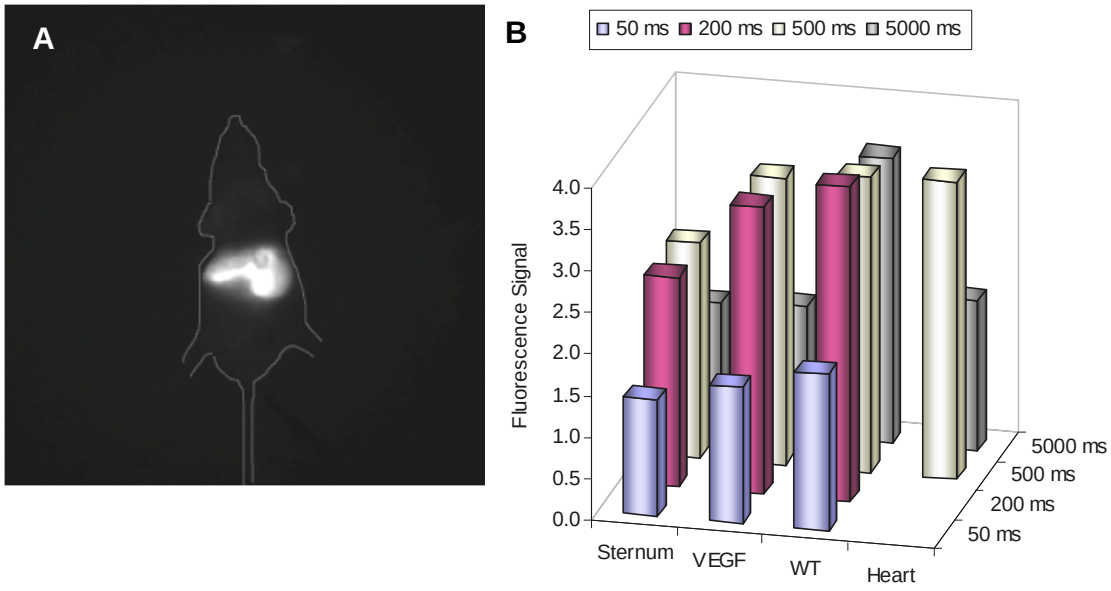

Figure 4.12 Results of *in vivo* imaging study with ICG nanoparticles. ICG nanoparticles were intravenously injected into mice that had a xenografts of wild-type (WT) and vascular endothelial growth factor (VEGF)-transfected human MCF-7 breast cancer cells. Photoacoustic computer tomography spectroscopy was used to detect the fluorescent signal from ICG. (A) Fluorescent image obtained with and ICG filter displays biodistribution of ICG nanoparticles and enhancement of tumor tissue. (B) Fluorescence intensity in sternum, tumors, and heart, relative to background at 50, 200, 500 and 5000 ms after injection.

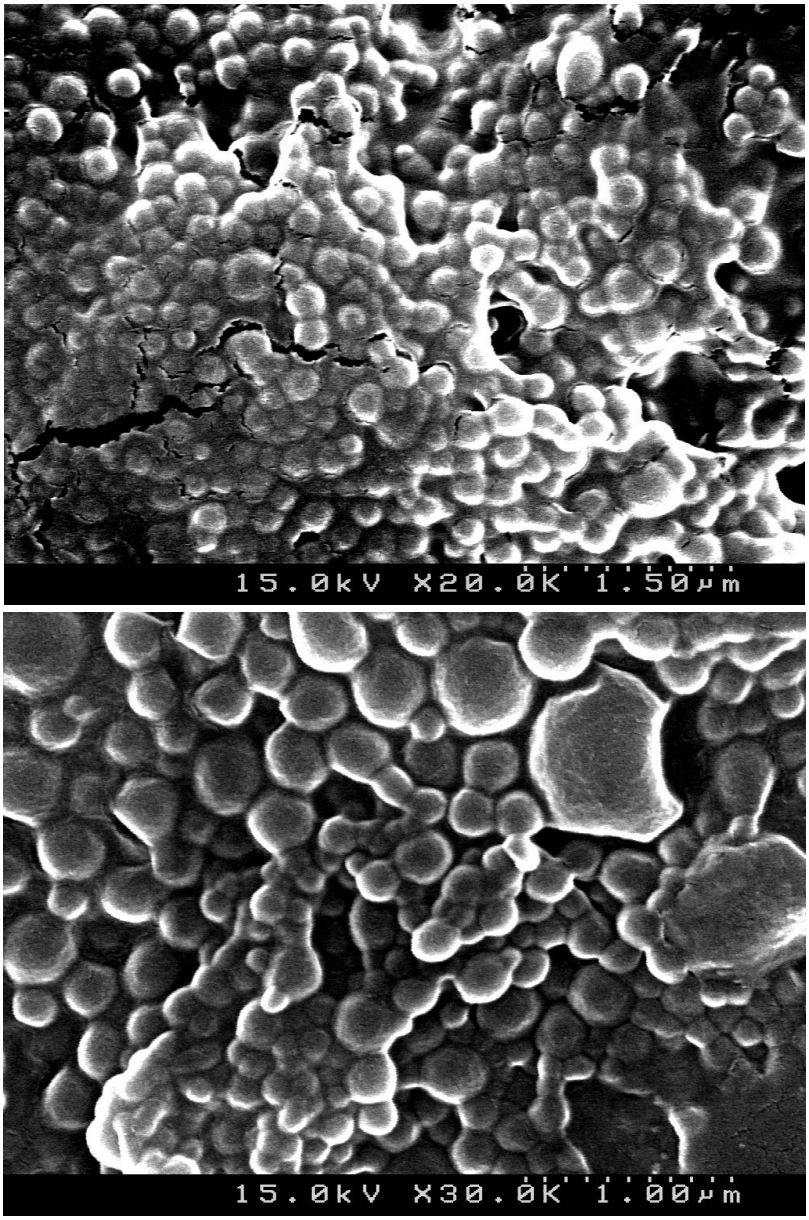

Figure 4.13 Scanning electron microscopy image of Gd-DTPA loaded particles prepared with acetone as the organic solvent, 500 µl of 7.6 mg/ml Gd-DTPA solution as the inner aqueous phase and bovine serum albumin solution as the outer aqueous phase. Particles are roughly spherical and are 200-300 nm.

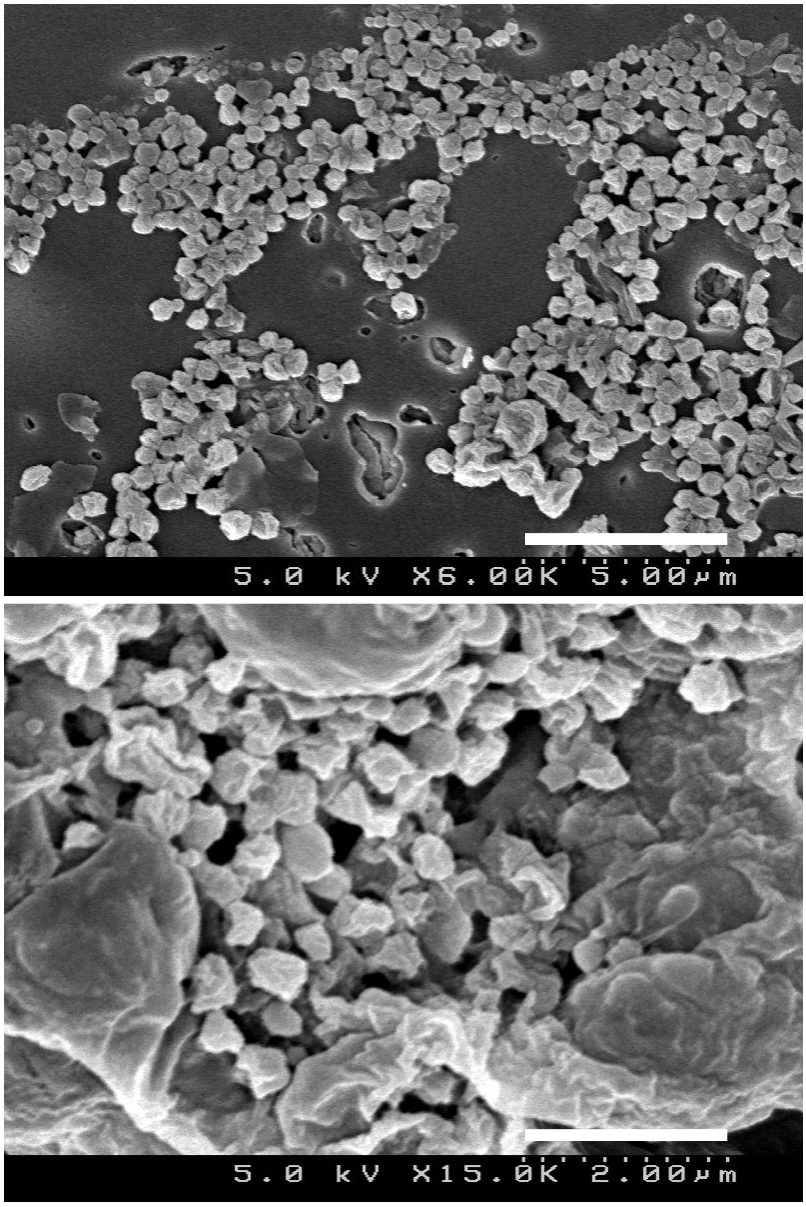

Figure 4.14 Scanning electron microscopy image of Gd-DTPA loaded particles prepared with ethyl acetate as the organic solvent, 500 µl of 14 mg/ml Gd-DTPA solution as the inner aqueous phase and bovine serum albumin solution as the outer aqueous phase. Particles in the size range of 500 nm are visible but are surrounded by a much larger polymeric precipitate. The morphology of the particles is corrugated. Bar represents 5 µm and 2 µm on the top and bottom images, respectively.

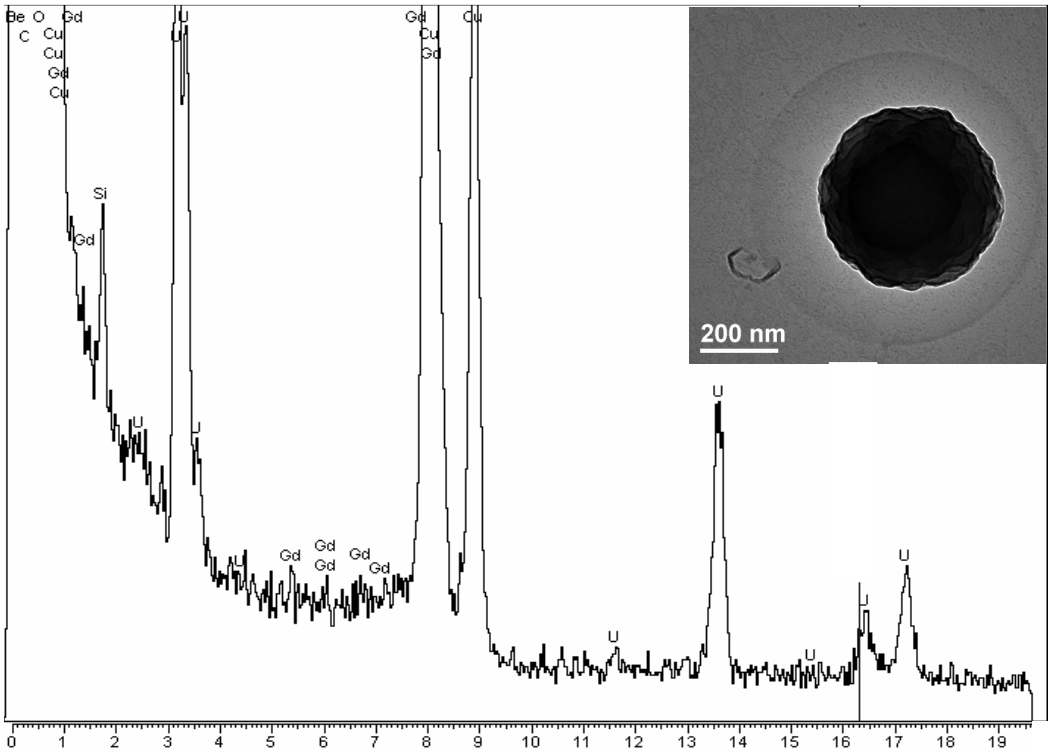

Figure 4.15 Transmission electron microscopy image and corresponding energy dispersive spectra (EDS) of poly(lactic-co-glycolic acid) nanoparticle loaded with Gd-DTPA . This batch of particles was prepared with acetone as the organic solvent, 500 μl of 7.8 mg/ml Gd-DTPA solution as the inner aqueous phase and bovine serum albumin solution as the outer aqueous phase. Gadolinium is identified in a single nanoparticle although most peaks are very close to the noise level.

4.5 REFERENCES

Arica, B. and A. Lamprecht (2005). "*In vitro* Evaluation of Betamethasone-Loaded Nanoparticles." Drug Development and Industrial Pharmacy 31(1): 19-24.

Bejiani, R. A., D. BenEzra, et al. (2005). "Nanoparticles for gene delivery to retinal pigment epithelial cells." Molecular Vision 11: 124-132.

Betancourt, T., B. Brown, et al. (2007). "Doxorubicin-loaded PLGA nanoparticles by nanoprecipitation: preparation, characterization and *in vitro* evaluation." Nanomedicine 2(2): 219-232.

de la Torre, M., X. Y. Hao, et al. (1993). "Characterization of four doxorubicin adapted human breast cancer cell lines with respect to chemotherapeutic drug sensitivity, drug resistance associated membrane proteins and glutathione transferases." Anticancer Research 13(5A): 1425-1430.

Desmettre, T., J. M. Devoisselle, et al. (2000). "Fluorescence properties and metabolic features of indocyanine green (ICG) as related to angiography." Survey of Ophthalmology 45(1): 15-27.

Faranesh, A. Z., M. T. Nastley, et al. (2004). "*In vitro* release of vascular endothelial growth factor from gadolinium-doped biodegradable microspheres." Magnetic Resonance in Medicine 51(6): 1265-1271.

Gathje, J., R. R. Steuer, et al. (1970). "Stability studies on indocyanine green dye." J Appl Physiol 29(2): 181-5.

Gear, A. R. (1974). "Rhodamine 6G. A potent inhibitor of mitochondrial oxidative phosphorilation." Journal of Biological Chemistry 249(11): 3628-3637.

Green, M. R., G. M. Manikhas, et al. (2006). "Abraxane, a novel Cremophor-free, albumin-bound particle form of paclitaxel for the treatment of advanced non-small-cell lung cancer." Annals of Oncology 17(8): 1263-1268.

Holzer, W., M. Mauerer, et al. (1998). "Photostability and thermal stability of indocyanine green." J Photochem Photobiol B 47(2-3): 155-64.

Hu, S., H. Zhao, et al. (2007). "Role of mitochondria in silica-induced apoptosis of alveolar macrophages: inhibition of apoptosis by rhodamine 6G and N-acetyl-L-cysteine." Journal of Toxicology and Environmental Health. Part A. 70(17): 1403-1415.

Kalliokoski, K. K., C. Scheede-Bergdahl, et al. (2006). "Muscle perfusion and metabolic heterogeneity: insights from noninvasive imaging techniques." Exerc Sport Sci Rev 34(4): 164-70.

Lamprecht, A., N. Ubrich, et al. (2001). "Design of rolipram-loaded nanoparticles: comparison of two preparation methods." Journal of Controlled Release 71(3): 297-306.

Leland, W. T. (1950). "The Isotopic Composition of Scandium, Gadolinium, and Dysprosium." Physical Reviews 77(5): 634-640.

Leo, E., C. Contado, et al. (2006). "Nanoparticle formulation may affect the stabilization of an antiischemic prodrug." International Journal of Pharmaceutics 307(1): 103-113.

Sarver, J. G., W. A. Klis, et al. (2002). "Microplate screening of the differential effects of test agents on Hoechst 33342, rhodamine 123, and rhodamine 6G accumulation in breast cancer cells that overexpress P-glycoprotein." Journal of Biomolecular Screening 7(1): 29-34.

Saxena, V., M. Sadoqi, et al. (2003). "Degradation kinetics of indocyanine green in aqueous solution." J Pharm Sci 92(10): 2090-7.

Saxena, V., M. Sadoqi, et al. (2004). "Enhanced photo-stability, thermal-stability and aqueous-stability of indocyanine green in polymeric nanoparticulate systems." J Photochem Photobiol B 74(1): 29-38.

Schneider, S. L., S. A. Fuqua, et al. (1990). "Isolation and characterization of an adriamycin-resistant breast tumor cell line." *In vitro* Cellular & Developmental Biology 26(6): 621-628.

Tang, H. W., X. B. Yang, et al. (2007). "Probing intrinsic and extrinsic components in single osteosarcoma cells by near-infrared surface-enhanced Raman scattering." Analytical Chemistry 79(10): 3646-3653.

Vila, A., H. Gill, et al. (2004). "Transport of PLA-PEG particles across the nasal mucosa: effect of particle size and PEG coating density`." Journal of Controlled Release 98(2): 231-244.

Vila, A., A. Sanchez, et al. (2004). "PEG-PLA nanoparticles as carriers for nasal vaccine delivery." Journal of Aerosol Medicine 17(2): 174-185.

Yoshimura, A., N. Shudo, et al. (1990). "Novel screening method for agents that overcome classical multidrug resistance in a human cell line." Cancer Letters 50(1): 45-51.

CHAPTER 5

STRATEGIES FOR PEGYLATION OF NANOPARTICLES

5.1 INTRODUCTION

As mentioned in Chapter 2, nanoparticle-based drug delivery systems are rapidly removed from the circulation upon intravenous injection by the reticuloendothelial system (Fawaz, Bonini et al. 1993; Brannon-Peppas and Blanchette 2004). Removal is dictated by the rapid absorption of plasma proteins, or opsonins, on the surface of the particles, which leads to recognition and sequestration by the Kupffer cells in the liver and macrophages in the spleen, both of which are part of the macrophage phagocytic system (Avgoustakis 2004). The short residence time of particulate drug delivery systems in the circulation limits their ability to reach the targeted disease tissue and, consequently, their effectiveness.

Incorporation of poly(ethylene glycol) (PEG) on the surface of nanoparticles, or PEGylation, confers them with stealth properties by creating a hydrophilic steric barrier that delays opsonization and rapid recognition by the macrophage phagocytic system (Stolnik, Dunn et al. 1994; Gref, Luck et al. 2000; Mehvar 2000; Hu, zhai et al. 2002; Otsuka, Nagasaki et al. 2003; Avgoustakis 2004). For example, a study of the biodistribution of liposomes in vivo in New Zealand White rabbits found that their circulation half life increased from 10-15 minutes to more than 1000 minutes as a result of PEGylation (Torchilin, Narula et al. 1996). PEGylation of nanoparticles also provides stability to the colloidal suspension through inter-particle steric repulsion (Avgoustakis 2004). The mechanism of protection offered by PEG has been associated with the high flexibility of the polymer chain which allows free rotation of the polymer units and the

high hydrophilicity that creates a shield around the particle, both of which prevent interaction of the particle with macromolecules in the body (Torchilin 1995).

Incorporation of PEG on the surface of particles has been attempted in the past through adsorption or covalent conjugation. However, it has been shown that the adsorption of surfactants containing PEG segments such as poloxamers and poloxamines does not confer permanent protection to the particles (Neal, Stolnik et al. 1998). Specifically, these surfactants have been shown to be displaced from PLGA nanoparticles by rat serum proteins *in vitro*. Such temporal surface protection limits the potential circulation time of the colloidal carriers. Covalent attachment of PEG to the nanoparticle polymer has been shown to be more effective than adsorbed PEG at reducing complement activation (Vittaz, Bazile et al. 1996), reducing interaction of the particles with the macrophage phagocytic system *in vitro* (Bazile, Prud'Homme et al. 1995; Barratt 2003), and reducing the uptake of the particles by the macrophage phagocytic system *in vivo* (Bazile, Prud'Homme et al. 1995).

Incorporation of PEG on the polymeric nanoparticles developed in the present research was carried out not only to increase the stability of the formulation and to provide the particles with improved circulation time once utilized *in vivo*, but also with the objective of utilizing surface PEG chains for attachment of targeting molecules such as antibodies, which could be utilized to direct the nanoparticles to the target cancerous tissue. Because of this, incorporation of PEG chains that included functional terminal groups was of outmost importance. The preparation of PEGylated nanoparticles has been widely investigated previously (Gref, Minamitake et al. 1994; Beletsi, Leontiadis et al. 1999; Zambaux, Bonneaux et al. 1999; Li, Pei et al. 2001; Avgoustakis, Beletsi et al. 2003). However, few reports have been made of the preparation of targeted nanoparticles that include functional PEG chains.

The use of the highly specific biotin-avidin interaction has been proposed as a means for the preparation of targeted drug delivery systems containing PEG. Specifically, the preparation of poly(lactic-acid)-PEG copolymers with biotinylated end gropus, which could be used for the preparation of targeted nanoparticles, has been reported (Cannizzaro, Padera et al. 1998; Salem, Cannizzaro et al. 2001). Also, nanoparticles of poly(ε-caprolactone)-PEG-biotin, which can be used for binding avidin-modified targeting agents, have been described in the literature (Gref, Couvreur et al. 2003). These systems, however, require that the targeting agent be chemically bound to avidin, a bulky glycoprotein that could interfere with the interaction of the targeting agent and its target receptor. One other interesting system involves the use of PLA-PEG-maleimide copolymers to create nanoparticles that can be bound to thiol-containing targeting agents (Gao, Tao et al. 2006). This technique is useful for site-specific conjugation to targeting agents because of the relatively low percentage of thiol-containing cysteine residues in most targeting agents –commonly antibodies, antibody fragments, peptides. However, most times it is necessary to add cysteines to these agents, thus increasing the possibility of altering their structure and reducing their activity.

In the present research, conjugation of targeting agents to functional PEG termini was performed with the use of electrophilic N-hydroxysuccinimide (NHS) esters of PEG carboxylic acids, as will be described in more detail in Chapter 6. Reaction between lysines or terminal amine groups of targeting agents and NHS-PEGs results in the formation of physiologically-stable amide bonds. The strategies for PEGylation of nanoparticles described in this chapter are focused on the use of PEG molecules containing NHS terminal groups, as shown on Figure 5.1, or others containing hydroxyl or carboxylic acid end groups which could be easily modified to include the NHS end group.

Four main strategies were studied in the present research for the incorporation of functional poly(ethylene glycol) (PEG) chains onto the surface of the nanoparticles. Two strategies were based on the use of blends of poly(lactic-co-glycolic acid) (PLGA) with PEG-containing polymers. The other strategies were based on covalently binding PLGA to heterofunctional PEG. For the latter strategy, synthesis of the copolymers was performed by polymerization of lactide and glycolide onto pre-made heterofunctional PEG or conjugation of pre-made poly(lactic-co-glycolic acid) to heterofunctional PEG.

5.1.1 Ring-Opening Polymerization of Lactide and Glycolide

Copolymers containing lactide and glycolide, including poly(lactic-co-glycolic acid) and poly(lactic acid) have traditionally been prepared by polycondensation from glycolic and/or lactic acids (Wang, Zhao et al. 2005) as shown on Figure 5.2, or more commonly by the ring-opening polymerization of the cyclic dimers of glycolide and lactide, shown on Figure 5.3. Polycondensation cannot normally produce polymers of acceptable molecular weight because this step polymerization reaches equilibrium prematurely when the water byproduct is not satisfactorily removed, i.e if the reaction is not continuously driven toward the polymer side (Dechy-Cabaret, Martin-Vaca et al. 2004). This equilibrium results in the formation of low molecular weight product. The ring-opening polymerization of lactide and glycolide is currently the preferred method for preparation of biodegradable polymers of these monomers as it can be easily controlled and can produce polymers with a wide range of molecular weights (Kiremitci-Gumusderelioglu and Deniz 1999; Jeong, Lim et al. 2000; Huh, Cho et al. 2003; Dechy-Cabaret, Martin-Vaca et al. 2004; Porjazoska, Karal-Yilmaz et al. 2004).

Lactide and glycolide cyclic dimers are among the few six-membered ring structures that can be polymerized. Thermodynamically, polymerization of all except six

membered rings is favored. Normally the stability of six-membered rings is too great to be overcome by the polymerization driving force. It is believed that the presence of two ester moieties in the dimers of lactide and glycolide causes sufficient strain to permit their polymerization (van Hummel, Harkema et al. 1982; Duda and Penczek 1990). The polymerization enthalpy of lactide, for example, was determined to be -22.9 kJ/mol (Duda and Penczek 1990), which is less favorable than that of 3-, 4- and 8-membered rings but similar to that of 5- and 7-membered cycloalkane rings (Odian 2004).

Ring opening polymerization of lactide and glycolide is normally carried out using stannous octoate as catalyst. Stannous octoate, also known as tin(II) bis(2-ethylhexanoate) or tin(II)octoate, is very effective, commercially available, easy to handle and is amenable to use in biomedical applications since it has been approved by the FDA for use as a food additive, although toxicity may still be an issue (Avgoustakis 2004; Dechy-Cabaret, Martin-Vaca et al. 2004). Stannous octoate is soluble in numerous organic solvents and in the melted monomers. Reaction times in the presence of stannous octoate at temperatures of 140 to 180°C are in the range of minutes to hours.

The mechanism of the catalyzed polymerization is believed to be of coordination-insertion (Dittrich and Schulz 1971; Du, Lemstra et al. 1995). The kinetics of polymerization have been reported to be first order with respect to the concentration of monomer (Dittrich and Schulz 1971). The reactivity of glycolide compared to that of lactide to polymerization has been reported to be about 10 times larger for the former versus the latter monomer (Gilding and Reed 1979). This fact played an important role in the results obtained in the present research, as will be discussed in later sections. The polymerization reaction can occur in a more controlled manner and at a faster speed in the presence of a protic agent such as an alcohol (Dechy-Cabaret, Martin-Vaca et al. 2004). This concept was also important for the use of ring-opening in the preparation of

functionalized copolymers in the present research. Importantly, impurities in the feed such as alcohols, lactic or glycolic acid and water can act as co-initiators. This is especially significant when the reaction is carried out without additional protic initiators.

The ring opening polymerization of lactide in the presence of alcohol-containing agents, including poly(ethylene glycol) and methyl ether terminated poly(ethylene glycol), has been utilized and studied previously (Kricheldrof and Meier-Haack 1993; Stolnik, Dunn et al. 1994; Bazile, Prud'Homme et al. 1995; Du, Lemstra et al. 1995; Tobio, Gref et al. 1998; Perez, Sanchez et al. 2001; Vila, Gill et al. 2004; Venkatraman, Jie et al. 2005; Vila, Sanchez et al. 2005). The polymerization is believed to begin with the activation of lactide by stannous octoate followed by the initiation of this active species with a hydroxyl group. Further lactide units coordinate at the end of the growing chain where the stannous octoate complex is located, and continue chain growth or chain transfer through either intra- or intermolecular attack. Intermolecular propagation commonly occurs with highly reactive initiators (Dechy-Cabaret, Martin-Vaca et al. 2004). When the initiator is a primary alcohol, such as PEG end groups, intermolecular attack is favored (Du, Lemstra et al. 1995). Importantly, when a high monomer-to-initiator ratio is used in the feed, the initiator is consumed rapidly (Du, Lemstra et al. 1995). The end groups of the polymer formed through this reaction are hydroxyls (Kricheldrof and Meier-Haack 1993). Initiation of the polymerization by secondary and tertiary alcohols occurs at slower rates than primary alcohols, as determined by comparing the reactions initiated by PEG and triethylene glycol as primary alcohols, methyl lactate and 2,3-butanediol as secondary alcohols, and pinacol and tertbutyl alcohol as tertiary alcohols (Du, Lemstra et al. 1995).

5.2 MATERIALS AND METHODS

5.2.1 Materials

Fluroescein-PEG-N-hydroxysuccinimide (FITC-PEG-NHS, molecular weight 5,000 g/mol) was purchased from Nektar Therapeutics (Huntsville, AL, USA). Heterofunctional PEGs including OH-PEG-COOH (molecular weight 3,400 g/mol) and HCl.NH_2-PEG-COOH (molecular weight 3400) were purchased from Nektar Therapeutics (Huntsville, AL, USA) and later from Laysan Bio, Inc. (Arab, AL, USA). Pluronic® F-127 (Poloxamer 407, molecular weight of 12,600 g/mol, hydrophilic-to-lipophilic balance 22, 101 ethylene oxide repeat units on each side of 56 central propylene oxide repeat units), stannous octoate (Tin(II) 2-ethylhexanoate), 2-(N-morpholino)ethanesulfonic acid (MES), N,N-dicyclohexylcarbodiimide (DCC), N-hydroxysuccinimide, poly(ethylene glycol) methyl ether ($mPEG_{2000}$, molecular weight of 2,000 g/mol) and poly(ethylene glycol) (molecular weight of 3,350 g/mol) were obtained from Sigma-Aldrich (Saint Louis, MO, USA).

Cyclic d,l-lactide (molecular weight 144.1) and glycolide (molecular weight 116.1) monomers were obtained from PolySciences, Inc. (Warrington, PA, USA). Poly(lactic-co-glycolic acid) (formerly PLGA 50:50 DL 2A, now 5050 DLGA 2A, 50/50 D,L-lactide to glycolide ratio, molecular weight 12,000 g/mol, carboxylic acid and hydroxyl end groups) was obtained from LakeShore Biomaterials (Birmingham, AL, USA).

The reagent 1-ethyl-3-(3-dimethylaminopropyl)carbodiimide hydrochloride (EDC) was obtained from Fluka. Anhydrous toluene and N,N-diisopropylethylamine were obtained from Acros Organics. Ethyl ether, acetone, ethyl acetate, dimethylformamide and methanol were obtained from Fisher Scientific.

5.2.2 Preparation of Nanoparticles with Blends of PLGA and PEG-Containing Polymers

Incorporation of PEG on nanoparticles through the use of polymer blends was pursued because it represented a rapid, simple and inexpensive method that could be translated rapidly into a clinical product. The hypothesis was that PEG or PEG-containing polymers could be incorporated into nanoparticles through hydrophobic interactions between the polymers. Specifically, PEG being a polymer that readily dissolves in numerous organic solvents such as acetone, dichloromethane, chloroform, acetonitrile, dimethylformamide, and methanol, as well as in water, it could be co-dissolved with PLGA in an organic solvent or mixture of solvents prior to precipitation or emulsification of the PLGA in an aqueous phase. Despite the fact that PEG would then partition between the organic and aqueous phases according to its solubility, it was expected that a significant amount would be incorporated within or on the surface of the nanoparticles.

Figure 5.4 shows the types of PEG-containing polymers that were investigated for incorporation within PLGA nanoparticles. Fluorescein-PEG-NHS (FITC-PEG-NHS) was used for easy monitoring and quantification of PEG incorporation as it offers similar properties and reactivity as unlabeled PEG derivatives containing the NHS group on one end such as methoxy-PEG-succinimidyl propionate (NektarTherapeutics 2005). Pluronic® F127 (PF127) is a tri-block copolymer of ethylene oxide and propylene oxide. The external ethylene oxide units are chemically identical to poly(ethylene glycol) and surround a more hydrophobic central domain of propylene oxide units. PF127 was used as opposed to other more commonly used poloxamers as it provides a relatively large

hydrophobic section (molecular weight ~ 3700 Da) compared to its hydrophilic ethylene oxide portions (molecular weight ~ 4400 Da on each side) while, at the same time having long-enough hydrophilic ends to provide protection to the particles. It was hypothesized that the higher hydrophobicity of poloxamers would enhance their incorporation within and on the surface of nanoparticles compared to simpler PEG derivatives because of improved hydrophobic interactions with the hydrophobic PLGA.

Preparation of polymeric nanoparticles including poloxamer blends have been reported previously (Moghimi, Muir et al. 1993; Li, Caldwell et al. 1994; Storm, Belliot et al. 1995; Moghimi and Hunter 2000; Csaba, Gonzalez et al. 2004; Csaba, Caamano et al. 2005; Csaba, Sanchez et al. 2006; Santander-Ortega, Jodar-Reyes et al. 2006); however, per our knowledge, no one has proposed the use of poloxamers for covalent attachment of targeting agents onto drug delivery nanoparticles.

For preparation of nanoparticles with FITC-PEG-NHS, 10 or 20 mg of PEG were dissolved in 1 ml of methanol and 100 mg of PLGA were dissolved in acetone. These two solutions were mixed to form the organic phase, which was then added to 10 ml of an aqueous solution containing bovine serum albumin (BSA), sodium cholate (SC) or poly(vinyl alcohol) (PVA) as surfactants. The mixture was sonicated and stirred at 500 rpm for 45 minutes under vacuum to evaporate the solvents. The nanoparticle suspension was then centrifuged with a Beckman J2-21 refrigerated centrifuge (Beckman Instruments, Palo Alto, CA, USA) for 10 minutes at 48,000 x g, and the supernatant collected for analysis of PEG-polymer incorporation. The nanoparticle pellet was then resuspended in the surfactant solution and centrifuged three more times to remove adsorbed PEG. Nanoparticle pellets were frozen at -20°C and freeze dried using a Labconco Freeze Dryer 4.5 (Kansas City, MO, USA).

Nanoparticles with poloxamer F-127 were prepared similarly, except that the poloxamers were not dissolved in methanol but directly co-dissolved in 6 ml of acetone with PLGA. For these nanoparticles, the ratio of poloxamer to PLGA used in the preparation was 50:50 (50 mg of PF127 and 50 mg of PLGA) or 25:75 (25 mg of PF127 and 75 mg of PLGA). No surfactant was used in the aqueous phase used to precipitate the polymer because its inclusion resulted in the formation of small micelles and a significant reduction in the yield to less than 4% according to initial studies. Nanoparticles were resuspended in 1ml of 50 mg/ml of glucose prior to freezing and freeze drying to try to minimize lyophilization-induced aggregation which led to batches that were impossible to resuspend in preliminary studies.

5.2.2.1 Physiochemical Characterization of PLGA/PEG-polymer Nanoparticles

Freeze dried nanoparticles were weighted to determine the yield or percent recovery compared to the mass of polymers that was used in the preparation of the particles. For determination of sizing, dried nanoparticles were resuspended in deionized water with sonication and sized using a Coulter® NanoSizer™ (Coulter Electronics LTD., Harpenden Herts, UK).

5.2.2.2 Determination of PEG-polymer Content on Nanoparticles

Incorporation of FITC-PEG-NHS was determined from spectrophotometric quantification of the FITC on supernatants from all wash/centrifugation cycles. Supernatants were collected and their volume and absorbance at 500 nm were measured. The concentration of FITC-PEG-NHS was determined based on a calibration curve ($r^2 > 0.99$) generated with solutions of known FITC-PEG-NHS concentration in the surfactant

solution used for each batch. The efficiency of incorporation was determined by comparing the mass of the polymer found in the supernatant to that which was used for preparation of the particles.

For determination of poloxamer content in nanoparticle batches, supernatants from all wash/centrifugation cycles were collected for analysis with a spectrophotometric assay based on the molar proportion of ions that coordinate around PEG chains (Skoog 1979). Specifically, 0.75 ml of 100 mM barium chloride solution was mixed with 0.375 ml of a solution that is 5 mM in Iodine and 15 mM in potassium chloride. To this, 3 ml of supernatant was added. The absorbance of the solution at 500 nm was used to determine the concentration of PEG or poloxamer in the supernatants based on a standard curve ($r^2 > 0.99$) generated with solutions of known poloxamer concentrations. PEG incorporation efficiency and PEG weight percent within nanoparticles was determined by comparing the amount of PEG in the supernatants to that used for preparation of the particles.

5.2.3 Preparation of PLGA-PEG Copolymers

The second main strategy used for incorporation of PEG on the nanoparticle formulation was based on covalently binding PEG to the nanoparticle core polymer. This strategy was expected to be superior as it assures incorporation of PEG and prevents premature loss of the PEG protective layer *in vivo,* which would result in rapid nanoparticle opsonization, sequestration by the macrophage phagocytic system and consequent undesired pharmacokinetics. As described next, the preparation of these copolymers was performed by conjugation of pre-made PEG and PLGA polymers (section 5.2.3.1) or by polymerization of lactide and glycolide monomers onto a different pre-made heterofunctional PEG (section 5.2.3.2).

5.2.3.1 Preparation of PLGA-NH-PEG-COOH Copolymers by Conjugation

Pre-made PLGA terminated in carboxylic acid and hydroxyl groups was conjugated to a heterofunctional PEG terminated on amine and carboxylic acid groups (NH_2-PEG-COOH) utilizing standard carbodiimide/NHS-mediated chemistry (Staros 1982; Hermanson 1996) using a method similar to that reported by Farokhzad and colleagues (Farokhzad, Cheng et al. 2006). Figure 5.5 is a schematic of the conjugation chemistry used in this protocol. PLGA was reacted with DCC and NHS in an organic solvent at room temperature and in the dark to activate the carboxylic acids to the semi-stable amine-reactive activated NHS-ester of PLGA (PLGA-NHS). After a specific reaction time, the polymer mixture was filtered with a 0.45 μm syringe filter to remove insoluble dicyclohexyl urea byproduct. The solution was then concentrated under vacuum while submerged in a water bath at 30°C. The solution was transferred to two 45-ml Teflon centrifuge tubes (less than 4ml of polymer solution per tube) and the polymer was precipitated by filling the rest of the tube with ethyl ether or -20°C methanol and mixing well. The precipitated polymer was pelleted by centrifugation for 10 minutes at 48,000 x g and the supernatant was removed. The pellet was dissolved in a small volume of dichloromethane (less than 1ml), precipitated and centrifuged once more. The purpose of the precipitation and centrifugation cycles is to remove excess DCC, NHS and remaining water-insoluble dicyclohexyl urea byproduct (Hermanson 1996).

If storage of the activated PLGA was required, the final pellet of activated PLGA was transferred to a Teflon beaker, dried in a vacuum dessicator, frozen at -20°C and freeze dried. Else, the pellet of activated PLGA was conjugated immediately. Activated PLGA was reacted with NH_2-PEG-COOH in an organic solvent in the presence of N,N-diisopropylethylamine to desalt the terminal PEG amine group. After a specific reaction

time the solution was concentrated under vacuum and the polymer was recovered and purified by three cycles of precipitation and centrifugation as described above. The purified copolymer pellet was transferred to a Teflon beaker, placed on a vacuum dessicator for 2 hours, frozen and freeze dried. The dried copolymer was stored under a nitrogen atmosphere and at -20°C. The conditions that were varied in the conjugation reaction included the molar ratio of PLGA to DCC/NHS (1:10, 1:50), the molar ratio of activated PLGA to PEG and to N,N-diisopropylethylamine, the solvent (dichloromethane, chloroform, or dimethylformamide) and the reaction time (2, 4 or 24 hours).

5.2.3.2 Conjugation of PEG After Nanoparticle Preparation

The method described for the preparation of copolymers by conjugation in the previous section also permitted conjugation of PEG to PLGA after nanoparticle preparation by utilizing protocols similar to those reported by Kasturi et al. for the preparation of polyethyleneimine-conjugated PLGA microspheres (Kasturi, Sachaphibulkij et al. 2005). Figure 5.6 shows the synthetic route used for activation PLGA in solid nanoparticles and conjugation of heterofunctional PEG on the particle surface.

Nanoparticles were first prepared by dissolving 100 mg of PLGA in 3 ml of acetone, adding this organic solution to 10 ml of 10 mg/ml aqueous poly(vinyl alcohol) solution, vortexing and sonicating for less than 1 minute. Solvent was removed by stirring under vacuum for 45 minutes. The nanoparticle suspension was centrifuged and washed three times with water to remove excess surfactant. Carboxylic acid groups on the surface of the nanoparticles were activated by resuspending the nanoparticles by sonication in isotonic 0.1M 2-[morpholino]ethylsulfonic acid (MES) buffer saline (1 or

10 ml), pH 5.5, and reacting for a specific time with EDC and NHS. A low-pH buffer was used to reduce the rate of hydrolysis of the NHS esters of PLGA that are formed in this step. The optimal reaction pH range is between 4.7 and 6 (Hermanson 1996). Importantly, this buffer was selected because the reaction medium must not contain amine or carboxylic acid groups which could compete in the reaction and which are found on other more commonly used buffers. Nanoparticles were then centrifuged and washed to remove excess EDC/NHS and the water-soluble isourea byproduct.

Activated nanoparticles were then resuspended in PBS buffer (1 or 10 ml) and reacted with NH_2-PEG-COOH for a specific period of time. Nanoparticles were centrifuged and washed to remove unbound PEG. The nanoparticles were resuspended in 1 ml of 50 mg/ml glucose or 8 ml of water with 400 mg of trehalose, frozen and freeze dried. The variables that were adjusted in the activation and conjugation steps were the reaction time and the molar ratio of PLGA to EDC/NHS or PEG, respectively, which assumes that 100% of the carboxylic acid end groups of PLGA are available on the surface of the nanoparticles.

The size and zeta potential of dry particles was determined after resuspending them in deionized water or 1mM KCl solution, respectively. Both sizing and zeta potential were obtained with a ZetaPlus® instrument (Brookhaven Instrument Corporation, Holtsville, NY, USA). The composition of these nanoparticles was determined by nuclear magnetic resonance, as described in more detail on Section 5.2.5. In addition, X-ray photoelectron spectroscopy (XPS) was used to analyze the surface composition of the nanoparticles. A dispersion of dry nanoparticles was analyzed with a PHI 5700 XPS instrument. The atomic composition of surface components was obtained.

5.2.3.3 Preparation of PLA-PEG-COOH Copolymers by Polymerization

Ring-opening polymerization of cyclic glycolide and/or lactide dimers initiated by the hydroxyl groups of PEG was carried out either as a melt of the reagents or in solution. Three types of PEG reagents were used: methyl ether PEG with hydroxyl groups on one end of the chain and a molecular weight of 2,000 g/mol ($mPEG_{2000}$), poly(ethylene glycol) with hydroxyl end groups on both sides of the molecule and a molecular weight of 3,350 g/mol (PEG_{3350}), and a heterofunctional PEG containing hydroxyl and carboxylic acid end groups and of a molecular weight of 3,400 g/mol (OH-PEG_{3400}-COOH). The first two types of PEG were used for all initial batches until the protocol had been optimized as they are significantly less expensive than the heterofunctional reagent. However, for preparation of targeted nanoparticles, the copolymer of the heterofunctional PEG was desired since it permits conjugation of targeting agents on the free carboxyl end group. Polymerization using this heterofunctional PEG has been reported previously (Farokhzad, Jon et al. 2004). Figure 5.7 is a schematic of the polymerization of lactide and glycolide initiated by the hydroxyl group of heterofunctional OH-PEG_{3400}-COOH.

Dimers of lactide and glycolide were first purified by recrystallization from ethyl acetate. Specifically, dimers were dissolved in 70°C ethyl acetate near their solubility and hot-filtered if needed. The dimer solutions were then allowed to cool down undisturbed to room temperature to permit formation of dimer crystals. After reaching room temperature, the samples were placed on an ice bath to try to maximize the formation of crystals. The crystals were recovered by vacuum filtration and dried in a vacuum desiccator for a few hours prior to freezing and freeze drying for more than 24 hours. Immediately after removing from the freeze drier, the dimers were polymerized as follows.

For preparation of the copolymers, the appropriate PEG and the dimers were added to a three-necked glass reaction flask that contained a magnetic stir bar. The mass of each reagent to be added was calculated based on the desired molecular weight and the assumption that each hydroxyl end group on each molecule of PEG polymer would initiate the polymerization of a single chain of PLGA or PLA. The reaction flask was closed with stopcocks and connected to a nitrogen line and a vacuum pump. The system was dried by cycles of vacuum and nitrogen for about 1 hour prior to starting the reaction. If the polymerization was to be carried out in solution, the solvent was then added while purging with nitrogen to prevent inflow of atmospheric gases. Polymerizations in solution were carried out in dimethylformamide at 140°C or in anhydrous toluene at 110°C.

The reaction flask was then immersed in a preheated silicon oil bath to allow the polymer and dimers to melt and/or go into solution. Once all reagents were liquid, stannous octoate was added while purging with nitrogen. The amount of stannous octoate was varied between 0.05 % of the total reagent mass, to a 1-to-1 molar ratio with respect to the hydroxyl groups of the PEG used, based on the amounts used in previous reports (Quellec, Gref et al. 1998; Kiremitci-Gumusderelioglu and Deniz 1999; Gref, Luck et al. 2000; Yoo and Park 2001). The reaction flask was then pressurized with 20 psi of nitrogen and sealed, and the reaction was allowed to occur for a specific period of time. At the end of the reaction time, or once the polymer had solidified, the reaction flask was removed from the heated bath and rapidly cooled in iced water. The polymer was then transferred to four Teflon centrifuge tubes if liquid, or mixed with dichloromethane if solid to try to dissolve it. The liquid polymer was precipitated by filling each centrifuge tube with ethyl ether, and centrifuged at 48,000 x g for 15 minutes to separate it from the supernatant. The pellets were dissolved in 1-2 ml of

dichloromethane per tube and again precipitated. This procedure was repeated once more so that the polymer was precipitated a total of 3 times. The pellets were then dried in a vacuum desiccator overnight, frozen at -20°C and freeze dried for 2 days.

If the polymer had solidified in the reaction flask or was unable to be dissolved after precipitation regardless of the volume of solvent used, the mixture of dissolved and solid polymer was filtered to remove the insoluble fraction. The polymer solution was then precipitated and purified as detailed above.

5.2.4 Characterization of Copolymers

Copolymers were characterized by proton nuclear magnetic resonance and gel permeation chromatography to determine their composition and molecular weight, respectively. Proton NMR was performed with a Varian INOVA-500 instrument (500 MHz, Palo Alto, CA, USA) after dissolving the polymers in deuterated chloroform or dimethyl sulfoxide at a concentration of 1 mg/ml and filtering the solution through a 0.2 μm syringe filter. Proton intensities corresponding to lactide methine quartets at 5.2 ppm, lactide methyl doublets at 1.6 ppm, glycolide protons at 4.8 ppm and PEG methylene protons at 3.6 ppm were used for determination of the composition of the copolymers, as described previously (Du, Lemstra et al. 1995; Hrkach, Peracchia et al. 1997; Heald, Stolnik et al. 2002; Garcia-Fuentes, Torres et al. 2004). Based on the area of PEG methylene proton peaks and the known number of protons associated with this area based on the starting molecular weight of PEG, a value of proton peak area per number of protons was determined. From this value, a molecular weight for the copolymer was estimated based on the peak areas for the lactide and glycolide protons. This calculation permitted the determination of PLGA-to-PEG ratios in the final copolymer.

The GPC system consisted of a two Polymer Labs columns in series designed for use with polymers of molecular weight between 200 and 2,000,000 g/mol, a Waters 515 HPLC pump, a multi-angle laser light scattering (MALLS) detector (DAWN EOS, Wyatt Techonology) that measures the light scattered by the polymers as they elute from the columns and permits determination of absolute weight-average molecular weight, and a refractometer (Optilab DSP, Wyatt Techonology) that measures changes in the refractive index with concentration. For analysis, polymers were dissolved in either tetahydrofuran or dimethylformamide depending on their solubility, and filtered through a 0.2 μm syringe filter prior to injection into the GPC system. Number average molecular weight (Mn) and polydispersity index are reported. The polydispersity index is the ratio of weight average to number average molecular weights and provides an indication of the width of the distribution of molecular weights of the chains that make up the polymer.

5.2.5 Preparation of Nanoparticles with PLGA-PEG or PLA-PEG Copolymers

Nanoparticles of PLA-PEG or PLGA-PEG copolymers were prepared by a nanoprecipitation solvent evaporation method (Fessi, Devissaguet et al. 1986; Barichello, Morishita et al. 1999; Betancourt, Brown et al. 2007). The copolymers were dissolved in 3 ml of acetone to form the organic phase. This organic phase was added to 10 ml of an aqueous solution with or without poly(vinyl alcohol) as a surfactant. After brief sonication, the solvent was removed by stirring the suspension under vacuum for 45 minutes. Nanoparticles were recovered through centrifugation, washed, and lyophilized with or without cryoprotectant. Glucose or trehalose were used as cryoprotectants. The composition of the nanoparticles was determined by nuclear magnetic resonance as described above for the characterization of copolymers.

Liquid state NMR of nanoparticles in suspension was also performed. For this, a batch of nanoparticles was prepared as above but not mixed with a cryoprotectant or freeze dried. Instead, the particles were centrifuged, resuspended in deuterated water and centrifuged again to try to remove as much water as possible without having to dry them. The pellet was then resuspended in deuterated water, filtered through a 0.45 μm syringe filter and analyzed. This method detects the resonance signal of nanoparticle components in intimate contact with the deuterated solvent but not that of solid components.

5.3 RESULTS AND DISCUSSION

5.3.1 Nanoparticles with Blends of PLGA and FITC-PEG-NHS

Table 5.1 summarizes the results of the preparation of nanoparticles with blends of PLGA and FITC-PEG-NHS. The yield of the formulations was approximately 60% for all batches prepared with PVA as a surfactant in the outer aqueous phase and was not dependent on the amount of PEG added during preparation ($p > 0.6$). Batches prepared with BSA as surfactant had an average yield of 68%, which is statistically different from that of particles with the same targeted PEG incorporation prepared with PVA ($p < 0.05$). Particles prepared with sodium cholate had a yield that was not significantly different from that of particles prepared with PVA with the same targeted PEG incorporation ($p > 0.2$).

The size of the nanoparticles before freeze drying was between 190 and 220 nm for batches made with PVA as surfactant and was also not influenced by the mass of PEG included in the formulation. Particles made with BSA had a significantly larger size in the range of 230 nm ($p < 0.05$), consistent with previous results of blank and doxorubicin-loaded nanoparticles described in Chapter 3 (Betancourt, Brown et al. 2007).

Batches prepared with SC had a significantly smaller size ($p < 0.05$) in the range of 180 nm, consistent with the results previously described for nanoparticles loaded with indocyanine green in Chapter 4. The size of the nanoparticles after freeze drying significantly increased for all formulations compared to that of the particles before freeze drying, but the type of surfactant continued being the major factor determining size. The size of nanoparticles made with BSA after freeze drying was not significantly different from that of those made with PVA. Because of the high variation in the size of the particles made with PVA and 9.2 wt.% PEG targeted incorporation, the size of particles made with SC after freeze drying was not statistically different; however, it was different from that of particles made with PVA without PEG.

Incorporation of FITC-PEG-NHS was significantly lower than desired, as can be seen in Table 5.1. Most of the PEG was removed in the first supernatant. The second supernatants contained at least one order of magnitude less PEG than the first. For the particles prepared with BSA, the average incorporation efficiency was negative possibly as a result in errors in the calibration curve, presence of particles in the supernatants, or errors in the measurement of supernatant volumes. These errors could also affect the data for all other formulations. The calculated PEG content in the nanoparticles was 0.1 or 0.8% by weight for particles made with PVA with a targeted wt% of 9.2 and 16.8% respectively, -0.2% for particles made with BSA and 1.1% for particles made with SC. In all cases, however, the incorporation efficiency achieved is less than desirable for the modification of the surface of the nanoparticles since PEG was expected to act as a shield preventing rapid opsonization and sequestration of the nanoparticles by the reticuloendothelial system *in vivo* and provide a conjugation site for targeting agents. In addition, the fact that PEG incorporated with this method is only physically entrapped within or adsorbed on the particles could be problematic when utilized *in vivo* as it could

diffuse out of the particles or be rapidly displaced as the particles interact with serum proteins. Finally, FITC-PEG-NHS, which was used because it facilitated quantification of PEG, is more hydrophobic than unlabeled PEG and, consequently, it is expected that preparation of particles with unlabeled PEG would result in even lower incorporation.

5.3.2 Nanoparticles with Blends of PLGA and Poloxamers

Table 5.2 summarizes the properties of nanoparticles prepared with blends of PLGA and PF127. Statistically significant differences were observed in the yield, size before and after freeze drying, incorporation efficiency and final PEG content between the two types of formulation with different PF127/PLGA ratios prepared ($p < 0.05$). The yield of the formulations was highly dependent on the ratio of the polymers blended, although it could be approximated to be about 60% of the PLGA mass used. However, this comparison can be misleading since, according to the measured incorporation efficiency, PF127 is in fact a significant part of the final nanoparticle composition. The lower yield and size of the particles prepared with higher PF127 content (PF127/PLGA ratio of 50:50) could be a result of the surfactant properties of the amphiphilic poloxamer which would lower the surface tension as the organic polymer-containing solution mixes with the aqueous solution, and would permit the formation of smaller particles. In addition, excess poloxamer not intimately associated with PLGA particles can form micelles of smaller sizes which would significantly decrease the percent recovery.

The large increase in particle size after freeze drying could be a result of the presence of the poloxamer on the surface of the particles. Poly(ethylene glycol), and consequently poly(ethylene oxide) chains, are known to crystallize upon freezing, thus causing major mechanical stresses on the particles and resulting in their aggregation (de Jaeghere, Allemann et al. 2000; Abdelwahed, Degobert et al. 2006). Batches that were

freeze dried without a cryoprotectant were impossible to resuspend after drying. The sizes shown in Table 5.2 are for batches that were frozen and freeze dried after addition of 50 mg of glucose to the nanoparticle suspension. Even in the presence of this cryoprotectant, particle aggregation to about four times the pre-dried sized occurred.

The incorporation efficiency of PF127, as determined by a colorimetric method, was higher in particles that were prepared with higher PF127/PLGA feed ratio. Increased poloxamer concentration, which led to the formation of smaller particles, could result in higher degree of association of the poloxamer with the particles as a result of increased nanoparticle surface area and the need for better stabilization of the thermodynamically unstable colloidal system. The final poloxamer content of the nanoparticles was of 12 or 43 wt.%, for the nanoparticles prepared with 25:75 or 50:50 PF127/PLGA mass ratios, respectively.

The zeta potential of the formulations was found not to be statistically different regardless of the amount of poloxamer used during preparation. However, the zeta potential of these formulations compared to that of other PLGA nanoparticles prepared with bovine serum albumin, sodium cholate or poly(vinyl alcohol) as surfactants is significantly different. Per our own data, the zeta potential of particles prepared with BSA, SC and PVA is of about -45mV, -50mV and -10mV, respectively. The difference in the zeta potential compared to these other formulations confirms the fact that the nanoparticles formulated with blends of PLGA and PF127 do in fact have a modified surface chemistry as a result of the presence of PF127.

5.3.3 Preparation of PLGA-NH-PEG-COOH Copolymers by Conjugation

Carbodiimide-mediated conjugation of PLGA to NH_2-PEG-COOH in solution, as shown on Figure 5.5, was used because of the extremely high efficiency of activation

achievable with DCC in anhydrous media since no hydrolysis of the active ester occurs as it does in bioconjugaiton methods that are carried out in aqueous suspensions using EDC (Hermanson 1996). Conjugation of PLGA to NH_2-PEG-COOH could have been performed using DCC without the presence of NHS. However, the O-acylurea intermediate formed upon reaction of the PLGA carboxyl with DCC can spontaneously rearrange to the inactive N-acylurea form, thus reducing the efficiency of the reaction (Hermanson 1996). This problem is specially important when the reaction is carried out in aprotic organic solvents such as dimethylformamide (Hermanson 1996). In addition, if no amine-containing molecule is available in the reaction medium to bind to the O-acylurea intermediate, it can react with other carboxyl groups in the system to form anhydrides (Hermanson 1996). NHS results in the formation of a more stable intermediate that can be subsequently reacted with the heterofunctional PEG, thus increasing the efficiency of conjugation. The half life of the intermediate created in the presence of NHS is of a few hours, as opposed to minutes or even seconds for the direct carbodiimide intermediate (Hermanson 1996).

A two step activation/conjugation method was used because direct reaction of heterofunctional PEG with NHS and EDC would have also resulted in activation of the carboxylic acid end groups of PEG, and very likely in the undesirable formation of PEG-PEG conjugates in addition to PLGA-PEG.

Proof-of-concept conjugations were performed to show that this method could be performed and that the resulting polymer composition could be regulated by varying the preparation variables. Nuclear magnetic resonance (NMR) and gel permeation chromatography were used to determine the resulting copolymer composition and molecular weight, respectively. Figure 5.8 displays the NMR spectra for various batches of copolymers. NMR confirmed the presence of both PLGA and PEG in all batches, and

allowed determination of the PLGA-to-PEG molar ratio of the resulting copolymer based on the areas of the proton peaks associated with each of the polymers. NMR spectra were run in deuterated chloroform, except for the copolymer in Figure 5.8C which was run in deuterated DMSO. Increasing peak size (area) of PEG protons at 3.6 ppm (*d*) relative to those of lactide at 5.2 ppm (*a*) and 1.6 ppm (*b*) and of glycolide at 4.8 ppm (*c*) was observed with increasing conjugation efficacy, as seen in the progression of copolymers from Figure 5.8 B through E.

Table 5.3 summarizes the results of these conjugations. For all conjugations, the desired PLGA to PEG end molar ratio based on the feed mass of each polymer was of 1 to 1. In Table 5.3 results are organized according to increasing actual molar ratio of PLGA-to-PEG as determined by NMR, and consequently of decreasing conjugation efficiency. Since conjugations were carried out with pre-made polymers, a molar ratio of PLGA to PEG greater than 1 means that there are PLGA chains that have not conjugated to PEG. Increased reaction time appeared to make a significant difference in the resulting copolymer composition. Decreasing reaction time resulted in decreasing conjugation efficiency. For equivalent reactions performed in chloroform, for example, a reaction time of 24 hours resulted in a copolymer that had 58% PLGA and 42% PEG (PLGA/PEG ratio of 1.4), while a reaction time of 2 hours resulted in a polymer that had 90% PLGA and only 10% PEG (PLGA/PEG ratio of 8.9). The solvent used in the reaction also appeared to make a difference in the resulting conjugation efficiency. For conjugations run for 4 hours, the use of dichloromethane or dimethylformamide as the solvent did not appear to make a difference. On the contrary, for reactions carried out for 2 hours, using chloroform as the reaction solvent led to significantly better results than using dichloromethane.

It was observed that the molar ratio of DCC and NHS to PLGA used for activation of carboxylic acids did not make a significant difference in the conjugation results at least within the ratios used (10:10:1 and 50:50:1). The same observation applies for the amount of N,N-diisopropylethylamine added for desalting the amine group of the PEG at least within the molar ratios used (PLGA/PEG/amine of 1:1:2 and 1:1:10). Addition of excess PEG to the reaction could have resulted in better conjugation efficiencies, but this was not feasible as a result of the high cost of the heterofunctional reagent.

According to gel permeation chromatography, the number average molecular weight of the starting polymers was of 5,395 with a polydispersity index (PI) of 1.13 for PEG and 11,160 with a PI of 1.26 for PLGA, although the PEG had a molecular weight of 3,400 according to the manufacturer. GPC analysis of the copolymers revealed that the number average molecular weight was very close to that of PLGA. One reason for this is that the resulting polymer may contain not only the co-polymer but also free PLGA and PEG chains which would skew the resulting average molecular weight toward that of the lower molecular weight components. Copolymers were purified by precipitation with cold methanol only or with ethyl ether and cold methanol. Methanol was used to try to remove unbound PEG since it is more soluble in this solvent than in ether; however, it is possible that some of the unbound PEG remained. Also, the fact that not all PLGA chains were conjugated to PEG would result in average molecular weights close to that of PLGA alone, depending on the extent of modification. Another reason why a definite difference between the number average molecular weight of PLGA and that of the copolymers was not seen could be related to the challenges of utilizing gel permeation chromatography with polymers of such small molecular weight. In all runs of these copolymers, the refractive index signal of the polymers was low and highly affected

by background noise. Also, the gel permeation chromatography columns used were designed for separating polymers of molecular weight in the wide range of 200 to 2,000,000 g/mol and were possibly not sufficiently sensitive to separate polymers that had only a 3,400 g/mol molecular weight difference. Finally, the multi-angle laser light scattering technique that was used to determine the molecular weight of the polymers assumes that the rate of change of the refractive index of the polymers with concentration is a constant, which is a good assumption for polymers of molecular weight above 10,000 g/mol but may result in more significant errors with polymers close to or below this size.

It is worth noting that polymer recovery ranged between 20 and 45% for most batches. The remaining polymer was lost during purification as a result of challenges with precipitating amphiphilic copolymers of relatively similar hydrophobic-to-hydrophilic chain sizes. These copolymers could easily remain in solution with less-than-ideal solvent amounts or solvent-to-precipitant ratios.

5.3.4 PEGylation of NPs by Surface Conjugation of PEG

Carbodiimide chemistry similar to that used in the previous method was utilized for conjugation of heterofunctional PEG directly to the surface of pre-made nanoparticles suspended in an aqueous medium. EDC was used for conjugation of NH_2-PEG-COOH to carboxyl groups on the surface of nanoparticles because it is widely used in bioconjugation strategies. The conjugation route is displayed in Figure 5.6. Table 5.4 summarizes the size and zeta potential of the resulting nanoparticles.

The size of PEGylated nanoparticles prepared with poly(vinyl alcohol) as the surfactant was of 245 nm in average and was not significantly different from that of non-PEGylated particles prior to freeze drying. The size of particles prepared without surfactant was significantly larger (324 nm, $p < 0.05$). These particles were prepared

with the hope of determining if surfactant adsorbed on the surface of the nanoparticles would be detrimental for the conjugation of PEG to terminal carboxylic acid groups of PLGA. Freeze drying of nanoparticles in the absence of a cryoprotectant was found to result in aggregation of particles which prevented their resuspension. This could be an indication of the presence of PEG in the formulation, but further studies will need to confirm this because aggregation of PLGA nanoparticles with the use of PVA has sometimes been observed in previous data from our laboratory. Glucose and trehalose, when used at the concentrations specified in the methods section, successfully prevented aggregation of the nanoparticles upon freeze drying ($p > 0.05$). The size of freeze dried PEGylated particles with cryoprotectant was not significantly different than that of non-PEGylated particles, regardless of the type of croprotectant used. Figure 5.9 shows a scanning electron microscopy image of nanoparticles to which PEG was conjugated in suspension after preparation.

The zeta potential of the PEGylated nanoparticles that were freeze dried with either glucose or trehalose was not significantly different than that of non-PEGylated nanoparticles. Zeta potential is commonly used to show the presence of PEG in formulation of nanoparticles prepared with copolymers of PLGA-PEG or PLA-PEG as it shifts it towards low but negative values according to the methyl ether or hydroxyl groups at the free end of PEG (Quellec, Gref et al. 1998; Gref, Luck et al. 2000; Li, Pei et al. 2001; Avgoustakis, Beletsi et al. 2003; Vila, Gill et al. 2004). However, in the present research, the free end group of the PEG is a carboxylic acid which confers the surface of the particles with a negative charge at neutral pH, similarly to that of a non-PEGylated PLGA nanoparticles. In addition, the use of poly(vinyl alcohol) as a surfactant also masks the surface of the nanoparticles and lowers the zeta potential to low negative values regardless of the presence of PEG in the formulation.

Proton NMR analysis of the dried particles after dissolution in either deuterated chloroform (for particles prepared without a surfactant) or dimethyl sulfoxide revealed that the PEG content of the formulations was low. For a conjugation that was carried out in dilute conditions (10 ml suspensions) with a 2-fold excess of NHS and EDC per PLGA chain and 20% excess PEG, the resulting molar ratio of PLGA to PEG according to NMR was of 1,732. For a conjugation that was carried out in concentrated conditions (1 ml suspensions) with 140% molar excess of PEG, the copolymer prepared had 787 PLGA chains for every PEG present. Figure 5.10 displays the NMR spectra of these two copolymers. Note the small peak near 3.6 ppm (*d*) associated with PEG.

It is worth noting that one batch of particles was prepared with bovine serum albumin as a surfactant instead of PVA to study whether it would make a positive impact on the conjugation. It was hypothesized that the presence of carboxylic acid groups on the protein would provide additional binding sites since it is known that a fraction of the albumin used as a surfactant in the preparation of the nanoparticles remains permanently bound on the surface of the particles (Bazile, Ropert et al. 1992; Verrecchia, Huve et al. 1993; Verrecchia, Spenlehauer et al. 1995). In addition, since albumin acts as a surfactant by exposing its hydrophilic, hydrogen-bonding domains toward the outer aqueous phase, it was expected that at least some of its carboxylic acids would be found at accessible locations on the surface for binding. Unfortunately, NMR analysis of this batch revealed no improvement in the conjugation efficacy.

Results for XPS analysis of control, activated and PEGylated nanoparticles are shown on Table 5.5. Theoretical atomic compositions of PLGA and PEG are also shown in this table. A decrease in the carbon and an increase in the oxygen content of the samples was expected upon PEGylation based on the carbon-to-oxygen ratio of PLGA and PEG. No significant differences were seen between the carbon and oxygen

compositions of the three nanoparticle samples, suggesting that the PEG amount on the surface of the sample, if any, is too small to make a significant difference. However, a difference was observed in the nitrogen content of both activated and PEGylated nanoparticles in comparison to control. The nitrogen content increased 10 times upon activation, suggesting the successful activation of the carboxylic acid end groups of PLGA with N-hydroxysuccinimide (NHS). Upon conjugation, the nitrogen content decreased, possibly as a result of surface masking of remaining NHS groups or amide linkages by any PEG that bound to the activated carboxylic acid groups. These results, similarly to NMR characterization, suggest that the surface of the nanoparticles is only being modified to a small extent.

PEGylation of PLGA nanoparticles by direct conjugation on their surface has a number of benefits and drawbacks. It permits preparation of PLGA nanoparticles without modification of protocols and so it may be used for encapsulation of agents through well-established methods that lead to acceptable drug loadings. PEGylation would occur after the agent has been encapsulated within the solid polymeric matrix so that key affinity of the drug to the polymer, such as hydrophobic or charge interactions, would not be disturbed. This is important because the loading of certain agents within particles of pre-made copolymers may be negatively affected as a result of poor interactions of the drug with the copolymer. Although the nanoparticles need to be exposed to an aqueous environment during conjugation, extensive loss of drug is not expected for moderately or hydrophobic drugs because the pH of the reaction can be adjusted within a relatively wide range without significantly affecting the rate of reaction and because the reaction is carried out at room temperature. Additionally, and in contrast to the preparation of copolymers by conjugation with carbodiimide chemistry that was discussed in the previous section, excess reagent and soluble byproducts can be easily

washed off since the particles and any associated PEG can be separated from the reaction medium by centrifugation.

On the other hand, the maximum possible surface PEG density that can be achieved is dependent on the number of PLGA carboxylic acid end groups that are available for reaction on the surface of the nanoparticles. This key factor could be possibly optimized by the use of various surfactants and nanoparticle preparation techniques that favor the presentation of these groups on the interface. Also, this type of conjugation technique is prone loss of efficiency to a number of competitive reactions of the O-acylisourea intermediate, such as that with sulfhydryl groups to form unstable thiol linkages, with oxygen atoms, and with water to regenerate the carboxylic acid group (Hermanson 1996). Although NMR analysis confirms the presence of PEG on the nanoparticles, the extent of PEGylation achieved with the experimental protocols used in the present research would not be sufficient for effective conjugation of targeting agents or for shielding of the particles in an *in vivo* setting.

5.3.5 Preparation of PLGA-PEG-COOH Copolymers by Polymerization

The ring-opening polymerization of lactide and glycolide using the hydroxyl group of the heterofunctional OH-PEG-COOH as an initiator was used to prepare PLGA-PEG-COOH copolymers, as shown on Figure 5.7. The reactions were catalyzed by stannous octoate, and run either as a melt of the monomer and PEG, or in the presence of a solvent. The two solvents that were utilized were dimethylformamide and toluene. The main requirement of the solvents was a high boiling point so that the reaction could be carried out at an elevated temperature, thus providing the necessary energy to favor the polymerization of these cyclic monomers. Dimethylformamide is a polar non-protic

solvent and has a boiling temperature of 153°C. Toluene is a non-polar solvent with a boiling temperature of 110.6°C.

Initially, a number of batches were prepared using unfunctionalized PEG of molecular weight 3,350 g/mol (PEG_{3350}) or monofunctional methyl ether PEG of molecular weight 2,000 g/mol ($mPEG_{2000}$) as these reagents are significantly less expensive than the heterofunctional PEG that was used to make the polymers to be used in the preparation of targeted nanoparticles (Chapter 6). Additionally, initial batches were designed to prepare copolymers with a 1-to-1 molar ratio of lactide to glycolide and a molecular weight of 11,000 to 15,000 g/mol with the purpose of recreating the PLGA polymer that had been used for all experiments of encapsulation of chemotherapeutic drugs and imaging agents described in Chapter 3 and 4. The theoretical molecular weight was controlled based on the number of moles of hydroxyl groups of PEG added to the reaction (two per chain for PEG_{3350} and one per chain for $mPEG_{2000}$), and assuming that each hydroxyl group on each chain of PEG would initiate the growth of a single chain of PLGA. Accordingly, PEG_{3350} would produce a triblock copolymer of the form PLGA-PEG-PLGA while $mPEG_{2000}$ produced a diblock copolymer of the form mPEG-PLGA. The size of these initial batches was limited to less than 2 grams, which is significantly smaller than batch sizes reported in the literature (Du, Lemstra et al. 1995; Quellec, Gref et al. 1998; Beletsi, Leontiadis et al. 1999; Kiremitci-Gumusderelioglu and Deniz 1999; Yoo and Park 2001; Porjazoska, Karal-Yilmaz et al. 2004).

Table 5.6 displays the results of some of these initial batches. Specifically, this table summarizes the results of batches carried out as a melt or in dimethylformamide. The main variables that were adjusted between batches were the type of PEG used, the temperature of reaction, the time of reaction and the amount of catalyst added. In all cases, the production of copolymer was experimentally observed as an increase in the

viscosity of the reagent medium with reaction time or, in some cases, with its solidification prior to the desired reaction time. After the completion of the desired reaction time, the reaction medium was cooled to room temperature. If possible, the viscous polymer was immediately precipitated and centrifuged to obtain a solid product.

Dichloromethane was then added to the solid copolymer (either to the one precipitated or to that which had solidified during reaction) to try to solubilize it for further purification. However, in most instances only a small portion of the solid dissolved regardless of the volume of solvent or the time allowed for solubilization. Other solvents, including ethyl acetate, chloroform and dimethylformamide were also used to see if these could better dissolve the solidified polymer but no significant differences were observed. Since solubilization was required for further purification, the portion that did not dissolve was removed by filtration, thus significantly reducing the yield for the batch. The yield reported in Table 5.6 is associated with the mass of polymer that was dissolved and precipitated at least 2 times. A few batches of of 50/50 PLGA-PEG were attempted in toluene (data not shown), but similar low yields of purified polymer were obtained. Although the insoluble polymer could have been kept without further purification since it probably did not contain significant amounts of monomer, it would not have been useful for the preparation of nanoparticles.

The generation of insoluble polymer could have a number of causes. One reason could be the presence of impurities in the feed reagents which would initiate side reactions and could possibly result in the formation of a crosslinked polymer. Both monomers were purified by recrystallization prior to use and the system was dried and maintained under a nitrogen atmosphere or under vacuum at all times during the reaction. Impurities, if any, could have come with the PEG. A second and more likely reason is the effect of higher reactivity of glycolide compared to lactide. As described earlier in

this chapter, glycolide has been observed to be about 10 times more reactive than lactide in this polymerization (Gilding and Reed 1979). It is possible, then, that long stretches of poly(glycolide) were being produced as opposed to a more randomly distributed PLGA. Since poly(glycolide) is insoluble in most organic solvents including ethyl acetate, dichloromethane, chloroform, acetone, dimethylformamide and tetrahydrofuran because of its high degree of crystallinity, it would not have been possible to dissolve it in the solvents that were available (Middleton and Tipton 2000). In addition, the melting point of poly(glycolide) is 225-230°C and that of 10:90 poly(lactic-co-glycolic acid) is 180-200°C, which would account for the solidification of the reaction medium during polymerization at temperatures as high as 180°C (Middleton and Tipton 2000; Huh, Cho et al. 2003). To remedy the formation of poly(glycolide) domains, one solution may be to add glycolide dimer either in a continuous manner or in portions so that the dimer composition in the reagent mix is lower than 50% glycolide at any given time, thus permitting the polymerization of lactide and the formation of a more random copolymer.

Proton NMR analysis of the soluble fraction of two of the 50/50 PLGA-PEG copolymers prepared was done. Figure 5.11 shows the NMR spectra of these two polymers, which were prepared in the melt at 140°C using PEG_{3350} and stannous octoate at 0.05 wt.% of the feed. As observed, the peaks for polymerized lactide and glycolide as well as for PEG are observed. From the area under the peaks for each of these agents, the composition of the copolymers was determined to be of 46/54 and 59/41 lactide-to-glycolide, which is close to the desired 50/50 copolymer. The molecular weight calculated from the NMR data was of 18,000 g/mol for both copolymers, i.e. slightly lower than the desired 25,000 g/mol. The low yield of these batches did not permit gel permeation chromatography analysis.

In contrast to the 50/50 PLGA-PEG copolymers, a number of batches of 75/25 PLGA-PEG and 100/0 PLA-PEG were successfully prepared in toluene at 110°C, as shown on Table 5.7. During polymerization, these batches increased in viscosity but never solidified as the polymerization continued. Also, after precipitation and centrifugation, the polymer pellets easily dissolved in small volumes of dichloromethane for purification. The yield of these batches was in the range of 65 to 81% for batches made with $mPEG_{2000}$ and of 52 to 87% for batches prepared with the heterofunctional OH-PEG_{3400}-COOH. The composition of these polymers was confirmed by NMR analysis. For all 75/25 copolymers made with $mPEG_{2000}$ the resulting copolymer contained between 71 and 76% lactide. All 100/0 PLA-PEG copolymers showed only the lactide and PEG protons, as expected. Figures 5.12, 5.13 and 5.14 show the NMR spectra of 75/25 PLGA-$mPEG_{2000}$, 100/0 PLA-$mPEG_{2000}$ and 100/0 PLA-PEG_{3400}-COOH copolymers, respectively. Note the absence of the glycolide peak at 4.8 ppm on 100/0 PLA-PEG copolymers.

The molecular weight of the copolymers as calculated from NMR composition data was in most cases very similar to the theoretical molecular weight which is based on the reagents fed to the reaction. Only for one batch the calculated molecular weight was close to two times the theoretical molecular weight. Gel permeation chromatography was used to determine the molecular weight distribution of the copolymers. As shown on Table 5.7, the number average molecular weight (Mn) was, in most instances, lower than the theoretical or NMR-calculated value, but mostly showed increased Mn with increased theoretical molecular weight, as expected. The polydispersity, or ratio of the weight average to the number average molecular weights of the polymers was low, mostly between 1.1 and 1.3. Only two batches had higher polydispersities. The increasing molecular weight of the copolymers can be seen from the NMR spectra, as the size of the

proton peaks associated with glycolide (4.8 ppm) and/or lactide (5.2 and 1.6 ppm) peaks increase relative to the proton peak associated with PEG at 3.6 ppm. This can be observed in Figures 5.12, 5.13 and 5.14 in which spectra are in order of increasing molecular weight, unless noted, for the three groups of copolymers.

NMR analysis permits determination of the monomer content in the final formulations. As the reagents are converted from monomers to polymers, the NMR peaks of the monomer decreases while that of the polymer increases. For lactide, the monomer doublets at 1.69 ppm and quartets at 5.03 ppm are replaced by broad polymer peaks at 1.6 and 5.2 ppm (Du, Lemstra et al. 1995). Figure 5.15 shows the NMR spectra of a PLA-mPEG copolymer that was precipitated only once without further purification. The monomer peaks are readily visible, although very small compared to the polymer peaks. It is important to note that all molecular weights calculated from NMR data were specific to the polymer peaks, i.e. not affected by the presence of residual monomer, if any.

Nanoparticles were prepared with the copolymers that were successfully prepared by polymerization of glycolide and/or lactide dimers onto PEG. Since these copolymers were chosen for preparation of targeted nanoparticles, detailed protocols and optimization of nanoparticle preparation variables are described in Chapter 6. In the present chapter, it is worth mentioning that nanoparticles prepared with these amphiphilic copolymers presented significant differences compared to PLGA nanoparticles. The former had significantly smaller sizes in the range of 150-180 before freeze drying as opposed to 200-300 nm for PLGA particles, were more stable in suspension and underwent severe aggregation when freeze dried without a cryoprotectant. All of these characteristics are consistent with the presence of PEG on their surface. Figure 5.16 shows a scanning electron microscopy image of some of these nanoparticles.

NMR analysis of the nanoparticles dissolved in deuterated dimethylsulfoxide after freeze drying confirmed that the composition of the nanoparticles was very similar to that of the copolymers used to make them. Figure 5.17 shows the NMR spectra for a batch of nanoparticles and for the PLA-mPEG$_{2000}$ copolymer with which they were prepared. Using the NMR peak intensities, the calculated molecular weight of the polymers of four identical nanoparticles batches to that in Figure 5.17C were found to be similar, although slightly lower than that of the starting copolymer. Specifically, the nanoparticle polymer molecular weights were calculated to be between 31,000 and 39,000 g/mol for all four batches, while the molecular weight of the copolymer was first determined to be 27,501 g/mol. It is possible that lower molecular weight polymer molecules were lost during preparation of the particles as a result of the formation of micelles, thus resulting in a lower average molecular after nanoparticle preparation. Importantly, no residual monomer is observed in the nanoparticles, as expected.

Nuclear magnetic resonance was also used to show the distribution of PEG within or around the nanoparticles. Specifically, Figure 5.18 shows the NMR spectra of a copolymer of PLA-PEG$_{3400}$-COOH dissolved in deuterated chloroform (B), of the nanoparticles prepared with this copolymer while suspended in deuterated water (C), and of the dried nanoparticles after being dissolved in deuterated dimethylsulfoxide (D). In the nanoparticles, PLA forms the hydrophobic core of the nanoparticle in which drugs or imaging agent can be encapsulated. PEG is localized at the surface of the nanoparticles and forms a hydrophilic shield that protects the nanoparticle from rapid recognition by the immune system, thus prolonging its circulation time. When nanoparticles are suspended in water, PLA remains solid and does not produce a resonance signal. PEG present on the surface of the nanoparticles, on the other hand, remains solvated and produces a signal in the NMR spectra, as shown in Figure 5.18C. Smaller peaks

observed in this spectra are associated with the surfactant (poly(vinyl alcohol)) and possibly with lactide protons that are in immediate proximity to PEG at the surfaced of the nanoparticles. After dissolving the dry particles, the copolymer composition can be once more confirmed.

Polymerization of lactide and glycolide onto PEG to form block copolymers is a viable method the incorporation of PEG onto nanoparticles. Copolymers of 75/25 PLGA-PEG or 100/0 PLA-PEG were successfully prepared in good yields and with good reproducibility. The polymerization method can be easily adjusted for the preparation of copolymers of varied composition and molecular weight, both of which are key factors in the resulting nanoparticle characteristics. In addition, and as will be confirmed in Chapter 6, the use of heterofunctional PEG containing both carboxylic acid and hydroxyl groups permits the preparation of copolymers that can be used for further derivatization.

5.4 CONCLUSION

This chapter describes various methods for the incorporation of poly(ethylene glycol) on the surface of PLGA nanoparticles. The preparation of nanoparticles with blends of PLGA and functionalized PEG did not prove to be effective as most of the hydrophilic PEG partitioned to the aqueous phase during preparation and further during nanoparticle washes. Blends of PLGA with Pluronic F127 did result in significant modification of the nanoparticle composition and surface charge, with up to 43% incorporation efficacy. However, this method does not provide permanent surface particle coverage, especially if the Pluronic is only adsorbed to the surface of the particles.

Three methods were used for covalent attachment of PEG to PLGA nanoparticles. Direct conjugation of PEG to the carboxylic acid groups of PLGA that were present on

the surface of the nanoparticles did not result in sufficient incorporation, possibly because of inaccessibility of these groups. Conjugation of PEG to PLGA in solution resulted in moderate copolymer conjugation efficiency depending on the specific conditions in which the conjugations were carried out. However, the main difficulty with this method was the purification of the copolymers by precipitation, which prevented the recovery of high yields. Finally, preparation of copolymers by the ring-opening polymerization of lactide and glycolide dimers onto PEG, methyl ether PEG, or OH-PEG-COOH was achieved. This last method could be used for the preparation of copolymers of a wide range of compositions and molecular weights. NMR analysis confirmed the composition of all copolymers in which PEG was covalently attached to PLGA or PLA. NMR also confirmed that the composition of the copolymers was maintained after preparation of nanoparticles, proving that PEG was in fact attached to the hydrophobic PLGA or PEG as opposed to simply associated to the polymer. Finally, NMR analysis of PLA-PEG nanoparticles in suspension confirmed that PEG was in fact being presented on the surface of the nanoparticles as a shielding layer that would protect them from rapid opsonization and sequestration by the reticuloendothelial system.

Chapter 3 and 4 described the preparation of PLGA nanoparticles loaded with chemotherapeutic and imaging agents, and their interaction with tumor cells *in vitro*. The present chapter describes how to modify these particles to include poly(ethylene glycol) on their surface so that targeting agents can be incorporated on their surface and so that they have a better chance of reaching the target diseased tissue *in vivo*. The following chapter describes the optimization of the parameters for the preparation of nanoparticles with PLA-PEG copolymers including cryoprotection, the encapsulation of chemotherapeutic and imaging agents within them, and the attachment of targeting agents to their surface.

Table 5.1 Summary of results for the incorporation of FITC-PEG-NHS in poly(lactic-co-glycolic acid) nanoparticles by blending of polymers. Abbreviations: poly(vinyl alcohol) (PVA), bovine serum albumin (BSA), sodium cholate (SC), poly(ethylene glycol) (PEG). Data are the average ± standard deviation for at least four independent samples.

Targeted FITC-PEG-NHS Incorporation (wt. %)	Type of Surfactant	Yield (%)	Size Before Freeze Drying (nm)	Size After Freeze Drying (nm)	Incorporation Efficiency (%)	PEG Content in Particles (wt. %)
0	PVA	60.9 ± 6	190 ± 3	263 ± 42	---	---
9.2	BSA	68.4 ± 11	236 ± 18	305 ± 21	-1.7 ± 7.6	-0.2 ± 0.8
9.2	PVA	58.9 ± 7	201 ± 11	331 ± 153	1.2 ± 8.0	0.1 ± 0.8
9.2	SC	56.9 ± 7	137 ± 16	179 ± 14	11.6 ± 12	1.1 ± 1.3
16.8	PVA	57.8 ± 11	217 ± 30	271 ± 14	4.1 ± 6.4	0.8 ± 1.3

Table 5.2 Incorporation of Pluronic F127 (PF127) in poly(lactic-co-glycolic acid) (PLGA) nanoparticles by blending of polymers. Data are the average ± standard deviation for at least three independent batches.

Ratio of PF127 / PLGA Used in Preparation	Yield (%)	Size Before Freeze Drying (nm)	Size After Freeze Drying (nm)	Zeta Potential (mV)	PF127 Incorporation Efficiency (%)	PF127 Content in Particles (wt. %)
50 : 50	27.7 ± 3.7	130 ± 12	493 ± 49	-27.9 ± 3.4	76.5 ± 2.4	43.3 ± 0.8
25 : 75	46.7 ± 3.3	168 ± 31	765 ± 133	-32.0 ± 3.5	42.0 ± 6.0	12.3 ± 1.5

Table 5.3 Preparation of PLGA-NH-PEG-COOH copolymers by conjugation of pre-made poly(lactic-co-glycolic acid) (PLGA) with heterofunctional poly(ethylene glycol) (PEG) mediated by carbodiimide chemistry. Results include the molar ratio of PLGA to PEG as determined by nuclear magnetic resonance (NMR) and the number average molecular weight (Mn) of the resulting copolymers as determined by gel permeation chromatography (GPC). Abbreviations: Chloroform ($CHCl_3$), dichloromethane (DCM), dimethylformamide (DMF), polydispersity index (PI).

Conjugation Solvent	Reaction Time (hr)	PLGA/PEG Molar Ratio From NMR	GPC Mn	GPC PI
$CHCl_3$	24	1.4		
DCM	4	2.0	10,760	1.2
DCM	4	2.9	12,400	1.3
DMF	4	3.4	8,458	1.3
DCM	4	4.8		
$CHCl_3$	2	8.9		
DCM	2	30.2		
DCM	2	43.3		

Table 5.4 Characteristics of nanoparticles PEGylated by conjugation of NH_2-PEG-COOH on their surface using carbodiimide chemistry in aqueous suspension. * Nanoparticles too large for sizing with ZetaPlus Instrument.

Sample	Surfactant	Cryoprotectant	Size Before Freeze Drying (nm)	Size After Freeze Drying (nm)	Zeta Potential (mV)
PEGylated	N/A	none	324 ± 31	*	*
PEGylated	PVA	none		*	*
PEGylated	PVA	glucose	245 ± 15	261 ± 25	-9.7 ± 1.3
PEGylated	PVA	trehalose		235 ± 3	-15.4 ± 2.7
Not PEGylated	PVA	trehalose	229 ± 5	234 ± 2	-10.8 ± 2.0

Table 5.5 Molar composition based on XPS analysis of nanoparticles (NPs) PEGylated after preparation by conjugation of NH_2-PEG-COOH on their surface using carbodiimide chemistry (EDC/NHS) in suspension. Values for PLGA and PEG are theoretical compositions based on the chemical structure of their repeating units.

Sample	Molar Composition (%)		
	Carbon	Oxygen	Nitrogen
PLGA (theoretical)	55.56	44.44	0
PEG (theoretical)	33.33	66.67	0
Control PLGA NPs (No surfactant & no activation)	58.51	41.42	0.07
Activated NPs (no PEG conjugation)	57.44	41.88	0.68
PEGylated NPs	59.03	40.76	0.21

Table 5.6 Summary of batches of 50/50 PLGA-PEG prepared by melt or solution polymerization in dimethylformamide.

Solvent	Feed Lact/Gly Ratio	Type of PEG	Theoretical Molecular Weight (g/mol)	Reaction Temperature (°C)	Reaction Time (hr)	Stannous Octoate Amount	Yield of Purified Polymer (%)
Melt	50/50	$mPEG_{2000}$	14,000	140	1	0.05 wt %	12.4
Melt	50/50	$mPEG_{2000}$	14,000	140	2	0.05 wt %	23.2
Melt	50/50	$mPEG_{2000}$	14,000	140	3	0.05 wt %	15.5
Melt	50/50	PEG_{3350}	25,000	140	0.2	0.05 wt %	3.9
Melt	50/50	PEG_{3350}	10,000	140	0.3	0.05 wt %	2.2
Melt	50/50	PEG_{3350}	25,000	140	0.3	0.05 wt %	12.7
Melt	50/50	PEG_{3350}	17,000	140	0.1	1:1 to PEG	25.3
Melt	50/50	PEG_{3350}	35,000	140	0.4	1:1 to PEG	18.3
DMF	50/50	$mPEG_{2000}$	14,000	140	24	1:1 to PEG	6.7
DMF	50/50	$mPEG_{2000}$	14,000	140	28	1:1 to PEG	0.0
DMF	50/50	$mPEG_{2000}$	14,000	140	48	1:1 to PEG	0.7
DMF	50/50	$mPEG_{2000}$	14,000	140	72	1:1 to PEG	2.4
DMF	50/50	$mPEG_{2000}$	14,000	140	90	1:2 to PEG	0.1
DMF	50/50	$mPEG_{2000}$	14,000	140	90	1:1 to PEG	0.7
DMF	50/50	PEG_{3350}	17,000	110	0.5	1:1 to PEG	7.4
DMF	50/50	PEG_{3350}	17,000	140	0.3	1:1 to PEG	10.0
DMF	50/50	PEG_{3350}	32,000	140	0.5	2:1 to PEG	3.6
DMF	50/50	PEG_{3350}	32,000	140	2	2:1 to PEG	1.4
DMF	50/50	PEG_{3350}	32,000	140	4	2:1 to PEG	6.2
DMF	50/50	PEG_{3350}	32,000	140	5	2:1 to PEG	1.3

Table 5.7 Characteristics of batches of PLGA-PEG or PLA-PEG copolymers prepared by solution polymerization in toluene at 110°C using a 1:1 molar ratio of PEG to stannous octoate catalyst. Abbreviations: Molecular weight (MW), nuclear magnetic resonance (NMR), number average molecular weight (Mn), polydispersity index (PI).

Feed Lact/Gly Ratio	Reaction Time (hr)	Type of PEG	Yield (%)	Theoretical MW	NMR MW	NMR Lact/Gly Ratio	GPC Mn	GPC PI
75/25	1	$mPEG_{2000}$	81.0	23,390	27,501	76 / 24	18,305	1.13
75/25	1	$mPEG_{2000}$	67.2	34,128	29,005	71 / 29	14,520	1.12
75/25	1	$mPEG_{2000}$	77.1	44,832	44,342	74 / 26	21,080	2.05
100/0	4	$mPEG_{2000}$	72.4	24,502	24,251	--	12,350	1.09
100/0	4	$mPEG_{2000}$	76.9	35,738	36,794	--	14,235	1.08
100/0	4	$mPEG_{2000}$	75.9	46,908	88,081	--	28,463	1.29
100/0	4	$OH\text{-}PEG_{3400}\text{-}COOH$	52.7	28,358	19,483	--	35,550	1.22
100/0	4	$OH\text{-}PEG_{3400}\text{-}COOH$	85.3	53,414	61,965	---	38,915	1.12
100/0	4	$OH\text{-}PEG_{3400}\text{-}COOH$	87.4	53,428	55,592	---	80,820	1.15
100/0	12	$OH\text{-}PEG_{3400}\text{-}COOH$	76.0	53,401	59,519	--	35,470	3.16

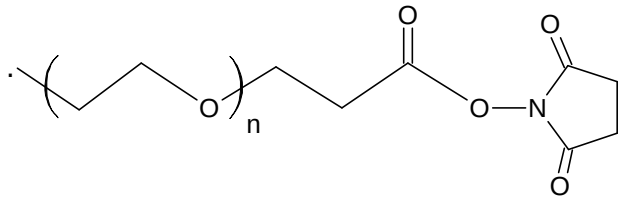

Figure 5.1 N-hydroxysuccinimide ester of poly(ethylene glycol) (PEG-NHS). The NHS functionality was a desired characteristic of the PEG-derivatives utilized in the design of the targeted nanoparticles. The electrophilic NHS functional group was used to form physiologically stable amide linkages with primary amine groups in the targeting agents.

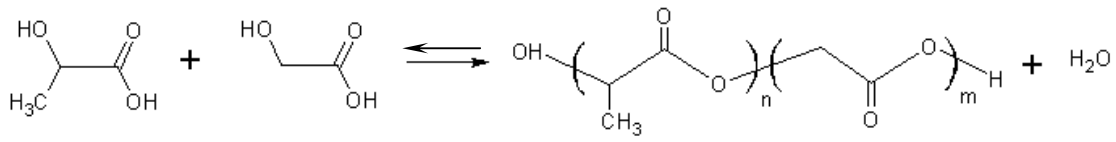

Figure 5.2 Polycondensation of lactic and glycolic acid to form poly(lactic co-glycolic acid)

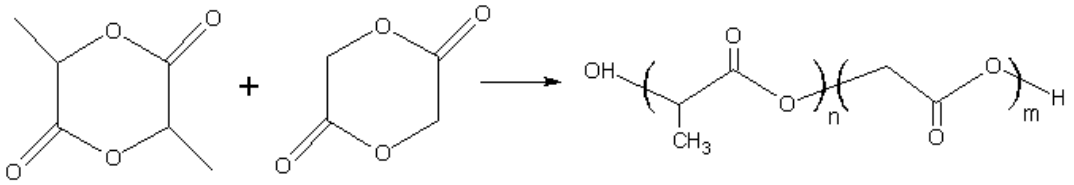

Figure 5.3 Ring opening polymerization of cyclic lactide and glycolide dimers to form poly(lactic-co-glycolic acid)

A

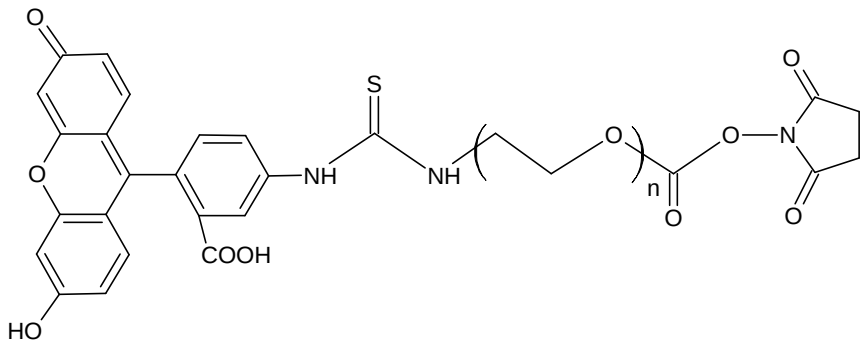

B

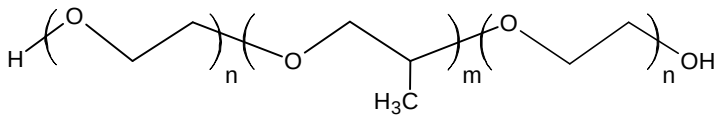

Figure 5.4 Chemical structure of PEG derivatives incorporated into PLGA nanoparticles through polymer blending. (A) Fluorescein-PEG-N-hydroxysuccinimide (FITC-PEG-NHS), and (B) Poloxamer F127 (n = 101 and m = 56).

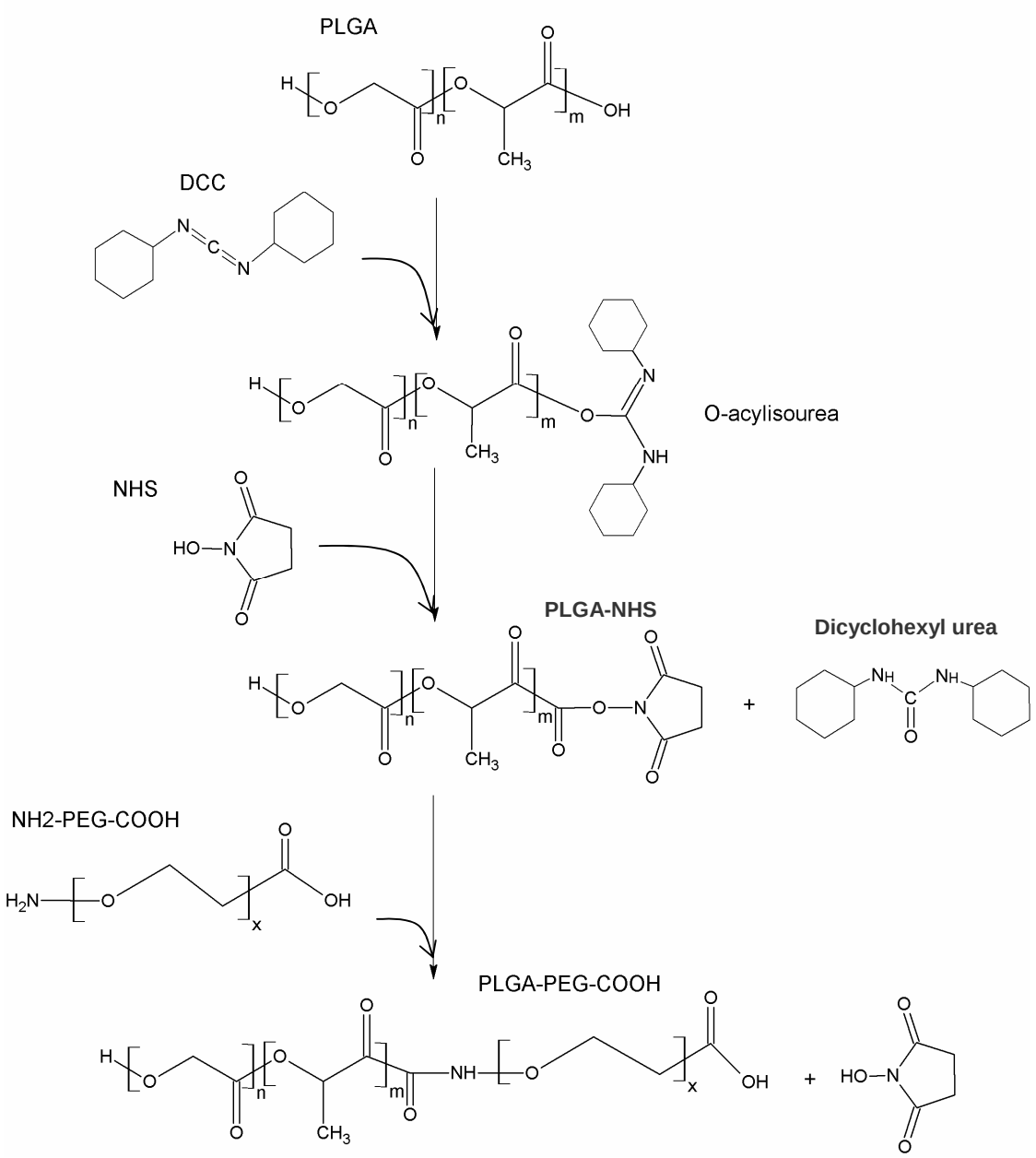

Figure 5.5 Conjugation of poly(lactic-co-glycolic acid) (PLGA) to heterofunctional poly(ethylene glycol) (PEG). Carboxyl groups of PLGA are activated with DCC and N-hydroxysuccinimide (NHS) to form an NHS-ester that is highly reactive to terminal amino groups on heterofunctional PEG. These react to form a stable amide linkage.

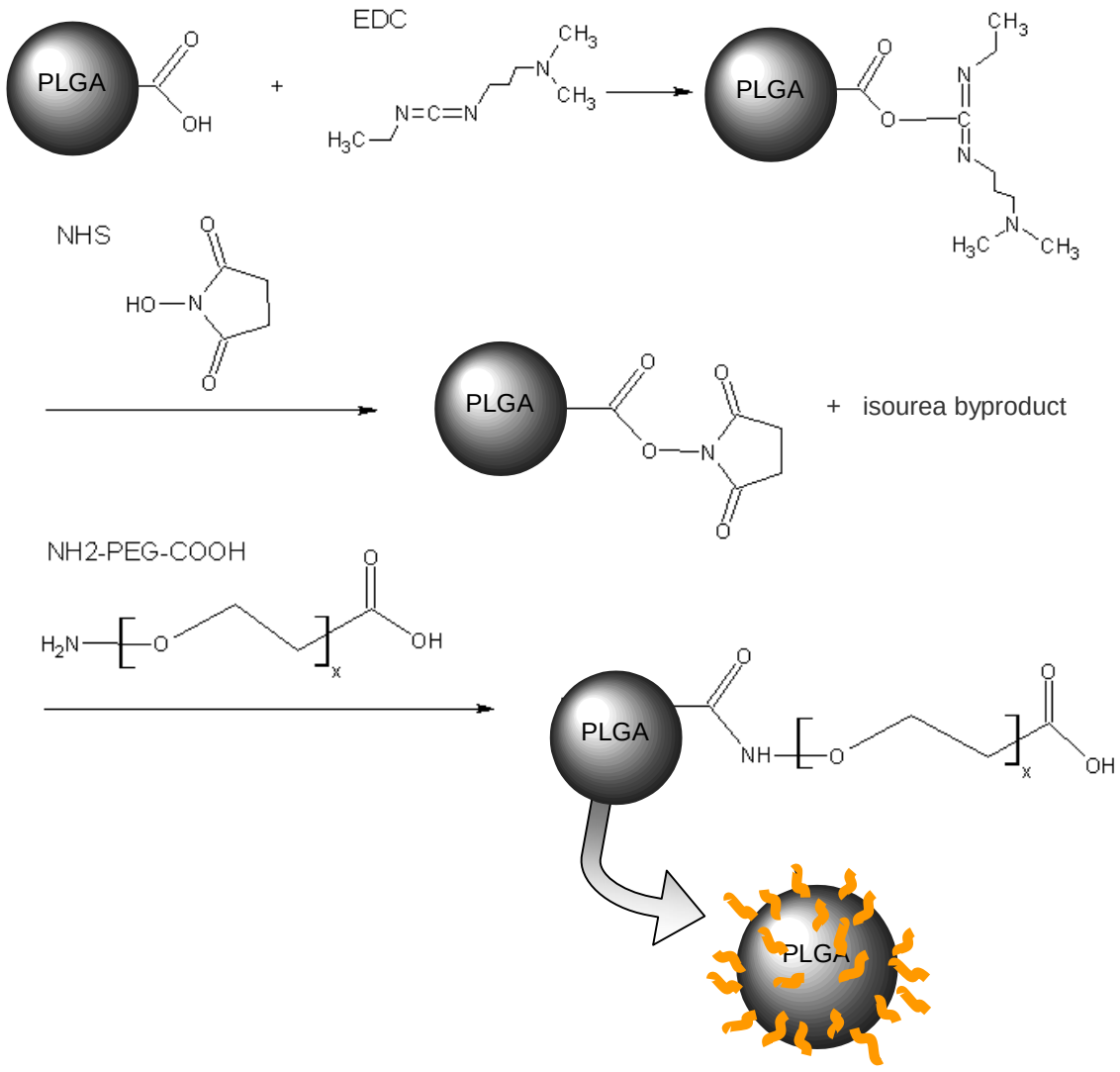

Figure 5.6 Conjugation of PEG to PLGA on the surface of pre-made nanoparticles. Carboxylic acid groups of PLGA present on the surface of the nanoparticles are activated with EDC and N-hydroxysuccinimide to form an NHS ester. This reacts with the primary amino group of heterofunctional PEG forming a stable amide bond.

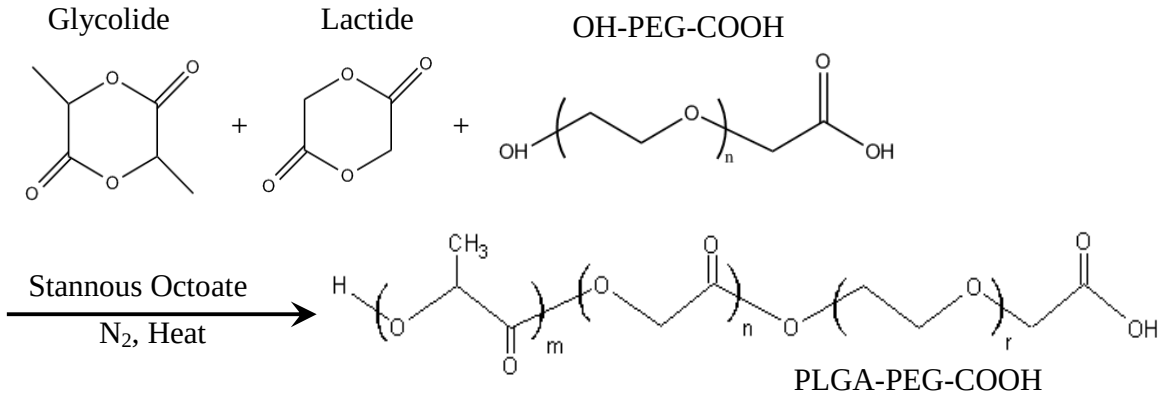

Figure 5.7 Ring-opening polymerization of lactide and glycolide initiated by the hydroxyl groups of heterofunctional OH-PEG-COOH.

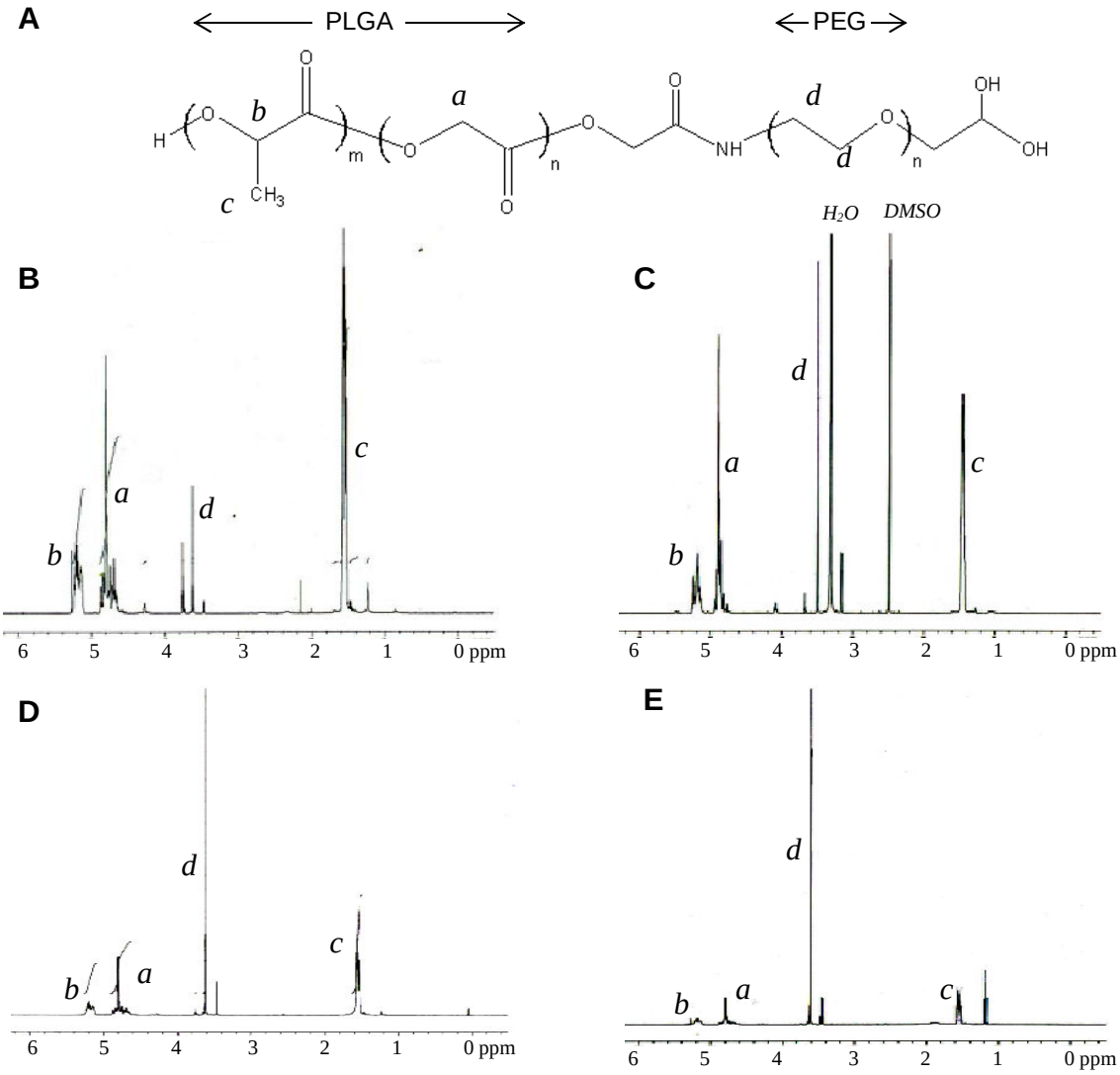

Figure 5.8 Nuclear magnetic resonance (NMR) spectra of PLGA-NH-PEG-COOH copolymers prepared by conjugation of PLGA and heterofunctional PEG. (A) Chemical structure of the copolymer and assignment of proton labels. Conjugations were carried out for (B) 2 hr in dichloromethane, (C) 2 hr in chloroform, (D) 4 hr in dichloromethane and (E) 24 hr in chloroform. Spectra are arranged in order of increasing conjugation efficiency (B through E). Note the increasing size of the PEG peak *d* at 3.6 ppm relative to the peaks of PLGA at 1.6 (*c*), 5.2 (*b*) and 4.8 ppm (*a*) with increasing conjugation efficiency. Spectrum in C was run in deuterated DMSO while all others were fun in deuterated chloroform.

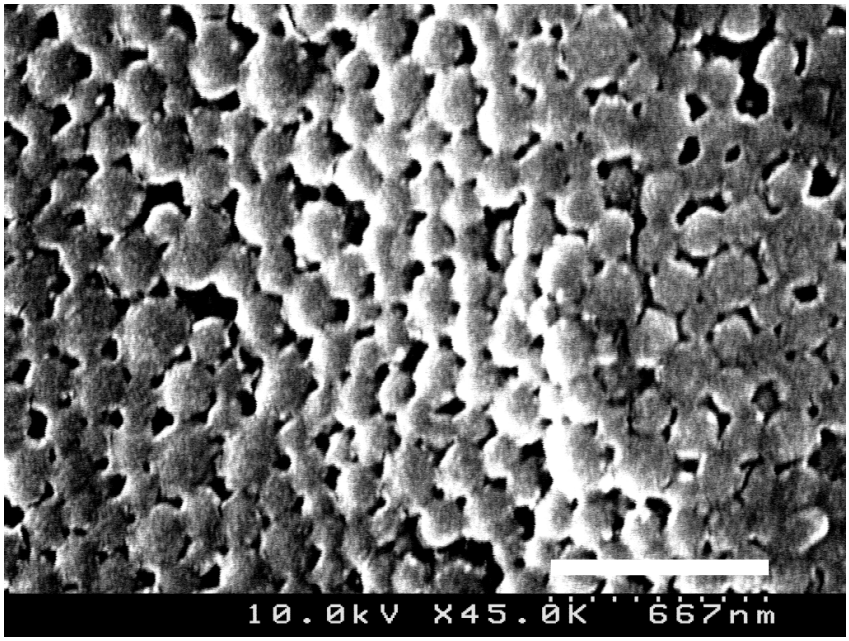

Figure 5.9 Scanning electron microscopy images of PLGA nanoparticles that were PEGylated in suspension after preparation using EDC and NHS. White bar represents a distance of 667 nm. Nanoparticle sizes are in the range of 200 nm.

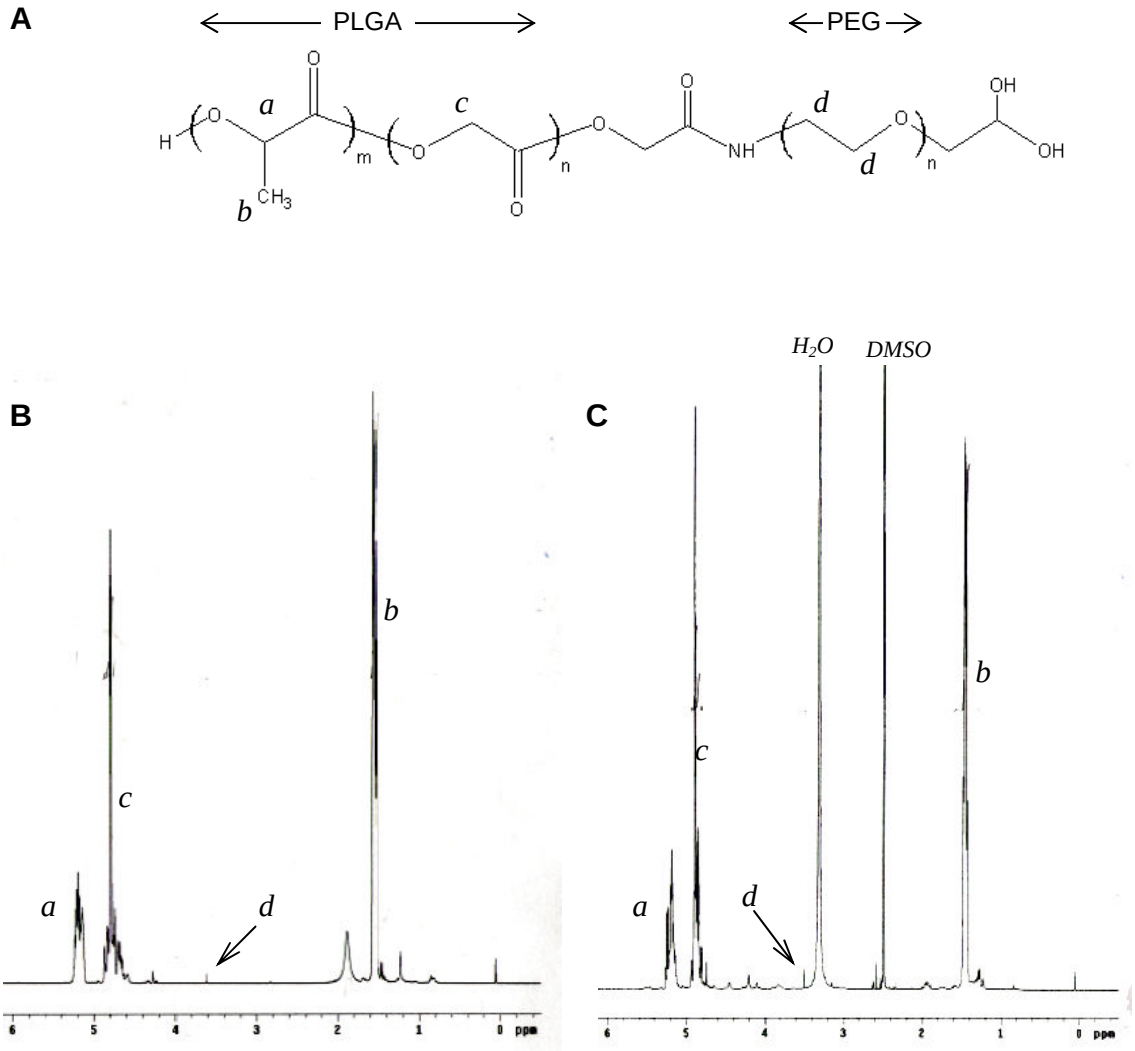

Figure 5.10 ^{1}H-NMR spectra of dried nanoparticles PEGylated by conjugation of NH2-PEG-COOH in suspension after nanoparticle preparation. (A) Structure of copolymers and assignment of peak labels. (B) Particles prepared without surfactant and freeze dried without a cryoprotectant. NMR spectra obtained after dissolving the particles in deuterated chloroform. (C) Nanoparticles prepared with poly(vinyl alcohol) as surfactant. This portion of the batch was freeze dried without cryoprotectant to prevent spectra interference with the polymers. Nanoparticles were dissolved in deuterated DMSO.

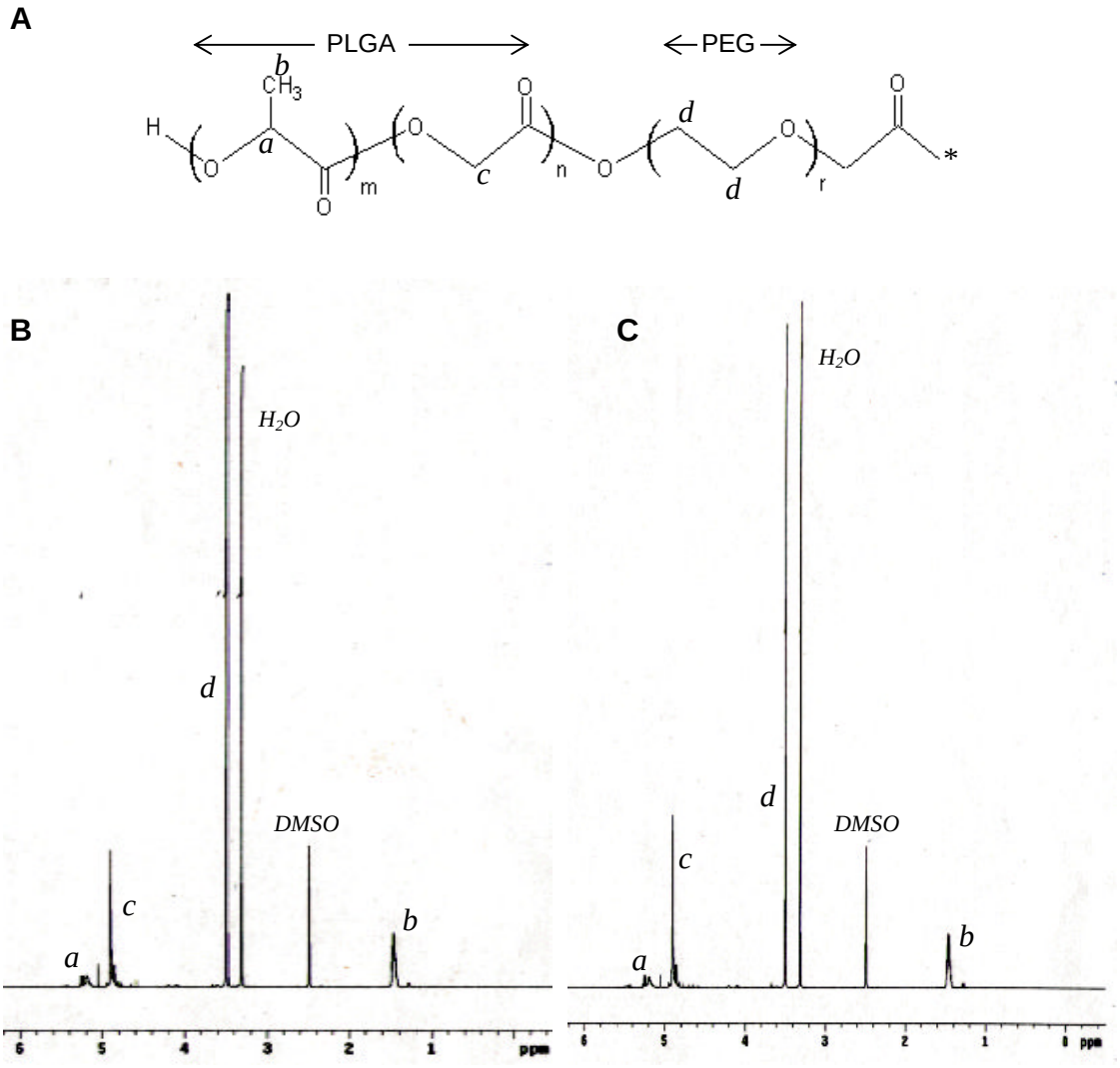

Figure 5.11 Proton NMR spectra of soluble portion of 50/50 PLGA-PEG copolymers prepared by melt polymerization (A) Chemical structure and peak assignment for PLGA-PEG. Note that the actual structure is a triblock copolymer (PLGA-PEG-PLGA) since PEG_{3350} has hydroxyl groups on both ends. (B and C) 1H-NMR spectra of both copolymers.

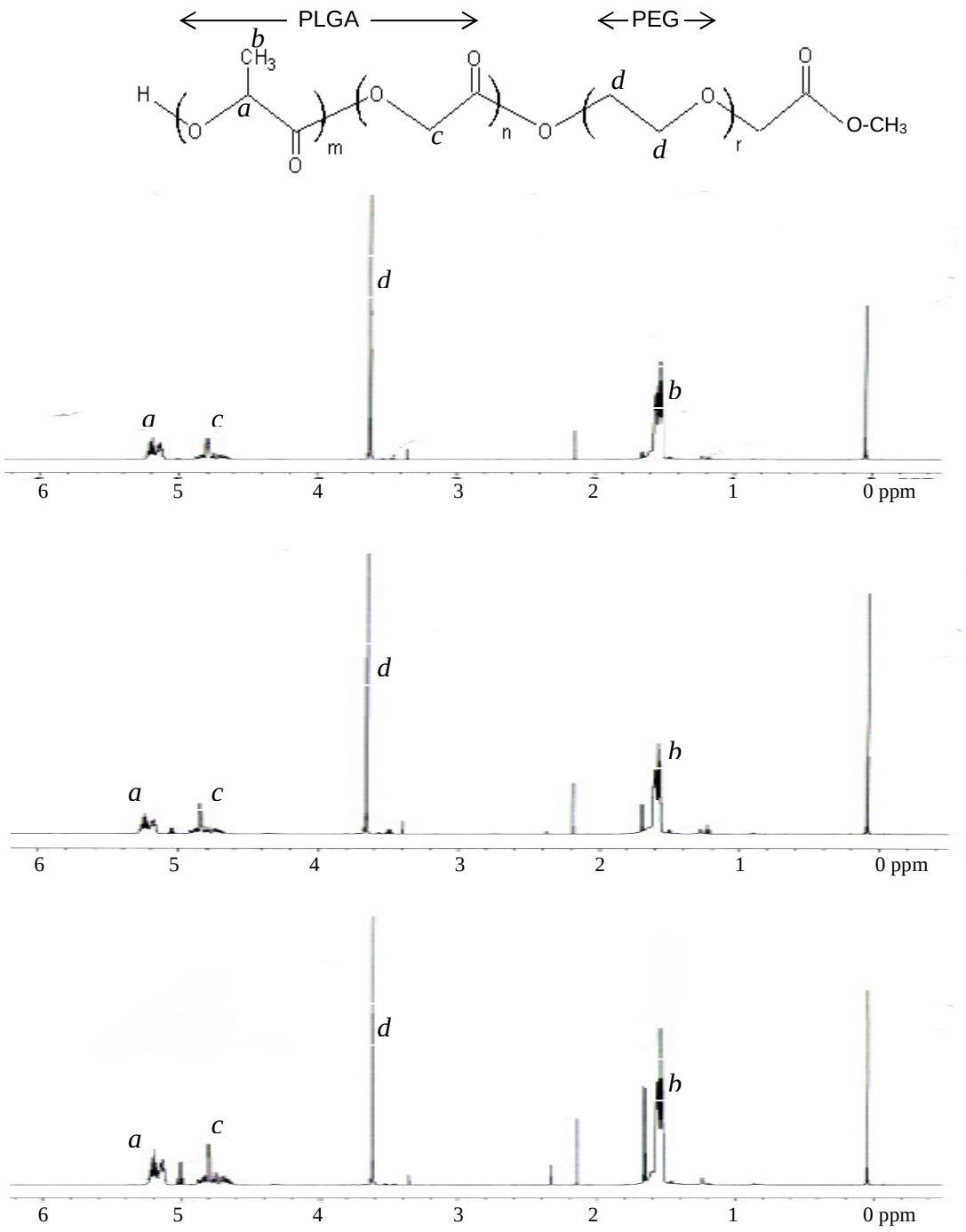

Figure 5.12 Proton NMR spectra of 75/25 PLGA-mPEG$_{2000}$ prepared in toluene in order of increasing theoretical and NMR-determined molecular weight.

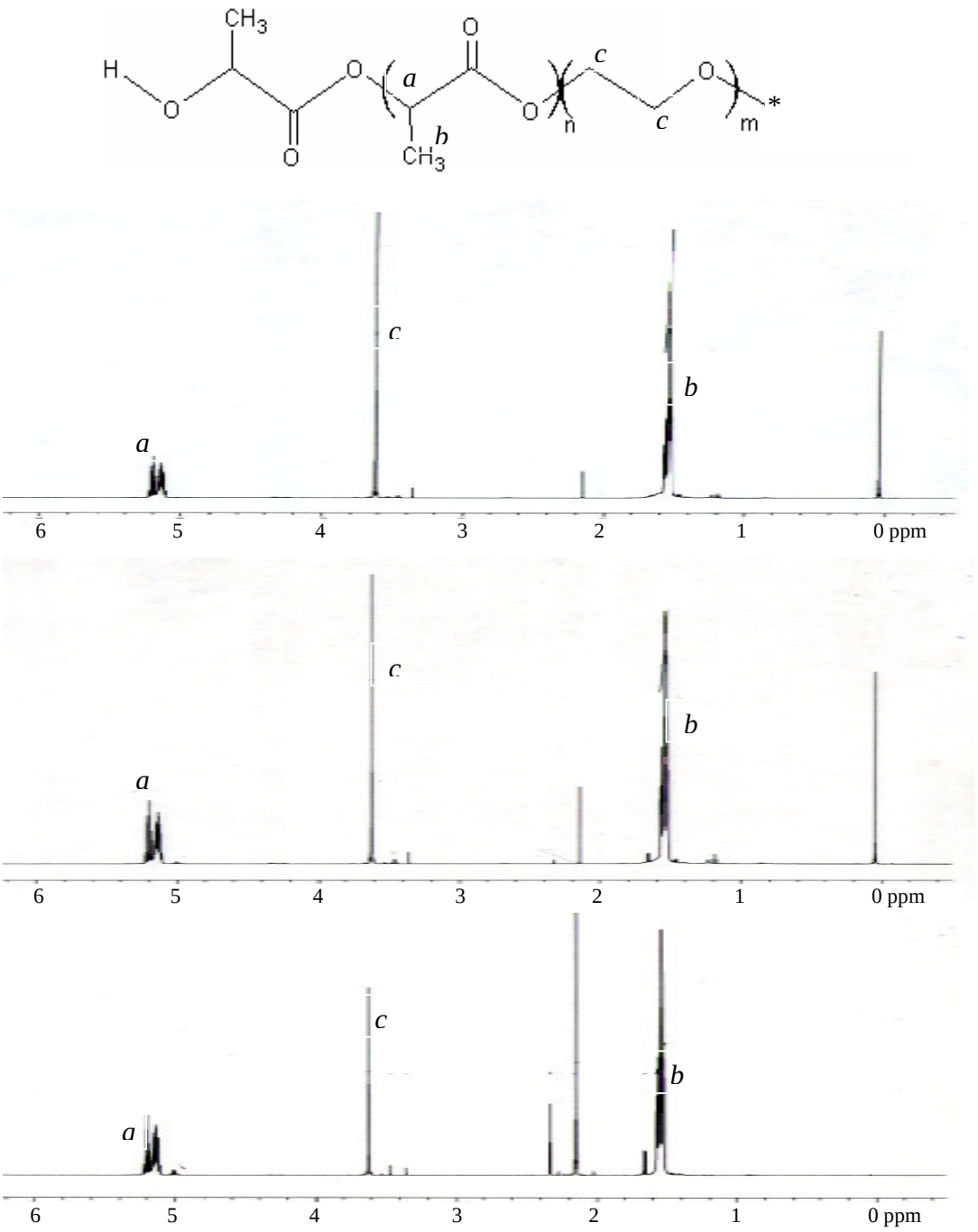

Figure 5.13 Proton NMR spectra of 100/0 PLA-mPEG$_{2000}$ prepared in toluene in order of increasing theoretical and NMR-determined molecular weight.

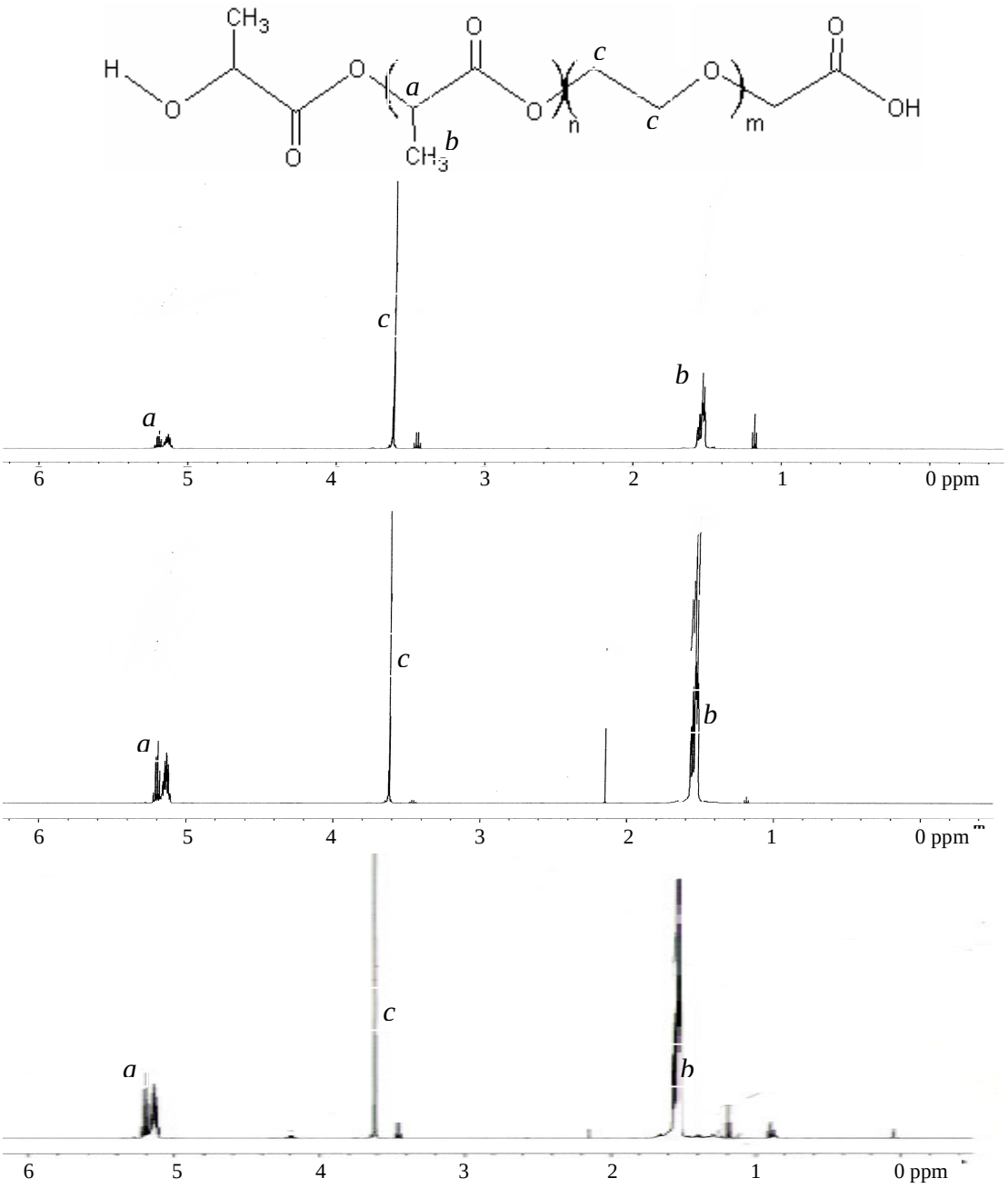

Figure 5.14 Proton NMR spectra of 100/0 PLA-PEG_{3400}-COOH prepared in toluene in order of increasing theoretical and NMR-determined molecular weight. Last two polymers had equal theoretical and very close NMR MW.

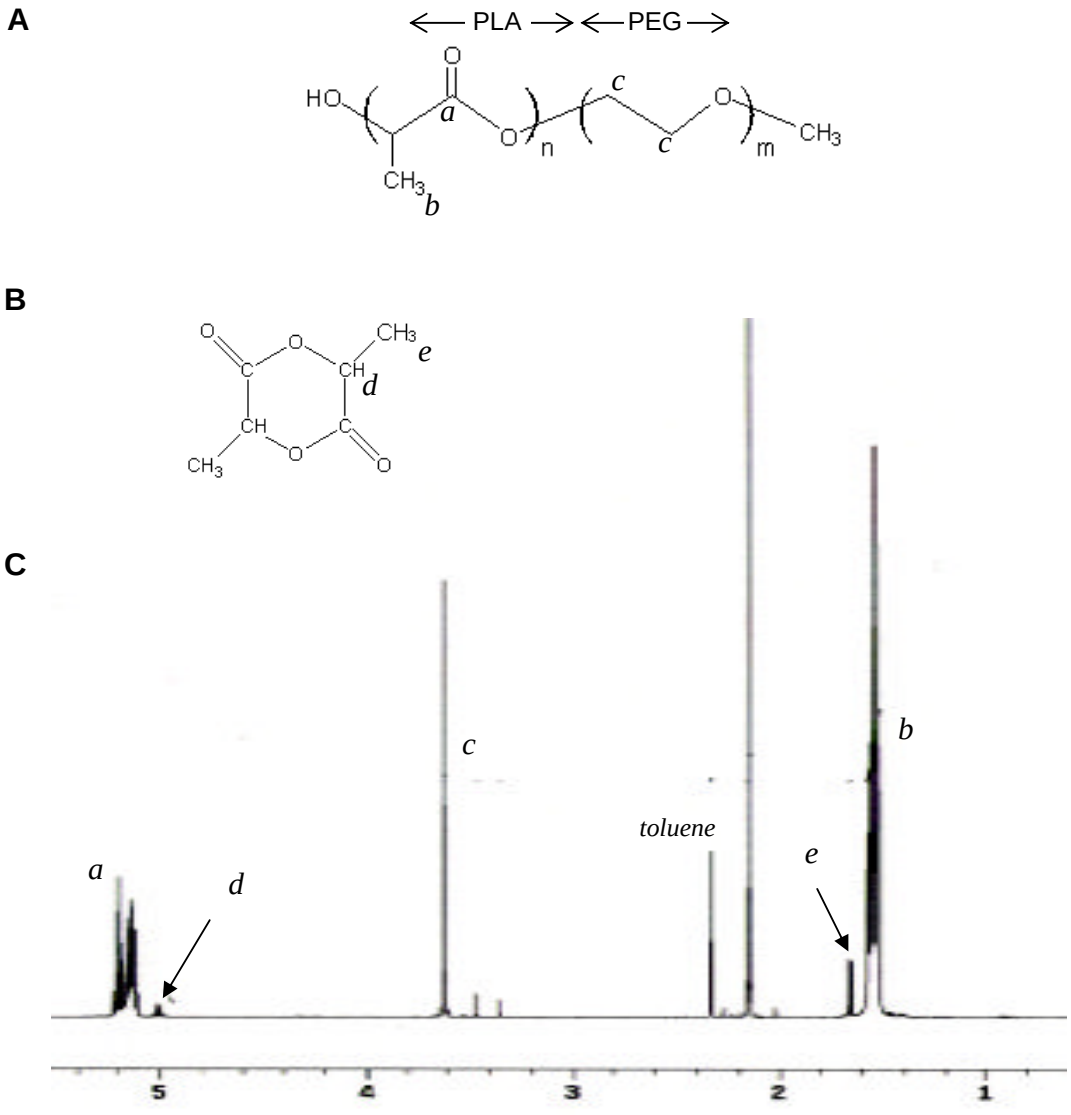

Figure 5.15 Chemical structure and proton NMR peak assignment (italics) for (A) PLA-$mPEG_{2000}$ copolymer and (B) lactide monomer. (C) NMR spectra of PLA-PEG copolymer prepared by ring-opening polymerization of lactide initiated by the hydroxyl group of OH-PEG-COOH with stannous octoate as catalyst. Reaction carried out in toluene for 4 hr at 110°C. This batch was precipitated in ethyl ether once but not further purified. Spectra show the presence of unreacted lactide monomer as well as poly(lactide).

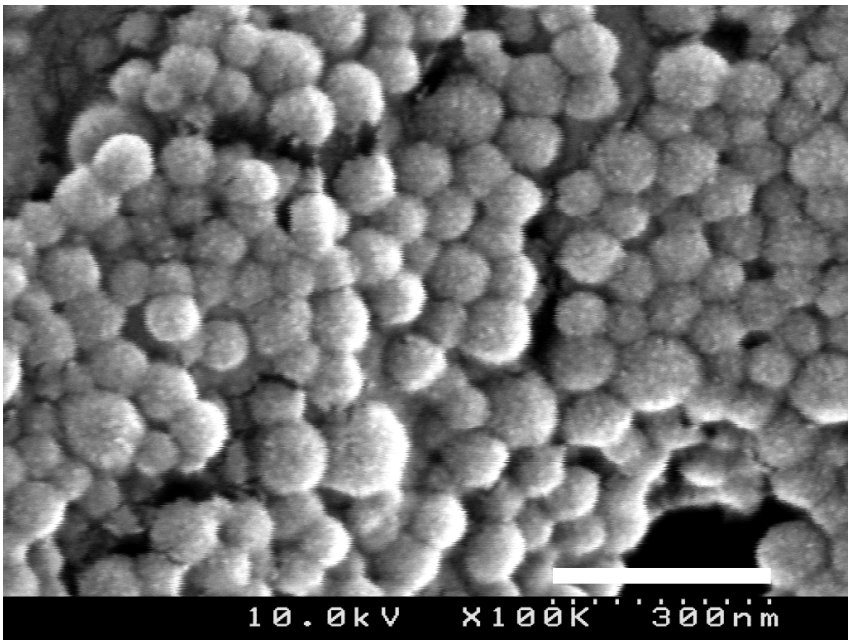

Figure 5.16 Scanning electron microscopy image of nanoparticles prepared with 100/0 PLA-PEG-COOH copolymer prepared by polymerization in solution. White bar represents 300 nm.

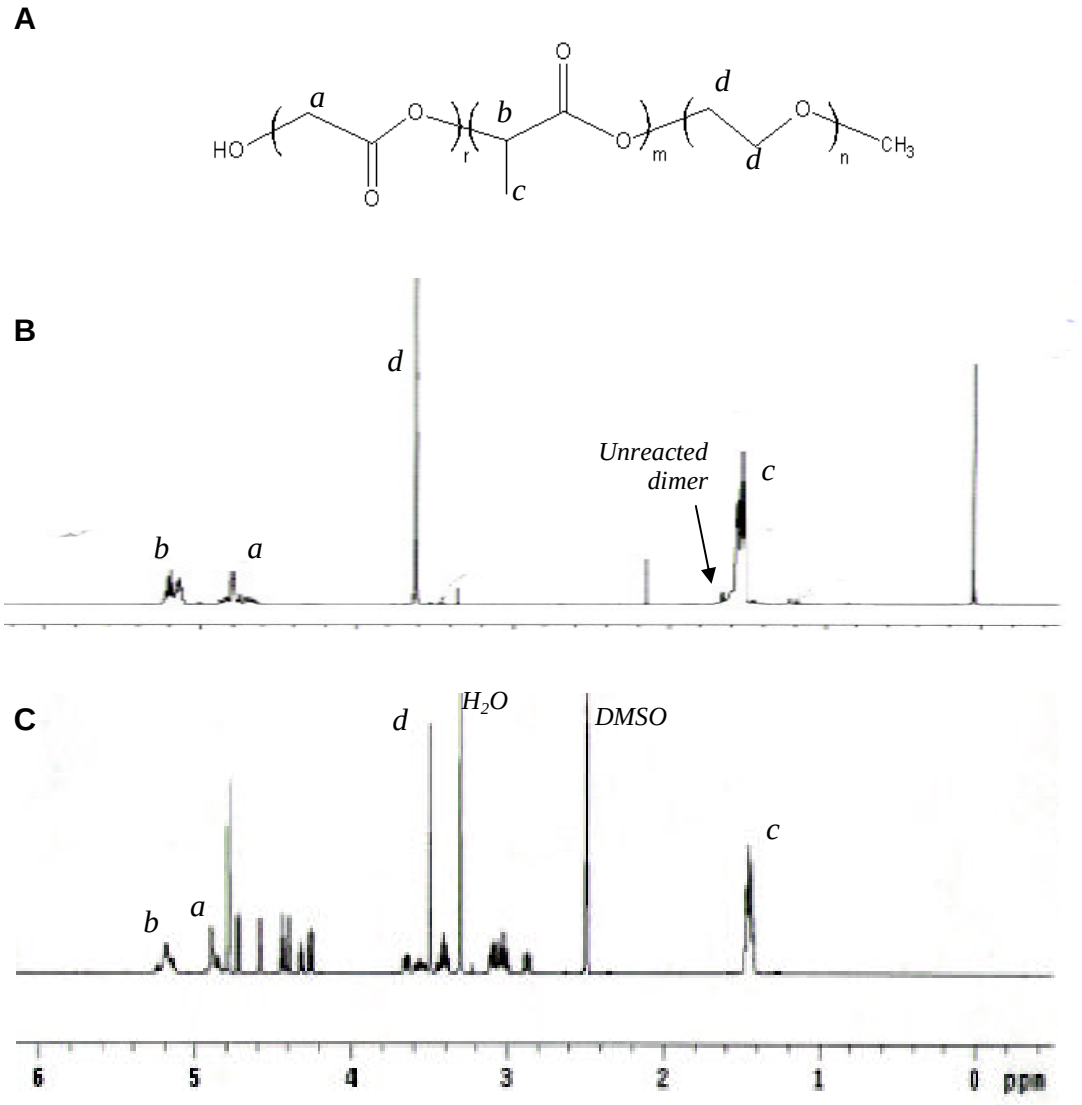

Figure 5.17 (A) Chemical structure and proton NMR peak assignment for PLGA-PEG copolymer. (B) 1H-NMR spectra of PLGA-mPEG$_{2000}$ prepared by polymerization and (C) nanoparticles prepared with this polymer. Additional peaks in nanoparticles correspond to glucose used as a cryoprotectant for the nanoparticles.

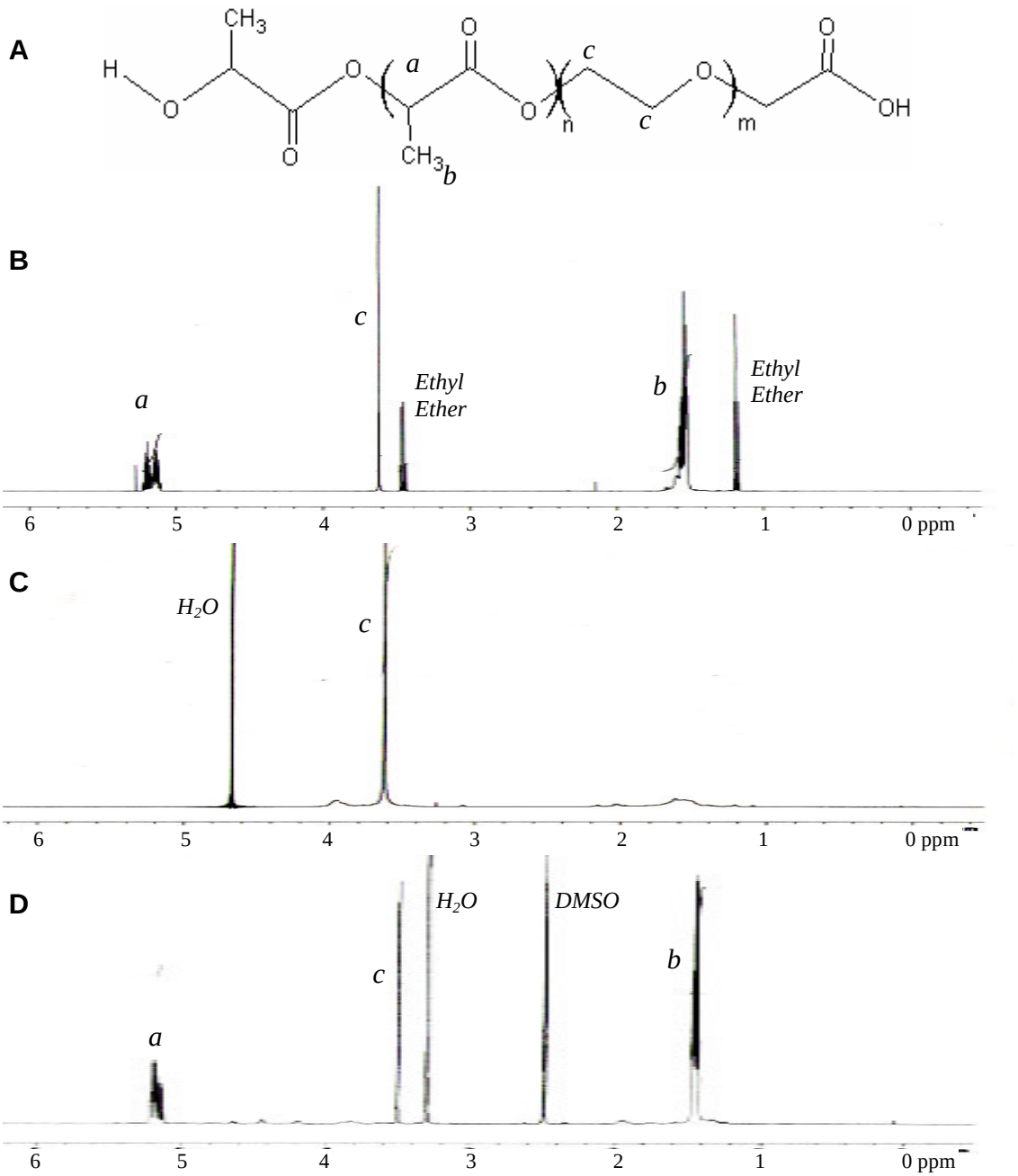

Figure 5.18 Nuclear magnetic resonance analysis of nanoparticles of PLA-PEG_{3400}-COOH. (A) Chemical structure and proton peak assignment. (B) NMR spectra of PLA-PEG-COOH copolymer used for nanoparticle preparation. (C) NMR spectra of nanoaparticles suspended in D_2O. No lactide peaks are observed. (D) Spectra of nanoparticles dissolved in d-DMSO.

5.5 REFERENCES

Abdelwahed, W., G. Degobert, et al. (2006). "Freeze-drying of nanoparticles: Formulation, process and storage considerations." Advanced Drug Delivery Reviews 58(15): 1688-1713.

Avgoustakis, K. (2004). "Pegylated poly(lactide) and poly(lactide-co-glycolide) nanoparticles: preparation, properties and possible applications in drug delivery." Current Drug Delivery 1: 321-333.

Avgoustakis, K., A. Beletsi, et al. (2003). "Effect of copolymer composition on the physicochemical characteristics, in vitro stability, and biodistribution of PLGA-mPEG nanoparticles." Int J Pharm 259(1-2): 115-27.

Barichello, J. M., M. Morishita, et al. (1999). "Encapsulation of Hydrophilic and Lipophilic Drugs in PLGA Nanoparticles by the Nanoprecipitation Method." Drug Development and Industrial Pharmacy 25(4): 471-476.

Barratt, G. (2003). "Colloidal drug carriers: achievements and perspectives." Cell Mol Life Sci 60(1): 21-37.

Bazile, D., C. Prud'Homme, et al. (1995). "Stealth Me.PEG-PLA Nanoparticles Avoid Uptake by the Mononuclear Phagocytes System." Journal of Pharmaceutical Sciences 84(4): 493-498.

Bazile, D. V., C. Ropert, et al. (1992). "Body distribution of fully biodegradable [14C]-poly(lactic acid) nanoparticles coated with albumin after parenteral administration to rats." Biomaterials 13(15): 1093-1102.

Beletsi, A., L. Leontiadis, et al. (1999). "Effect of preparative variables on the properties of poly(dl-lactide-co-glycolide)-methoxypoly(ethyleneglycol) copolymers related to their application in controlled drug delivery." International Journal of Pharmaceutics 182(2): 187-197.

Betancourt, T., B. Brown, et al. (2007). "Doxorubicin-loaded PLGA nanoparticles by nanoprecipitation: preparation, characterization and in vitro evaluation." Nanomedicine 2(2): 219-232.

Brannon-Peppas, L. and J. O. Blanchette (2004). "Nanoparticle and targeted systems for cancer therapy." Advanced Drug Delivery Reviews 56(11): 1649-1659.

Cannizzaro, S. M., R. F. Padera, et al. (1998). "A novel biotinylated degradable polymer for cell-interactive applications." Biotechnol Bioeng 58(5): 529-35.

Csaba, N., P. Caamano, et al. (2005). "PLGA:Poloxamer and PLGA:Poloxamine Blend Nanoparticles: New Carriers for Gene Delivery." Biomacromolecules 6: 271-278.

Csaba, N., L. Gonzalez, et al. (2004). "Design and characterisation of new nanoparticulate polymer blends for drug delivery." J Biomater Sci Polym Ed 15(9): 1137-51.

Csaba, N., A. Sanchez, et al. (2006). "PLGA:poloxamer and PLGA:poloxamine blend nanostructures as carriers for nasal gene delivery." J Control Release 113(2): 164-72.

de Jaeghere, F., E. Allemann, et al. (2000). "Freeze-Drying and Lyopreservation of Diblock and Triblock Poly(Lactic Acid)-Poly(Ethylene Oxide) (PLA-PEO) Copolymer Nanoparticles." Pharmaceutical Development and Technology 5(4): 473-483.

Dechy-Cabaret, O., B. Martin-Vaca, et al. (2004). "Controlled Ring-Opening Polymerization of Lactide and Glycolide." Chemical Reviews 104(12): 6147-6176.

Dittrich, V. W. and R. C. Schulz (1971). "Kinetic und mechanismus der ringöffnenden polymerisation von L(-)-lactid." Angewandte Makromolekulare Chemie 15(1): 109-126.

Du, Y. J., P. J. Lemstra, et al. (1995). "ABA Type Copolymers of Lactide with Poly(ethylene glycol). Kinetic, Mechanistic, and Model Studies." Macromolecules 28: 2124-2132.

Duda, A. and S. Penczek (1990). "Thermodynamics of L-lactide polymerization. Equilibrium Monomer Concentration." Macromolecules 23(66): 1636-1639.

Farokhzad, O. C., J. Cheng, et al. (2006). "Targeted nanoparticle-aptamer bioconjugates for cancer chemotherapy in vivo." Proc Natl Acad Sci U S A 103(16): 6315-20.

Farokhzad, O. C., S. Jon, et al. (2004). "Nanoparticle-aptamer bioconjugates: a new approach for targeting prostate cancer cells." Cancer Res 64(21): 7668-72.

Fawaz, F., F. Bonini, et al. (1993). "Influence of poly(DL-lactide) on the biliary clearance and enterohepatic circulation of indomethacin in the rabbit." Pharmaceutical Research 10(5): 750-756.

Fessi, H., J. P. Devissaguet, et al. (1986). Procédé de préparation des systèmes colloïdaux dispersibles dune substance sous forme de nanoparticules. F. P. Application. French.

Gao, X., W. Tao, et al. (2006). "Lectin-conjugated PEG-PLA nanoparticles: preparation and brain delivery after intranasal administration." Biomaterials 27(18): 3482-90.

Garcia-Fuentes, M., D. Torres, et al. (2004). "Application of NMR spectroscopy to the characterization of PEG-stabilized lipid nanoparticles." Langmuir 20(20): 8839-45.

Gilding, D. K. and A. M. Reed (1979). "Biodegradable polymers for use in surgery-polyglycolic/poly(lactic acid) homo- and copolymers: 1." Polymer 20(12): 1459-1464.

Gref, R., P. Couvreur, et al. (2003). "Surface-engineered nanoparticles for multiple ligand coupling." Biomaterials 24(24): 4529-37.

Gref, R., M. Luck, et al. (2000). "'Stealth' corona-core nanoparticles surface modified by polyethylene glycol (PEG): influences of the corona (PEG chain length and surface density) and of the core composition on phagocytic uptake and plasma protein adsorption." Colloids Surf B Biointerfaces 18(3-4): 301-313.

Gref, R., Y. Minamitake, et al. (1994). "Biodegradable Long-Circulating Polymeric Nanospheres." Science 263(5153): 1600-1603.

Heald, C. R., S. Stolnik, et al. (2002). "Poly(lactic acid)-poly(ethylene oxide) (PLA-PEG) nanoparticles: NMR studies of the central solid like PLA core and the liquid PEG corona." Langmuir 18: 3669-3675.

Hermanson, G. T. (1996). Bioconjugate Techniques. San Diego, CA, Academic Press, Inc.

Hrkach, J. S., M. T. Peracchia, et al. (1997). "Nanotechnology for biomaterials engineering: structural characterization of amphiphilic polymeric nanoparticles by 1H NMR spectroscopy." Biomaterials 18: 27-30.

Hu, R. G., Q. W. zhai, et al. (2002). "Bioactivities of ricin retained and its immunoreactivity to anti-ricin polyclonal antibodies alleviated through pegylation." International Journal of Biochemistry and Cell Biology 34(4): 396-402.

Huh, K. M., Y. W. Cho, et al. (2003). "PLGA-PEG Copolymers." Drug Delivery Technology 3(5)?

Jeong, J. H., D. W. Lim, et al. (2000). "Synthesis, characterization and protein adsorption behaviors of PLGA/PEG di-block co-polymer blend films." Colloids Surf B Biointerfaces 18(3-4): 371-379.

Kasturi, S. P., K. Sachaphibulkij, et al. (2005). "Covalent conjugation of polyethyleneimine on biodegradable microparticles for delivery of plasmid DNA vaccines." Biomaterials 26(32): 6375-6385.

Kiremitci-Gumusderelioglu, M. and G. Deniz (1999). "Synthesis, characterization and in vitro degradation of poly(DL-lactide)/poly(dl-lactide-co-glycolide) films." Turkish Journal of Chemistry 23: 153-161.

Kricheldrof, H. R. and J. Meier-Haack (1993). "Polylactones. XXII: ABA triblock copolymers of L-lactide and poly(ethylene glycol)." J. Makromol. Chem. 194(2): 715-725.

Li, J.-T., K. D. Caldwell, et al. (1994). "Surface Properties of Pluronic-Coated Polymeric Colloids." Langmuir 10: 4475-4482.

Li, Y., Y. Pei, et al. (2001). "PEGylated PLGA nanoparticles as protein carriers: synthesis, preparation and biodistribution in rats." J Control Release 71(2): 203-11.

Mehvar, R. (2000). "Modulation of the pharmacokinetics and pharmacodynamics of proteins by polyethylene glycol conjugation." Journal of Pharmacy and Pharmacetuical Sciences 3(1): 125-136.

Middleton, J. C. and A. J. Tipton (2000). "Synthetic biodegradable polymers as orthopedic devices." Biomaterials 21(23): 2335-2346.

Moghimi, S. M. and A. C. Hunter (2000). "Poloxamers and poloxamines in nanoparticle engineering and experimental medicine." Trends Biotechnol 18(10): 412-20.

Moghimi, S. M., I. S. Muir, et al. (1993). "Coating particles with a block co-polymer (poloxamine-908) suppresses opsonization but permits the activity of dysopsonins in the serum." Biochim Biophys Acta 1179(2): 157-65.

Neal, J. C., S. Stolnik, et al. (1998). "Modification of the copolymers poloxamer 407 and poloxamine 908 can affect the physical and biological properties of surface modified nanospheres." Pharm Res 15(2): 318-24.

NektarTherapeutics (2005). Nektar Advanced PEGylation - Catalog 2005-2006.

Odian, G. (2004). Principles of Polymerization. Hoboken, NJ, John Wiley & Sons.

Otsuka, H., Y. Nagasaki, et al. (2003). "PEGylated nanoaprticles for biological and pharmaceutical applications." Advanced Drug Delivery Reviews 55(3): 403-419.

Perez, C., A. Sanchez, et al. (2001). "Poly(lactic acid)-poly(ethylene glycol) nanoparticles as new carriers for the delivery of plasmid DNA." J Control Release 75(1-2): 211-24.

Porjazoska, A., O. Karal-Yilmaz, et al. (2004). "Biocompatible polymer blends of poly(D,L-lactic acid-co-glycolic acid) and triblock PCL-PDMS-PCL copolymers: Their Characterizations and Degradations." Croatia Chemica Acta 77(4): 545-551.

Quellec, P., R. Gref, et al. (1998). "Protein encapsulation within polyethylene glycol-coated nanospheres. I. Physicochemical characterization." J Biomed Mater Res 42(1): 45-54.

Salem, A. K., S. M. Cannizzaro, et al. (2001). "Synthesis and characterisation of a degradable poly(lactic acid)-poly(ethylene glycol) copolymer with biotinylated end groups." Biomacromolecules 2(2): 575-80.

Santander-Ortega, M. J., A. B. Jodar-Reyes, et al. (2006). "Colloidal stability of pluronic F68-coated PLGA nanoparticles: a variety of stabilisation mechanisms." J Colloid Interface Sci 302(2): 522-9.

Skoog, B. (1979). "Determination of polyethylene glycols 4000 and 6000 in plasma protein preparations." Vox Sang 37: 345-349.

Staros, J. V. (1982). "N-hydroxysuccinimide active esters: Bis(N-hydroxysulfosuccinimide) esters of two dicarboxylic acids are hydrophilic, membrane impermeant, protein cross-linkers." Biochemistry 21: 3950-3955.

Stolnik, S., S. E. Dunn, et al. (1994). "Surface modification of poly(lactide-co-glycolide) nanospheres by biodegradable poly(lactide)-poly(ethylene glycol) copolymers." Pharm Res 11(12): 1800-8.

Storm, G., S. O. Belliot, et al. (1995). "Surface modification of nanoparticles to oppose uptake by the mononuclear phagocyte system." Advanced Drug Delivery Reviews 17: 31-48.

Tobio, M., R. Gref, et al. (1998). "Stealth PLA-PEG nanoparticles as protein carriers for nasal administration." Pharm Res 15(2): 270-5.

Torchilin, V. P. (1995). "Which polymer can make nanoparticulate drug carriers long-circulating?" Advanced Drug Delivery Reviews 16(2-3): 141-155.

Torchilin, V. P., J. Narula, et al. (1996). "Poly(ethylene glycol)-coated anti-cardiac myosin immunoliposomes: factors influencing targeted accumulation in the infarcted myocardium." Biochimica Biophysica Acta 1279: 75-83.

van Hummel, G. J., S. Harkema, et al. (1982). "Structure of 3,6-dimethyl-1,4-dioxane-2,5-dione [D-,D-(L-,L-)lactide]." Acta Crystallographica B38: 1679-1681.

Venkatraman, S. S., P. Jie, et al. (2005). "Micelle-like nanoparticles of PLA-PEG-PLA triblock copolymer as chemotherapeutic carrier." Int J Pharm 298(1): 219-32.

Verrecchia, T., P. Huve, et al. (1993). "Adsorption/desorption of human serum albumin at the surface of poly(lactic acid) nanoparticles prepared by a solvent evaporation technique." Journal of Biomedical Materials Research 27(8): 1019-1028.

Verrecchia, T., G. Spenlehauer, et al. (1995). "Non-stealth (poly(lactic acid/albumin)) and stealth (poly(lactic acid-polyethylene glycol)) nanoparticles as injectable drug carriers." Journal of Controlled Release 36(1-2): 49-61.

Vila, A., H. Gill, et al. (2004). "Transport of PLA-PEG particles across the nasal mucosa: effect of particle size and PEG coating density`." Journal of Controlled Release 98(2): 231-244.

Vila, A., A. Sanchez, et al. (2005). "PLA-PEG particles as nasal protein carriers: the influence of the particle size." Int J Pharm 292(1-2): 43-52.

Vittaz, M., D. Bazile, et al. (1996). "Effect of PEO surface density on long-circulating PLA-PEO nanoparticles which are very low complement activators." Biomaterials 17(16): 1575-81.

Wang, Z.-Y., Y.-M. Zhao, et al. (2005). "Syntheses of Poly(lactic acid-co-glycolic acid) Serial Biodegradable Polymer Materials via Direct Melt Polycondensation and Their Characterization." Journal of Applied Polymer Science 99: 244-252.

Yoo, H. S. and T. G. Park (2001). "Biodegradable Polymeric Micelles Composed of Doxorubicin Conjugated PLGA-PEG Block Copolymer." Journal of Controlled Release 70(1-2): 63-70.

Zambaux, M. F., F. Bonneaux, et al. (1999). "MPEO-PLA nanoparticles: effect of MPEO content on some of their surface properties." J Biomed Mater Res 44(1): 109-15.

CHAPTER 6

FORMULATION AND CHARACTERIZATION OF TARGETED NANOPARTICLES

6.1 INTRODUCTION

Chapter 3 and 4 described the methods for preparation of biodegradable poly(lactic-co-glycolic acid) nanoparticles encapsulating the chemotherapeutic agent doxorubicin and the imaging agents rhodamine 6G, indocyanine green and gadopentetic acid. Chapter 5 presented various methods for the incorporation of poly(ethylene glycol) (PEG) on these types of nanoparticles, including the formulation of particles with polymer blends of PLGA and PEG-containing polymers, the covalent conjugation of PEG on the surface of pre-made nanoparticles using carbodiimide-mediated chemistry, and the preparation of covalently-bound block copolymers of poly(lactic-co-glycolic acid) (PLGA) and PEG by conjugation and polymerization. Based on the results described in Chapter 5, the polymerization of lactide and/or glycolide monomers initiated by hydroxyl groups on heterofunctional OH-PEG-COOH provided the best method for the synthesis of functional copolymers that could be used for preparation of nanoparticles with a high PEG surface coverage. In this chapter, the preparation of nanoparticles with these copolymers, the encapsulation of chemotherapeutic and imaging agents within them, and the attachment of targeting antibodies to their surface is described.

6.1.1 Preparation and Characteristics of PEGylated Nanoparticles

Nanoparticles made with block copolymers of PLGA and PEG have been investigated in the past because of their ability to circulate in the bloodstream for

extended periods compared to their unmodified PLGA counterparts (Moghimi, Porter et al. 1991; Gref, Minamitake et al. 1994; Stolnik, Dunn et al. 1994; Gref, Domb et al. 1995; Torchilin, Narula et al. 1996; Gref, Luck et al. 2000; Riley, Stolnik et al. 2001; Avgoustakis 2004). PEGylated nanoparticles are also known to adsorb less plasma protein with increased PEG content. Speficically, as much as 43% and 64% reduction in protein adsorption was observed in PLA-PEG nanoparticles with a PLA-to-PEG molecular weight ratio of 45,000/2,000 and 45,000/5,000, respectively (Gref, Luck et al. 2000). Surface PEG has also been observed to modify the biodistribution of nanoparticles as a result of surface chemistry differences. In addition to prolonged residence time in the blood pool, surface modification of PLGA nanoparticles with PEG resulted in significantly lower accumulation in the liver and higher accumulation in the spleen, intestines, and bones (Avgoustakis, Beletsi et al. 2003). A separate study revealed increased accumulation of PLGA-PEG nanoparticles in the lungs and decreased accumulation in the kidneys compared to unmodified PLGA nanoparticles (Li, Pei et al. 2001).

In addition to surface properties, the size of particles also has a great effect on their *in vivo* activity. For intravenous administration, the size of solid nanoparticles has to be significantly smaller than that of capillaries, i.e. less than 5 μm (Avgoustakis 2004). Nanoparticles of less than 200 nm have been found to be better able to avoid filtration by the spleen (Moghimi, Porter et al. 1991). Nanoparticles are also known to accumulate in tumors when their size is less than 100 nm (Kim and Nie 2005).

A number of different methods have been used for the preparation of nanoparticles with PLGA-PEG or PLA-PEG copolymers. Among these, emulsification/solvent evaporation (Gref, Luck et al. 2000; Li, Pei et al. 2001) and nanoprecipitation (Fessi, Devissaguet et al. 1986; Fessi, Puisieux et al. 1989;

Avgoustakis, Beletsi et al. 2003) are the most commonly used. Nanoprecipitation is also commonly described as solvent diffusion or solvent displacement method. In both methods, the copolymer is first dissolved in an organic solvent together with the active agent to be encapsulated. This organic phase is mixed with an aqueous solution to form the nanoparticles. In the emulsification method, a water immiscible solvent, such as ethyl acetate or dichloromethane, is used. Input of energy, in the form of sonication, homogenization or vigorous vortexing is necessary to emulsify the organic solution within the aqueous outer phase. The organic solvent must then be evaporated to solidify the polymer droplets. In the nanoprecipitation method, on the other hand, a water miscible solvent such as acetone or acetonitrile is used to dissolve the polymers and drug. Upon mixing, the organic solvent diffuses into the added aqueous phase, thus lowering the surface tension between the two phases and resulting in the spontaneous formation of an oil-in-water nanometric emulsion. Surfactants are not necessary for the preparation of PEGylated particles as PEG is able to stabilize the colloidal system through steric interactions. However, surfactants do improve the resuspension of particles after mechanically-induced sedimentation (Avgoustakis 2004).

The structure of nanoparticles made from amphiphilic copolymers such as PLGA-PEG and PLA-PEG is known to be highly influenced by the overall molecular weight of the polymer as well as the ratio of the molecular weights of the hydrophilic and hydrophobic domains. With larger size ratio of the hydrophilic to the hydrophobic domain, the structure of the nanoparticles becomes more dynamic or micelle-like (Avgoustakis 2004). A molecular weight ratio of 45/5 for the hydrophobic domain relative to the hydrophilic domain has been suggested for preparation of solid nanoparticles of PLA-PEG. With lower ratios, particle formation is thought to occur through self-assembly of the polymers into micelle-like structures, instead of by

precipitation of the hydrophobic polymer regions when in contact with the outer continuous aqueous phase.

6.1.2 Freeze Drying of PEGylated Nanoparticles

Freeze drying is a process that is commonly used in the pharmaceutical industry for preservation of moisture-sensitive formulations including nanoparticles, liposomes and nanoemulsions (Abdelwahed, Degobert et al. 2006). This process consists of three steps: freezing of the formulation, removal of water by sublimation or primary drying, and desorption of residual water. During freeze drying, however, the stability of colloidal formulations can be compromised because of the various mechanical stresses that the samples must be subjected. A number of formulation variables can be adjusted to increase the ability of nanoparticles to undergo freeze drying and maintain their stability. These variables include the type of surfactant used for stabilization of the nanoparticle suspensions, the type of polymer making the nanoparticles, the presence of agents bound to the surface of the particles, and the use of cryoprotectants (Abdelwahed, Degobert et al. 2006).

The freezing step of the freeze drying process can be highly influential with respect to the ability of the formulation to be reconstituted after drying. Freezing of colloidal suspensions occurs through the formation of pure water crystals. This separation of phases results in the segregation of nanoparticle into dehydrated domains which ultimately solidify in amorphous form at their glass transition temperature (Abdelwahed, Degobert et al. 2006). Aggregation of nanoparticles can occur at this step since the particles are physically concentrated within these domains. In addition, formation of water crystals around the nanoparticle domains can induce mechanical stresses that result in particle destabilization. During the primary drying step, the sample

is subjected to high vacuum. As the sample absorbs heat from the surrounding environment, water crystals sublimate and the water travels in vapor form from the sample to the freeze dryer condenser, where it solidifies. During this step, samples must be maintained below a critical temperature above which the sample loses its macroscopic porous network structure and collapses, thus preventing efficient sublimation of water. This critical temperature is usually about 2°C higher than the glass transition temperature of the amorphous domains (Abdelwahed, Degobert et al. 2006).

The use of excipients called cryoprotectants has been suggested for prevention of particle aggregation as a result of freeze drying stresses. Some commonly used cryoprotectants include sucrose, lactose, trehalose, glycerol, mannitol, sorbitol, glycine, alanine, lysine, polyethylene glycol, dextran and poly(vinyl pyrrolidone) (Abdelwahed, Degobert et al. 2006). These agents solidify in amorphous conformation below their glass transition temperature, thus protecting the particles from mechanical stress caused by the formation of water crystals. Trehalose has been suggested to be a preferred cryoprotectant because it is less hydroscopic than other cryoprotectants, has a low chemical reactivity, does not present internal hydrogen bonding, and has a higher glass transition temperature (-30°C) than other sugars such as glucose (-41°C). This latter fact is important because in order for the freezing and sublimation processes to proceed until completion, these steps must be done under the glass transition temperature of the cryoprotectant-nanoparticle domains (Abdelwahed, Degobert et al. 2006). In addition to the type of cryoprotectant used, the concentration of this agent and that of the nanoparticle suspension have been reported to be important for successful freeze drying of nanoparticles (de Jaeghere, Allemann et al. 2000; Abdelwahed, Degobert et al. 2006).

Freeze drying of nanoparticles containing poly(ethylene glycol) is known to result in particle aggregation (de Jaeghere, Allemann et al. 1999). In fact, previous studies have

demonstrated a relationship between the amount and molecular weight of PEG and the aggregation of the formulation (de Jaeghere, Allemann et al. 2000; Abdelwahed, Degobert et al. 2006). This phenomenon has been attributed to the crystallization of PEG during the freezing step (Izutsu, Yoshioka et al. 1996). Trehalose has been used to protect PEGylated poly(lactic acid) nanoparticles during freeze drying successfully (de Jaeghere, Allemann et al. 2000). Trehalose protects PEGylated nanoparticle suspensions by preventing PEG crystallization with the formation of an amorphous matrix around the nanoparticles and creating hydrogen bonds with PEG (Abdelwahed, Degobert et al. 2006).

6.1.3 Antibodies as Targeting Agents for Ovarian Cancer

Antibodies are immunoglobulins capable of recognizing a specific antigen. Structurally, antibodies are Y-shaped molecules composed of two identical heavy chains and two antigen-specific variable light chains. Commonly antibodies are produced by immunizing a susceptible animal with an antigen and collecting the immunoglobulins that are specific to the antigen from the animal's blood. This mixture of immunoglobulins will contain antibodies to various epitopes of the same antigen and, consequently, constitutes a polyclonal antibody mixture (Greener 2005). Monoclonal antibodies, on the other hand, contain only one type of antibody specific to a given epitope of the antigen molecule. Monoclonal antibodies are normally produced in hybridoma cell lines, which consist of fused B lymphocytes and immortal myeloma cells (Greener 2005).

No monoclonal antibodies specific to the follicle stimulating hormone receptor are commercially available to date. The group of Dr. James A. Dias from the Wadsworth Center of the New York State Department of Health kindly provided a monoclonal

antibody that his group developed for investigation of the binding site of follicle stimulating hormone to FSHR. This antibody, labeled mAb106-105, is an immunoglobulin of IgG2b isotype that is specific to the extracellular domain of human FSHR (Lindau-Shepard, Brumberg et al. 2001). It was derived from mice immunized with a recombinant protein expressed by insect cells representing the extra-cellular domain of human FSHR, and produced by hybridoma cells. The epitope of this antibody is located within amino acid residues 300-315 of FSHR, as determined by ELISA Binding of mAb106-105 to the extracellular domain of FSHR was determined by ELISA and SDS-PAGE/Western immunoblot (Lindau-Shepard, Brumberg et al. 2001). Binding of the mAb106-105 antibody to FSHR-expressing cells was determined by flow cytometry (Lindau-Shepard, Brumberg et al. 2001).

Binding of the mAb106-105 antibody to FSHR was shown to block binding of the follicle stimulating hormone to the receptor and consequent cAMP production in a concentration-dependent manner in Y1-R FSHR-expressing cells (Lindau-Shepard, Brumberg et al. 2001). Specifically, a mass of 10 μg of the monoclonal antibody was shown to completely inhibit hormone binding (Lindau-Shepard, Brumberg et al. 2001). Inhibition of hormone binding and function was observed to be reversed by increased concentration of FSH. Binding of 10 μg of antibody was determined to be disrupted by addition of 30ng or more of the follicle stimulating hormone in a dose dependent manner (Lindau-Shepard, Brumberg et al. 2001). It has also been shown that binding of this antibody to the target receptor does not cause adenyl cyclase activation and subsequent signaling events (Lindau-Shepard, Brumberg et al. 2001). The mAb106-105 monoclonal antibody has been used by other groups for investigation of the role of FSHR in ovarian cancer development (Choi, Choi et al. 2004).

Development of monoclonal antibodies to FSHR has also been reported by Vannier and colleagues (Vannier, Loosfelt et al. 1996). These antibodies were produced by immunizing mice with a fusion protein containing the extracellular domain of FSHR. All antibodies produced were shown to recognize the 172-358 amino acid fragment of the receptor, although most had different epitopes and could bind simultaneously. These antibodies were shown to cause little cAMP production (Vannier, Loosfelt et al. 1996). Cell studies demonstrated that these antibodies recognized and bound to the cell membrane of cells expressing FSHR but not to control cells (Vannier, Loosfelt et al. 1996). Antibodies labeled 323 and 156 resulted in the strongest immunohistochemical labeling.

6.2 MATERIALS AND METHODS

6.2.1 Materials

Heterofunctional PEG containing hydroxyl and carboxylic acid end groups (OH-PEG-COOH) of molecular weight 3,400 g/mol was purchased from Laysan Bio Inc. (Arab, AL, USA). Stannous octoate (Tin(II) 2-ethylhexanoate), poly(vinyl alcohol) (87-90% hydrolyzed, molecular weight average of 30,000 to 70,000), 2-(N-morpholino)ethylsulfonic acid (MES), N-hydroxysuccinimide, 3,3'5,5'-tretramethylbenzidine dihydrochloride (TMB) tablets, bovine serum albumin, phosphate buffered saline packages pH 7.4 were purchased from Sigma-Aldrich (Saint Louis, MO, USA). D-(+)-trehalose dihydrate was obtained from ACROS. The reagent 1-ethyl-3-(3-dimethylaminopropyl)carbodiimide hydrochloride (EDC) was obtained from Fluka.

Cyclic d,l-lactide (molecular weight 144.1) and glycolide (molecular weight 116.1) monomers were obtained from PolySciences, Inc. (Warrington, PA, USA). Poly(lactic-co-glycolic acid) (formerly PLGA 50:50 DL 2A, now 5050 DLGA 2A, 50/50 D,L-lactide to glycolide ratio, molecular weight 12,000 g/mol, carboxylic acid and hydroxyl end groups) was obtained from LakeShore Biomaterials (Birmingham, AL, USA). Doxorubicin hydrochloride, ethyl ether, acetone, dimethylsulfoxide, ethyl acetate, dimethylformamide, methanol, and sulfuric acid were obtained from Fisher Scientific. Sodium hydroxide was obtained from JT Baker.

Mouse purified IgG, used as a model antibody for protocol validation, was purchased from Biomeda (Foster City, CA, USA). Monoclonal antibody mAb 106-105 specific to the extracellular domain of the follicle stimulating hormone receptor was generously provided by Dr. James Dias from the Wadsworth Center (Albany, NY, USA). Purified IgG2b isotype control from murine myeloma and goat anti-mouse IgG (whole molecule) horseradish peroxidase conjugate were obtained from Sigma (Saint Louis, MO, USA).

6.2.2 Preparation of Copolymers

PLA-PEG-COOH copolymers were prepared by the solution polymerization of cyclic lactide initiated by the terminal hydroxyl group of heterofunctional PEG containing hydroxyl and carboxylic acid end groups (OH-PEG-COOH) (Laysan Bio Inc., Arab, AL, USA), as described in Chaper 5. The polymerization was catalyzed by stannous octoate (1:1 molar ratio to PEG) and carried out for four hours in anhydrous toluene at 110°C. Copolymers were purified by three cycles of dissolution in dichloromethane and precipitation in ethyl ether. Copolymers were then dried overnight in a vacuum desiccator, frozen and freeze dried. Copolymers were prepared in a manner

to give theoretical molecular weights between 24,500 and 53,000 g/mol. For all batches of nanoparticles containing imaging agents, therapeutic agents or antibodies, the copolymer used had a theoretical molecular weight of 53,000 g/mol, which was confirmed by nuclear magnetic resonance analysis of the copolymer composition.

6.2.3 Preparation of Targeted Nanoparticles with PLA-PEG-COOH Copolymer

The preparation of targeted nanoparticles was carried out in three consecutive steps, as displayed in Figure 6.1. First, nanoparticles of the PLA-PEG-COOH copolymers were prepared by oil-in-water nanoprecipitation. Next, the terminal carboxylic acid groups of PEG, which were expected to be exposed on the surface of the nanoparticles, were activated using carbodiimide chemistry to create an amine-reactive semi-stable N-hydroxysuccinimide ester. Finally, antibodies were reacted with the activated carboxyls on the nanoparticles. Each of these steps is described in detail below.

6.2.3.1 Preparation of Nanoparticles with PLA-PEG-COOH Copolymer

Nanoparticles of the PLA-PEG-COOH copolymers were prepared by oil-in-water nanoprecipitation. A mass of 100±0.2 mg of PLA-PEG-COOH copolymer was dissolved in 3 ml of acetone. After the polymer was completely dissolved, 1 ml of methanol or a solution of drug or imaging agent in methanol was added and the solution was briefly mixed. Methanol, although not required for preparation of blank nanoparticles, was added to simulate the preparation of nanoparticles loaded with methanol-soluble drugs or imaging agents. The polymer solution was filtered through a 0.2 μm nylon syringe filter directly onto 10 ml of an aqueous solution of 10 mg/ml PVA. The purpose of the filtering step was to remove any impurities that may have accumulated in the copolymers

during their preparation and handling. The suspension was rapidly vortexed and sonicated for 5 seconds each to form a homogeneous system. Organic solvent was removed by stirring the suspension in a vacuum flask at 500 rpm for 45 minutes while at room temperature and under 400 mmHg of vacuum. The nanoparticle suspension was transferred to a 45 ml polycarbonate centrifuge tube. The vacuum flask was rinsed with 10 ml of water and the rinse was transferred to the same centrifuge tube. The nanoparticle suspension was then centrifuged in a Beckman J2-21 refrigerated centrifuge for 1 hour at 43,600 x g. The supernatant was removed, the pellet was again resuspended in water by vortexing and sonication, and the sample was centrifuged again at 43,600 x g for one more hour to remove excess surfactant from the surface of the nanoparticles.

Nanoparticles loaded with drug or imaging agents were prepared similarly, except that the agent was included in the initial organic phase of the polymer in acetone and methanol. Specifically, rhodamine 6G (RHO) nanoparticles were made by dissolving rhodamine in acetone at a concentration of 0.3 mg/ml, using 3 ml of this solution to dissolve the copolymer and then adding 1 ml of methanol to form the organic phase. Indocyanine green (ICG) loaded nanoparticles were prepared by dissolving ICG in methanol at a concentration of 10 mg/ml and adding 1 ml to a solution of the copolymer in acetone. Finally, doxorubicin (DOX) loaded nanoparticles were prepared by first dissolving doxorubicin at a concentration of 1.33 mg/ml in methanol and then adding a volume in the range of 1.5 to 2.25 ml of this solution to 3ml of pre-dissolved copolymer in acetone, depending on the loading desired. Nanoparticles loaded with active agents were washed three times after solvent evaporation by cycles of centrifugation and resuspension in water to remove unencapsulated agent.

6.2.3.2 Activation of Surface Carboxylic Acid Groups

Immediately after preparation and removal of excess surfactant, the nanoparticle pellet was resuspended in 0.99 ml of 0.01 M MES buffer (pH 5.5) using sonication and vortexing. EDC and NHS were then added immediately after being dissolved in 50 μl of 0.01 M MES buffer, each, at a 50:1 molar ratio compared to the moles of PLA-PEG-COOH used to make the batch of nanoparticles. The reaction was allowed to occur for 15 minutes at room temperature while shaking, after which 19 ml of 0.01M MES buffer were added and the suspension was centrifuged for 15 minutes to remove excess NHS, EDC and isourea byproduct. The supernatant was removed and the nanoparticles were immediately conjugated to targeting antibodies as described below.

6.2.3.3 Conjugation of Targeting Antibodies to Activated Nanoparticles

The pellet of activated nanoparticles was rapidly resuspended in 1 ml of 0.1 M PBS buffer (pH 7.5) with sonication and vortexing. The appropriate amount of antibody solution was added and the system was allowed to react for 3 hours at room temperature while shaking. After reaction, 19 ml of PBS were added and the suspension was centrifuged at 19,000 rpm for 1 hour. The nanoparticles were resuspended in 20 ml of PBS buffer by pipetting with a Pasteur pipet and again centrifuged. It is important to note that no sonication or vortexing were used after antibody conjugation to prevent loss of antibody activity. The nanoparticles were then resuspended in 8 ml of water by pipetting with a Pasteur pipette. One fourth of this suspension was frozen at -80°C and freeze dried for 2 days in the absence of a cryoprotectant for determination of batch yield and drug loading. A second fourth of the batch was used for determination of antibody conjugation efficiency. The last one half of the batch was freeze dried in the presence of a cryoprotectant, as described next, at stored at -20°C for further studies.

6.2.3.4 Freeze Drying of Nanoparticles

Long term storage of nanoparticles requires that water be removed from the formulation to prevent premature drug release and polymer degradation. The process most commonly used for this purpose is lyophilization, or freeze drying. As the name implies, the process consists of two main steps: freezing of the formulation and subsequent drying by sublimation of ice. Unfortunately, formulations containing PEG are known to undergo aggregation after this process as a result of PEG crystallization. The use of cryoprotectants, and specifically of trehalose, has been suggested for minimization of particle aggregation during freeze drying (de Jaeghere, Allemann et al. 2000).

An initial study was done to determine the optimal variables for freeze drying of the nanoparticles to permit reconstitution after storage. The variables studied were the concentration of nanoparticles in suspension, the mass of trehalose with respect to the mass of nanoparticles, and the freezing temperature. The concentration of nanoparticles in the suspension was varied between 7.5, 10, 12.5 and 15 mg/ml while the ratio of the mass of D-(+)-trehalose dihydrate to that of nanoparticles was increased between 0 and 10 mg/ml. Particles were frozen in a -80°C freezer after being transferred to a borosilicate glass vial, or in a liquid nitrogen tank (-196°C) after being transferred to a polypropylene cryogenic vial. Suspension volumes were of about 1 ml total. Nanoparticles were left freezing overnight for at least 3 hours if frozen at -80°C, or for 10 minutes if frozen in liquid nitrogen. Nanoparticles were then freeze dried for 2 days in a Labconco Freeze Dryer 4.5 (Kansas City, MO, USA).

After determining the optimal conditions for freeze drying, as described in the results section, all washed particles encapsulating active agents or with targeting

antibodies were resuspended in 8 ml of water with sonication. A fraction of this suspension was transferred to a vial that contained trehalose (200± 0.1 mg of trehalose per 4 ml of nanoparticle suspension) as a cryoprotectant, and frozen at -80°C. The remaining fraction was frozen without trehalose for determination of batch yield and drug loading, when applicable. The frozen nanoparticle suspensions were freeze dried for 2 days and stored at -20°C. The volume of water used to resuspend each batch of nanoparticles and the amount of trehalose used for cryoprotection were designed to create a 12.5 mg/ml nanoparticle suspension (based on starting mass of polymer) that has 50 mg/ml trehalose, conditions that were found to be optimal for cryoprotection of these PLA-PEG nanoparticles in the above study.

6.2.3.5 Preparation of Sterile Nanoparticles

For the preparation of nanoparticles that would be used for in vitro cellular studies, as described in Chapter 7, nanoparticles were prepared under aseptic conditions to prevent contamination, which occurred during preliminary studies. All vials, flask and pipets used during nanoparticle preparation, lyophilization and storage were either purchased in pre-sterilized form, autoclaved or subjected to ultraviolet light for > 12 hours. These included vacuum flasks, centrifuge tubes, and Pasteur pipets. All feed solutions, including the polymer/drug organic solution, aqueous surfactant solution, buffers, activation reagents, antibody solutions, and trehalose solutions were filtered through 0.2 μm sterile syringe filters. All filtered solutions or particle suspensions were handled inside a laminar flow cell culture hood unless securely sealed inside a sterile container such as a vial or centrifuge tube. Vacuum solvent removal was carried out with the nanoparticle-containing flasks inside laminar flow hood, but connected to a vacuum

pump located outside of the hood through vacuum tubing. No mechanical stirring was used during this step.

For freeze drying of nanoparticle batches under aseptic conditions, frozen nanoparticle suspensions were placed inside a freeze drying flask and connected to the freeze dryer through two glass stopcocks, as displayed in Figure 6.2. These stopcocks were closed at all times unless the particles were under vacuum in which case all flow would be going from the samples through the freeze dryer and out from the vacuum pump. After the freeze drying cycle, both stopcocks were closed and the sample was removed from the freeze dryer while still under vacuum. Vacuum was released inside a laminar flow hood. Sterile freeze-dried particles were handled inside the laminar flow hood whenever needed, and stored in a well sealed flask at -20°C.

6.2.4 Physiochemical Characterization of Nanoparticles

Nanoparticles were characterized with respect to batch yield, size, zeta potential, morphology, and agent loading when applicable. The yield of each batch was determined from the dry weight of the fraction of the nanoparticle suspension that was frozen and freeze dried without cryoprotectant. For determination of size and zeta potential, and for preparation of samples for scanning electron microscopy, approximately 20mg of nanoparticles originally freeze dried with cryoprotectant (nanoparticle/trehalose blends) were resuspended in 10 ml of water and centrifuged to remove excess trehalose. The pellets were then resuspended in 500 μl of water and diluted in the respective solvent as described below. For size determination, nanoparticles were further diluted in deionized water and sized by dynamic light scattering with a ZetaPlus® instrument (Brookhaven Instrument Coorporation, Holtsville, NY, USA). Each batch was sized for 2 minutes. Zeta potential was determined with this same instrument after dilution of the concentrated

nanoparticle suspension with 1mM potassium chloride solution to make a 1 mg/ml nanoparticle suspension. For each batch at least 10 readings of zeta potential were averaged.

A Hitachi S-4500 field emission scanning electron microscope (SEM) was used for observation of nanoparticle morphology and confirmation of nanoparticle size. After removal of trehalose from freeze dried nanoparticles as described above, nanoparticle suspensions in water were placed on top of a SEM stub covered with a conductive carbon tab (Electron Microscopy Sciences, Hatfield, PA, USA) and allowed to dry at room temperature. Samples were then sputter coated with gold plasma prior to imaging.

Transmission electron microscopy was also used to image the nanoparticles. A sample of pre-dried nanoparticles suspended in water was applied to a 300 mesh copper TEM grid with a carbon film. The sample was stained with uranyl acetate and rinsed once before allowing it to dry at room temperature.

6.2.4.1 Determination of Agent Loading

For determination of the doxorubicin, rhodamine and ICG content within nanoparticles, a known mass of dry nanoparticles was dissolved in a known volume of dimethylsulfoxide (DMSO) at a concentration equal or lower than 1mg of nanoparticles per milliliter. When necessary, the solutions were diluted in DMSO until the absorbance of doxorubicin, rhodamine or ICG was within the standard curve for the specific agent in DMSO. Samples were placed in quartz cuvettes and a Shimadzu UV-1201 spectrophotometer was utilized for reading their absorbance. The mass of the agent in the sample was determined based on a standard curve of known concentrations of the agent in DMSO. The loading, or weight percent of the agent in the nanoparticle

formulation was determined by dividing the mass of the agent found by the mass of nanoparticles that were dissolved.

6.2.4.2 In Vitro Agent Release

The release of doxorubicin and rhodamine from PLA-PEG-COOH nanoparticles that had been conjugated with model antibodies or without antibodies was investigated. A known mass of nanoparticles was suspended in phosphate buffered saline of pH 7.4 or pH 6.0. These suspensions were maintained in the dark in poly(carbonate) centrifuge tubes in a 37°C water bath. At specific time points, the samples were centrifuged for 1 hour at 19,000 rpm while maintaining the centrifuge rotor temperature at 35°C, and a sample of the supernatant was removed for analysis.

For doxorubicin-loaded nanoparticles, nanoparticles were first suspended in 4 ml of buffer. Since the concentration of doxorubicin was very low, samples of 100 μl were taken and no fresh buffer was added during the course of the experiment. Doxorubicin samples were analyzed by fluorescence spectroscopy for determination of drug content based on a standard curve in the appropriate buffer. A BioTek FLX 800 microplate fluorescence reader was used for this purpose. Samples were excited with light of 484 nm and emission was read at 645 nm. Rhodamine-loaded nanoparticles were suspended in 4 ml of PBS buffer pH 6.0 or 10 ml of PBS buffer pH 7.4. These samples were analyzed by absorbance spectrophotometry.

6.2.4.3 Determination of Antibody Conjugation Efficiency

Detection and quantification of antibodies bound to the surface of the targeted nanoparticles were carried out with the tetramethylbenzidine (TMB)-horseradish

peroxidase assay, as described previously for PEGylated silica/gold nanoshells conjugated to anti-HER2 antibodies (Lowery, Gobin et al. 2006). This assay is based on the time-dependent oxidation of TMB under the enzymatic action of horseradish peroxidase, which results in the formation of a blue soluble product (Josephy, Thomas et al. 1982; Menegazzi, Zabucchi et al. 1992). As such, this sensitive assay is dependent on the presence of the secondary antibody conjugated to the peroxidase enzyme, which in turn is specific to the primary antibody that is to be quantified. This method is superior to more commonly-used protein quantification techniques which are commonly less sensitive and influenced by the presence of surfactants, ions, carbohydrates, and protein contamination (Bradford 1976). The TMB assay permited visual inspection of the reaction, and was able to detect concentrations of antibody as low as 0.3 ng/ml.

First, 10 mg of bovine serum albumin were dissolved in 1 ml of a nanoparticle suspension of $1/8^{th}$ of each batch in water and allowed to interact for 1 hour to block non-specific sites. After 1 hour, 9 ml of 0.01 M PBS were added and the nanoparticles were centrifuged for 30 minutes at 19,000 rpm. The nanoparticle pellet was resuspended by pipetting in 450 μl of 0.01 M PBS and 49 μl of 0.51 μg/μl goat anti-mouse IgG-horseradish peroxidase conjugate were added and allowed to react for 1 hour at room temperature while shaking. A volume of 19 ml of 0.01 M PBS was added and the nanoparticle suspension was centrifuged for 30 minutes at 43,600 x g. The supernatant was removed and the particles were washed again with 10 ml of 0.01 M PBS.

The TMB substrate solution was prepared as suggested by the manufacturer: one tablet of TMB was dissolved in 10 ml of 0.05 M phosphate/citrate buffer pH 5.0 and 2 μl of 30% hydrogen peroxide were added immediately prior to use. The nanoparticle pellet was resuspended in 2 ml of 0.05 M phosphate/citrate buffer (pH 5.0) by pipetting. A volume of 1μl of this nanoparticle suspension was diluted in 99 μl of buffer in 96 well

plates and reacted with 100 µl of TMB substrate solution. After 15 min of reaction, 50 µl of 4 N sulfuric acid were added to stop the reaction. The absorbance of the solution was read a 450 nm and the amount of antibody present was determined based on a calibration curve generated with known concentrations of goat anti-mouse IgG – horseradish peroxidase antibody ranging from 0.3 to 20 ng/ml.

6.3 RESULTS

6.3.1 Preparation of Nanoparticles with PLA-PEG-COOH Copolymers

Preparation of nanoparticles was carried out by emulsification or nanoprecipitation methods, as described previously for nanoparticles of poly(lactic-co-glycolic acid) (PLGA) in Chapters 3 and 4. Clear differences were observed in the colloidal suspension characteristics, including the significant size decrease, as will be described in more detail later in this section, and improved stability of the colloids. Two main variables had to be optimized for the production of nanoparticles with reproducible yields and sizes: recovery and lyophilization.

6.3.1.1 Nanoparticle Recovery

During initial experiments, the recovery of the nanoparticles by centrifugation was very low as a result of the small size of the particles. The size of the nanoparticles was in average 170 nm before freeze drying, which is at least 40% smaller than that of PLGA nanoparticles prepared with bovine serum albumin or poly(vinyl alcohol) as surfactants, as reported in Chapters 3 and 4 (See Tables 3.1 and 4.2 for example). Per Stokes' Law applied to dilute suspensions of spherical particles, as described in Equation

6.1, the rate of sedimentation (V) is proportional to the square of the size of the particles (d), the square of the angular velocity of centrifugation (ω), the density difference between the particles (ρ_s) and the liquid medium in which they are suspended (ρ_l), and the radius of rotation of the centrifugation system (r), while being inversely proportional to the kinematic viscosity of the medium (η) (Darby 1996).

$$V = \frac{d^2 \cdot (\rho_s - \rho_l) \cdot \omega^2 \cdot r_s}{18 \cdot \eta} \tag{6.1}$$

Since the size of the PLA-PEG particles decreased by a factor of 0.6 compared to PLGA nanoparticles, the velocity of sedimentation was effectively reduced to 36% of that of PLGA nanoparticles under the same centrifugation conditions. Consequently, it was necessary to increase the time of centrifugation by at least 3.8 fold, from 10 to 38 minutes, to achieve the same trajectory along the centrifugation tube. In addition, since the poly(ethylene glycol) chains were expected to form a hydrophilic brush along the surface of each particle, it was expected that the actual speed of sedimentation would be even lower as a result of increased friction or interaction between the particle surface and the liquid medium. A centrifugation time of 1 hour was finally selected to minimize loss of mass during the repeated wash steps that the nanoparticles were subjected to. Size analysis of the particles remaining in the supernatants even after 1 hour of centrifugation suggests that particles of size in the range of or smaller than 110 nm were not successfully recovered.

6.3.1.2 Effect of Copolymer Molecular Weight on Nanoparticle Size

The effect of copolymer molecular weight on the size of the particles and recovery was also studied. Since PEG of constant molecular weight was used to initiate

the polymerization of the copolymers, increased copolymer molecular weight was dependent on larger poly(lactic acid) (PLA) domains and increased PLGA to PLA ratio. As is displayed in Figure 6.3A, and although most of the data points are not statistically significantly different, the size of the nanoparticles, both in the centrifuged pellet and remaining in the supernatants after centrifugation, appeared to follow an almost-linear increasing trend with increasing theoretical molecular weight. At the same time, the mass of dried supernatants, which includes 100 mg of poly(vinyl alcohol), decreased with increased copolymer theoretical molecular weight, suggesting that particles were more efficiently sedimented as a result of their larger size. Figure 6.3B shows an image of the nanoparticle suspension and the combined particle-laden supernatants for the same batch. It is important to note that the theoretical molecular weight of the copolymers (24,500 to 53,400 g/mol) was, in all cases, larger than the number average molecular weight measured by gel permeation chromatography (12,350 to 35,500 g/mol) although they followed the same increasing trends.

6.3.1.3 Effect of Cryoprotectant on Nanoparticle Reconstitution

Trehalose was used for cryoprotection of the nanoparticles during freezing and lyophilization (freeze drying). Studies were performed to determine the optimal concentration of nanoparticles and trehalose, and the optimal freezing temperature that would best protect the nanoparticles from aggregation. Table 6.1 summarizes the effect of these variables on the ratio of the size of the particles before and after freeze drying. As shown, particles dried without a cryoprotectant (trehalose/NP ratio of 0/1) aggregated so significantly that the particles could not be sized regardless of the nanoparticle concentration or freezing temperature. Qualitatively, particle aggregates of up to several hundreds of microns were observed by visual inspection for most of these batches. With

inclusion of trehalose at a ratio of 0.25/1 to nanoparticles, the size ratio decreased to between 1.8 and 60 depending on the concentration of the particles and the freezing temperature. As the ratio of the mass of trehalose to the mass of nanoparticles in the formulation was increased from 0.25 to 2, the size of the dried particles decreased to nearly that of the pre-lyophilized particles. No further improvement was observed with trehalose concentrations greater than 2 or 4 times that of the nanoparticles, as is graphically displayed in Figure 6.4.

The influence of the nanoparticle concentration on the final size of the particles was determined to not be nearly as significant as the amount of trehalose, at least within the concentration range tested. For the lowest nanoparticle concentrations tested (7.5 and 10 mg/ml), the size ratio was greater than 1.2 for all trehalose/nanoparticle. The best nanoparticle reconstitution was achieved with a nanoparticle concentration of 12.5 mg/ml for all nanoparticle/trehalose ratios.

The data in Table 6.1 also suggested that freezing the particles in a -80°C freezer resulted in less particle aggregation at the lower trehalose concentrations, contrary to what other authors have reported (de Jaeghere, Allemann et al. 2000). It is possible that the containers on which the particles were frozen could have had an impact in the actual rate of freezing regardless of the temperature. When being frozen in liquid nitrogen, particle suspensions were put into polypropylene cryogenic tubes that are designed to be used for cryopreservation of cells, while particles frozen at -80°C were put in borosilicate glass containers. Glass has a higher coefficient of thermal conductivity than the polymer, which could result in better heat transfer from the samples frozen in these the borosilicate glass vials and consequently in a more favorable rate of freezing. Based on these data, a nanoparticle concentration of 12.5 mg/ml with a trehalose-to-nanoparticle mass ratio of

4/1 and a freezing temperature of -80°C was selected for safe freezing and drying of the PLA-PEG nanoparticles.

6.3.2 Physiochemical Characteristics of PLA-PEG-COOH Nanoparticles

Table 6.2 summarizes some of the characteristics of PLA-PEG-COOH nanoparticles that were prepared, including those without an agent (blank), and those loaded with doxorubicin (DOX), rhodamine 6G (RHO), and indocyanine green (ICG). Three types of antibodies were utilized in the preparation of some of these batches. Mouse IgG was used as a model antibody for optimization of antibody binding protocols and also as a control. A number of batches of nanoparticles were prepared by adsorbing or conjugating this antibody. When adsorbing the antibody, nanoparticles were not activated with EDC and NHS, but just incubated with the antibody under the same conditions in which the antibody conjugations were carried out. The antibody mAb106-105 was used as the targeting agent as it is specific to the extracellular domain of the FSHR receptor. The IgG2b antibody was used as an isotype control for mAb106-105. These two later antibodies were only conjugated to the nanoparticles, not adsorbed. It should be noted that only two batches of blank and DOX-loaded nanoparticles with mAb106-105, two batches of blank nanoparticles with IgG2b, and one batch of DOX-loaded particles with IgG2b were prepared because of the availability or cost of these antibodies.

The percent recovery, or yield achieved was in the range of 35 to 73%, which is still lower than that achieved previously with PLGA nanoparticles. Recovery of blank nanoparticles with antibodies, DOX-loaded nanoparticles, RHO-loaded nanoparticles or ICG-loaded nanoparticles was not statistically different from that of blank nanoparticles without antibody. Longer centrifugation times or faster centrifugation speed would have

improved recovery; however, this was not possible because the Beckman J2-21 centrifuge was already being used at its maximum rated speed, and the already-extended centrifugation times appeared to be causing mechanical problems in this instrument.

The size of the nanoparticles prepared with poly(vinyl alcohol) as surfactant (blank, DOX-loaded and RHO-loaded particles) was consistently in the range of 140 - 190 nm and not statistically different from that of blank nanoparticles without antibody before freeze drying. ICG nanoparticles, which were prepared with sodium cholate as the surfactant, were significantly smaller. Most batches aggregated to between 1.2 and 2 times the initial size after freeze drying despite the use of the optimized freeze drying conditions that were described previously. RHO-loaded nanoparticles with conjugated IgG appeared to be almost 5 times as big as pre-dried nanoparticles. It is important to note, however, that nanoparticle batches to which antibodies had been adsorbed or conjugated were resuspended by pipetting instead of sonication prior to freeze drying. This could have resulted in incomplete nanoparticle resuspension in the cryoprotectant solution, and consequently in less than optimal freeze drying conditions. Also, it is worth noting that the preliminary studies of optimization of nanoparticle freeze drying conditions were performed in a smaller scale (~1 ml samples) while the batches presented in Table 6.2 were at least 4 times larger. The increased sample size could have had a negative impact on the speed of sample freezing, possibly allowing the separation of the components and formation of trehalose-free nanoparticle-rich pockets which would have led to particle aggregation.

No significant difference was observed in the morphology or surface characteristics of the particles with the different loaded agents or types of antibodies, as can be seen from scanning electron microscopy (SEM) images on Figures 6.5, 6.6, 6.7 and 6.8 for blank, doxorubicin-loaded, rhodamine-loaded and indocyanine green-loaded

nanoparticles, respectively. SEM images of the batches in fact revealed the presence of polymer aggregates, as shown for doxorubicin-loaded nanoparticles in Figure 6.6A. However, these were far less numerous than the spherical nanoparticles that were all around them when the magnification was increased, as seen in Figure 6.6B for the same batch. Transmission electron microscopy images, as shown on Figure 6.9, confirm the spherical shape of the particles. Both scanning and electron microscopy images suggest, however, that the actual nanoparticle size is closer to 100 nm as opposed to 170 nm, as measured with the ZetaPlus instrument. This is expected since this instrument reports an effective diameter that is influenced by the diameter of the larger polymeric aggregates, despite the fact that they are significantly outnumbered by the small nanoparticles.

The zeta potential of all batches, similarly to the size of the particles, was determined to be mainly influenced by the type of surfactant used. All batches prepared with poly(vinyl alcohol), including those loaded with agents and with or without antibodies, were in the range of -5 to -12 mV, and not statistically different from blank nanoparticles without antibody. ICG nanoparticles, prepared with sodium cholate, had a more charged surface with a statistically different average of -15 mV. This is expected as sodium cholate is an anionic surfactant derived from cholesterol.

6.3.3 Encapsulation of Chemotherapeutic and Imaging Agents

Loading of chemotherapeutic and imaging agents, as seen in Table 6.3, was very different to that previously observed with PLGA nanoparticles. The calculated doxorubicin loading was of only about 7% the desired amount regardless of antibody conjugation, with an average loading of 0.2 wt.%. In comparison, the loading achieved with PLGA nanoparticles was of about 80% of the desired amount at similar targeted loadings, as presented in Table 3.2 of Chapter 3. Most of the drug partitioned to the

water phase of the suspension upon nanoparticle precipitation and was subsequently removed in the first few supernatants. Figure 6.10, however, shows how after the first two or three washes the drug that had been encapsulated within the particles remained entrapped instead of continuously leaching from them, as can be seen from the clear doxorubicin color contrast between the pellet to that the supernatant.

Encapsulation of rhodamine similarly was reduced compared to that achieved in PLGA nanoparticles. For the same targeted loading of 0.3 wt.%, the calculated loading was 0.29 wt. % in PLGA nanoparticles compared to a maximum of 0.2 wt.% in PLA-PEG nanoparticles. In addition, rhodamine appeared to continue leaching from the particles as these were exposed to aqueous media during conjugation of antibodies, thus resulting in a significantly lower loading of less than half that achieved without antibody conjugation.

Possible reasons for the reduction in encapsulation efficiencies include the reduction in nanoparticle size which significantly increases the surface area in contact with the aqueous medium and available for agent diffusion. On the other hand, an ionic interaction between the basic doxorubicin and the carboxylic acid groups of PLGA had been hypothesized in Chapter 3. In PLA-PEG-COOH nanoparticles the carboxylic acid end group is no longer associated with the core of the nanoparticles, but rather with the terminal end of the surface brush-like PEG shell. Consequently, any such interaction between doxorubicin and the polymer would have been lost. A similar theory could be applied to rhodamine 6G which also contains a positively-charged protonated amine group at physiological pH, as can be seen from Figure 4.1A in Chapter 4.

Loading of indocyanine green into PLA-PEG-COOH nanoparticles, on the other hand, improved compared to that achieved with PLGA nanoparticles prepared with identical protocols. Specifically, for the same targeted loading of 9.1 wt.%, PLGA

nanoparticles were able to encapsulate only an average of 0.1 wt.% as shown on Table 4.3 of Chapter 4. PLA-PEG nanoparticles, on the other had, were able to encapsulate one order of magnitude more ICG. It is possible that the increased hydrophilicitiy of the nanoparticles as a result of the incorporation of PEG provided sufficient drive for such different partitioning of ICG between the organic polymeric phase and the outer aqueous phase.

6.3.4 *In Vitro* Release of Chemotherapeutic and Imaging Agents

The release of doxorubicin and rhodamine 6G from PLA-PEG–COOH nanoparticles was investigated. Figure 6.11 shows the release profile obtained for doxorubicin-loaded particles at physiological and acidic pH. As observed, an initial burst release of only 10% of the drug was observed within the first three hours in both conditions. After this, the release occurred at a nearly-constant rate for up to 4 days. No significant differences were observed in the release of the drug in the different pH buffers during the first 20 hours of release. Afterwards, statistically significant differences were observed at the two pH values, with the drug releasing slightly faster at pH 7.4.

Results are very different from those obtained with PLGA nanoparticles, as described in Section 3.4.3 and displayed in Figure 3.2 of Chapter 3. The release from PLGA particles occurred at a significantly higher rate and was highly influenced by pH. At pH 7.4, almost 50% of the drug had been released from PLGA nanoparticles within one day, while less than half of that was released from PLA-PEG-COOH nanoparticles. In pH 4.0, release from PLGA nanoparticles occurred very fast, with about 70% of the drug being released within the first hour and about 93% during the first day. The release rate from PLA-PEG-COOH nanoparticles at pH 6.0 cannot, however, be directly compared to that of PLGA nanoparticles which was studied at pH 4.0. Nonetheless, the

pH dependency of drug release from PLA-PEG-COOH nanoparticle appears to be less significant.

In Chapter 3, the dependence of release on pH was suggested to be associated with the interaction between the deprotonated carboxyl end groups of PLGA and the protonated amine group of doxorubicin. As the pH was lowered, the carboxyl groups would become protonated and the charge attraction between the polymer and the drug would have been lost, thus permitting diffusion of the drug from the particles. With the PLA-PEG-COOH nanoparticles, and as discussed above for the loading capacity of these particles, the carboxyl groups are no longer present in the core of the particles but rather on the surface at the terminal end of the PEG chains. Consequently, no such charge attraction occurs and changes in pH do not affect the release of the drug so significantly.

Figure 6.12 shows the time release of rhodamine 6G from PLA-PEG nanoparticles. Differences are observed in the release of rhodamine from particles conjugated to antibodies compared to those that did not have antibody at physiological pH. It is possible that more rapid release of the agent from particles without antibodies is caused by the higher loading of rhodamine in these particles. As mentioned earlier, rhodamine was observed to continuously leach out of the particles during all activation, conjugation and purification steps, thus leading to lower rhodamine content in the particles than in those that were not subjected to these steps. The loading was of 0.093 and 0.204 wt.% rhodamine in particles conjugated to antibody and without antibody, respectively.

The release of rhodamine from PLA-PEG-COOH particles at pH 7.4 was significantly faster than the release from PLGA nanoparticles which is summarized in Figure 4.4 and discussed on section 4.3.1 of Chapter 4. Within the first 2 hours, between 40 and 50% of the agent was released from PLA-PEG-COOH nanoparticles, while less

than 5% had been released from PLGA particles (Figure 4.4). Within 4 days, almost 90% of the rhodamine was released from PLA-PEG-COOH particles, while only 30 to 45% had been released from PLGA particles.

The rate of release of rhodamine from the same batch of PLA-PEG nanoparticles conjugated to mouse IgG at pH 6 was found to be faster than at pH 7.4, with an initial release of approximately 55% of the drug during the first 2 hours and 96% within 3 days. From this release behavior and the fact that the agent was observed to continue leaching during all preparation steps, it is possible that rhodamine was associated with the surface and consequently with the PEG shell. As such, as the pH was lowered to 6.0, the charge attraction between the positively-charged amine group of rhodamine and the carboxyl groups of PLA-PEG-COOH would have lost some affinity, thus resulting in the moderate release rate increase observed.

6.3.5 Conjugation of Antibodies to the Nanoparticles

An Elisa-based assay was used for the determination of antibody binding to nanoparticles. A secondary antibody conjugated to horseradish peroxidase was reacted with nanoparticles that had antibodies either adsorbed to their surface or conjugated to the terminal hydroxyl groups of PEG. The oxidation of TMB into a soluble blue compound, mediated by horseradish peroxidase, was used to determine the amount of primary antibody associated with the nanoparticles. Figure 6.13 shows the result of control experiments on the attachment of mouse IgG to blank nanoparticles. In the presence of no primary antibody, the adsorption of secondary antibody and resulting TMB oxidation was low. Blank nanoparticles to which IgG was adsorbed instead of conjugated showed no significant difference compared to nanoparticles with no primary antibody. Nanoparticles to which IgG was conjugated, on the other had, showed clear

incorporation of the antibody, with an average of 319 ng attached per milligram of nanoparticles, which is equivalent to a 23% incorporation efficiency based on the 50 μg of antibody that were used for conjugation to each batch of nanoparticles.

Figure 6.14 shows the results of conjugation of antibodies on blank, doxorubicin- and rhodamine-loaded nanoparticles. As presented, no difference was observed in the attachment of mouse IgG between blank, doxorubicin- or rhodamine-loaded nanoparticles. However, conjugation of the isotype control IgG2b antibody and the anti-FSHR mAb106-105 antibody to blank and doxorubicin-loaded nanoparticles was less effective. Possible reasons could be differences in the quality of the primary antibodies or dissimilar interaction between these primary antibodies and the secondary horseradish peroxidase conjugated antibody. Nonetheless, conjugation of these antibodies is clear compared to nanoparticles with no antibodies or with adsorbed primary antibody.

It is important to note that no interference from the absorption of doxorubicin or rhodamine was observed. Doxorubicin absorbs light in the range of 480 to 550 nm, with peak absorption at 480 nm. Rhodamine absorbs from 475 to 550 nm, with peak absorption at 520 nm. As shown on Figure 6.15 for doxorubicin-loaded nanoparticles, the concentration of nanoparticles that was used for quantification of the antibody was too low for the absorption of the loaded agent to be detected and, consequently, for it to interfere with the quantification of the antibody. Equivalent results were obtained with rhodamine-loaded nanoparticles.

The number of antibodies per individual nanoparticle was calculated based on the mass ratio of antibody-to-nanoparticle shown on Figure 6.14 and the mass of a single nanoparticle. Using a nanoparticle density of 1.27 g/ml, based on poly(lactic acid), the mass of a nanoparticle was calculated for three different average nanoparticle sizes: 100, 200 and 300 nm. Table 6.4 displays the average number of antibody molecules per

nanoparticle. The number of antibodies per particle increases with the third power of the nanoparticle diameter. With decreasing nanoparticle size, the number of nanoparticles per batch increases drastically. Consequently, even small changes in nanoparticle size result in significant variations in the number of antibodies per nanoparticle. For nanoparticles of size below 100 nm, the antibody conjugated would not be enough for each particle to present one on its surface. However, for particles of 200 nm in average, from 2 to 7 antibodies could have been bound per nanoparticle, depending on antibody incorporation efficiency. Since the average size of nanoparticles before freeze drying was in the range of 150 to 200 nm, as determined by dynamic light scattering and presented in Table 6.2, the average number of antibodies bound per nanoparticle was in the range of 1 to 7 molecules. Although the use of higher amounts of antibody in the conjugation would have resulted in better modification of the nanoparticles, this was not possible as a result of monoclonal antibody availability.

6.4 CONCLUSIONS

This Chapter describes the preparation of nanoparticles using amphiphilic copolymers of poly(lactic acid) and poly(ethylene glycol). Use of these copolymers was identified as the best method for incorporation of poly(ethylene glycol) on the surface of the nanoparticles in Chapter 5. Here, the preparation of PEGylated nanoparticles incorporating surface-bound antibodies for the targeted delivery of chemotherapeutic and imaging agents is reported.

Three main variables were optimized in the preparation of these nanoparticles: recovery, freeze drying conditions and antibody conjugation. Recovery of nanoparticles was achieved by increasing centrifugation time to account for decreased nanoparticle size and dynamic surface layer. Aggregation of nanoparticles induced by freeze drying

processes was minimized with the use of trehalose as a cryoprotectant. Trehalose minimizes mechanical stresses on the particles as a result of crystallization of water and PEG on the surface of the nanoparticles by creating hydrogen bonds with PEG and forming an amorphous matrix around the particles. Antibody conjugation was carried out by activation of terminal carbolxylic acid groups on the surface of the nanoparticles using carbodiimide chemistry. Conjugation of antibodies to the activated nanoparticles with up to 30% incorporation efficiency was confirmed with an Elisa-like assay.

Encapsulation of the chemotherapeutic agent doxorubicin and the imaging agents rhodamine 6G and indocyanine green within PEGylated nanoparticles was investigated and compared to the results previously described with PLGA nanoparticles in Chapters 3 and 4. Clear differences were observed in the encapsulation capacity of the PEGylated nanoparticles. Doxorubicin was encapsulated at a significantly lower loading, but the release of this drug was better controlled at an almost linear rate over a period of 4 days with a minimal burst of 10% during the first three hours. Rhodamine was also loaded less efficiently but also appeared to be released from the particles at a faster rate than from PLGA nanoparticles. Indocyanine green, on the other hand, was encapsulated better in PEGylated nanoparticles compared to PLGA particles. Differences in loading capacity and release profiles were suggested to be caused mainly by the decreased particle size and the loss of agent-polymer charge attractions as a result of the relocation of terminal carboxyl groups from the core in PLGA nanoparticles to the outer surface of the particles in the PEGylated counterparts. The effect of loading and release parameters, PEGylation and targeting antibody presentation on the surface of these nanoparticles on their interaction with cancer cells is described in Chapter 7.

Table 6.1 Optimization of cryoprotection for PLA-PEG nanoparticles. *Size too large for measurement by dynamic light scattering.

NP Concentration (mg/ml)	Freezing Temp (°C)	Trehalose/NP Weight Ratio	Size Before Drying (nm)	Size After Drying (nm)	Size Ratio (nm/nm)
10.0	-80	0/1	178	*	*
		0.25/1	168	308	1.8
		0.5/1	168	252	1.5
		1/1	168	208	1.2
		2/1	168	201	1.2
		5/1	178	208	1.2
		10/1	178	205	1.2
10.0	-196	0/1	178	*	*
		0.25/1	168	1,557	9.3
		0.5/1	168	386	2.3
		1/1	168	343	2.0
		2/1	168	279	1.7
		5/1	178	251	1.4
		10/1	178	225	1.3
12.5	-80	0/1	171	*	*
		0.25/1	180	759	4.2
		0.5/1	180	252	1.4
		1/1	180	263	1.5
		2/1	180	203	1.1
		4/1	171	179	1.0
		8/1	171	203	1.2
12.5	-196	0/1	171	237	1.4
		0.25/1	180	1,426	7.9
		0.5/1	180	2,639	14.7
		1/1	180	5,603	31.1
		2/1	180	204	1.1
		4/1	171	270	1.6
		8/1	171	198	1.2
15.0	-80	0/1	173	*	*
		0.25/1	170	10,280	60.4
		0.5/1	170	288	1.7
		1/1	170	375	2.2
		2/1	170	222	1.3
		4/1	173	161	0.9
		8/1	173	169	1.0
15.0	-196	0/1	173	2,044	11.8
		0.25/1	170	2,678	15.7
		0.5/1	170	1,903	11.2
		1/1	170	407	2.4
		2/1	170	209	1.2
		4/1	173	182	1.1
		8/1	173	180	1.0

TABLE 6.2 Characteristics of PLA-PEG nanoparticles (NPs). Abbreviations: poly(vinyl alcohol) (PVA), sodium cholate (SC), doxorubicin (DOX), rhodamine 6G (RHO), indocyanine green (ICG).

Type of Particles	Type of Antibody	Mass or Antibody (mg)	Type of Surfactant	Yield (%)	Size Before Freeze Drying (nm)	Size After Freeze Drying (nm)	Zeta Potential (mV)
Blank NPs	No Antibody	0	PVA	57 ± 19	184 ± 30	305 ± 110	-9.9 ± 3.0
	IgG Adsorbed	50	PVA	58 ± 12	176 ± 49	243 ± 18	-8.8 ± 4.0
	IgG Conjugated	50	PVA	47 ± 14	175 ± 35	280 ± 57	-9.1 ± 3.2
	mAb106-105 Conjugated	50	PVA	40 ± 17	138 ± 14	250 ± 46	-12.2 ± 3.4
	IgG2b Conjugated	50	PVA	35 ± 4	151 ± 16	268 ± 59	-7.3 ± 1.0
DOX NPs	No Antibody	0	PVA	64 ± 9.8	152 ± 5	312 ± 60	-7.5 ± 1.7
	IgG Conjugated	50	PVA	69 ± 10	164 ± 9	218 ± 33	-8.6 ± 1.1
	mAb106-105 Conjugated	50	PVA	63 ± 12	156 ± 6	301 ± 55	-5.6 ± 0.7
	IgG2b Conjugated	50	PVA	78	161	289	-12.9
RHO NPs	No Antibody	0	PVA	39 ± 8	160 ± 7	191 ± 5	-8.7 ± 0.2
	IgG Conjugated	50	PVA	55 ± 10	191 ± 35	922 ± 161	-6.9 ± 1.7
ICG NPs	No Antibody	0	SC	39.3 ± 7	139 ± 4	191 ± 19	-15.7 ± 5.0

Table 6.3 Loading of chemotherapeutic and imaging agents within PLA-PEG-COOH nanoparticles. Abbreviations: doxorubicin (DOX), rhodamine 6G (RHO), indocyanine green (ICG).

Type of Particles	Type of Antibody	Targeted Loading (wt. %)	Calculated Loading (wt. %)
DOX NPs	No Antibody	2.9	0.22
	IgG Conjugated	2.0	0.20 ± 0.02
	IgG Conjugated	2.9	0.18 ± 0.03
	mAb106-105 Conjugated	2.9	0.23 ± 0.07
	IgG2b Conjugated	2.9	0.2
RHO NPs	No Antibody	0.3	0.2 ± 0.017
	IgG Conjugated		0.09 ± 0.004
ICG NPs	No Antibody	9.1	1.2 ± 0.158

Table 6.4 Molecules of mouse IgG, mAb106-105 and IgG2b isotype antibodies bound per individual nanoparticle as a function of nanoparticle size for blank and doxorubicin-loaded nanoparticles. Data are based on the wt. % content of antibodies in the nanoparticles, as calculated with the TMB assay, and using a particle specific gravity of 1.27.

Number of Antibody Molecules per Nanoparticles						
NP Size (nm)	IgG		mAb106/105		IgG2b	
	Blank	DOX	Blank	DOX	Blank	DOX
100	0.78	0.89	0.24	0.46	0.33	0.30
200	6.23	7.14	1.92	3.69	2.67	2.39
300	21.03	24.08	6.49	12.45	9.01	8.06

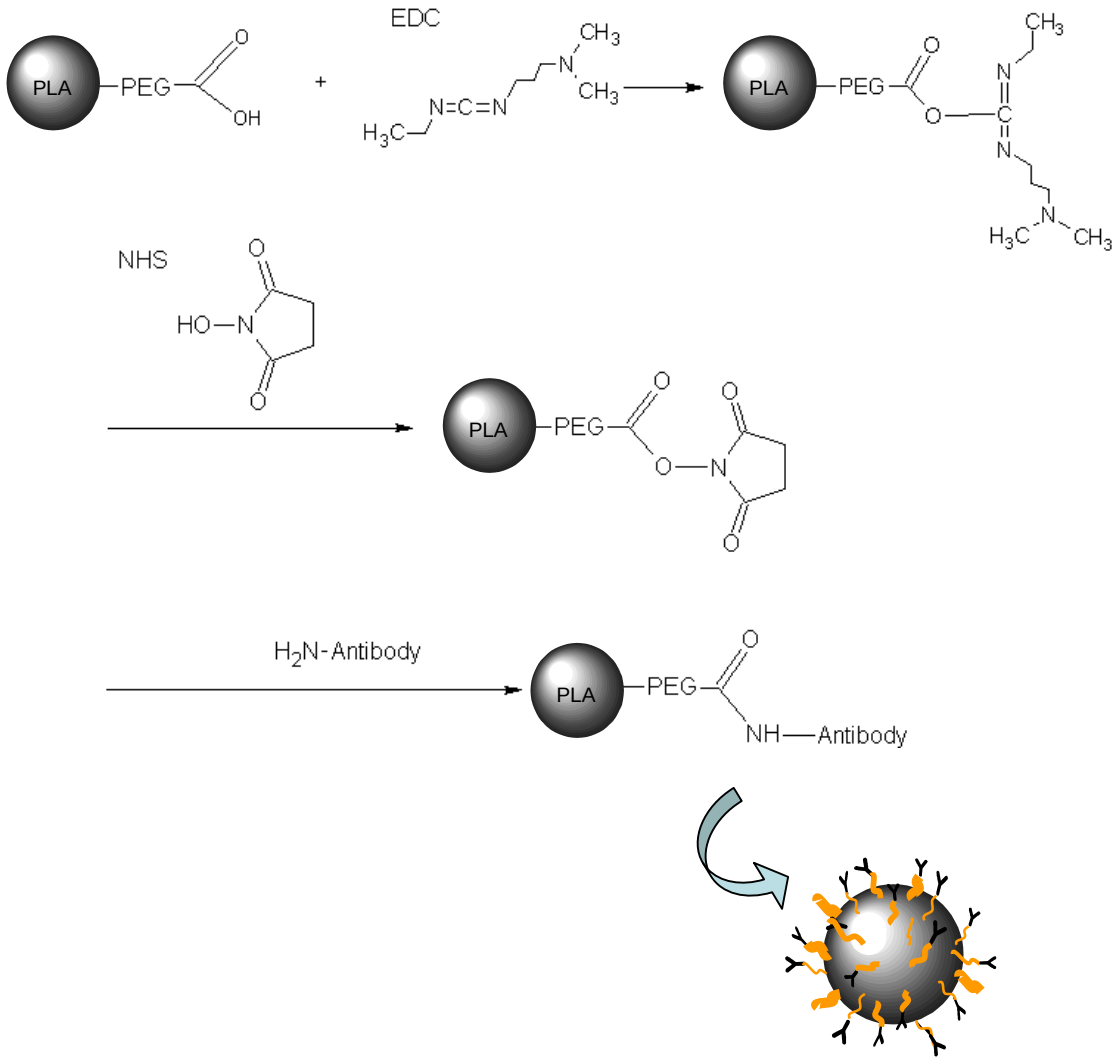

Figure 6.1 Schematic of chemical route for conjugation of antibodies to the surface of poly(lactic acid)-co-poly(ethylene glycol) (PLA-PEG-COOH) nanoparticles. Carboxylic acid groups on the terminal end of surface-exposed PEG were activated to NHS esters using carbodiimide chemistry and conjugated to amine groups on the antibodies to form stable amide bonds.

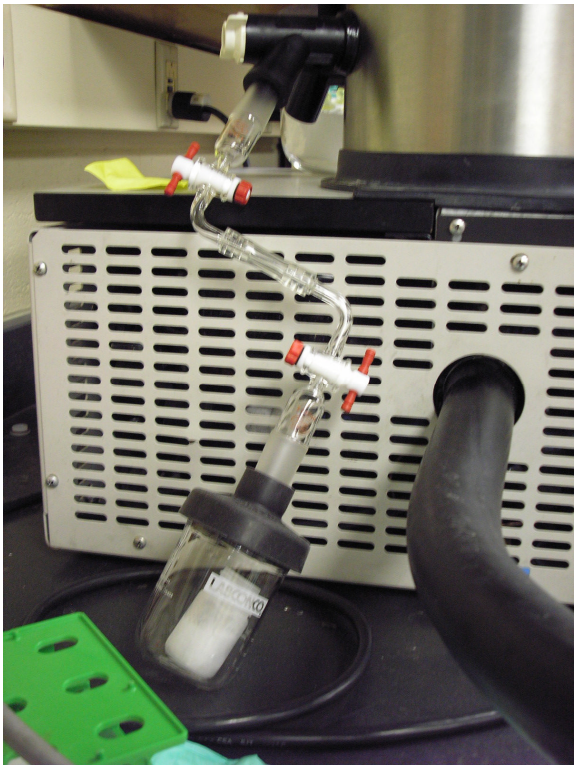

Figure 6.2 Setup utilized for freeze drying of sterile nanoparticles. Red stopcock valves were closed at all times unless the system was under vacuum which assured one-directional flow from the sample to the freeze dryer. Valves were closed and removed from the freeze dryer while maintaining the sample under vacuum at the end of the freeze drying process.

A

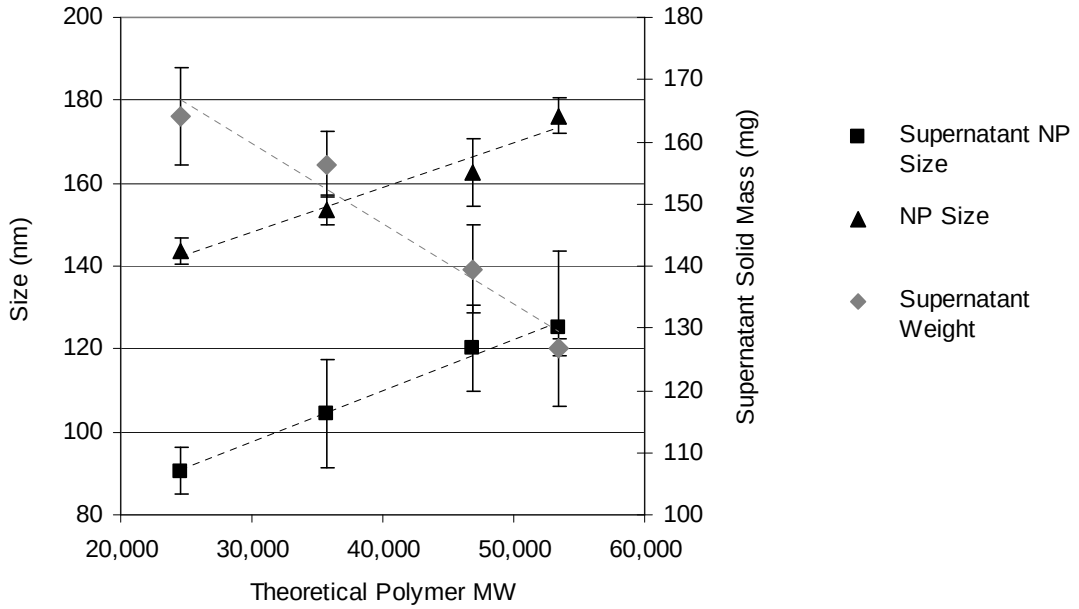

B

Figure 6.3 **(A)** Effect of copolymer molecular weight on the size of the PLA-PEG nanoparticles, the size of the particles remaining on the supernatants of centrifugation, and the mass of dried combined supernatants (which includes 100 mg of surfactant). (B) Image of final nanoparticle suspension (left) and combined supernatants (right) for batch prepared with copolymer of 53,400 g/mol molecular weight. Each batch was prepared with 100 mg of copolymer and was submitted to three 10-minute centrifugation cycles at 48,000 x g.

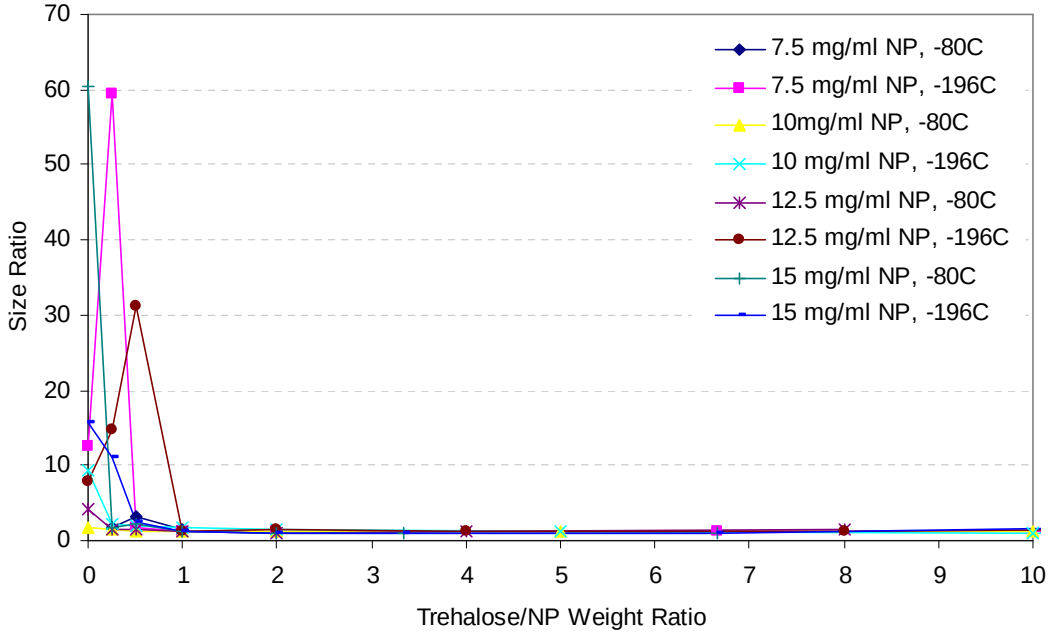

Figure 6.4 Effect of the mass ratio of D-trehalose to nanoparticles (NP) on the size of freeze dried particles. The y axis represent the ratio of the size of the particles after being freeze dried compared to the pre-dried size. As the ratio of trehalose to nanoparticles increases from 0.25 to 2.0, the size of the particles nears the pre-dried size (size ratio closer to 1). No further improvement was observed with trehalose/NP ratios greater than 2.

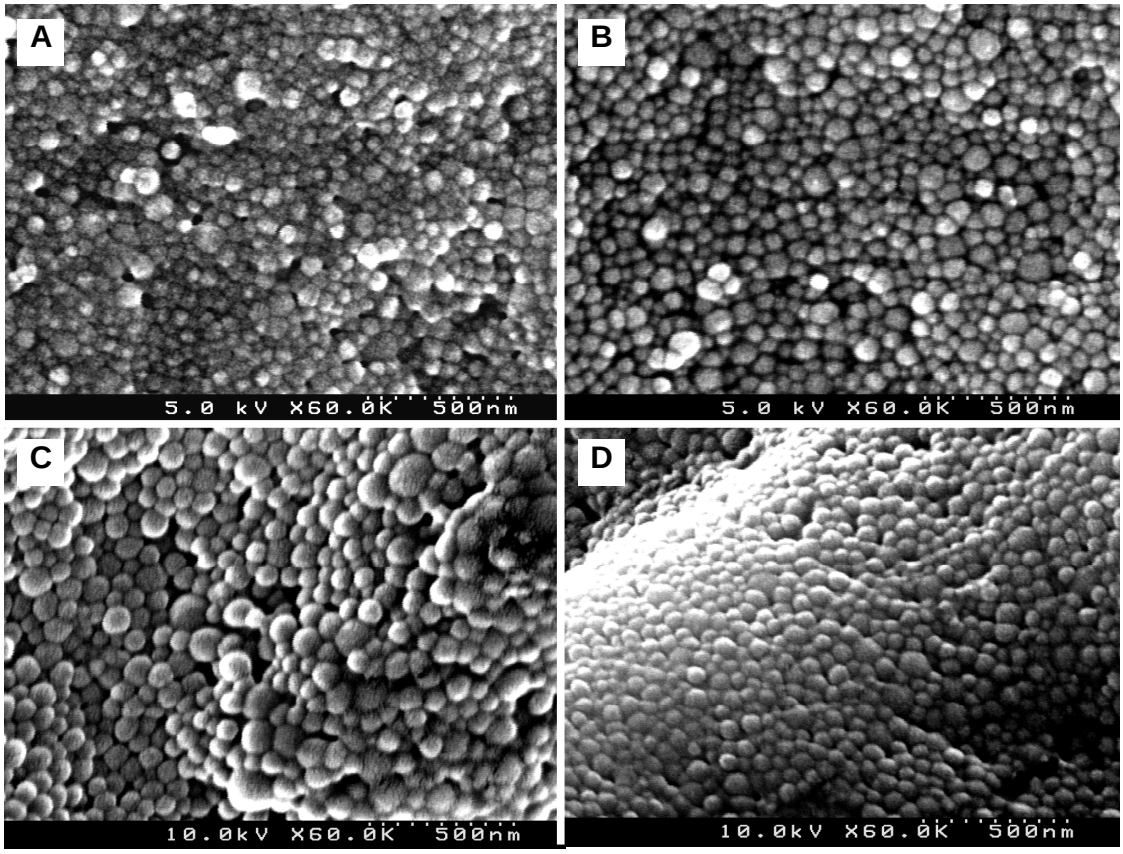

Figure 6.5 Scanning electron images of blank PLA-PEG-COOH nanoparticles. (A) Nanoparticles that were activated with EDC/NHS but not conjugated to an antibody. (B) Nanoparticles with adsorbed mouse IgG. (C) Nanoparticles conjugated to mouse IgG. (D) Nanoparticles conjugated to anti-FSHR antibody mAb106-105

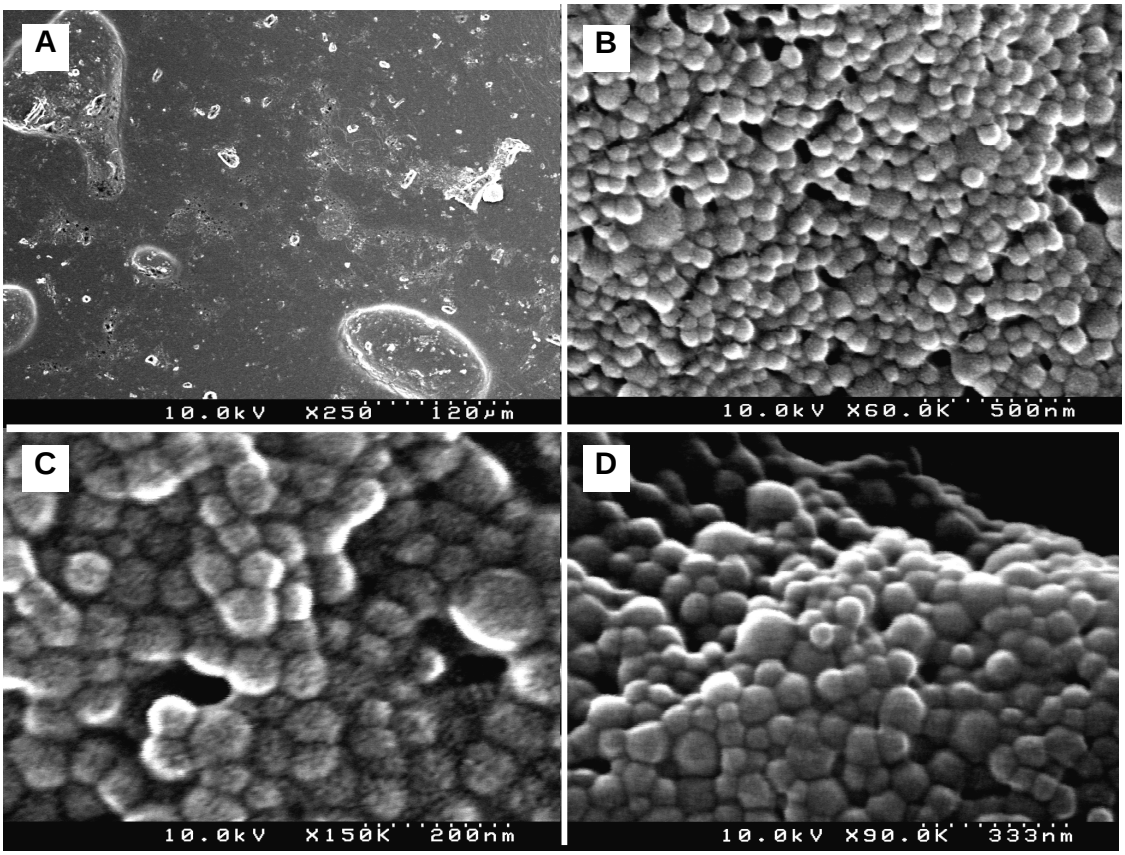

Figure 6.6 Scanning electron images of doxorubicin-loaded PLA-PEG-COOH nanoparticles. (A and B) Images of batch of particles conjugated to anti-FSHR antibody mAb106-105. Image at low magnification shows the presence of polymeric aggregates (A), which are numerically insignificant compared to the smaller particles observed at high magnification (B). (C) Nanoparticles conjugated to isotype control antibody IgG2b. (D) Nanoparticles conjugated to mouse IgG.

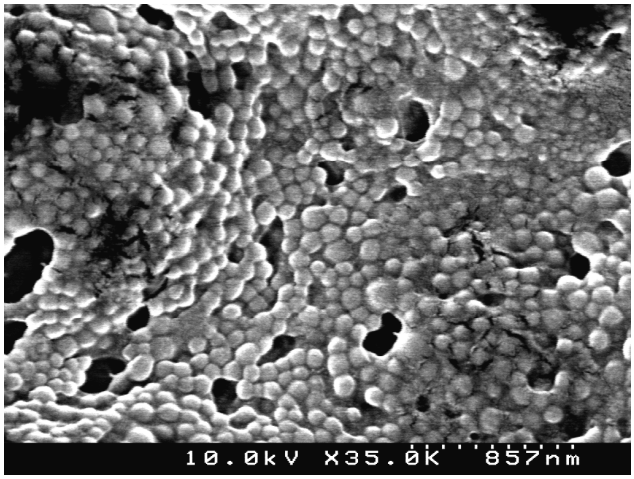

Figure 6.7 Scanning electron microscopy images of rhodamine 6G-loaded PLA-PEG-COOH nanoparticles.

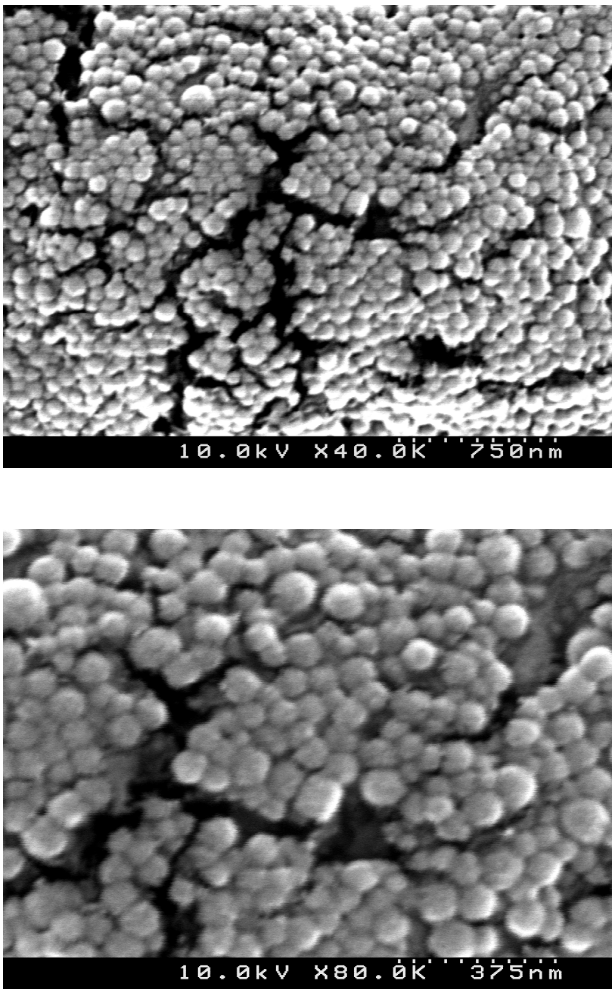

Figure 6.8 Scanning electron microscopy image of PLA-PEG-COOH nanoparticles loaded with indocyanine green.

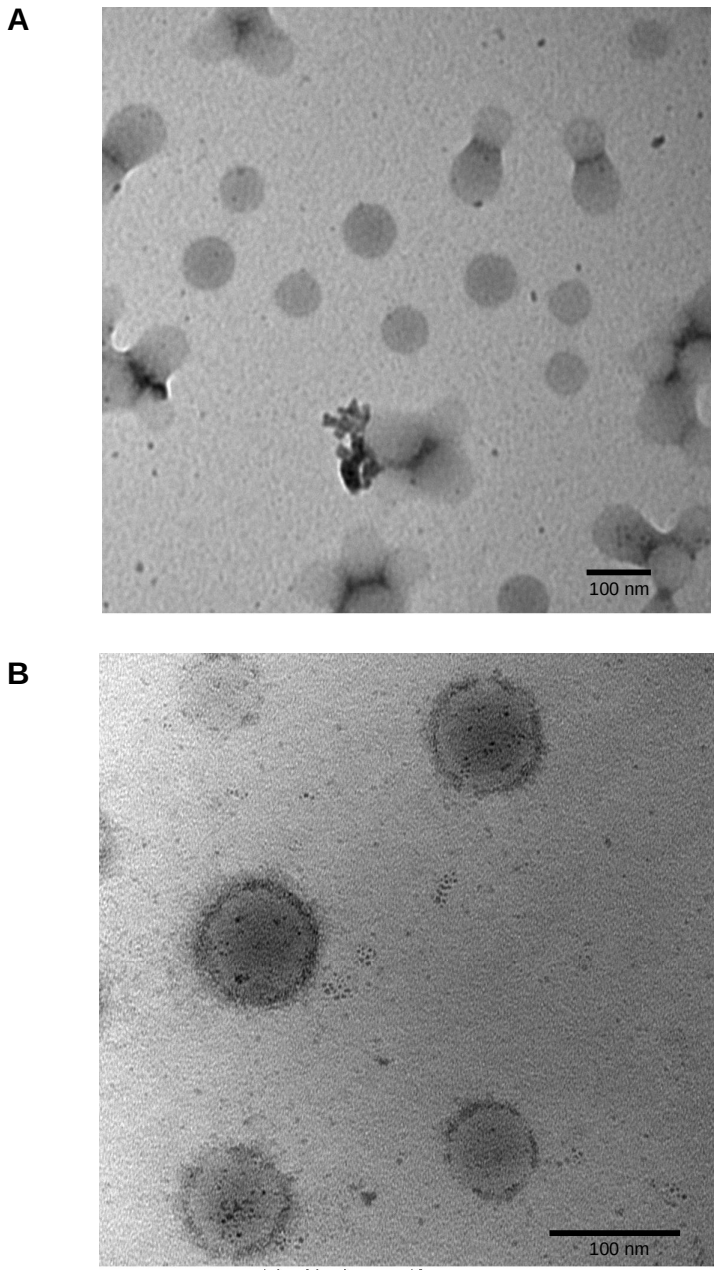

Figure 6.9 Transmission electron microscopy images of blank PLA-PEG-COOH nanoparticles conjugated to mouse IgG at (A) 89,000 and (B) 180,000x magnification.

Figure 6.10 Image of doxorubicin loaded nanoparticle pellet and supernatant showing clear encapsulation of the drug within the PLA-PEG nanoparticles

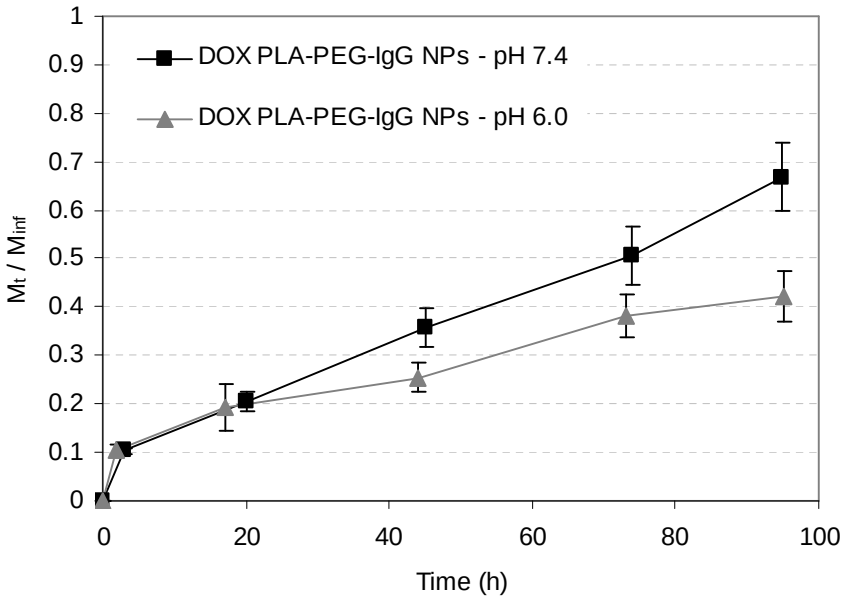

Figure 6.11 *In vitro* release of doxorubicin from PLA-PEG-IgG nanoparticles at physiological and acidic pH. Error bars represent the standard deviation between three independent samples.

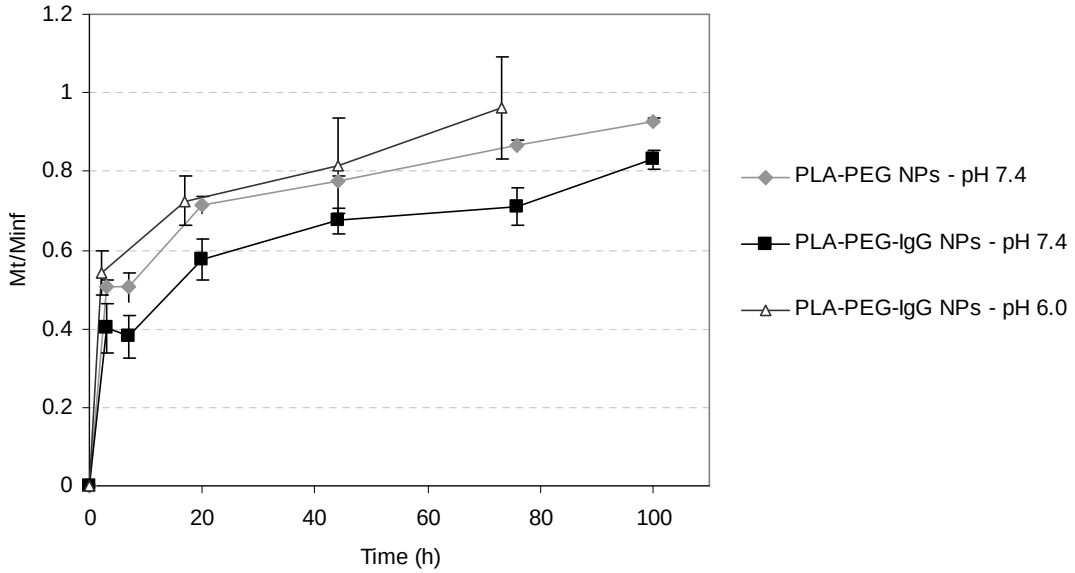

Figure 6.12 *In vitro* release of rhodamine from PLA-PEG nanoparticles without antibody or conjugated to mouse IgG as a model antibody at physiological (pH 7.4) or acidic conditions (pH 6.0). Y bars represent the standard deviation between three independent samples.

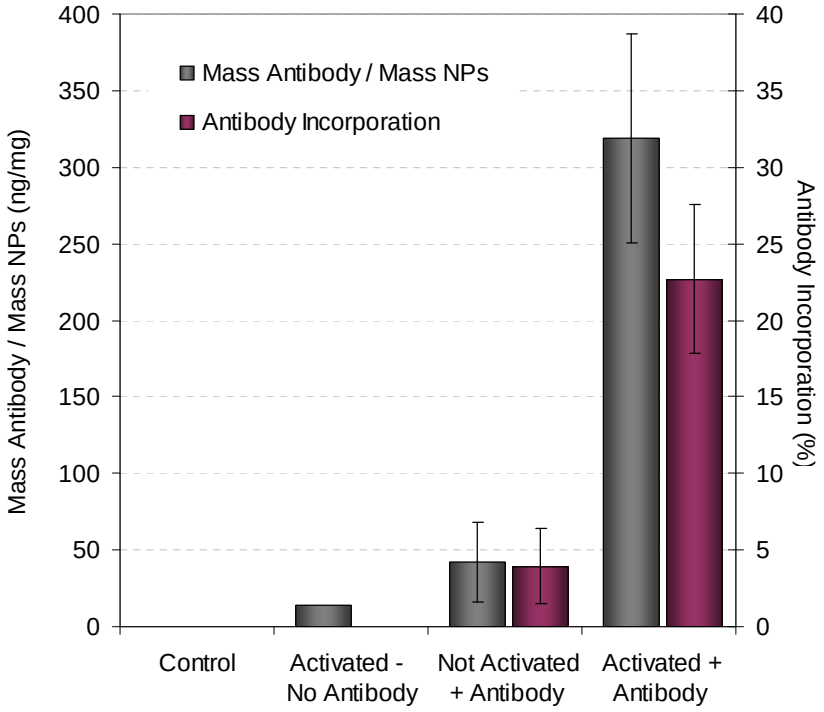

Figure 6.13 Efficiency of conjugation of mouse IgG as a model antibody on PLA-PEG-COOH nanoparticles. Data are displayed as mass of antibody conjugated per mass of nanoparticles and as percent antibody incorporated out of that used in the preparation of the particles (50 μg).

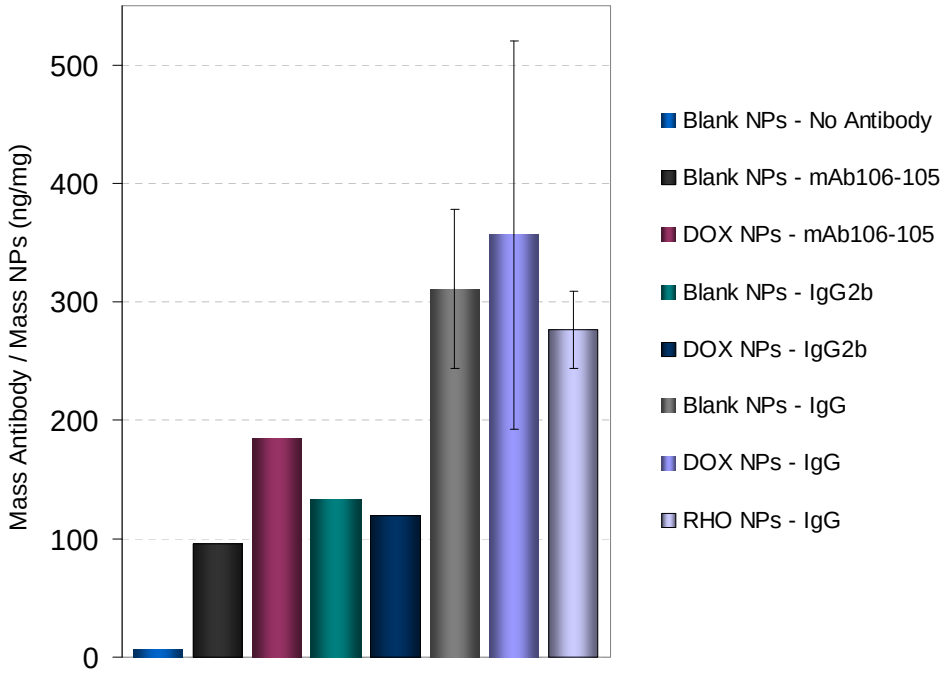

Figure 6.14 Conjugation of antibodies to blank, doxorubicin- and rhodamine-loaded nanoparticles. Data presented as mass of antibody per mass of nanoparticles (ng/mg).

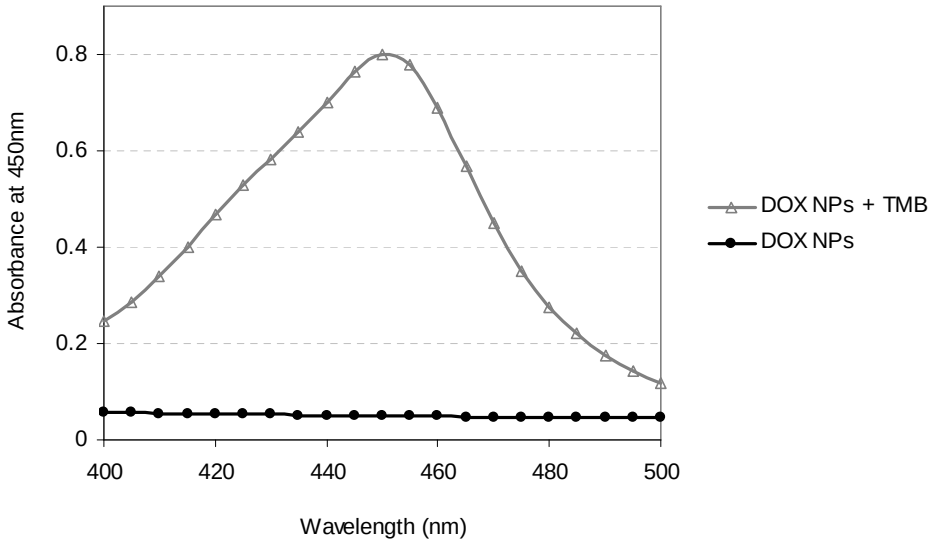

Figure 6.15 Absorbance spectra of doxorubicin-loaded nanoparticles conjugated to anti-FHSR mAb106-105 antibody (black) and of the same batch of nanoparticles at the same concentration after reaction with TMB for antibody quantification. The nanoparticle concentration is too low for the absorption of doxorubicin (maxima at 480nm) to interfere with the antibody quantification assay.

6.5 REFERENCES

Abdelwahed, W., G. Degobert, et al. (2006). "Freeze-drying of nanoparticles: Formulation, process and storage considerations." Advanced Drug Delivery Reviews 58(15): 1688-1713.

Avgoustakis, K. (2004). "Pegylated poly(lactide) and poly(lactide-co-glycolide) nanoparticles: preparation, properties and possible applications in drug delivery." Current Drug Delivery 1: 321-333.

Avgoustakis, K., A. Beletsi, et al. (2003). "Effect of copolymer composition on the physicochemical characteristics, in vitro stability, and biodistribution of PLGA-mPEG nanoparticles." Int J Pharm 259(1-2): 115-27.

Bradford, M. M. (1976). "A rapid and sensitive method for the quantitation of microgram quantities of protein utilizing the principle of protein-dye binding." Anal Biochem 72: 248-54.

Choi, J.-H., K.-C. Choi, et al. (2004). "Overexpression of Follicle-Stimulating Hormone Receptor Activates Oncogenic Pathways in Preneoplastic Ovarian Surface Epithelial Cells." The Journal of Clinical Endocrinology & Metabolism 89(11): 5508-5516.

Darby, R. (1996). Chemical Engineering Fluid Mechanics. New York, NY, Marcel Dekker, Inc.

de Jaeghere, F., E. Allemann, et al. (2000). "Freeze-Drying and Lyopreservation of Diblock and Triblock Poly(Lactic Acid)-Poly(Ethylene Oxide) (PLA-PEO) Copolymer Nanoparticles." Pharmaceutical Development and Technology 5(4): 473-483.

de Jaeghere, F., E. Allemann, et al. (1999). "Formulation and lyoprotection of poly(lactic-acid-co-ethylene oxide) nanoparticles: influence of physical stability and in vitro cell uptake." Pharmaceutical Research 16(6): 859-866.

Fessi, H., J. P. Devissaguet, et al. (1986). Procédé de préparation des systèmes colloïdaux dispersibles dune substance sous forme de nanoparticules. F. P. Application. French.

Fessi, H., F. Puisieux, et al. (1989). "Nanocapsule formation by interfacial deposition following solvent displacement." International Journal of Pharmaceutics 55: R1-R4.

Greener, M. (2005). "MAbs Turn 30." The Scientist: 14-16.

Gref, R., A. Domb, et al. (1995). "The controlled intravenous delivery of drugs using PEG-coated sterically stabilized nanospheres." Advanced Drug Delivery Reviews 16(2): 215-233.

Gref, R., M. Luck, et al. (2000). "'Stealth' corona-core nanoparticles surface modified by polyethylene glycol (PEG): influences of the corona (PEG chain length and surface density) and of the core composition on phagocytic uptake and plasma protein adsorption." Colloids Surf B Biointerfaces 18(3-4): 301-313.

Gref, R., Y. Minamitake, et al. (1994). "Biodegradable Long-Circulating Polymeric Nanospheres." Science 263(5153): 1600-1603.

Izutsu, K., S. Yoshioka, et al. (1996). "Effects of sugars and polymers on crystallization of poly(ethylene glycol) in frozen solutions: phase separation between incompatible polymers." Pharmaceutical Research 13(9): 1393-1400.

Josephy, P. D., e. Thomas, et al. (1982). "The horseradish peroxidase-catalyzed oxidation of 3,5,3',5'-tetramethylbenzidine." The Journal of Biological Chemistry 257(7): 3669-3675.

Kim, G. J. and S. Nie (2005). "Targeted cancer nanotherapy." Nanotoday 8(8, Supplement 1): 28-33.

Li, Y., Y. Pei, et al. (2001). "PEGylated PLGA nanoparticles as protein carriers: synthesis, preparation and biodistribution in rats." J Control Release 71(2): 203-11.

Lindau-Shepard, B., H. A. Brumberg, et al. (2001). "Reversible immunoneutralization of human follitropin receptor." Journal of Reproductive Immunology 49: 1-19.

Lowery, A. R., A. M. Gobin, et al. (2006). "Immunonanoshells for targeted photothermal ablation of tumor cells." Int J Nanomedicine 1(2): 149-54.

Menegazzi, R., G. Zabucchi, et al. (1992). "A new, one-step assay on whole cell suspensions for peroxidase secretion by human neutrophils and eosinophils." Journal of Leukocyte Biology 52: 619-624.

Moghimi, S. M., C. J. Porter, et al. (1991). "Non-phagocytic uptake of intravenously injected microspheres in rat spleen: influence of particle size and hydrophilic coating." Biochem Biophys Res Commun 177(2): 861-6.

Riley, T., S. Stolnik, et al. (2001). "Physiochemical evaluation of nanoparticles assembled from poly(lactic acid)-poly(ethylene glycol) (PLA-PEG) block copolymers as drug delivery vehicles." Langmuir 17: 3168-3174.

Stolnik, S., S. E. Dunn, et al. (1994). "Surface modification of poly(lactide-co-glycolide) nanospheres by biodegradable poly(lactide)-poly(ethylene glycol) copolymers." Pharm Res 11(12): 1800-8.

Torchilin, V. P., J. Narula, et al. (1996). "Poly(ethylene glycol)-coated anti-cardiac myosin immunoliposomes: factors influencing targeted accumulation in the infarcted myocardium." Biochimica Biophysica Acta 1279: 75-83.

Vannier, B., H. Loosfelt, et al. (1996). "Anti-Human FSH Receptor Monoclonal Antibodies: Immunochemical and Immunocytochemical Characterization of the Receptor." Biochemistry 35: 1358-1366.

CHAPTER 7

IN VITRO CELLULAR EVALUATION OF TARGETED NANOPARTICLES

7.1 INTRODUCTION

Three cells lines were used as *in vitro* models for the evaluation of targeted nanoparticles. The main criteria used for screening of these cell lines were expression of the follicle stimulating hormone receptor (FSHR) and sensitivity or resistance to chemotherapeutic agents such as doxorubicin. The cell lines chosen are described below.

7.1.1 Ovarian Cancer Cell Line NIH:OVCAR-3

OVCAR-3 cells are epithelial, adherent cells isolated in 1982 from the ascites of a 60-year old Caucasian female patient with poorly differentiated ovarian adenocarcinoma (Hamilton, Young et al. 1983). This cell line grows in tightly interconnected colonies in culture and is known to express androgen and estrogen receptors (Hamilton, Young et al. 1983). This cell line is known to be resistant to clinically chemotherapeutic drugs including doxorubicin, cisplatin and melphalan at clinically-relevant concentrations of 0.03, 0.15 and 1.5 μg/ml, respectively (Hamilton, Young et al. 1983). These concentrations of chemotherapeutic agents are equivalent to 10% of the achievable peak plasma levels of doxorubicin and cisplatin, and 3-fold more than the maximum achievable plasma levels for melphalan. This cell line is one of the 60 human cancer cell lines used by the National Cancer Institute to screen new anti-cancer drugs (Nishizuka,

Charboneau et al. 2003) and has been suggested to be an appropriate model system for the study of drug resistance in ovarian cancer.

OVCAR-3 cell line has been previously shown to express high levels of the follicle stimulating hormone receptor by Southern immunoblot analysis and high levels of FSHR mRNA by RT-PCR (Choi, Choi et al. 2004; Choi, Choi et al. 2006). This cell line has also been shown to overexpress EGFR, K-Ras, HER-2/neu and c-myc oncogenes (Choi, Choi et al. 2006).

7.1.2 Ovarian Cancer Cell Line Caov-3

Caov-3 cells are ovarian adenocarcinoma adherent cells of epithelial morphology derived from a 54-year old caucasian female (ATCC). This cell line is known to be sensitive to doxorubicin treatment (Fan, Twu et al. 1998; Sugiyama, Imai et al. 2005). Reports of FSHR expression levels in Caov-3 cells in the literature have been contradicting: Choi, et al., reported in 2004 that this cell line had high levels of the FSHR protein at the translational level similar to OVCAR-3 cells by immunoblot, although the data was not shown (Choi, Choi et al. 2004). The same group in 2006 reported that the mRNA transcriptional level of FSHR produced by Caov-3 cells was less than 10% of that of OVCAR-3 cells and SKOV-3 cells as determined by real-time PCR (Choi, Choi et al. 2006). According to an email discussion with Dr. K. C. Choi, the discrepancy could be a result post-transcriptional regulation of FSHR, different culture conditions of Caov-3 during the studies, and of the quality of the anti-FSHR antibody used in their investigation (Choi 2007). The antibody used by this group is the same mAb106-105 monoclonal antibody developed by the group of Dr. James Dias at the Wadsworth Center (Albany, NY) that was utilized in the research presented here as a targeting agent for delivery of nanoparticles to ovarian cancer cells.

7.1.3 Breast Cancer Cell Line MDA-MB-231

MDA-MB-231 cells are epithelial adenocarcinoma cells derived from pleural effusion of a 54-year old Caucasian female (Cailleau, Young et al. 1974; Cailleau, Olive et al. 1978). As reported in previous accounts, FSHR expression is limited to cells of ovarian origin (Richards and Midgley 1976; Kangasniemi, Kaipia et al. 1990; Simoni, Gromoll et al. 1997; Meduri, Charnaux et al. 2002). Consequently, this cell line was used as a control for studying the interaction of the targeted nanoparticles with cells not expressing the target receptor. This cell line is also one of the 60 human cancer cell lines used by the National Cancer Institute for screening of new anti-neoplastic drugs (Nishizuka, Charboneau et al. 2003). This cell line is known to be sensitive to doxorubicin treatment (Smith, Watson et al. 2006; Betancourt, Brown et al. 2007; Pero, Shukla et al. 2007).

7.2 METHODS

7.2.1 Materials

The reagent 3-[4,5-dimethylthiazol-2-yl]-2,5-diphenyl tetrazolium bromide (MTT) and formaldehyde (37%, formalin) were obtained from Sigma-Aldrich (Saint Louis, MO, USA). Ethylenediamine-tetraacetic acid (EDTA) and dimethylsulfoxide were purchased form Fisher Scientific (Waltham, MA, USA). Sodium azide was obtained from ACROS Organics.

Blank or doxorubicin-loaded poly(lactic acid)-co-poly(ethylene glycol) (PLA-PEG) nanoparticles with or without conjugated antibodies were prepared and characterized as described in Chapter 6. Blank or doxorubicin-loaded poly(lactic-co-

glycolic acid) (PLGA) nanoparticles with no targeting antibodies were prepared and characterized as described in Chapter 3.

7.2.2 Cell Culture

Ovarian cancer cell lines were obtained from American Type Tissue Culture (Manassas, VA, USA) while the MDA-MB-231 cell line was generously provided by Dr. Suranganie Dharmawardane, formerly from the School of Biological Sciences of The University of Texas at Austin. Caov-3 and MDA-MB-231 cells were cultured with Dulbecco's Modified Eagle's Medium (DMEM, Mediatech, Manassas, VA, USA) supplemented with 10% fetal bovine serum (Tissue Culture Biologicals, Tulare, CA, USA), 10 mM HEPES buffer (Gibco, Carlsbad, CA, USA) and 1% penicillin/streptomycin. NIH-OVCAR-3 cells were grown in RPMI medium (Mediatech, Manassas, VA, USA) supplemented with 20% fetal bovine serum, 10 mM HEPES buffer, 1% penicillin/streptomycin, and 0.01 mg/ml bovine insulin (Sigma, Saint Louis, MO, USA). Cells were grown in T75 flasks in an incubator at 37°C and 5% CO_2 atmosphere.

7.2.3 Determination of Target Receptor Expression by Cell Lines

The relative expression levels of the follicle stimulating hormone receptor (FSHR) was determined on ovarian cancer cell lines Caov-3 and NIH:OVCAR-3. Breast cancer cell line MDA-MB-231 was used as a control. For determination of FSHR expression an immunocytochemical study was carried out. Cells were grown in T-75 flasks to near confluency, washed twice with 5 ml of DPBS without calcium or magnesium ions (referred to as DPBS throughout this section), and once with a solution

of 2mM EDTA in DPBS. Cells were then detached by incubation in EDTA solution. Detached cells of each cell line were transferred to six separate 15-ml conical tubes at a concentration of 300,000 cells per tube, centrifuged for 5 minutes at 500 x g to remove EDTA and incubated at 4°C for 30 minutes in 1 ml of 5% goat serum (SIGMA, St. Louis, Missouri, USA) in DPBS with 0.02% sodium azide (DPBS-SA) to block non-specific sites. The presence of sodium azide prevents modification of the antibody-antigen complex after recognition and binding.

Cells were then centrifuged and resuspended in 200 µl of a solution of the primary antibody mAb106-105 from murine origin (IgG_{2b} isotype, generously provided by Dr. James Dias from the Wadsworth Center, Albany, NY) at a concentration of 2.5 µg/tube, mouse IgG2b (SIGMA, Saint Louis, Missouri, USA) as an isotype control at the same concentration, or DPBS-SA as a negative control for 1 hour at 4°C. Each of these primary antibody treatments were repeated in 2 of the conical tubes of each cell line. Cells were then centrifuged, washed with DPBS-SA, centrifuged again and resuspended in 200 µl of secondary FITC-conjugated goat anti-mouse IgG (H+L) antibody (Biomeda, Foster City, CA, USA) or DPBS-SA as a negative control and incubated at 4°C for 30 minutes. Cells were then centrifuged, washed with DPBS-SA, resuspended in DPBS-SA with 2% formaldehyde, kept cold and analyzed soon after by flow cytometry (FACSCalibur, Becton and Dickinson, Franklin, NJ, USA). All voltage and gain settings were maintained constant during analysis to be able to do a comparative analysis of the fluorescence associated with each sample.

The fluorescence levels of these three cell lines after exposure to the primary and secondary antibodies were confirmed by confocal microscopy. Samples from the fixed cells of the above study were mounted onto microscopy slides and observed with a Leica

SP2 AOBS confocal fluorescence microscope while maintaining all microscope and software settings constant for comparison between samples.

7.2.4 Determination of Therapeutic Efficacy of Targeted Nanoparticles

Each of the three cell lines was seeded at a concentration of 5,000 cells per well in the central 60 wells of nine 96-well plates with 100 μl of complete growth media. The remaining 36 wells of each plate were filled with 200 μl of DPBS to minimize loss of moisture from the plates. Two days after seeding, the cell media was replaced with 100 μl of complete media containing one of a series of formulations. These formulations included blank or doxorubicin-loaded PLA-PEG nanoparticles conjugated to anti-FSHR antibody mAb106-105, IgG2b control antibody or no antibody, blank and doxorubicin-loaded PLGA nanoparticles, free doxorubicin in solution or unmodified media as a control. Each formulation was repeated in 5 wells.

The concentration of nanoparticles was such that the doxorubicin content was maintained constant between samples. Nanoparticle samples with no doxorubicin were added at the same nanoparticle concentration as doxorubicin-loaded nanoparticles with the same antibody. The mass of each nanoparticle formulation to be used was calculated from the desired doxorubicin concentration, the known weight percent of doxorubicin in each batch, and the nanoparticle-to-trehalose ratio that was determined for each batch. Nanoparticles were first weighed, resuspended in 10 ml of cold sterile water and centrifuged for 1 hour in a Beckman J2-21 refrigerated centrifuge (Beckman Instruments Inc., Palo Alto, CA, USA) at 43,000 x g to remove excess trehalose. The nanoparticle pellets were then resuspended in 0.6 ml of DPBS with Ca/Mg. A volume of 0.4 ml of these suspensions was further diluted in 1.6 ml of DMEM media for the Caov-3 and

MDA-MB-231 cells, while the remaining 0.2 ml were diluted in RPMI media for the OVCAR-3 cells. The doxorubicin concentrations tested were 0.1, 1.0 and 10.0 μg/ml.

Cells were incubated for 24 hours in these formulations, after which the media was removed and the cells were washed three times with DPBS with Ca/Mg ions. Complete growth media was then added to the cells and these were incubated for 2 days to allow the drug to act as the cells attempted to replicate. After this incubation period, 10 μl of 5 mg/ml MTT solution in DPBS with Ca/Mg was added and the cells were incubated for 4 hours. After this incubation period, the cell media was removed by inverting the plates and gently tapping them against paper towels. Then, 200 μl of dimethylsulfoxide were added to each well to solubilize formazan crystals produced by live cells. After confirming solubilization of crystals by microscopy, the absorbance of each well was read at 570 and 690 nm using a BioTek Synergy™ HT microplate reader (Winooski, VT, USA). The absorbance difference at these two wavelengths was used to determine the viability of the cells exposed to each formulation relative to control cells not exposed to any formulation.

It should be noted that the PLA-PEG nanoparticle formulations used contained doxorubicin-loadings in the range of 0.196 to 0.282 wt. % and nanoparticle-to-trehalose ratios of 0.11 to 0.18 depending on the encapsulation efficiency and yield of each batch. The PLGA batch, on the other had, had a doxorubicin content of 1.69 wt.% and no trehalose. Nonetheless, the actual doxorubicin concentrations that the cells were exposed to were maintained constant, as described above.

7.2.5 Microscopy Study of Interactions of Nanoparticles with Cells

Each of the cell lines was seeded at a concentration of 5,000 cells per well in 8-welled Lab-Tek™ chambered coverglass (Nalge Nunc International, Rochester, NY) in

complete growth media and incubated at 37°C and 5% CO_2 atmosphere for 4 days before beginning the study to permit enough time for the cells to attach to the less-favorable glass substrate and begin replicating. To begin the study, the media was removed and replaced with complete media containing various nanoparticle or drug formulations. Specifically, the six formulations tested were doxorubicin-loaded PLA-PEG nanoparticles conjugated to mAb106-105 anti-FSHR antibody, IgG2b isotype control antibody or no antibody, doxorubicin-loaded PLGA nanoparticles, free doxorubicin in solution and free media as a control.

The concentration of nanoparticles was adjusted so that the doxorubicin concentration was maintained at 10 μg/ml in all the formulations. The mass of each nanoparticle formulation to be used was calculated from the desired doxorubicin concentration, the weight percent of doxorubicin in each batch, and the nanoparticle-to-trehalose ratio of each batch. The PLA-PEG nanoparticle batches used had a doxorubicin content of 0.18 to 0.22 wt. %, while the PLGA batch had a doxorubicin content of 1.69 wt.%. The PLA-PEG nanoparticle batches also had a nanoparticle-to-trehalose ratio in the range of 0.14 to 0.18 by weight, while the PLGA nanoparticle batches contained no trhalose. The desired mass of nanoparticles was resuspended in 10 ml of cold sterile water and centrifuged for 1 hour at 43,000 x g to remove excess trehalose. The nanoparticle pellets were then resuspended in the appropriate complete cell culture media depending on the cell line, and added to the cells.

After 3 hours of cell exposure to the formulations, the media was removed, the cells were washed three times, and complete growth media was added. Cells were immediately imaged with a Leica SP2 AOBS confocal microscope utilizing the natural fluorescence of doxorubicin to determine the interaction of the nanoparticles with the

cells. All laser and detection settings were maintained constant during the study for comparison of fluorescence intensities between formulations.

7.3 RESULTS

7.3.1 Expression of FSHR by Cell Lines

Figure 7.1 displays the results of immunocytochemical detection of FSHR expression by the three cell lines to be used in these studies. In the control breast cancer cell line MDA-MB-231, only minor increases in mean fluorescence intensities were observed with exposure to FITC-conjugated secondary antibody, regardless of the type of primary antibody, thus confirming the absence of the FSHR receptors on the surface of these cells. In OVCAR-3 cells, slightly higher fluorescence was observed in all samples exposed to the labeled secondary antibody; however, significantly higher fluorescence was detected from the samples exposed to the anti-FSHR antibody and the secondary antibody in comparison to all other samples and cell lines, thus confirming expression of the target receptor, as expected based on prior reports (Choi, Choi et al. 2004; Choi, Choi et al. 2006).

In Caov-3 cells, no significant difference was observed between all samples, including those exposed to the anti-FSHR antibody, thus suggesting that the cells do not express this receptor. This result is contrary previous reports of high expression levels of FSHR that were determined by immunoblot (Choi, Choi et al. 2004). It is possible that different expression levels are manifested based on cell culture conditions. In addition, the fact that previous studies had observed low FSHR mRNA but high FSHR protein levels could suggest that the expression of this receptor is modulated by the cells

according to various stimuli and, consequently, the expression of this receptor varies with time and conditions even in culture.

7.3.2 *In Vitro* Therapeutic Effect of Formulations

The MTT assay was used for determination of cell viability after exposure to various nanoparticle formulations. This assay is based on the cleavage of the tetrazolium ring of the MTT reagent by action of mitochondrial dehydrogenases of viable cells (Mossman 1983). This cleavage results in the formation of formazan crystals which are insoluble in aqueous solutions, but are soluble in acidified isopropanol or dimethylsulfoxide. The concentration of soluble formazan, as determined spectrophotometrically, is proportional to the number of live cells in the sample, thus indicating the effect of the various formulations on cell growth. The MTT assay among the few that can be used for determination the activity of doxorubicin-containing formulations because the absorbance and fluorescence of this drug interferes with most other cytotoxicity or live/dead assays.

Figures 7.3, 7.4 and 7.5 display the viability of the OVCAR-3, Caov-3 and MDA-MB-231 cells after exposure to the various formulations. For all three cell lines, a decrease in cell viability was observed with increased dose, including after exposure with blank and doxorubicin-loaded nanoparticles. Significant reductions in cell viability by doxorubicin-loaded nanoparticles compared to blank nanoparticles were observed for most samples at the highest exposure concentration equivalent to 10 μg/ml and in a few samples at the intermediate concentration of 1.0 μg/ml. No significant decrease in cell viability was caused by the nanoparticles containing conjugated anti-FSHR antibody mAb106-105 in any of the cell lines compared to nanoparticles with the control antibody IgG2b or without an antibody at the highest dose, which is the dose at which the cell

viability decreased caused by doxorubicin-loaded nanoparticles was significantly lower than that caused by blank nanoparticles.

The reduced cell viability encountered after exposure to all nanoparticle formulations could suggest that trace amounts of monomers, catalysts, solvents, antibody conjugation reagents and trehalose could have remained in the formulations; however, this hypothesis does not explain reduction in cell viability for every single formulation since those batches without antibodies had not been exposed to the conjugation reagents and those made with PLGA had not been exposed to trehalose. On the other hand, in this study the concentration of nanoparticles used at the highest dose was in the range of 4.4 to 6.4 mg/ml for PLA-PEG batches as a result of their low doxorubicin content. This concentration, and the number of particles that it represents, is quite high and possibly resulted in reduction in cell viability as a result of mechanical shear stresses caused by the Brownian motion of the colloids in suspension. Nonetheless, at this dose the effect of doxorubicin on cell growth was observed, thus indicating the drug activity is maintained.

In this study, cells were exposed to the various formulations for 24 hours, in contrast to the 2 hours used in the study presented in Chapter 3 (Figure 3.5). This longer exposure time was chosen because of the slower rate of drug release observed with doxorubicin-loaded PLA-PEG nanoparticles, which limited the amount of free drug to less than 25% of the total during this incubation time at both pH 7.4 and 6.0 according to the release studies described in Chapter 6. At the same time, however, this increased the time that the cells were subjected to the unfavorable nanoparticle suspension, thus resulting in cell death that is not associated with the action of the drug.

Despite these problems, the data show that no significant increase in cell death is caused by the targeted doxorubicin-loaded nanoparticles on the cells expressing the target FSH receptor. It is possible that the number of antibodies conjugated per nanoparticle is

too low for favorable interaction of the nanoparticles with the target receptors. As described in Chapter 6, the number of antibodies per nanoparticle was calculated to be in the range of 1 to 7. In addition, the chemistry used for conjugation of the antibodies, as described in Chapter 6, does not discriminate between the N-terminal and lysine amine groups in the antibody (Hermanson 1996). As such, conjugation can occur at any one of a number of locations in an antibody, which could result in blockage of the antigen binding domain and consequent reduction in biological activity (Chapman 2002). The binding potential of antibodies after random conjugation to poly(ethylene glycol) chains was reported to decrease from 20 to 90% depending on the antibody type, number of conjugations per antibody and PEG molecular weight, as reviewed previously (Chapman 2002). Conjugation to nanoparticles can, in addition, prevent proper antibody-receptor recognition and binding as a result of steric hindrance by surrounding PEG chains.

7.3.3 Microscopy Study of Cell-Nanoparticle Interaction

Cells were imaged while live with a confocal microscope using the natural fluorescence of doxorubicin to investigate the interaction of the PLA-PEG and PLGA nanoparticles with ovarian and breast cancer cells. Figures 7.6, 7.7 and 7.8 display images of the fluorescence associated with each sample after a 3 hour exposure to doxorubicin-loaded PLA-PEG nanoparticles with anti-FSHR antibody mAb106-105 (PLA-PEG-mAb), with isotype control antibody IgG2b (PLA-PEG-IgG2b) or without an antibody (PLA-PEG-NA), doxorubicin-loaded PLGA nanoparticles or free doxorubicin in solution. As presented, in OVCAR-3 cells that express the FSHR receptor, a similar low level of fluorescence is observed in cells exposed to PLA-PEG-mAb, PLGA nanoparticles or free doxorubicin in solution. A slightly higher level of fluorescence was observed in cells exposed to PLA-PEG-IgG2b nanoparticles. The fluorescence intensity

of cells exposed to PLA-PEG-NA nanoparticles was, however, drastically higher than with all other formulations.

In cells exposed to doxorubicin-loaded PLA-PEG nanoparticles, the distribution of the fluorescence signal was limited to the cytoplasm of the cells, thus suggesting that the drug is still associated with the nanoparticles. In cells exposed to PLGA nanoparticles or doxorubicin solution, the drug was mostly associated with the nucleus of the cells, as previously observed in studies described in Chapter 3 (Figures 3.6 and 3.7). Nuclear localization requires, however, that the drug be dissociated from the nanoparticles for transport across nuclear pores. These results agree with the drug release behavior of PLA-PEG nanoparticles described in Chapter 5 which found no differences in the release of the drug at physiological pH of 7.4 or acidic pH of 6.0 during the first day and that from PLGA nanoparticles described in Chapter 3 (Figure 3.2) which found a significantly accelerated at acidic pH. When the nanoparticles are endocytosed, exposure to acidic conditions in the endolysosomal compartments leads to rapid release of the drug from PLGA nanoparticles, but not so from PLA-PEG nanoparticles.

Similar increased fluorescence signal in addition to some nuclear fluorescence was observed in Caov-3 and MDA-MB-231 cells exposed to PLA-PEG-NA nanoparticles compared to those bound to the anti-FSHR mAb106-105 or IgG2b antibody. In addition, increased nuclear localization in cells exposed to PLGA nanoparticles was observed in comparison to cells exposed to free doxorubicin in both of these cell lines, as previously described in Chapter 3 for the breast cancer cell line.

Results suggest that the conjugation of antibodies, whether mAb106-105 or isotype control IgG2b, on the surface of the nanoparticles decreases their ability to interact with the cells in comparison to PLA-PEG nanoparticles with no antibody. Zeta potential measurements, presented in Chapter 6, did not show significant differences

between these formulations. During conjugation of the antibody, the terminal carboxyl groups of PEG are activated to their N-hydroxysuccinimide (NHS) ester, as shown on Figure 6.1. After conjugation of the antibodies, all free NHS esters would by hydrolyzed back to the carboxylic acid in the presence of water at neutral or higher pH. The half life of these NHS esters has been reported to be in the order of less than 30 minutes at this pH 7-9 (Hermanson 1996; NektarTherapeutics 2005). The conjugations were carried out for 3 hours in PBS buffer pH 7.4 and further washes were done in this buffer. Consequently, the actual surface chemistry of the particles conjugated to antibodies or without these would not be significantly different

The hydrophilic surface PEG coating and the negatively charged end groups of the PLA-PEG nanoparticles in theory would impede their uptake into the cells through the hydrophobic and also negatively charged cell membrane. Consequently, some type of active transport must be facilitating the uptake of the PEGylated nanoparticles into the cytoplasm of the cells.

Similarly to what was observed from therapeutic efficacy studies described in the previous section, the results show that no increased cell-nanoparticle interaction was facilitated by the anti-FSHR antibody on the FSHR-positive cells. As described, it is possible that the number and activity of the antibodies bound to the surface of the nanoparticles are not sufficient to mediate active binding and/or transport into the cells.

7.4 CONCLUSIONS

Cellular studies described in this chapter evaluated the efficacy of targeted PEGylated nanoparticles at interacting with cells expressing the target follicle stimulating hormone receptor and causing decrease in cell growth compared to the free chemotherapeutic agent doxorubicin and to non-targeted and non-PEGylated

formulations. Cytotoxicity studies determined that no increased cell viability reduction was caused by exposure to the targeted nanoparticles in comparison to non-targeted or non-PEGylated nanoparticles. A reduction of cell viability compared to control was observed after exposure to most of the formulations at the three doses tested possibly as a result of shear forces on the cell by the colloids or the presence of trace non-biocompatible compounds in the nanoparticles, although formulations including doxorubicin caused higher reductions in cell viability than blank nanoparticles at intermediate and higher doses, as expected. *In vitro* imaging studies also revealed that the interaction of nanoparticles with cells was decreased in formulations that had been conjugated to antibodies, regardless of the antibody type. No increased association of targeted nanoparticles was seen in FSHR-positive OVCAR-3 cells. All results suggest that the number of antibodies conjugated to the nanoparticles was not sufficient to permit specific recognition, binding and transport of the targeted nanoparticles with the target FSH receptor.

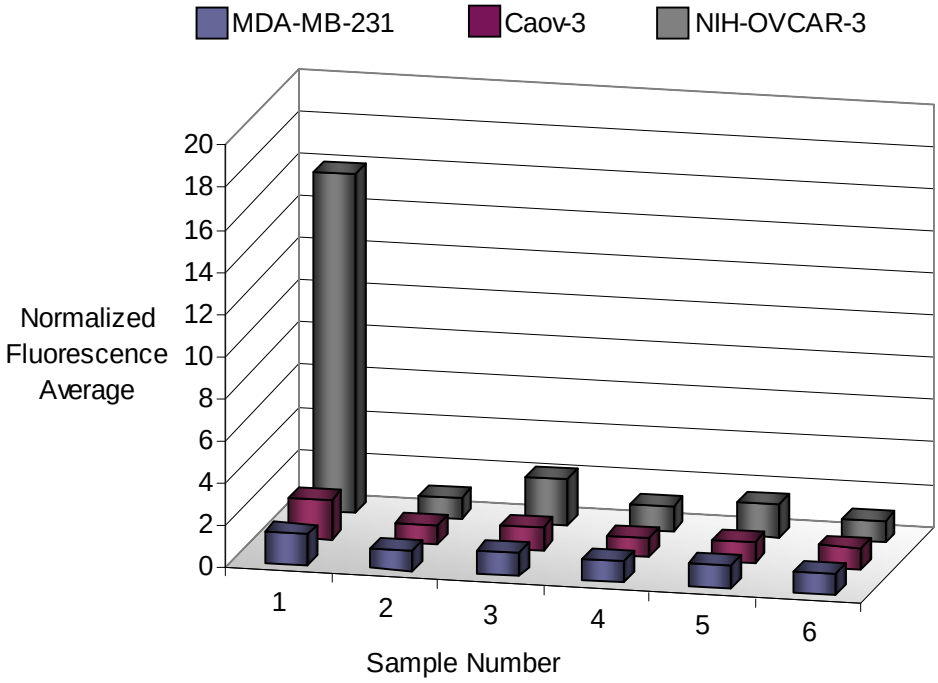

Sample Number	Primary Antibody	Secondary Antibody
1	Anti-FHSR (mAb106-105)	Yes
2	Anti-FHSR (mAb106-105)	No
3	IgG2b control	Yes
4	IgG2b control	No
5	None	Yes
6	None	No

Figure 7.1 Immunocytochemical determination of FSHR expression in model cell lines. Data show clear expression of FSHR by OVCAR-3 cells.

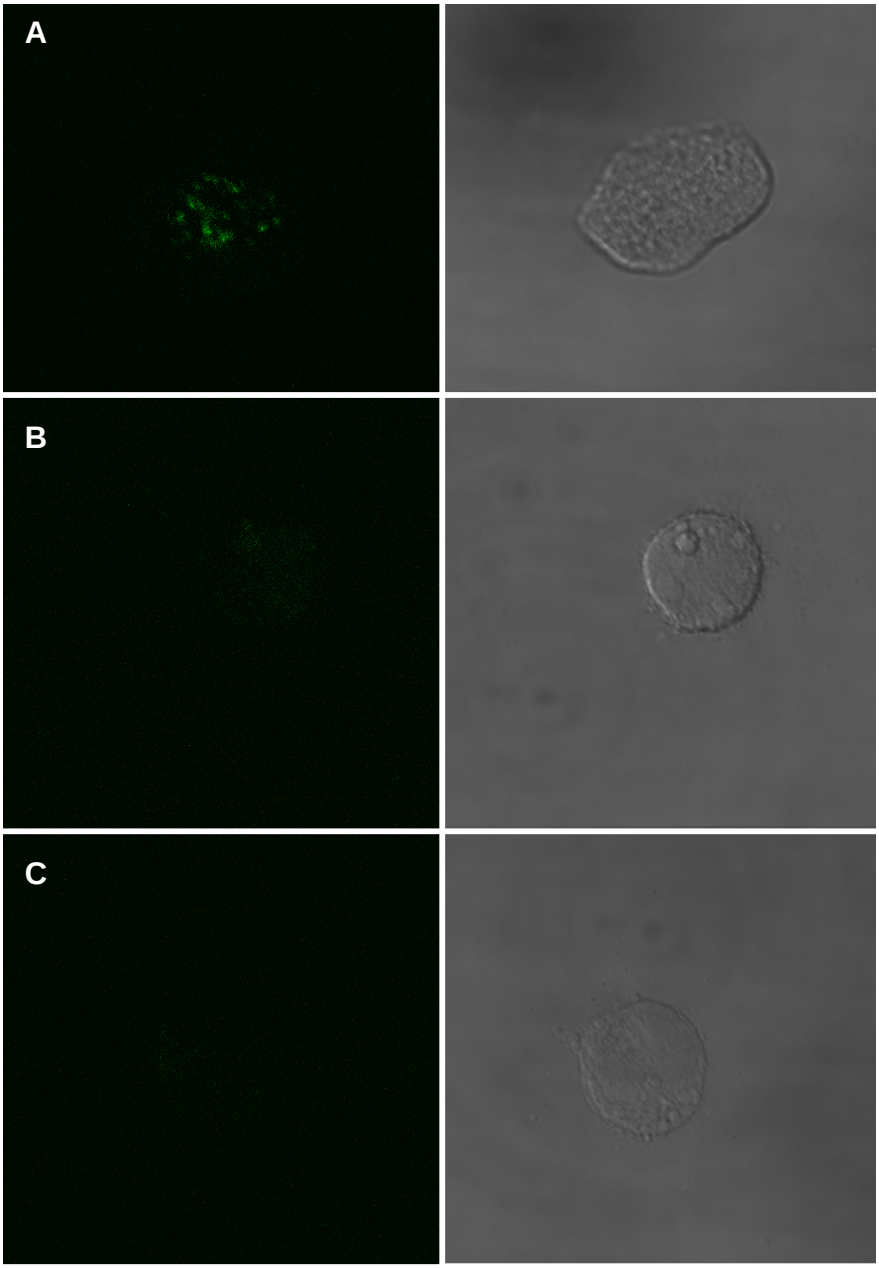

Figure 7.2 Fluorescence and corresponding differential interference contrast microscopy images of (A) OVCAR-3 ovarian cancer cells, (B) Caov-3 ovarian cancer cells and (C) MDA-MB-231 breast cancer cells. The intensity of fluorescence represents the expression of the follicle-stimulating hormone receptor by the cells.

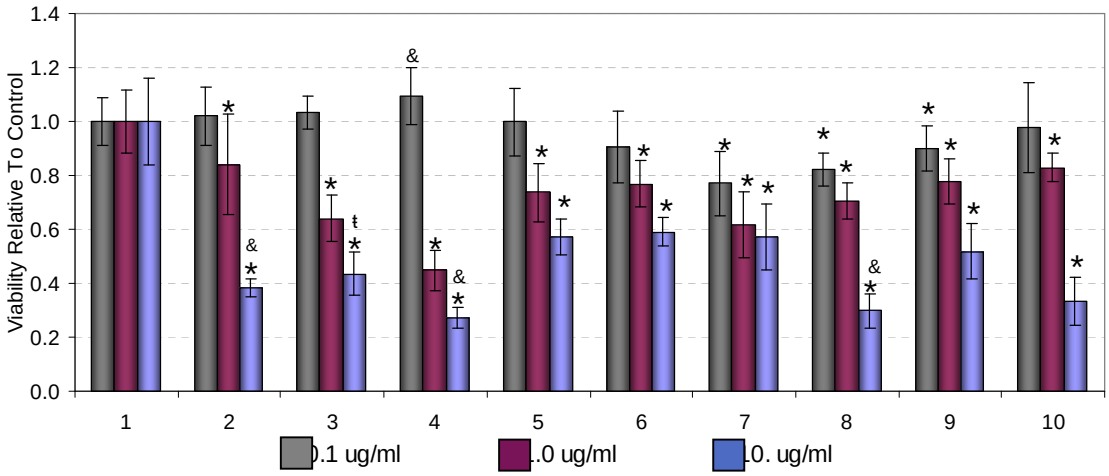

Sample No.	Description
1	Control
2	DOX - PLA-PEG-mAb106-105 NPs
3	DOX - PLA-PEG-IgG2b NPs
4	DOX - PLA-PEG NPs - No Antibody
5	Blank - PLA-PEG-mAb106-105 NPs
6	Blank - PLA-PEG-IgG2b NPs
7	Blank - PLA-PEG NPs - No Antibody
8	DOX - PLGA NPs
9	Blank - PLGA NPs
10	DOX solution

Figure 7.3 Viability of NIH:OVCAR-3 cells after exposure to blank and doxorubicin-loaded PLA-PEG and PLGA nanoparticles with or without targeting antibodies as determined by the MTT assay. Viability presented as a fraction relative to control cells maintained in complete growth media without nanoparticles or drug. Error bars represent the standard deviation between 5 repetitions for each condition. * Significantly different from control. & Significantly different from blank nanoparticles of same polymer and antibody.

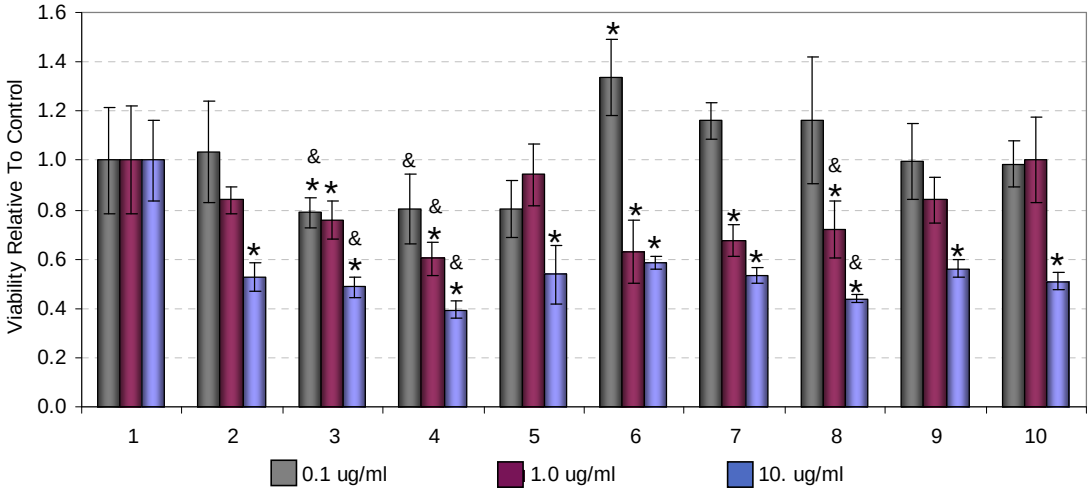

Sample No.	Description
1	Control
2	DOX - PLA-PEG-mAb106-105 NPs
3	DOX - PLA-PEG-IgG2b NPs
4	DOX - PLA-PEG NPs - No Antibody
5	Blank - PLA-PEG-mAb106-105 NPs
6	Blank - PLA-PEG-IgG2b NPs
7	Blank - PLA-PEG NPs - No Antibody
8	DOX - PLGA NPs
9	Blank - PLGA NPs
10	DOX solution

Figure 7.4 Viability Caov-3 cells after exposure to blank and doxorubicin-loaded PLA-PEG and PLGA nanoparticles with or without targeting antibodies as determined by the MTT assay. Viability presented as a fraction relative to control cells maintained in complete growth media without nanoparticles or drug. Error bars represent the standard deviation between 5 repetitions for each condition. * Significantly different from control. & Significantly different from blank nanoparticles of same polymer and antibody.

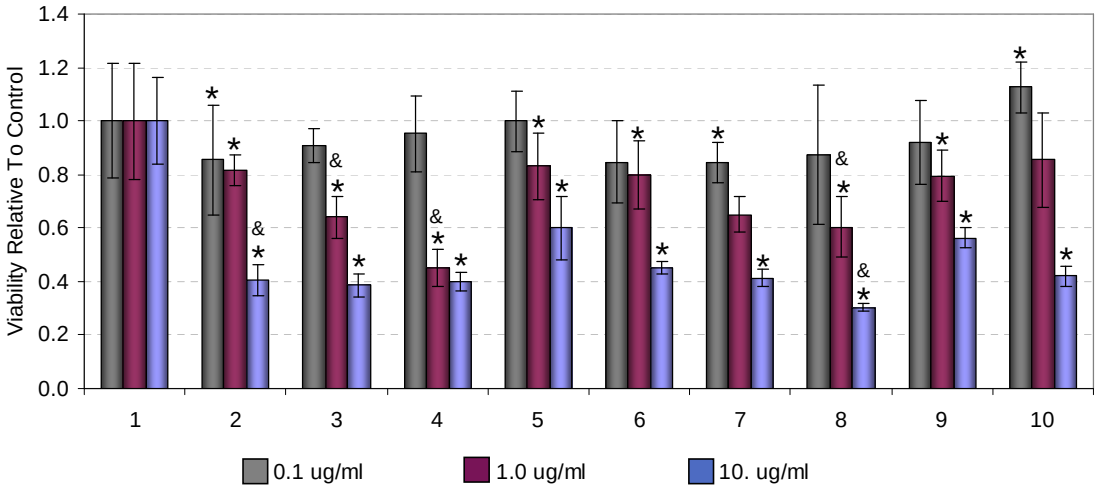

Sample No.	Description
1	Control
2	DOX - PLA-PEG-mAb106-105 NPs
3	DOX - PLA-PEG-IgG2b NPs
4	DOX - PLA-PEG NPs - No Antibody
5	Blank - PLA-PEG-mAb106-105 NPs
6	Blank - PLA-PEG-IgG2b NPs
7	Blank - PLA-PEG NPs - No Antibody
8	DOX - PLGA NPs
9	Blank - PLGA NPs
10	DOX solution

Figure 7.5 Viability MDA-MB-231 cells after exposure to blank and doxorubicin-loaded PLA-PEG and PLGA nanoparticles with or without targeting antibodies as determined by the MTT assay. Viability presented as a fraction relative to control cells maintained in complete growth media without nanoparticles or drug. Error bars represent the standard deviation between 5 repetitions for each condition. * Significantly different from control. & Significantly different from blank nanoparticles of same polymer and antibody.

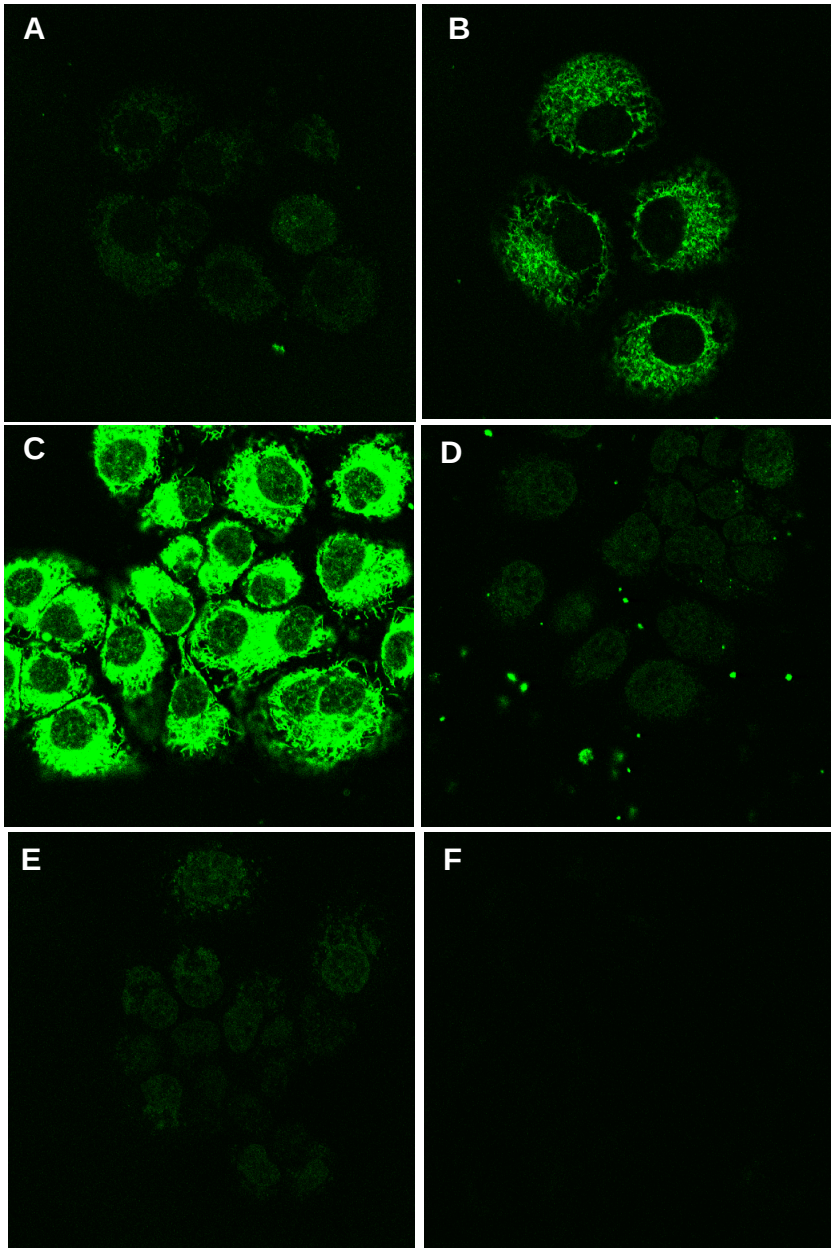

Figure 7.6 Confocal microscopy images of OVCAR-3 cells exposed to doxorubicin-loaded PLA-PEG nanoparticles with anti-FSHR mAb106-105 antibody (A), IgG2b antibody (B), or no antibody (C), DOX-loaded PLGA nanoparticles (D), free DOX (E) or cell media (F) for 3 hours.

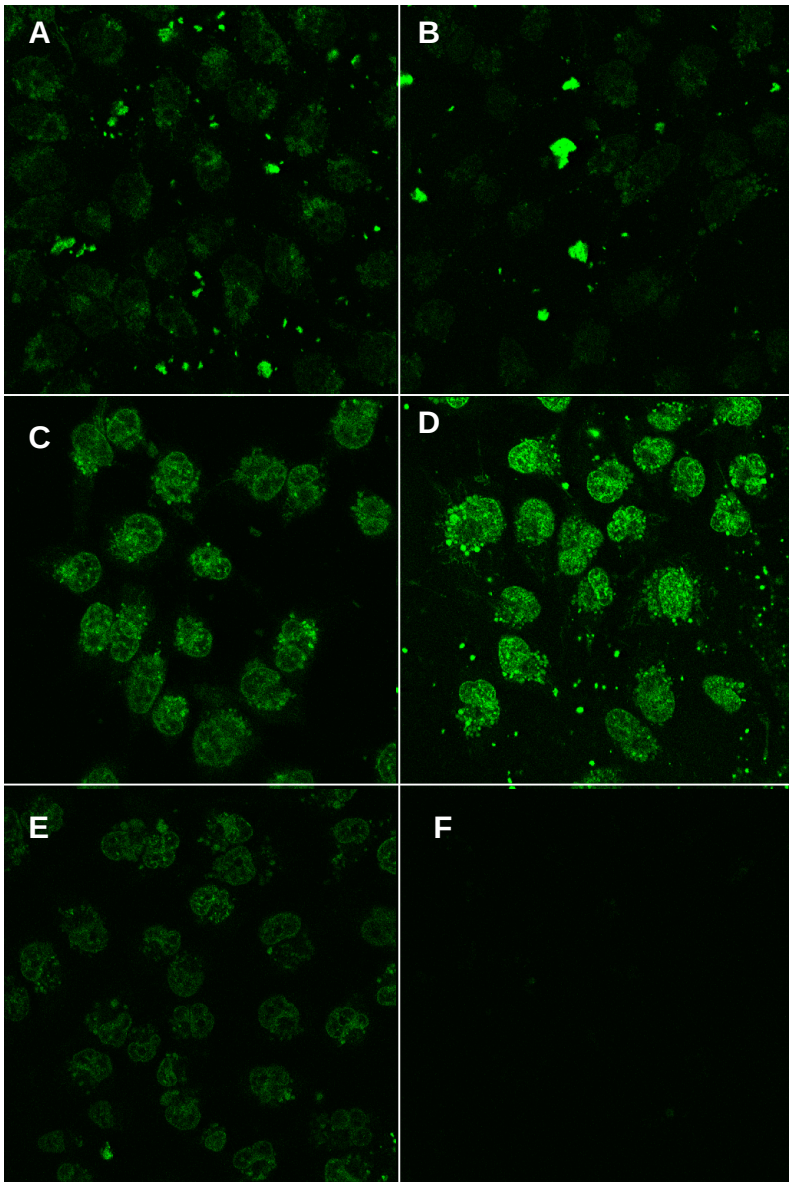

Figure 7.7 Confocal microscopy images of Caov-3 cells exposed to doxorubicin-loaded PLA-PEG nanoparticles with anti-FSHR mAb106-105 antibody (A), IgG2b antibody (B), or no antibody (C), DOX-loaded PLGA nanoparticles (D), free DOX (E) or cell media (F) for 3 hours.

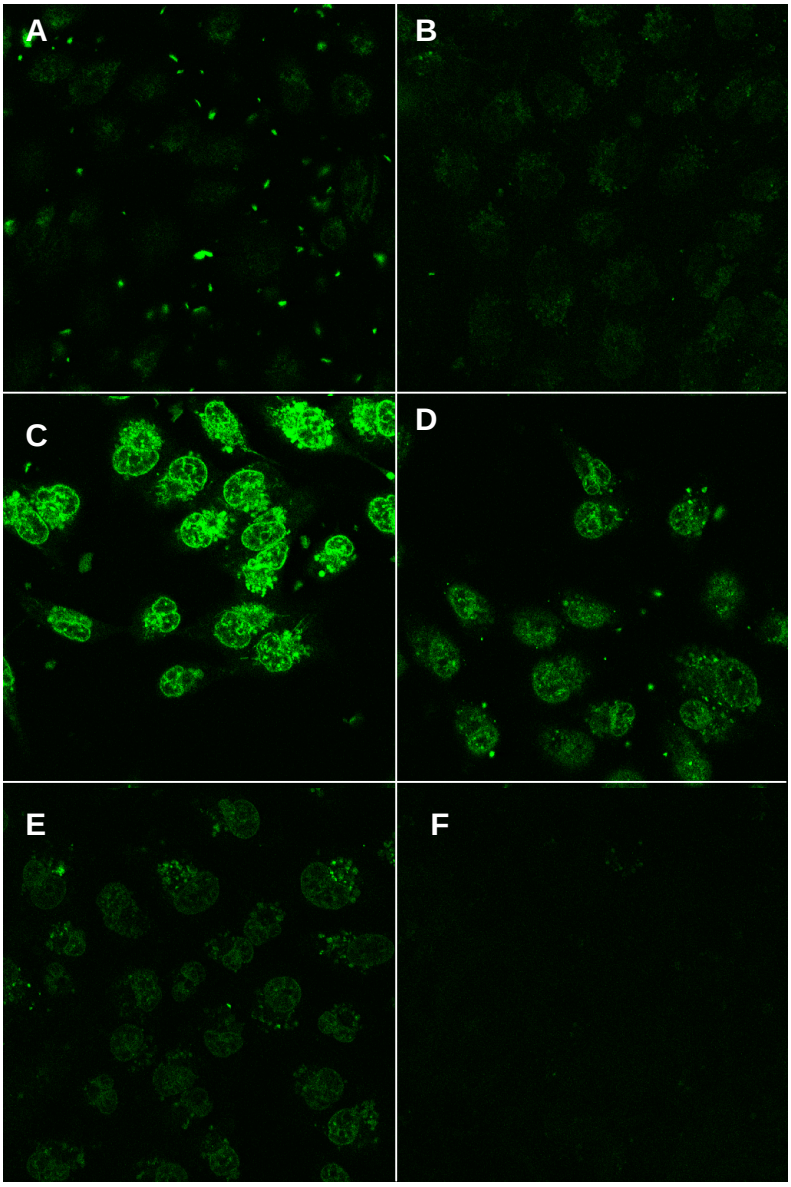

Figure 7.8 Confocal microscopy images of MDA-MB-231 cells exposed to doxorubicin-loaded PLA-PEG nanoparticles with anti-FSHR mAb106-105 antibody (A), IgG2b antibody (B), or no antibody (C), DOX-loaded PLGA nanoparticles (D), free DOX (E) or cell media (F) for 3 hours.

7.4 REFERENCES

Betancourt, T., B. Brown, et al. (2007). "Doxorubicin-loaded PLGA nanoparticles by nanoprecipitation: preparation, characterization and in vitro evaluation." Nanomedicine 2(2): 219-232.

Cailleau, R., M. Olive, et al. (1978). "Long-term human breast carcinoma cell lines of metastatic origin: preliminary characterization." In Vitro 14(11): 911-915.

Cailleau, R., R. Young, et al. (1974). "Breast tumor cell lines from pleural effusions." Journal of the National Cancer Institute 53(3): 661-674.

Chapman, A. P. (2002). "PEGylated Antibodies and Antibody Fragments for Improved Therapy: a Review." Advanced Drug Delivery Reviews 54(4): 531-545.

Choi, J.-H., K.-C. Choi, et al. (2004). "Overexpression of Follicle-Stimulating Hormone Receptor Activates Oncogenic Pathways in Preneoplastic Ovarian Surface Epithelial Cells." The Journal of Clinical Endocrinology & Metabolism 89(11): 5508-5516.

Choi, J. H., K. C. Choi, et al. (2006). "Differential regulation of two forms of gonadotropin-releasing hormone messenger ribonucleic acid by gonadotropins in human immortalized ovarian surface epithelium and ovarian cancer cells." Endocr Relat Cancer 13(2): 641-51.

Choi, K. C. (2007). T. Betancourt. Vancouver, British Columbia, Canada: Electronic mail discussion.

Fan, S., N. F. Twu, et al. (1998). "Down-regulation of BRCA1 and BRCA2 in human ovarian cancer cells exposed to adriamycin and ultraviolet radiation." Int J Cancer 77(4): 600-9.

Hamilton, T. C., R. C. Young, et al. (1983). "Characterization of a human ovarian carcinoma cell line (NIH:OVCAR-3) with androgen and estrogen receptors." Cancer Res 43(11): 5379-89.

Hermanson, G. T. (1996). Bioconjugate Techniques. San Diego, CA, Academic Press, Inc.

Kangasniemi, M., A. Kaipia, et al. (1990). "Cellular regulation of follicle-stimulating hormone (FSH) binding in rat seminiferous tubules." J Androl 11(4): 336-43.

Meduri, G., N. Charnaux, et al. (2002). "Follicle-stimulating hormone receptors in oocytes?" J Clin Endocrinol Metab 87(5): 2266-76.

Mossman, T. (1983). "Rapid colorimetric assay for cellular growth and survival: application to proliferation and cytotoxicity assays." Journal of Immunological Methods 65: 55-63.

NektarTherapeutics (2005). Nektar Advanced PEGylation - Catalog 2005-2006.

Nishizuka, S., L. Charboneau, et al. (2003). "Proteomic profiling of the NCI-60 cancer cell lines using new high-density reverse-phase lysate microarrays." Proc Natl Acad Sci U S A 100(24): 14229-34.

Pero, S. C., G. S. Shukla, et al. (2007). "Combination treatment with Grb7 peptide and Doxorubicin or Trastuzumab (Herceptin) results in cooperative cell growth inhibition in breast cancer cells." Br J Cancer 96(10): 1520-5.

Richards, J. S. and A. R. Midgley, Jr. (1976). "Protein hormone action: a key to understanding ovarian follicular and luteal cell development." Biol Reprod 14(1): 82-94.

Simoni, M., J. Gromoll, et al. (1997). "The follicle-stimulating hormone receptor: biochemistry, molecular biology, physiology, and pathophysiology." Endocr Rev 18(6): 739-73.

Smith, L., M. B. Watson, et al. (2006). "The analysis of doxorubicin resistance in human breast cancer cells using antibody microarrays." Mol Cancer Ther 5(8): 2115-20.

Sugiyama, M., A. Imai, et al. (2005). "Gonadotropin-releasing hormone retards doxorubicin-induced apoptosis and serine/threonine phosphatase inhibition in ovarian cancer cells." Oncol Rep 13(5): 813-7.

CHAPTER 8

CONCLUSIONS

The need for improved therapies for the treatment of cancer is still great despite decades of research. The development of engineered drug delivery systems is one of the strategies that are currently being investigated for improvement of patient quality of life during treatment and outcome after treatment. These systems promise to improve the pharmacological behavior of anticancer drugs *in vivo* in order to improve the therapeutic effect while minimizing dose-limiting side effects.

The systems developed in this research were designed for targeted and controlled delivery of the chemotherapeutic agent doxorubicin to ovarian tumors. Specifically, the design of this drug delivery carrier consisted of nanoparticles with a core of a biodegradable polyester of the poly(lactic-co-glycolic acid) family and surface pendant chains of functional poly(ethylene glycol) to which antibodies specific to the follicle stimulating hormone receptor were conjugated. These nanoparticles were expected to be superior to normal bolus administration of the drug because the use of nanoparticles would improve the lifetime of the drug in the circulation, increase the accumulation of the drug at the tumor site, increase the time that the tumor would be exposed to the drug, and minimize the amount of drug able to enter healthy tissue as a result of the entrapment of the drug within a macromolecular matrix. In addition, by use of targeting antibodies, these particles were designed to be able to actively recognize and bind to the diseased ovarian tissue.

In the course of the research, the first studies were focused on the encapsulation of the chemotherapeutic agent doxorubicin in the core of nanoparticles of poly(lactic-co-glycolic acid). A nanoprecipitation method was successfully employed to this end, leading to the preparation of spherical nanoparticles of size in the range of 200 nm with a relatively high content of the drug compared to that achieved in a number of previously reported formulations. The encapsulation of doxorubicin with this method proved to be reproducible and efficient, thus maximizing the use of the drug. *In vitro* studies showed that doxorubicin was released form these particles in a controlled and pH-dependent manner. Under normal physiological conditions the drug would be more protected within the core of the particles while in the more acidic tumor extracellular fluid and after endocytosis into the cells, the nanoparticles would rapidly release the drug thus allowing it to act on the cells. The pH dependency of the drug release was hypothesized to be associated with charge interactions between positively charged amine groups of doxorubicin and negatively charged terminal carboxyl groups of the polymer.

Studies of the interaction of these particles with breast cancer cells *in vitro* showed that short exposure of the cells to the particles resulted in as much therapeutic effect as the free drug at the same dose. These results were encouraging because *in vivo* the amount of drug that would reach the tumor was expected to be significantly higher for the nanoparticle-based formulation than for the drug alone. Microscopy studies with these cells also showed that the drug was taken up by the cells faster and in a greater amount when presented to them encapsulated within nanoparticles than when in solution. The same nuclear localization of the drug within the cells was observed with both formulations, thus confirming the activity of the drug even after encapsulation.

After having successfully synthesized nanoparticles loaded with a high payload of the chemotherapeutic agent doxorubicin, the focus of the research was then to prepare

nanoparticles loaded with imaging agents for *in vitro* and *in vivo* monitoring of the fate of these formulations. For this purpose, the various formulations would need to have similar physiochemical characteristics so very similar preparation methods were utilized. The imaging agents rhodamine 6G, indocyanine green and gadopentetic acid were encapsulated within poly(lactic-co-glycolic acid) nanoparticles. Rhodamine encapsulation was achieved with high efficiency. Rhodamine-loaded nanoparticles were optimal for fluorescence microscopy studies as they retained the fluorescent agent for extended periods of time so that all significant fluorescence signal detected would be associated with the particles during *in vitro* studies. Cellular studies also showed improved intake of the agent by the cells when encapsulated within nanoparticles than when in solution. Indocyanine green encapsulation was much less efficient than that of doxorubicin of rhodamine as a result of its high hydrophilicity, but the content of indocyanine green within nanoparticles was determined to be sufficient for detection of the particles in animal studies. Confirmation of the encapsulation of the paramagnetic and electron dense agent gadopentetic acid was challenging as a result of its unique properties. Studies with inductively coupled plasma mass spectroscopy and energy dispersive spectroscopy showed that incorporation of gadopentetic acid within nanoparticles was low if any at all. Although alternative nanoparticles preparation methods could have resulted in higher encapsulation efficiency indocyanine green or gadopentetic acid, the need for preparation of imaging nanoparticles that had similar properties to those of doxorubicin-loaded particles negated this option.

Having prepared particles with chemotherapeutic and imaging agents that could be used *in vitro*, the next step of the research was to modify the surface of the nanoparticles to improve their *in vivo* potential by incorporation of functional poly(ethylene glycol) (PEG). Various methods were investigated to this end, including

the use of polymer blends, the conjugation of pre-made polymers and the preparation of copolymers by polymerization of the core polyester onto pre-made heterofunctional PEG. The effectiveness of incorporation of PEG in formulations prepared with polymer blends was highly dependent on the characteristics of the polymers. Incorporation of simple functional PEG was minimal. Triblock copolymers of poly(propylene oxide) (PPO) and PEG were, on the other hand, incorporated with up to 76% efficiency as a result of the higher hydrophobicity of the central PPO domain. These two latter methods, however, could not assure permanent modification of the particle surfaces since they relied on physical association. Covalent conjugation of PEG to the terminal carboxyl groups of the biodegradable polyester in solution was effective when the reaction conditions were optimized. However, purification and recovery of the polymer proved to be challenging as a result of the amphiphilic character of the copolymers synthesized. Conjugation of PEG directly to the surface of the nanoparticles using the exposed carboxyl groups of the core polyester was significantly less efficient, possibly as a result of inaccessibility of these groups because of adsorbed surfactant. The most reproducible and efficient method of preparation was the ring-opening polymerization of the polyester onto pre-made heterofunctional PEG. These copolymers were synthesized reproducibly and in high yields. Also, by varying the reagent amounts, the composition and molecular weight of the copolymers was adjusted.

The encapsulation of the previously-discussed chemotherapeutic and imaging agents in nanoparticles prepared with the copolymers was then assessed. In addition, targeting antibodies were conjugated to the terminal carboxyl groups of PEG on the surface of these nanoparticles. All formulations were significantly different than those solely prepared with poly(lactic-co-glycolic acid). The encapsulation efficiency of doxorubicin and rhodamine decreased, possibly as a result of significant decrease in the

size of the nanoparticles and translocation of the negative charge of the polymer terminal groups from the core of the particles to the terminal end of the PEG chains on the surface of the particles. However, the release of doxorubicin from the modified formulation was better controlled. Rhodamine, on the other hand, was found to escape more easily from the nanoparticles prepared with the copolymers. Encapsulation of indocyanine green in nanoparticles made with the copolymer was increased, possibly as a result of the higher hydrophilicity of the particles as a result of the presence of poly(ethylene glycol). Conjugation of targeting or control antibodies to the surface of the nanoparticles was successfully confirmed by an Elisa-like assay.

The interaction of targeted nanoparticles with or without the drug was evaluated in the ovarian cancer cell lines OVCAR-3 and Caov-3, in addition to the MDA-MB-231 breast cancer cells used for evaluation of the unmodified doxorubicin and rhodamine nanoparticles. These studies showed that the nanoparticles containing the targeting antibodies did not result in improved interactions or therapeutic effect than nanoparticles without these antibodies, possibly because the small number of antibodies conjugated per nanoparticle were not sufficient to mediate active recognition and binding to the target receptor. In addition, these studies suggested that the nanoparticle formulations caused reduction of cell viability in the absence of the chemotherapeutic drug, possibly because of negative mechanical or chemical interaction of the nanoparticles with the cells.

Future improvements in the development of this targeted drug delivery system for ovarian cancer should address the physiochemical characteristics of the nanoparticle formulation that could be interfering with cell viability. In addition, to achieve the targeting potential of the nanoparticles, further studies will need to investigate the effect of increased targeting agent presentation on their interactions with target cells. Also, the effect of the choice of targeting agent between antibodies, antibody fragments, targeting

peptides and aptamers on the interaction of the nanoparticles with the *in vitro* models of tumors should be studied.

The present research contributed to the understanding of key parameters in the preparation of polymeric nanoparticles for therapeutic and imaging purposes in biological systems. In addition, it demonstrated the significant differences in the interaction of chemotherapeutic drugs with cancer cells that can be mediated by the use of nanomeric drug delivery systems.

Bibliography

Abdelwahed, W., G. Degobert, et al. (2006). "Freeze-drying of nanoparticles: Formulation, process and storage considerations." Advanced Drug Delivery Reviews 58(15): 1688-1713.

Akiyoshi, K., I. Taniguchi, et al. (1996). "Hydrogel nanoparticle formed by self-assembly of hydrophobized polysaccharide. Stabilization of Adriamycin by complexation." European Journal of Pharmaceutics and Biopharmaceutics 42(4): 286-290.

American Cancer Society (2005). Cancer Facts & Figures 2005. Atlanta, GA, American Cancer Society.

Arencibia, J. M., A. V. Schally, et al. (2001). "In vitro targeting of a cytotoxic analog of luteinizing hormone-releasing hormone AN-207 to ES-2 human ovarian cancer cells as demonstrated by microsatellite analyses." Anticancer Drugs 12(1): 71-8.

Arica, B. and A. Lamprecht (2005). "In Vitro Evaluation of Betamethasone-Loaded Nanoparticles." Drug Development and Industrial Pharmacy 31(1): 19-24.

Astete, C. E. and C. M. Sabliov (2006). "Synthesis and characterization of PLGA nanoparticles." Journal of Biomaterials Science Polymer Edition 17(3): 247-289.

Avgoustakis, K. (2004). "Pegylated poly(lactide) and poly(lactide-co-glycolide) nanoparticles: preparation, properties and possible applications in drug delivery." Current Drug Delivery 1: 321-333.

Avgoustakis, K., A. Beletsi, et al. (2003). "Effect of copolymer composition on the physicochemical characteristics, in vitro stability, and biodistribution of PLGA-mPEG nanoparticles." Int J Pharm 259(1-2): 115-27.

Barichello, J. M., M. Morishita, et al. (1999). "Encapsulation of Hydrophilic and Lipophilic Drugs in PLGA Nanoparticles by the Nanoprecipitation Method." Drug Development and Industrial Pharmacy 25(4): 471-476.

Barratt, G. (2003). "Colloidal drug carriers: achievements and perspectives." Cell Mol Life Sci 60(1): 21-37.

Barraud, L., P. Merle, et al. (2005). "Increase of doxorubicin sensitivity by doxorubicin-loading into nanoparticles for hepatocellular carcinoma cells in vitro and in vivo." Journal of Hepatology 42: 736-343.

Bazile, D. V., C. Ropert, et al. (1992). "Body distribution of fully biodegradable [14C]-poly(lactic acid) nanoparticles coated with albumin after parenteral administration to rats." Biomaterials 13(15): 1093-1102.

Bazile, D., C. Prud'Homme, et al. (1995). "Stealth Me.PEG-PLA Nanoparticles Avoid Uptake by the Mononuclear Phagocytes System." Journal of Pharmaceutical Sciences 84(4): 493-498.

Bejiani, R. A., D. BenEzra, et al. (2005). "Nanoparticles for gene delivery to retinal pigment epithelial cells." Molecular Vision 11: 124-132.

Beletsi, A., L. Leontiadis, et al. (1999). "Effect of preparative variables on the properties of poly(dl-lactide-co-glycolide)-methoxypoly(ethyleneglycol) copolymers related to their application in controlled drug delivery." International Journal of Pharmaceutics 182(2): 187-197.

Betancourt, T. and L. Brannon-Peppas (2006). "Micro- and nanofabrication methods in nanotechnological medical and pharmaceutical devices." International Journal of Nanomedicine 1(4): 483-495.

Betancourt, T., B. Brown, et al. (2007). "Doxorubicin-loaded PLGA nanoparticles by nanoprecipitation: preparation, characterization and in vitro evaluation." Nanomedicine 2(2): 219-232.

Birnbaum, D. T. and L. Brannon-Peppas (2003). "Molecular weight distribution changes during degradation and release of PLGA nanoparticles containing epirubicin HCl." Journal of Biomaterials Science Polymer Edition 14(1): 87-102.

Birnbaum, D. T., J. D. Kosmala, et al. (2000). "Optimization of preparation techniques for poly(lactic acid-co-glycolic acid) nanoparticles." Journal of Nanoparticle Research 2(2): 173-181.

Blanchette, J. and N. A. Peppas (2005). "Oral chemotherapeutic delivery: design and cellular response." Ann Biomed Eng 33(2): 142-9.

Blanco, D. and M. J. Alonso (1998). "Protein encapsulation and release from poly(lactide-co-glycolide) microspheres: effect of the protein and polymer properties and of the co-encapsulation of surfactants." Eur J Pharm Biopharm 45(3): 285-294.

Blasiak, J., E. Gloc, et al. (2002). "A comparison of the in vitro genotoxicity of anticancer drugs idarubicin and mitoxantrone." Acta Biochimica Polonica 49(1): 145-155.

Bradford, M. M. (1976). "A rapid and sensitive method for the quantitation of microgram quantities of protein utilizing the principle of protein-dye binding." Anal Biochem 72: 248-54.

Brannon-Peppas, L. (1995). "Recent advances on the use of biodegradable microparticles and nanoparticles in controlled drug delivery." Int J Pharm. 116(1): 1-9.

Brannon-Peppas, L. (1997). "Polymers in Controlled Drug Delivery." Medical Plastics and Biomaterials Magazine 4: 34-44.

Brannon-Peppas, L. and D. T. Birnbaum (2000). Process to Scale-Up the Production of Biodegradable Nanoparticles. American Institute of Chemical Engineers Annual Meeting, Los Angeles, CA.

Brannon-Peppas, L. and J. O. Blanchette (2004). "Nanoparticle and targeted systems for cancer therapy." Advanced Drug Delivery Reviews 56(11): 1649-1659.

Cailleau, R., M. Olive, et al. (1978). "Long-term human breast carcinoma cell lines of metastatic origin: preliminary characterization." In Vitro 14(11): 911-915.

Cailleau, R., R. Young, et al. (1974). "Breast tumor cell lines from pleural effusions." Journal of the National Cancer Institute 53(3): 661-674.

Cannizzaro, S. M., R. F. Padera, et al. (1998). "A novel biotinylated degradable polymer for cell-interactive applications." Biotechnol Bioeng 58(5): 529-35.

Chapman, A. P. (2002). "PEGylated Antibodies and Antibody Fragments for Improved Therapy: a Review." Advanced Drug Delivery Reviews 54(4): 531-545.

Cheng, J., B. A. Teply, et al. (2007). "Formulation of functionalized PLGA-PEG nanoparticles for in vivo targeted drug delivery." Biomaterials 28(5): 869-76.

Chertok, B., B. A. Moffat, et al. (2007). "Iron oxide nanoparticles as a drug delivery vehicle for MRI monitored magnetic targeting of brain tumors." Biomaterials.

Choi, J. H., K. C. Choi, et al. (2006). "Differential regulation of two forms of gonadotropin-releasing hormone messenger ribonucleic acid by gonadotropins in human immortalized ovarian surface epithelium and ovarian cancer cells." Endocr Relat Cancer 13(2): 641-51.

Choi, J.-H., K.-C. Choi, et al. (2004). "Overexpression of Follicle-Stimulating Hormone Receptor Activates Oncogenic Pathways in Preneoplastic Ovarian Surface Epithelial Cells." The Journal of Clinical Endocrinology & Metabolism 89(11): 5508-5516.

Choi, K. C. (2007). T. Betancourt. Vancouver, British Columbia, Canada: Electronic mail discussion.

Conner, S. D. and S. L. Schmid (2003). "Regulated portals of entry into the cell." Nature 422(6927): 37-44.

Couvreur, P., C. Dubernet, et al. (1995). "Controlled Drug Delivery with Nanoparticles: Current Possibilities and Future Trends." European Journal of Pharmaceutics and Biopharmaceutics 41(1): 2-13.

Csaba, N., A. Sanchez, et al. (2006). "PLGA:poloxamer and PLGA:poloxamine blend nanostructures as carriers for nasal gene delivery." J Control Release 113(2): 164-72.

Csaba, N., L. Gonzalez, et al. (2004). "Design and characterisation of new nanoparticulate polymer blends for drug delivery." J Biomater Sci Polym Ed 15(9): 1137-51.

Csaba, N., P. Caamano, et al. (2005). "PLGA:Poloxamer and PLGA:Poloxamine Blend Nanoparticles: New Carriers for Gene Delivery." Biomacromolecules 6: 271-278.

Darby, R. (1996). Chemical Engineering Fluid Mechanics. New York, NY, Marcel Dekker, Inc.

D'Arceuil, H. E., A. J. de Crespigny, et al. (2004). "An MRA study of vascular stenosis in a pig model using CH3-DTPA-Gd (NMS60) and Gd-DTPA." Magn Reson Imaging 22(9): 1243-8.

de Jaeghere, F., E. Allemann, et al. (1999). "Formulation and lyoprotection of poly(lactic-acid-co-ethylene oxide) nanoparticles: influence of physical stability and in vitro cell uptake." Pharmaceutical Research 16(6): 859-866.

de Jaeghere, F., E. Allemann, et al. (2000). "Freeze-Drying and Lyopreservation of Diblock and Triblock Poly(Lactic Acid)-Poly(Ethylene Oxide) (PLA-PEO) Copolymer Nanoparticles." Pharmaceutical Development and Technology 5(4): 473-483.

de la Torre, M., X. Y. Hao, et al. (1993). "Characterization of four doxorubicin adapted human breast cancer cell lines with respect to chemotherapeutic drug sensitivity, drug resistance associated membrane proteins and glutathione transferases." Anticancer Research 13(5A): 1425-1430.

Dechy-Cabaret, O., B. Martin-Vaca, et al. (2004). "Controlled Ring-Opening Polymerization of Lactide and Glycolide." Chemical Reviews 104(12): 6147-6176.

Desai, K. G., S. R. Mallery, et al. (2007). "Formulation and Characterization of Injectable Poly(DL: -lactide-co-glycolide) Implants Loaded with N-Acetylcysteine, a MMP Inhibitor." Pharm Res.

Desmettre, T., J. M. Devoisselle, et al. (2000). "Fluorescence properties and metabolic features of indocyanine green (ICG) as related to angiography." Survey of Ophthalmology 45(1): 15-27.

Dharap, S. S., B. Qiu, et al. (2003). "Molecular targeting of drug delivery systems to ovarian cancer by BH3 and LHRH peptides." Journal of Controlled Release 91(1-2): 61-73.

Dharap, S. S., Y. Wang, et al. (2005). "Tumor-specific targeting of an anticancer drug delivery system by LHRH peptide." Proc Natl Acad Sci U S A 102(36): 12962-7.

Dias, J. A., B. Lindau-Shepard, et al. (1998). "Human Follicle-Stimulating Hormone Structure-Activity Relationships." Biology of Reproduction 58: 1331-1336.

Dittrich, V. W. and R. C. Schulz (1971). "Kinetic und mechanismus der ringöffnenden polymerisation von L(-)-lactid." Angewandte Makromolekulare Chemie 15(1): 109-126.

Du, Y. J., P. J. Lemstra, et al. (1995). "ABA Type Copolymers of Lactide with Poly(ethylene glycol). Kinetic, Mechanistic, and Model Studies." Macromolecules 28: 2124-2132.

Duda, A. and S. Penczek (1990). "Thermodynamics of L-lactide polymerization. Equilibrium Monomer Concentration." Macromolecules 23(66): 1636-1639.

Fahmy, T. M., R. M. Samstein, et al. (2005). "Surface modification of biodegradable polyesters with fatty acid conjugates for improved drug targeting." Biomaterials 26.

Fan, S., N. F. Twu, et al. (1998). "Down-regulation of BRCA1 and BRCA2 in human ovarian cancer cells exposed to adriamycin and ultraviolet radiation." Int J Cancer 77(4): 600-9.

Faranesh, A. Z., M. T. Nastley, et al. (2004). "In vitro release of vascular endothelial growth factor from gadolinium-doped biodegradable microspheres." Magnetic Resonance in Medicine 51(6): 1265-1271.

Farokhzad, O. C., J. Cheng, et al. (2006). "Targeted nanoparticle-aptamer bioconjugates for cancer chemotherapy in vivo." Proc Natl Acad Sci U S A 103(16): 6315-20.

Farokhzad, O. C., J. M. Karp, et al. (2006). "Nanoparticle-aptamer bioconjugates for cancer targeting." Expert Opin Drug Deliv 3(3): 311-24.

Farokhzad, O. C., S. Jon, et al. (2004). "Nanoparticle-aptamer bioconjugates: a new approach for targeting prostate cancer cells." Cancer Res 64(21): 7668-72.

Fattal, E., S. Pecquet, et al. (2002). "Biodegradable microparticles for the mucosal delivery of antibacterial and dietary antigens." Int J Pharm. 242(1-2): 15-24.

Fawaz, F., F. Bonini, et al. (1993). "Influence of poly(DL-lactide) on the biliary clearance and enterohepatic circulation of indomethacin in the rabbit." Pharmaceutical Research 10(5): 750-756.

Feng, S. S., L. Mu, et al. (2004). "Nanoparticles of biodegradable polymer for clinical administration of paclitaxel." Current Medicinal Chemistry 11(4): 413-424.

Ferlay, J., F. Bray, et al. (2004). GLOBOCAN 2002: Cancer Incidence, Mortality and Prevalence Worldwide. IARC CancerBase No. 5. Lyon, IARC Press.

Fessi, H., F. Puisieux, et al. (1989). "Nanocapsule formation by interfacial deposition following solvent displacement." International Journal of Pharmaceutics 55: R1-R4.

Fessi, H., J. P. Devissaguet, et al. (1986). Procédé de préparation des systèmes colloïdaux dispersibles dune substance sous forme de nanoparticules. F. P. Application. French.

Folkman, J. (2003). "Fundamental Concepts of the Angiogenic Process." Current Molecular Medicine 3(7): 6423-651.

Folkman, J., E. Merler, et al. (1971). "Isolation of a Tumor Factor Responsible for Angiogenesis." The Journal of Experimental Medicine 133(2): 275-288.

Freitas, S., H. P. Merkle, et al. (2005). "Microencapsulation by solvent extraction/evaporation: reviewing the state of art of microsphere preparation process technology." Journal of Controlled Release 102(2): 313-332.

Friess, W. (2004). Biopolymers for Parenteral Drug Delivery in Cancer Therapy. Drug Delivery Systems in Cancer Therapy. D. M. Brown. Totowa, New Jersey, Humana Press: 62-95.

Furtado Mosquera, V. C., P. Legrand, et al. (2000). "Poly(D,L-Lactide) Nanocapsules Prepared by a Solvent Displacement Process: Influence of the Composition on Physiochemical and Structural Properties." Journal of Pharmaceutical Sciences 89(5): 614-626.

Gabizon, A. A. (2001). "Pegylated Liposomal Doxorubicin: Metamorphosis of an Old Drug into a New Form of Chemotherapy." Cancer Investigation 19(4): 424-436.

Gao, X., W. Tao, et al. (2006). "Lectin-conjugated PEG-PLA nanoparticles: preparation and brain delivery after intranasal administration." Biomaterials 27(18): 3482-90.

Gao, X., Y. Cui, et al. (2004). "In vivo cancer targeting and imaging with semiconductor quantum dots." Nature Biotechnology 22(8): 969-971.

Garcia-Fuentes, M., D. Torres, et al. (2004). "Application of NMR spectroscopy to the characterization of PEG-stabilized lipid nanoparticles." Langmuir 20(20): 8839-45.

Gathje, J., R. R. Steuer, et al. (1970). "Stability studies on indocyanine green dye." J Appl Physiol 29(2): 181-5.

Gear, A. R. (1974). "Rhodamine 6G. A potent inhibitor of mitochondrial oxidative phosphorilation." Journal of Biological Chemistry 249(11): 3628-3637.

Gilding, D. K. and A. M. Reed (1979). "Biodegradable polymers for use in surgery-polyglycolic/poly(lactic acid) homo- and copolymers: 1." Polymer 20(12): 1459-1464.

Graham, N. B. (1987). Poly(ethylene oxide) and related hydrogels. Hydrogels in Medicine and Pharmacy; Volume II Polymers. N. A. Peppas. Boca Raton, FL, CRC Press: 95-114.

Green, M. R., G. M. Manikhas, et al. (2006). "Abraxane, a novel cremophor-free, albumin-bound particle form of paclitaxel for the treatment of advanced non-small-cell lung cancer." Annals of Oncology 17(8): 1263-1268.

Greener, M. (2005). "MAbs Turn 30." The Scientist: 14-16.

Gref, R., A. Domb, et al. (1995). "The controlled intravenous delivery of drugs using PEG-coated sterically stabilized nanospheres." Advanced Drug Delivery Reviews 16(2): 215-233.

Gref, R., M. Luck, et al. (2000). "'Stealth' corona-core nanoparticles surface modified by polyethylene glycol (PEG): influences of the corona (PEG chain length and surface density) and of the core composition on phagocytic uptake and plasma protein adsorption." Colloids Surf B Biointerfaces 18(3-4): 301-313.

Gref, R., P. Couvreur, et al. (2003). "Surface-engineered nanoparticles for multiple ligand coupling." Biomaterials 24(24): 4529-37.

Gref, R., Y. Minamitake, et al. (1994). "Biodegradable Long-Circulating Polymeric Nanospheres." Science 263(5153): 1600-1603.

Hamilton, T. C., R. C. Young, et al. (1983). "Characterization of a human ovarian carcinoma cell line (NIH:OVCAR-3) with androgen and estrogen receptors." Cancer Res 43(11): 5379-89.

Heald, C. R., S. Stolnik, et al. (2002). "Poly(lactic acid)-poly(ethylene oxide) (PLA-PEG) nanoparticles: NMR studies of the central solid like PLA core and the liquid PEG corona." Langmuir 18: 3669-3675.

Hermanson, G. T. (1996). Bioconjugate Techniques. San Diego, CA, Academic Press, Inc.

Heurtault, B., P. Saulnier, et al. (2003). "Physico-chemical stability of colloidal lipid particles." Biomaterials 24: 4283-4300.

Holzer, W., M. Mauerer, et al. (1998). "Photostability and thermal stability of indocyanine green." J Photochem Photobiol B 47(2-3): 155-64.

Hrkach, J. S., M. T. Peracchia, et al. (1997). "Nanotechnology for biomaterials engineering: structural characterization of amphiphilic polymeric nanoparticles by 1H NMR spectroscopy." Biomaterials 18: 27-30.

Hu, R. G., Q. W. zhai, et al. (2002). "Bioactivities of ricin retained and its immunoreactivity to anti-ricin polyclonal antibodies alleviated through pegylation." International Journal of Biochemistry and Cell Biology 34(4): 396-402.

Hu, S., H. Zhao, et al. (2007). "Role of mitochondria in silica-induced apoptosis of alveolar macrophages: inhibition of apoptosis by rhodamine 6G and N-acetyl-L-cysteine." Journal of Toxicology and Environmental Health. Part A. 70(17): 1403-1415.

Huh, K. M., Y. W. Cho, et al. (2003). "PLGA-PEG Copolymers." Drug Delivery Technology 3(5).

Huolman, R. and N. Ashammakhi (2007). "New multifunctional anti-osteolytic releasing bioabsorbable implant." J Craniofac Surg 18(2): 295-301.

IARC (1976). IARC Monographs on the Evaluation of the Carcinogenic Risk of Chemicals to Man. Some Naturally Occurring Substances. I. A. f. R. o. Cancer. Lyon, France, IARC. 10: 353 pp.

Ike, O., Y. Shimizu, et al. (1991). "Biodegradation and antitumor effect of adriamycin-containing poly(L-lactid acid) microspheres." Biomaterials 12(8): 757-762.

Izutsu, K., S. Yoshioka, et al. (1996). "Effects of sugars and polymers on crystallization of poly(ethylene glycol) in frozen solutions: phase separation between incompatible polymers." Pharmaceutical Research 13(9): 1393-1400.

Jacobs, I. and R. C. Bast (1989). "The CA 125 tumor-associated antigen: a review of the literature." Human Reproduction 4(1): 1-12.

Jain, R. A. (2000). "The manufacturing techniques of various drug loaded biodegradable poly(lactide-co-glycolide) (PLGA) devices." Biomaterials 21(23): 2475-2490.

Janes, K. A., M. P. Fresneau, et al. (2001). "Chitosan nanoparticles as delivery systems for doxorubicin." Journal of Controlled Release 73(2-3): 255-267.

Janes, K. A., P. Calvo, et al. (2001). "Polysaccharide colloidal particles as delivery systems for macromolecules." Adv Drug Deliv Rev 47(1): 83-97.

Jeong, J. H., D. W. Lim, et al. (2000). "Synthesis, characterization and protein adsorption behaviors of PLGA/PEG di-block co-polymer blend films." Colloids Surf B Biointerfaces 18(3-4): 371-379.

Jeong, Y.-I., H.-S. Na, et al. (2006). "Adriamycin release from self-assembling nanospheres of poly(D,L-lactide-co-glycolide)-grafted pullulan." International Journal of Pharmaceutics 322(1-2): 154-160.

Jiang, X., M. Dreano, et al. (1995). "Structural predictions for the ligand-binding region of glycoprotein hormone receptors and the nature of hormone-receptor interactions." Structure 3(12): 1341-53.

Josephy, P. D., e. Thomas, et al. (1982). "The horseradish peroxidase-catalyzed oxidation of 3,5,3',5'-tetramethylbenzidine." The Journal of Biological Chemistry 257(7): 3669-3675.

Kalliokoski, K. K., C. Scheede-Bergdahl, et al. (2006). "Muscle perfusion and metabolic heterogeneity: insights from noninvasive imaging techniques." Exerc Sport Sci Rev 34(4): 164-70.

Kangasniemi, M., A. Kaipia, et al. (1990). "Cellular regulation of follicle-stimulating hormone (FSH) binding in rat seminiferous tubules." J Androl 11(4): 336-43.

Kasturi, S. P., K. Sachaphibulkij, et al. (2005). "Covalent conjugation of polyethyleneimine on biodegradable microparticles for delivery of plasmid DNA vaccines." Biomaterials 26(32): 6375-6385.

Kim, G. J. and S. Nie (2005). "Targeted cancer nanotherapy." Nanotoday 8(8, Supplement 1): 28-33.

Kiremitci-Gumusderelioglu, M. and G. Deniz (1999). "Synthesis, characterization and in vitro degradation of poly(DL-lactide)/poly(dl-lactide-co-glycolide) films." Turkish Journal of Chemistry 23: 153-161.

Kontakis, G. M., J. E. Pagkalos, et al. (2007). "Bioabsorbable materials in orthopaedics." Acta Orthop Belg 73(2): 159-69.

Kou G, G. J., Wang H, Chen H, Li B, Zhang D, Wang S, Hou S, Qian W, Dai J, Zhong Y, Guo Y (2007). "Preparation and Characterization of Paclitaxel-loaded PLGA nanoparticles coated with cationic SM5-1 single-chain antibody." Journal of Biochemistry and Molecular Biology 40(5): 731-739.

Kricheldrof, H. R. and J. Meier-Haack (1993). "Polylactones. XXII: ABA triblock copolymers of L-lactide and poly(ethylene glycol)." J. Makromol. Chem. 194(2): 715-725.

Kukowska-Latallo, J. F., K. A. Candido, et al. (2005). "Nanoparticle Targeting of Anticancer Drug Improves Therapeutic Response in Animal Model of Human Epithelial Cancer." Cancer Research 65(12): 5317-5324.

Kumar, C. S., C. Leuschner, et al. (2007). "Glutaric acid as a spacer facilitates improved intracellular uptake of LHRH-SPION into human breast cancer cells." Int J Nanomedicine 2(2): 175-9.

Lamprecht, A., N. Ubrich, et al. (2001). "Design of rolipram-loaded nanoparticles: comparison of two preparation methods." Journal of Controlled Release 71(3): 297-306.

Lanza, G. M., P. Winter, et al. (2004). "Novel paramagnetic contrast agents for molecular imaging and targeted drug delivery." Curr Pharm Biotechnol 5(6): 495-507.

Lee, E. S., K. Na, et al. (2005). "Doxorubicin loaded pH-sensitive polymeric micelles for reversal of resistant MCF-7 tumpr." Journal of Controlled Release 103: 405-418.

Lee, E. S., K. Na, et al. (2005). "Doxorubicin loaded pH-sensitive polymeric micelles for reversal of resistant MCF-7 tumor." Journal of Controlled Release 103(2): 405-418.

Lee, H. S., M. Hu, et al. (2007). "Apoptotic epidermal growth factor (EGF)-conjugated block copolymer micelles as a nanotechnology platform for targeted combination therapy." Molecular Pharmaceutics 4(5): 769-781.

Lee, J. H. and A. P. Koretsky (2004). "Manganese enhanced magnetic resonance imaging." Curr Pharm Biotechnol 5(6): 529-37.

Lee, J. H., A. C. Silva, et al. (2005). "Manganese-enhanced magnetic resonance imaging of mouse brain after systemic administration of MnCl2: dose-dependent and temporal evolution of T1 contrast." Magn Reson Med 53(3): 640-8.

Lee, J. W., J. Y. Lu, et al. (2002). "Synthesis and evaluation of taxol-folic acid conjugates as targeted antineoplastics." Bioorg Med Chem 10(7): 2397-414.

Legrand, P., G. Barratt, et al. (1999). "Polymeric Nanocapsules as Drug Delivery Systems." S.T.P. Pharma Sciences 9(5): 411-418.

Leland, W. T. (1950). "The Isotopic Composition of Scandium, Gadolinium, and Dysprosium." Physical Reviews 77(5): 634-640.

Leo, E., C. Contado, et al. (2006). "Nanoparticle formulation may affect the stabilization of an antiischemic prodrug." International Journal of Pharmaceutics 307(1): 103-113.

Lewis, D. H. (1990). Controlled Release of Bioactive Agents from Lactide/Glycolide Polymers. Biodegradable Polymers as Drug Delivery Systems. M. Chasin and R. Langer. New York, Marcerl Dekker: 1-41.

Li, J.-T., K. D. Caldwell, et al. (1994). "Surface Properties of Pluronic-Coated Polymeric Colloids." Langmuir 10: 4475-4482.

Li, R. H. (1998). "Materials for Immunoisolated Cell Transplantation." Advanced Drug Delivery Reviews 33: 87-109.

Li, Y., Y. Pei, et al. (2001). "PEGylated PLGA nanoparticles as protein carriers: synthesis, preparation and biodistribution in rats." J Control Release 71(2): 203-11.

Liang, H.-F., C.-T. Chen, et al. (2006). "Paclitaxel-loaded poly(γ-glutamic acid)-poly(lactide) nanoparticles as a targeted drug delivery system for the treatment of liver cancer." Biomaterials 27(9): 2051-2059.

Lin, R., L. S. Ng, et al. (2005). "In vitro study of anticancer drug doxorubicin in PLGA-based microparticles." Biomaterials 26: 4476-4485.

Lindau-Shepard, B., H. A. Brumberg, et al. (2001). "Reversible immunoneutralization of human follitropin receptor." Journal of Reproductive Immunology 49: 1-19.

Liu S.Q., W. N., Gao SJ, Tong Y. W., Yang Y. Y. (2007). "Bio-functional micelles self-assembled from a folate-conjugated block copolymer for targeted intracellular delivery of anticancer drugs." Biomaterials 28(7): 1423-1433.

Liu, S. Q., Y. W. Tong, et al. (2005). "Incorporation and in vitro release of doxorubicin in thermally sensitive micelles made from poly(N-isopropylacrylamine-co-N,N-dimethylacrylamide)-b-poly(D,L-lactide-co-glycolide) with varying compositions." Biomaterials 26: 5064-5074.

Liu, W., H. Dahnke, et al. (2007). "In vivo MRI using positive-contrast techniques in detection of cells labeled with superparamagnetic iron oxide nanoparticles." NMR Biomed.

Lowery, A. R., A. M. Gobin, et al. (2006). "Immunonanoshells for targeted photothermal ablation of tumor cells." Int J Nanomedicine 1(2): 149-54.

Lu, J. J., Y. Zheng, et al. (2000). "Decreased Luteinizing Hormone Receptor mRNA Expression in Human Ovarian Epithelial Cancer." Gynecologic Oncology 79: 158-168.

Lum, B. L., J. M. Svec, et al. (1985). "Doxorubicin: alteration of dose scheduling as a means of reducing cardiotoxicity." Drug Intelligence & Clinical Pharmacy 19(4): 259-264.

Luo Y, B. N., Lu ZR, Kopecek J, Prestwich GD (2002). "Targeted delivery of doxorubicin by HPMA copolymer-hyaluronan bioconjugates." Pharmaceutical Research 19(4): 396-402.

Lutsenko SV, F. N., Severin SE (2002). "Cytotoxic and antitumor activities of doxorubicin conjugates with the epidermal growth factor and its receptor-binding fragment." Journal of Drug Targeting 10(7): 567-571.

Majoros, I. J., A. Myc, et al. (2006). "PANAM dendrimer-based multifunctional conjugate for cancer therapy: synthesis, characterization, and functionality." Biomacromolecules 7(2): 572-579.

Mamot, C., R. Ritschard, et al. (2006). "EGFR-targeted immunoliposomes derived from the monoclonal antibody EMD72000 mediate specific and efficient drug delivery to a variety of colorectal cancer cells." Journal of Drug Targeting 14(4): 215-223.

McDonald, D. M. and P. Baluk (2002). "Significance of Blood Vessel Leakiness in Cancer." Cancer Research 62(18): 5381-5385.

Meduri, G., N. Charnaux, et al. (2002). "Follicle-stimulating hormone receptors in oocytes?" J Clin Endocrinol Metab 87(5): 2266-76.

Mehvar, R. (2000). "Modulation of the pharmacokinetics and pharmacodynamics of proteins by polyethylene glycol conjugation." Journal of Pharmacy and Pharmacetuical Sciences 3(1): 125-136.

Menegazzi, R., G. Zabucchi, et al. (1992). "A new, one-step assay on whole cell suspensions for peroxidase secretion by human neutrophils and eosinophils." Journal of Leukocyte Biology 52: 619-624.

Mhaka, A., S. R. Denmeade, et al. (2002). "A 5-fluorodeoxyuridine prodrug as targeted therapy for prostate cancer." Bioorganic & Medicinal Chemistry Letters 12(17): 2459-2461.

Middleton, J. C. and A. J. Tipton (2000). "Synthetic biodegradable polymers as orthopedic devices." Biomaterials 21(23): 2335-2346.

Moghimi, S. M. and A. C. Hunter (2000). "Poloxamers and poloxamines in nanoparticle engineering and experimental medicine." Trends Biotechnol 18(10): 412-20.

Moghimi, S. M., C. J. Porter, et al. (1991). "Non-phagocytic uptake of intravenously injected microspheres in rat spleen: influence of particle size and hydrophilic coating." Biochem Biophys Res Commun 177(2): 861-6.

Moghimi, S. M., I. S. Muir, et al. (1993). "Coating particles with a block co-polymer (poloxamine-908) suppresses opsonization but permits the activity of dysopsonins in the serum." Biochim Biophys Acta 1179(2): 157-65.

Morello, A. P., 3rd, R. Burrill, et al. (2007). "Preparation and characterization of poly(methyl methacrylate) - iron (III) oxide microparticles using a modified solvent evaporation method." J Microencapsul 24(5): 476-91.

Mossman, T. (1983). "Rapid colorimetric assay for cellular growth and survival: application to proliferation and cytotoxicity assays." Journal of Immunological Methods 65: 55-63.

Murillo, M., M. M. Goni, et al. (2002). "Modulation of the cellular immune response after oral or subcutaneous immunization with microparticles containing brucella ovis antigens." J Control Release. 85(1-3): 237-246.

Nakano, R., S. Kitayama, et al. (1989). "Localization of gonadotropin binding sites in human ovarian neoplasms." Am J Obstet Gynecol 161(4): 905-10.

Nakaoka, R., Y. Tabata, et al. (1997). "Prolongation of the serum half-life period of superoxide dismutase by poly(ethylene glycol) modification." Journal of Controlled Release 46(3): 253-261.

Nan, A., H. Ghandehari, et al. (2005). "Water-soluble polymers for targeted drug delivery to human squamous carcinoma of head and neck." Journal of Drug Targeting 13(3): 189-197.

Nasongkla, N., E. Bey, et al. (2006). "Multifunctional Polymeric Micelles as Cancer-Targed, MRI-Ultrasensitive Drug Delivery Systems." Nano Letters 6(11): 2427-2430.

Neal, J. C., S. Stolnik, et al. (1998). "Modification of the copolymers poloxamer 407 and poloxamine 908 can affect the physical and biological properties of surface modified nanospheres." Pharm Res 15(2): 318-24.

NektarTherapeutics (2005). Nektar Advanced PEGylation - Catalog 2005-2006.

Nishizuka, S., L. Charboneau, et al. (2003). "Proteomic profiling of the NCI-60 cancer cell lines using new high-density reverse-phase lysate microarrays." Proc Natl Acad Sci U S A 100(24): 14229-34.

Nitta, M., H. Katabuchi, et al. (2001). "Characterization and Tumorigenecity of Human Ovarian Surface Epithelial Cells Immortalized by SV40 Large T Antigen." Gynecologic Oncology 81: 10-17.

Odian, G. (2004). Principles of Polymerization. Hoboken, NJ, John Wiley & Sons.

Otsuka, H., Y. Nagasaki, et al. (2003). "PEGylated nanoaprticles for biological and pharmaceutical applications." Advanced Drug Delivery Reviews 55(3): 403-419.

Panyam, J. and V. Labhasetwar (2003). "Biodegradable nanoparticles for drug and gene delivery to cells and tissue." Advanced Drug Delivery Reviews 55(3): 329-347.

Panyam, J., S. K. Sahoo, et al. (2003). "Fluorescence and electron microscopy probes for cellular and tissue uptake of poly(D,L-lactide-co-glycolide) nanoparticles." International Journal of Pharmaceutics 262(1-2): 1-11.

Park, S. N., H. J. Jang, et al. (2007). "Preparation and characterization of biodegradable anti-adhesive membrane for peritoneal wound healing." J Mater Sci Mater Med 18(3): 475-82.

Park, E. K., S. B. Lee, et al. (2005). "Preparation and characterization of methoxy poly(ethylene glycol)/poly(epsilon-caprolactone) amphiphilic block copolymeric nanospheres for tumor-specific folate-mediated targeting of anticancer drugs." Biomaterials 26(9): 1053-61.

Park, E. K., S. Y. Kim, et al. (2005). "Folate-conjugated methoxy poly(ethylene glycol)/poly(epsilon-caprolactone) amphiphilic block copolymeric micelles for tumor-targeted drug delivery." J Control Release 109(1-3): 158-68.

Parrott, J. A., V. Doraiswamy, et al. (2001). "Expression and actions of both the follicle stimulating hormone receptor and the luteinizing hormone receptor in normal

ovarian surface epithelium and ovarian cancer." Mol Cell Endocrinol 172(1-2): 213-22.

Peltonen, L., P. Koistinen, et al. (2003). "Preparation of Nanoparticles by the Nanoprecipitation of low molecular weight poly(l)lactide." S.T.P. Pharma Sciences 13(5): 299-304.

Peppas, N. A. (2006). "Intelligent Biomaterials as Pharmaceutical Carriers in Microfabricated and Nanoscale Devices." MRS Bulletin 31: 888-893.

Peppas, N. A., K. M. Wood, et al. (2004). "Hydrogels for oral delivery of therapeutic proteins." Expert Opin Biol Ther 4(6): 881-7.

Perez, C., A. Sanchez, et al. (2001). "Poly(lactic acid)-poly(ethylene glycol) nanoparticles as new carriers for the delivery of plasmid DNA." J Control Release 75(1-2): 211-24.

Pero, S. C., G. S. Shukla, et al. (2007). "Combination treatment with Grb7 peptide and Doxorubicin or Trastuzumab (Herceptin) results in cooperative cell growth inhibition in breast cancer cells." Br J Cancer 96(10): 1520-5.

Porjazoska, A., O. Karal-Yilmaz, et al. (2004). "Biocompatible polymer blends of poly(D,L-lactic acid-co-glycolic acid) and triblock PCL-PDMS-PCL copolymers: Their Characterizations and Degradations." Croatia Chemica Acta 77(4): 545-551.

Pun SH, T. F., Bellocq NC, Cheng J, Grubbs BH, Jensen GS, Davis ME, Brewster M, Janicot M, Janssens B, Floren W, Bakker A (2004). "Targeted delivery of RNA-cleaving DNA enzyme (DNAzyme) to tumor tissue by transferrin-modified, cyclodextrin-based particles." Cancer Biology & Therapy 3(7): 641-650.

Quellec, P., R. Gref, et al. (1998). "Protein encapsulation within polyethylene glycol-coated nanospheres. I. Physicochemical characterization." J Biomed Mater Res 42(1): 45-54.

Richards, J. S. and A. R. Midgley, Jr. (1976). "Protein hormone action: a key to understanding ovarian follicular and luteal cell development." Biol Reprod 14(1): 82-94.

Riley, T., S. Stolnik, et al. (2001). "Physiochemical evaluation of nanoparticles assembled from poly(lactic acid)-poly(ethylene glycol) (PLA-PEG) block copolymers as drug delivery vehicles." Langmuir 17: 3168-3174.

Ross, J. F., H. Wang, et al. (1999). "Folate receptor type beta is a neutrophilic lineage marker and is differentially expressed in myeloid leukemia." Cancer 85(2): 348-57.

Roth, A., D. C. Drummond, et al. (2007). "Anti-CD166 single chain antibody-mediated intracellular delivery of liposomal drugs to prostate cancer cells." Molecular Cancer Therapeutics 6(10): 2737.

Sahoo, S. K. and V. Labhasetwar (2005). "Enhanced antiproliferative activity of transferrin-conjugated paclitaxel-loaded nanoparticles is mediated via sustained intracellular drug retention." Molecular Pharmaceutics 2(5): 373-383.

Sahoo, S. K., M. Wenxue, et al. (2004). "Efficacy of transferrin-conjugated paclitaxel-loaded nanoparticles in a murine model of prostate cancer." International Journal of Cancer 112(2): 335-340.

Salem, A. K., S. M. Cannizzaro, et al. (2001). "Synthesis and characterisation of a degradable poly(lactic acid)-poly(ethylene glycol) copolymer with biotinylated end groups." Biomacromolecules 2(2): 575-80.

Santander-Ortega, M. J., A. B. Jodar-Reyes, et al. (2006). "Colloidal stability of pluronic F68-coated PLGA nanoparticles: a variety of stabilisation mechanisms." J Colloid Interface Sci 302(2): 522-9.

Sarver, J. G., W. A. Klis, et al. (2002). "Microplate screening of the differential effects of test agents on Hoechst 33342, rhodamine 123, and rhodamine 6G accumulation in breast cancer cells that overexpress P-glycoprotein." Journal of Biomolecular Screening 7(1): 29-34.

Sawant, R. M., J. P. Hurley, et al. (2006). ""SMART" drug delivery systems: double-targeted pH-responsive pharmaceutical nanocarriers." Bioconjug Chem 17(4): 943-9.

Saxena, V., M. Sadoqi, et al. (2003). "Degradation kinetics of indocyanine green in aqueous solution." J Pharm Sci 92(10): 2090-7.

Saxena, V., M. Sadoqi, et al. (2004). "Enhanced photo-stability, thermal-stability and aqueous-stability of indocyanine green in polymeric nanoparticulate systems." J Photochem Photobiol B 74(1): 29-38.

Schiffelers, R. M., G. A. Koning, et al. (2003). "Anti-tumor efficacy of tumor vasculature-targeted liposomal doxorubicin." Journal of Controlled Release 91: 115-122.

Schneider, S. L., S. A. Fuqua, et al. (1990). "Isolation and characterization of an adriamycin-resistant breast tumor cell line." In vitro Cellular & Developmental Biology 26(6): 621-628.

Shen, F., J. F. Ross, et al. (1994). "Identification of a novel folate receptor, a truncated receptor, and receptor type beta in hematopoietic cells: cDNA cloning,

expression, immunoreactivity, and tissue specificity." Biochemistry 33(5): 1209-15.

Shive, M. S. and J. M. Anderson (1997). "Biodegradation and biocompatibility of PLA and PLGA microspheres." Advanced Drug Delivery Reviews 28(1): 5-24.

Silva, A. C., J. H. Lee, et al. (2007). "Detection of cortical laminar architecture using manganese-enhanced MRI." J Neurosci Methods.

Simoni, M., J. Gromoll, et al. (1997). "The follicle-stimulating hormone receptor: biochemistry, molecular biology, physiology, and pathophysiology." Endocr Rev 18(6): 739-73.

Skoog, B. (1979). "Determination of polyethylene glycols 4000 and 6000 in plasma protein preparations." Vox Sang 37: 345-349.

Smith, L., M. B. Watson, et al. (2006). "The analysis of doxorubicin resistance in human breast cancer cells using antibody microarrays." Mol Cancer Ther 5(8): 2115-20.

Staros, J. V. (1982). "N-hydroxysuccinimide active esters: Bis(N-hydroxysulfosuccinimide) esters of two dicarboxylic acids are hydrophilic, membrane impermeant, protein cross-linkers." Biochemistry 21: 3950-3955.

Stayton, P. S., M. E. El-Sayed, et al. (2005). "'Smart' delivery systems for biomolecular therapeutics." Orthod Craniofac Res 8(3): 219-25.

Stolnik, S., S. E. Dunn, et al. (1994). "Surface modification of poly(lactide-co-glycolide) nanospheres by biodegradable poly(lactide)-poly(ethylene glycol) copolymers." Pharm Res 11(12): 1800-8.

Storm, G., S. O. Belliot, et al. (1995). "Surface modification of nanoparticles to oppose uptake by the mononuclear phagocyte system." Advanced Drug Delivery Reviews 17: 31-48.

Sturgeon, R. J. and S. G. Schulman (1977). "Electronic Absorption Spectra and Protolytic Equilibria of Doxorubicin: Direct Spectrophotometric Determination of Microconstants." Journal of Pharmaceutical Sciences 66(7): 958-961.

Sudimack, J. and R. J. Lee (2000). "Targeted drug delivery via the folate receptor." Adv Drug Deliv Rev 41(2): 147-62.

Sugiyama, M., A. Imai, et al. (2005). "Gonadotropin-releasing hormone retards doxorubicin-induced apoptosis and serine/threonine phosphatase inhibition in ovarian cancer cells." Oncol Rep 13(5): 813-7.

Sun B, R. B., Feng SS (2007). "Multifunctional poly(d,l-lactide-co-glycolide)/montmorillonite (PLGA/MMT) nanoparticles decorated by Trastuzumab for targeted chemotherapy of breast cancer." Biomaterials In Press.

Syed, V., G. Ulinski, et al. (2001). "Expression of gonadotropin receptor and growth responses to key reproductive hormones in normal and malignant human ovarian surface epithelial cells." Cancer Res 61(18): 6768-76.

Tan, E. C., R. Lin, et al. (2005). "Fabrication of double-walled microspheres for sustained release of doxorubicin." Journal of Colloild and Interface Science 291: 134-143.

Tang, H. W., X. B. Yang, et al. (2007). "Probing intrinsic and extrinsic components in single osteosarcoma cells by near-infrared surface-enhanced Raman scattering." Analytical Chemistry 79(10): 3646-3653.

Tobio, M., R. Gref, et al. (1998). "Stealth PLA-PEG nanoparticles as protein carriers for nasal administration." Pharm Res 15(2): 270-5.

Torchilin, V. P. (1995). "Which polymer can make nanoparticulate drug carriers long-circulating?" Advanced Drug Delivery Reviews 16(2-3): 141-155.

Torchilin, V. P. (2002). Strategies and Means for Drug Targeting: An Overview. Biomedical Aspects of Drug Targeting. V. R. Muzykantov and V. P. Torchilin, Kluwer Academic Publishers: 3-26.

Torchilin, V. P., J. Narula, et al. (1996). "Poly(ethylene glycol)-coated anti-cardiac myosin immunoliposomes: factors influencing targeted accumulation in the infarcted myocardium." Biochimica Biophysica Acta 1279: 75-83.

Torres-Lugo, M., M. Garcia, et al. (2002). "pH-Sensitive hydrogels as gastrointestinal tract absorption enhancers: transport mechanisms of salmon calcitonin and other model molecules using the Caco-2 cell model." Biotechnol Prog 18(3): 612-6.

Turk, M. J., D. J. Waters, et al. (2004). "Folate-conjugated liposomes preferentially target macrophages associated with ovarian carcinoma." Cancer Lett 213(2): 165-72.

Twardowski, P. and K. Margolin (2002). Targeting Vascular Endothelium With Antibodies. Cancer Drug Discovery and Development: Tumor Targeting in Cancer Therapy. M. Pagé. Totowa, NJ, Humana Press Inc.: 199-210.

van Hummel, G. J., S. Harkema, et al. (1982). "Structure of 3,6-dimethyl-1,4-dioxane-2,5-dione [D-,D-(L-,L-)lactide]." Acta Crystallographica B38: 1679-1681.

Vannier, B., H. Loosfelt, et al. (1996). "Anti-Human FSH Receptor Monoclonal Antibodies: Immunochemical and Immunocytochemical Characterization of the Receptor." Biochemistry 35: 1358-1366.

Vega J, K. S., Fan Z, Wallace S, Charsangavej C, Li C (2003). "Targeting doxorubicin to epidermal growth factor receptors by site-specific conjugation of C225 to poly(L-glutamic acid) through a polyethylene glycol spacer." Pharmaceutical Research 20(5): 826-832.

Veggian, R., S. Fasolato, et al. (1989). "Immunohistochemical reactivity of a monoclonal antibody prepared against human ovarian carcinoma on normal and pathological female genital tissues." Tumori 75(5): 510-3.

Venkatraman, S. S., P. Jie, et al. (2005). "Micelle-like nanoparticles of PLA-PEG-PLA triblock copolymer as chemotherapeutic carrier." Int J Pharm 298(1): 219-32.

Verrecchia, T., G. Spenlehauer, et al. (1995). "Non-stealth (poly(lactic acid/albumin)) and stealth (poly(lactic acid-polyethylene glycol)) nanoparticles as injectable drug carriers." Journal of Controlled Release 36(1-2): 49-61.

Verrecchia, T., P. Huve, et al. (1993). "Adsorption/desorption of human serum albumin at the surface of poly(lactic acid) nanoparticles prepared by a solvent evaporation technique." Journal of Biomedical Materials Research 27(8): 1019-1028.

Vila, A., A. Sanchez, et al. (2004). "PEG-PLA nanoparticles as carriers for nasal vaccine delivery." Journal of Aerosol Medicine 17(2): 174-185.

Vila, A., A. Sanchez, et al. (2005). "PLA-PEG particles as nasal protein carriers: the influence of the particle size." Int J Pharm 292(1-2): 43-52.

Vila, A., H. Gill, et al. (2004). "Transport of PLA-PEG particles across the nasal mucosa: effect of particle size and PEG coating density`." Journal of Controlled Release 98(2): 231-244.

Vittaz, M., D. Bazile, et al. (1996). "Effect of PEO surface density on long-circulating PLA-PEO nanoparticles which are very low complement activators." Biomaterials 17(16): 1575-81.

Wang, J., L. Lin, et al. (2003). "Quantitative analysis of follicle-stimulating hormone receptor in ovarian epithelial tumors: a novel approach to explain the field of ovarian cancer development in secondary mullerian systems." International Journal of Cancer 103(3): 328-334.

Wang, Z.-Y., Y.-M. Zhao, et al. (2005). "Syntheses of Poly(lactic acid-co-glycolic acid) Serial Biodegradable Polymer Materials via Direct Melt Polycondensation and Their Characterization." Journal of Applied Polymer Science 99: 244-252.

Wei, J. S., H. B. Zeng, et al. (2005). "Temperature- and pH-sensitive core-shell nanoparticles self-assembled from poly(n-isopropylacrylamide-co-acrylic acid-co-

cholesteryl acrylate) for intracellular delivery of anticancer drugs." Front Biosci 10: 3058-67.

Weitman, S. D., R. H. Lark, et al. (1992). "Distribution of the folate receptor GP38 in normal and malignant cell lines and tissues." Cancer Res 52(12): 3396-401.

Wong, H. L., A. M. Rauth, et al. (2006). "A New Polymer-Lipid Hybrid Nanoparticle System Increases Cytotoxicity of Doxorubicin Against Multidrug-Resistant Human Breast Cancer Cells." Pharmaceutical Research 23(7): 1574-1585.

Wu J, L. Y., Lee A, Pan X, Yang X, Zhao X, Lee RJ (2007). "Reversal of multidrug resistance by tranferrin-conjugated liposomes co-encapsulating doxorubicin and verapamil." Journal of Pharmacy and Pharmacetuical Sciences 10(3): 350-357.

Xu, J.-P., J. Ji, et al. (2005). "Novel biomimetic polymersomes as polymer therapeutics for drug delivery." Journal of Controlled Release 107(3): 502-512.

Yang, C. Q., K. Y. K. Chan, et al. (2006). "Single Nucleotide Polymorphisms of Follicle-Stimulating Hormone Receptor are Associated with Ovarian Cancer Susceptibility." Carcinogenesis 27(7): 1502-1506.

Yang, X., W. Deng, et al. (2007). "Folate-functionalized polymeric micelles for tumor targeted delivery of a potent multidrug-resistance modulator FG020326." J Biomed Mater Res A.

Yokoyama, M. and T. Okano (1996). "Targetable Drug Carriers: Present Status and Future Perspectives." Advanced Drug Delivery Reviews 21(2): 77-80.

Yoo, H. S. and T. G. Park (2001). "Biodegradable Polymeric Micelles Composed of Doxorubicin Conjugated PLGA-PEG Block Copolymer." Journal of Controlled Release 70(1-2): 63-70.

Yoo, H. S. and T. G. Park (2004). "Folate receptor targeted biodegradable polymeric doxorubicin micelles." Journal of Controlled Release 96(2): 273-283.

Yoo, H. S. and T. G. Park (2004). "Folate-receptor-targeted delivery of doxorubicin nano-aggregates stabilized by doxorubicin-PEG-folate conjugate." Journal of Controlled Release 100(2): 247--256.

Yoo, H. S., J. E. Oh, et al. (1999). "Biodegradable Nanoparticles Containing Doxorubicin-PLGA Conjugate for Sustained Release." Pharmaceutical Research 16(7): 1114-1118.

Yoshimura, A., N. Shudo, et al. (1990). "Novel screening method for agents that overcome classical multidrug resistance in a human cell line." Cancer Letters 50(1): 45-51.

Zambaux, M. F., F. Bonneaux, et al. (1999). "MPEO-PLA nanoparticles: effect of MPEO content on some of their surface properties." J Biomed Mater Res 44(1): 109-15.

Zeng, F., H. Lee, et al. (2006). "Epidermal growth factor-conjugated poly(ethylene glycol)-block- poly(delta-valerolactone) copolymer micelles for targeted delivery of chemotherapeutics." Bioconjugate Chemistry 17(2): 399-409.

Zhang, Z., S. H. Lee, et al. (2007). "Folate-decorated poly(lactic-co-glycolide)-vitamin E TPGS nanoparticles for targeted drug delivery." Biomaterials 28(10): 1889-1899.

Zheng, W., J. J. Lu, et al. (2000). "Ovarian epithelial tumor growth promotion by follicle-stimulating hormone and inhibition of the effect by luteinizing hormone." Gynecol Oncol 76(1): 80-8.

Vita

Tania Betancourt was born in Bogota, Colombia, on July 24, 1981, to her parents Nydia Bustos and Juan Betancourt. She completed high school in Colegio del Rosario de Santo Domingo in Bogota, and immediately moved with her mother to The United States of America where she began pursuing her higher education. She received her Bachelor of Science degree in Chemical Engineering from Texas A&M Universtiy in December of 2002. After graduation, she worked with the Crop Protection group of DuPont for eight months as a production engineer. She began her work towards a Doctorate in Biomedical Engineering in August 2003 under the supervision of Professor Lisa Brannon-Peppas. During her doctorate work, she published one review article on the applications of micro- and nano-fabrication in the pharmaceutical and biomedical fields, and one research article on the preparation, characterization and evaluation of doxorubicin-loaded nanoparticles. She also participated in the publication of two book chapters with her advisor, Dr. Lisa Brannon-Peppas. She is expected to complete her Doctor of Philosophy degree in December of 2007.

Permanent address: 2207 Wickersham Lane # 1106, Austin, Texas 78741

This dissertation was typed by the author.